1974

Studies in the distribution of nonmetallic inclusions in metal ingots

I. D. Simpson
Wollongong University College

THE UNIVERSITY OF NEW SOUTH WALES

WOLLONGONG UNIVERSITY COLLEGE

SCHOOL OF METALLURGY

THESIS

FOR THE DEGREE OF DOCTOR OF PHILOSOPHY

"STUDIES IN THE DISTRIBUTION OF NONMETALLIC INCLUSIONS IN METAL INGOTS"

I. D. SIMPSON, B.Sc. (Hon)

NOVEMBER 1974

8080147

ACKNOWLEDGEMENTS

The author wishes to express his sincere thanks to Professor G. Brinson for his support and to Associate Professor N. Standish for his invaluable help and guidance during this research program.

Formative discussions with Mr. M. Atkinson and the development of the computer program by Dr. S. Cumming are also gratefully acknowledged. Appreciation is expressed to Mr. L. Auran and Mr. A. Malin for electron probe microanalyses.

The author is indebted to the Australian Iron and Steel Pty. Ltd. for the opportunity to conduct this research and to both the Chemical and Computer Departments for services given. Thanks are also due to the Electrolytic Refining and Smelting Co. Pty. Ltd. for donating electrolytic copper and for chemical analysis of samples.

The author also wishes to express his gratitude to Mrs M. Standen for her photography of diagrams and to his wife for her encouragement and typing of this thesis.

SYNOPSIS

The size-frequency distribution of nonmetallic inclusions in the volume of metal was estimated from the distribution of inclusion sections on a polished plane. The estimation process involved the description of both distributions by log-normal functions and the calculation of one from the other by the method of moments.

The significance of the fit of the three parameter log-normal form to the assessed section distributions were tested with the chi-square test. Most samples gave a significant fit at the 10% confidence level, while those which did not, on further examination were shown to be heterogeneous in either inclusion shape or type.

The inclusion's shape was approximated to that of a general ellipsoid, so that once the shape distribution had been determined the spatial inclusion distribution could be estimated. The significance of the fit of both the spatial distribution and shape distribution was tested by comparing the values of the inclusions' volume fraction and surface area per unit volume determined from the distributions with that determined by quantitative metallographic methods.

Of the inclusions examined in small 3 Kg ingots, alumina particles with a hexagonal plate morphology were

approximated by oblate ellipsoids of revolution with a mean eccentricity of 0.85, while partially deformed oxy-sulphide inclusions in industrial hot rolled plate were successfully represented by ellipsoids of revolution with a constant axial ratio.

The spatial distributions of oxides from different ingot positions in both the 3 Kg ingots and a 12 ton ingot were compared by testing the equivalence of the distribution parameters with the standard statistical F and t tests. Small perturbations in inclusion growth rates were discerned from the results of these tests.

Microscopic examinations of several of the aluminium deoxidized copper and iron 3 Kg ingots produced from induction stirred melts, provided evidence supporting the theory that the mixing of the deoxidant in the melt takes a considerable time. Also the examination of alumina clusters present in these ingots indicated that the clusters had formed by an aggregation followed by a partial sintering process.

TABLE OF CONTENTS

APPENDICES

1.0 INTRODUCTION

The investigations discussed in this thesis were subject to changing aims and motivations. The original aim was to examine the causes for the formation of a base cone of inclusions in industrial size, fully-killed, steel ingots. Small ingots of iron and copper were cast from laboratory melts which had been deoxidized by aluminium. After numerous attempts under varying casting conditions none of the ingots had an observable base cone. Thus, it was concluded that the phenomena operative in commercial size ingots were not reproducible in small scale laboratory ingots (3-7 Kg). The high inclusion flotation rates, short solidification times, high inclusion removal rate from the induction stirred heats because of the large ratio of crucible area to melt volume and difficulties in producing an equiaxed cone region were reasons for abandoning this investigation.

The results of these studies, however, are discussed in Appendix 3 as the subsequent examination and assessment of the inclusion distributions in these ingots can be meaningfully considered only when the ingot's history is known.

The change in the thesis from a study of the base cone

phenomenon to that of quantitative description of the inclusions size-frequency distributions was a consequence of two events. A discussion with Mr. M. Atkinson (W.U.C.) indicated the extent of previous attempts to achieve this important description of the inclusions and also there was the realization that this information was urgently needed for the interpretation of the influence of inclusions on the matrix and mechanical properties of the inclusion-steel composite (168-170). In fact in a recent review (217) by Pickering this point was high-lighted by the continual reference to the relationship between inclusion size and shape distributions and the toughness, ductility and weldability of steel.

The inadequacies of the existing techniques based on cleanness indices or average measures of the inclusion concentration (144,148) to supply these much needed data will inevitably force a re-examination of the methods of determining the inclusion size-distributions in the steel volume. Previous size-distribution analysis, such as those of Guellard (166) Main (218) and Russell (219), considered only the size distribution of particle sections . It is the size-distribution of the inclusions in the bulk of the steel, however, which is of importance when investigating

correlations between inclusions and the steel's properties.

Thus the aim of these present investigations is to pursue the statistical approach which was either suggested (110) or tentatively used (218, 219) by previous investigators to its logical limits. This involves the clarification of the relationship between the distribution of particle sections seen on the polished section plane and that of the un-sectioned inclusions in the bulk of the sample by defining both distributions in mathematical functional forms. Such a proceedure greatly simplifies the estimation of one distribution from another.

During the development of this model for the inclusion size distributions it was also necessary to develop a shape model, as size and shape cannot be separated when estimating the spatial distribution (179). The general ellipsoid model was developed in preference to the more commonly used spherical model, as particles with elongated morphologies can be better represented by an ellipsoid than a sphere.

2.0 NON-METALLIC INCLUSIONS IN STEEL

Non-metallic inclusions have been defined as "particles of sulphide, silicate, oxide or nitride, which either occur in the raw materials from which steel is made, or are picked up from the furnace gases, or are a result of contamination by refractories, or by the reaction products of the steelmaking and deoxidation practice" (1). There is no logical reason for the exclusion from this definition of carbides or those intermetallic compounds which lack ductility and other properties commonly associated with metals, other than it has been customary to do so (2).

The above definition implies that the origin of inclusions can be explicitly identified. This, however, is not always the case and is the reason why Sims' system of classifying inclusions was difficult to apply. Sims (3) classified inclusions as exogenous or endogenous. Exogenous inclusions were defined as those of origin foreign to the steel, such as admixed slags, erosion products and impurities in raw materials and alloy additions, etc., which have become entrapped in the steel, whilst endogenous inclusions were defined as those whose origin was the

result of chemical reactions within the steel.

The difficulty of Sims' classification by origin is that a metallographic study of inclusions does not always establish their origin (2,4,5). For example, during solidification a continuous change can occur in the inclusion structure and composition as a result of reactions with the molten steel. Consequently there may be endogenous precipitation on exogeneous nuclei which would result in a problematic classification.

A more convenient classification of inclusions based on their composition was proposed by Kiessling (5), who used this fundamental concept to present inclusion types in a systematic manner independent of their origin, (4).

Simultaneously with these attempts to provide a logical framework within which inclusions could be identified, the thermodynamic and kinetic studies of the chemical reactions and growth mechanisms which occur during deoxidation were also taking place. Although both these aspects of deoxidation have been studied continuously since the beginning of this century, even now neither aspect can be considered to be completely understood. The relative importance of heterogeneous and homogeneous nucleation is still debated as is retarded nucleation or flotation

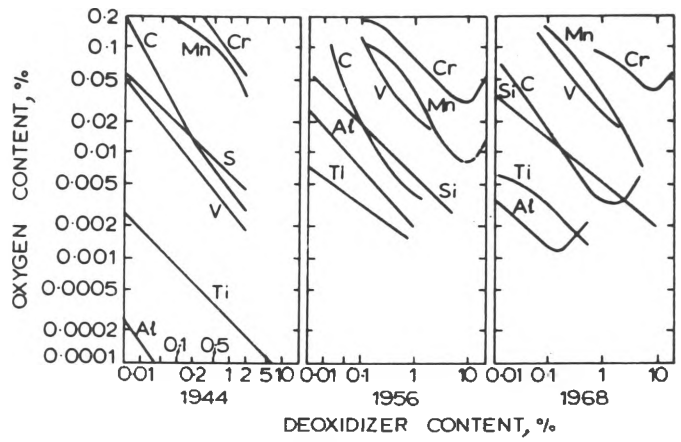

Fig. 2-1 Deoxidizing capacity of C, Mn, Si, V, Ti, and Al in molten iron as determined in 1944, 1956 and 1968 (7).

mechanism as the major influence controlling the deoxidation rate. The importance given to each of these by the many investigators is reflected in their mathematical models and interpretations of their experimental findings.

Before reviewing some important but controversial kinetic concepts, the thermodynamics of deoxidation should first be considered. This area of inclusion studies is the most complete and so only a brief review is necessary to highlight certain anomalies in the existing thermodynamic data.

2.1 THERMODYNAMIC CONSIDERATIONS.

Since 1930 the evaluation of the equilibrium constant, K, for the various deoxidants added to steel has motivated many investigations. Inspite of the considerable number of these investigations (6) there are still some uncertainties in the equilibrium data. Figure 2-1 shows the changes which have occurred between 1944 and 1968 in the relative deoxidizing capacity of some elements (7). These changes have been explained in many different ways, for example, anomalies in the equilibrium constant for aluminium deoxidation were explained by Repetylo et al (8) as resulting from the gradual flotation of the alumina from

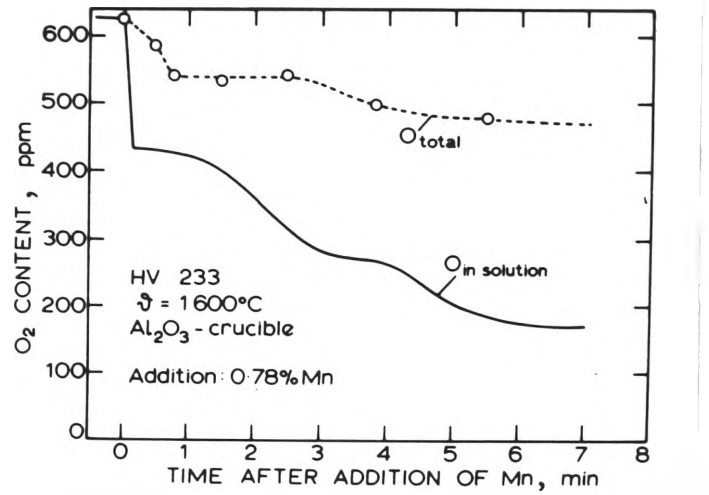

Fig. 2-2 Oxygen concentration curves for the time period after the addition of electrolytic manganese (11).

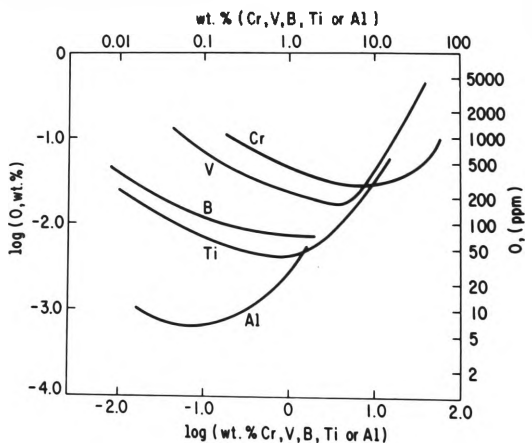

Fig. 2-3 The influence of various elements on the oxygen solubility in liquid steel at 1600°C (B at 1550 °C) (12).

the bath. This explanation is most probably correct and can also explain the low equilibrium values for deoxidation by manganese obtained by Luzgin et al (9) and also those of von Bogdandy et al (10) presented in Fig. 2-2 (11). It would appear then that manganese is a stronger deoxidizer than is commonly accepted. The formation of a manganese oxide in suspension in these experiments had kept the total oxygen content of the bath high, thereby affecting the values of the constant.

A general trend which can be observed from a number of deoxidation studies of the Fe-De-O systems is that as the oxide of the deoxidant (De) becomes more stable, the minimum oxygen solubility decreases and the minimum occurs at lower deoxidant concentration (Fig. 2-3) (12).

This phenomenon was explained by Samarin (7, 13) as resulting from two opposing effects during deoxidation.

1. a reduction of the partial pressure of oxygen which lowers its solubility in the melt, and
2. a decrease in the activity of oxygen which increases the solubility.

The result of these two effects is a minimum in the equilibrium curve as shown in Fig. 2-3.

Minima have also been reported in the equilibrium curves for Cr, Al, Co (13) C (14) and Ti (12, 15) in iron.

The concentration of the deoxidant at which this minimum soluble oxygen content occurs is usually above that normally required to "kill" the steel, thus the minimum oxygen content that is obtained depends on the kinetics of the deoxidation reaction.

2.2 KINETICS OF DEOXIDATION

Studies of deoxidation kinetics can be divided into four general categories:-

(a) solution of deoxidizer in melt

(b) nucleation of oxides

(c) growth of oxides

(d) elimination of oxides

In most studies (16-21) little consideration was given to the first stage in the deoxidation sequence as homogeneous mixing was usually assumed (17, 19), while the last two categories have taken considerable prominence especially in the theories of alumina cluster formation.

2.2.1 Dissolution of Deoxidizer

The time for the attainment of the homogeneity of mixing of deoxidizers depends on the free energy change of dissolution (22). Silicon and aluminium for instance require a shorter time than manganese or chromium.

Another factor which was considered to have a considerable influence on the rate of mixing of deoxidizers was the presence in the melt of any currents either natural or induced. Thus, many experimenters reported increased rates of mixing for deoxidizers added to induction stirred melts (16, 19-21), but this mixing may not be as rapid or as complete as these investigations imply.

Studies of the dissolution of deoxidizers Ti and Fe-Mn by Kojima et al (22) revealed that mixing occurred by laminar flow even though the experiments were performed in high frequency induction furnaces. This is but one example of the numerous experimental results which support the hypothesis that mixing of deoxidizers occurs inhomogeneously. Other examples which can be quoted from the literature are:

1. Manganese heterogeneity resulting from the formation of areas enclosed by galaxite films (23, 24).

2. Slow decrease in dissolved oxygen caused by a layer rich in fine alumina particles preventing diffusion of aluminium (25).

3. The presence of spinel inclusions under conditions such that the equilibrium phase was alumina (26).

These and other experimental observations can be explained by a hypothesis of Chipman (27). He proposed that dissolution and complete mixing of a deoxidizer in a molten steel bath was slow and as a consequence stabilizing films formed at the interface of regions with a high content of deoxidizing agent and a high content of oxygen, while non-equilibrium phases can form in low deoxidizer, high oxygen containing regions of the melt.

2.2.2 Nucleation

The formation of oxide nuclei from the reaction:

$$x\ De + y\ O \longrightarrow (De)_x O_y \qquad (2\text{-}1)$$

has generally been considered in terms of the classical nucleation theory of Volmer and Weber and its subsequent

improvements by Becker and Doring (28). In this theory, embryos randomly form and disappear if they are thermodynamically unstable. The smallest embryo in equilibrium with its surroundings and able to grow Volmer called a "nucleus". The size of the nucleus may be determined from an equation proposed by von Bogdandy et al (29) and based on the Gibbs-Thompson equation:

$$r^* = \frac{2\sigma_{m\text{-}ox} M}{\rho RT \ln \frac{K^1}{K^1_e}} \qquad (2.3)$$

where $\sigma_{m\text{-}ox}$ = interfacial tension at the oxide-metal interface (erg/cm^2)

M = molecular weight of oxide (g/mole)

ρ = density of nucleus (g/cm^3)

r^* = critical radius of nucleus (cm)

K^1/K^1_e is the supersaturation ratio, where $K^1_e = (De)^x \cdot (O)^y$ is the solubility product for homogeneous nucleation.

Although nucleation has generally been considered using this classical theory, calculations by Popel' (30) of the supersaturations required to homogeneously nucleate inclusions with surface tensions of 1000 $ergs/cm^2$ or more, showed that such oxides would only nucleate heterogeneously.

Experimental evidence has been produced which both supports and contradicts Popel's conclusion. For example alumina was observed to nucleate only heterogeneously on the walls of the container (31) inspite of a high supersaturation in the melt. Also, von Bogdandy concluded from his deoxidation studies that Al, and Ti and Zr can nucleate homogeneously, whereas Si and Mn only nucleate heterogeneously (29, 32). In a more recent study however using an oxygen probe, Sigworth and Elliott (33) state that their results indicate that silica can also nucleate homogeneously at a supersaturation ratio of about 80. On the other hand, Hoff and Kugel (34) found that in their experiments silicon did not nucleate homogeneously. The difficulty of ensuring freedom from particles which can act as nuclei and from the nucleation of FeO rich phases complicates the interpretation and the experimental study of homogeneous nucleation.

As is well known in the absence of nucleants there are three possible ways to achieve the degree of supersaturation required for homogeneous nucleation. They are:

1. by quenching an equilibrium melt from a high temperature;

Species	Interfacial energy σ	Nucleus size and nucleation rate	C/C_s supersaturation degree				
			1.5	3	5	10	100
SiO_2	420	r_I^*	59	22	16	11	7.4
		I	10^{-760}	10^{-102}	$3\cdot10^{-37}$	$2\cdot10^{2}$	10^{21}
MnO	620	r_I^*	24	9.1	6.1	4.6	3.1
		I	$5\cdot10^{-196}$	50	$7\cdot10^{20}$	$2\cdot10^{27}$	$3\cdot10^{32}$
FeO-MnO-SiO_2	700	r_I^*	42	16	71	7.5	5.0
		I	10^{-820}	$3\cdot10^{-70}$	$2\cdot10^{-16}$	$2\cdot10^{10}$	$2\cdot10^{25}$

r^* in Å, I in nuclei/cm³ sec, σ in erg/cm².

Table 2-1 Calculated nucleus sizes and nucleation rates (19).

2. during dissolution of the deoxidizer, and
3. by segregation of oxygen and deoxidizer to the residual liquid during solidification

These possibilities have been examined experimentally by several workers. In analysing their subcooling experiments Turpin and Elliott (35) found that because of competition among several possible types of oxides for nucleation during Si or Al deoxidation, FeO or FeO-containing oxides were nucleated rather than SiO_2 or Al_2O_3. The FeO containing oxides most probably nucleated because of their lower supersaturation ratio and higher nucleation rate (see Table 2-1, (19)).

The work of Torssell reported by Pomey and Trentini (36) also showed that rapid cooling from 1650 to 1550°C of a silicon-killed steel produced no homogeneous nucleation as oxygen activity curves determined by the oxygen probe and the silicon activity calculated from its concentration in samples, were in agreement.

In a study of the dissolution of various deoxidizers (22), supersaturation ratios of 120 to 200 were calculated for homogeneous nucleation and only Al, Ti and Si were

reported as achieving this level during the dissolution step.

Concerning oxygen segregation several authors have shown that during solidification oxygen is segregated in the residual liquid to a considerable degree, while silicon and aluminium only to a lesser degree (37, 38). The critical supersaturation required for homogeneous nucleation has been suggested as arising chiefly from the increased oxygen concentration in the melt (37). It should be noted that as heterogeneous nucleation on the iron dendrite is unlikely (37) then in the absence of foreign nucleating particles, homogeneous nucleation would be expected to occur in the interdendrite interstices during solidification. The results of quenched 0.01% Si melts of Turpin and Elliott (35) and the formation of small FeO inclusions in iron containing less than 0.01% Si (39), lend support to the above hypothesis.

In the presence of small nuclei, however, heterogeneous nucleation of deoxidation products can occur. This is because a lower supersaturation is required for heterogeneous nucleation as compared with homogeneous nucleation (30, 35). It should be noted that for steelmaking conditions the supersaturation ratio is normally less than 50 (40), and as there are approximately 10^4

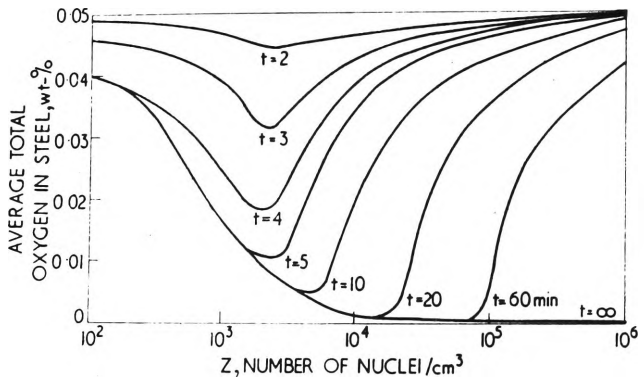

Fig. 2-4 Average total oxygen content as a function of the number of nuclei in a stagnant steel melt. Initial oxygen concentration of 0.05 wt% and equilibrium concentration of 0 wt% and a liquid steel depth of 2 metres (40).

nuclei/cc (41) in the liquid steel, heterogeneous nucleation would be the favoured mechanism. In fact, Turkdogan (40) showed that the number of nuclei present at the beginning of deoxidation can have a pronounced effect on the average total oxygen content of the solidified steel (See Fig. 2-4).

It should also be borne in mind that heterogeneous nucleation can occur not only on foreign nuclei but also on homogeneously nucleated FeO and MnO particles (30, 35, 42). In fact, Straube et al found in both aluminium (43) and titanium (44) deoxidized melts that Al_2O_3 and Ti_2O_3 were nucleated by FeO, MnO particles. Similar observations by other authors of deoxidized melts revealed the existence of SiO_2 inclusions containing FeO after silicon deoxidation (45, 46, 47) and FeO - Al_2O_3 inclusions after aluminium deoxidation (47, 48, 49). The formation of these complex inclusions probably results from direct reduction of the FeO or MnO inclusions by the deoxidant dissolved in the liquid iron (50).

The formation of FeO - Al_2O_3 inclusions can be adequately explained by invoking Chipman's incomplete mixing theory, as this theory explains quite satisfactorily the formation of thermodynamically unstable nuclei (49) whilst the formation of liquid deoxidation products during

aluminium deoxidation and the formation of aluminates or silicates when the equilibrium phase should have been alumina or silica, can all result from a non-uniform concentration of the deoxidant in the melt.

Also, not only can new oxides nucleate on existing oxides but the nucleation of iron and manganese sulphides on, or in, Al_2O_3-MnO-SiO_2 inclusions have been observed by Maunder and Charles (51). Thus there are many possible nucleation mechanisms and only actual deoxidizing conditions will determine which one, or combination of, mechanisms will be operative.

Finally, the composition of the growing inclusion is determined by the powerful deoxidizers, such as aluminium, titanium and calcium, (51). These deoxidizers, need not be added intentionally but may be tramp elements in the added ferroalloys. In fact, even small percentages of trace elements between approximately 0.1% and 2% (52) of the ferroalloys have been found to make a significant contribution to the inclusion composition (53).

2.2.3 Clusters of Alumina

The formation of a characteristic morphology

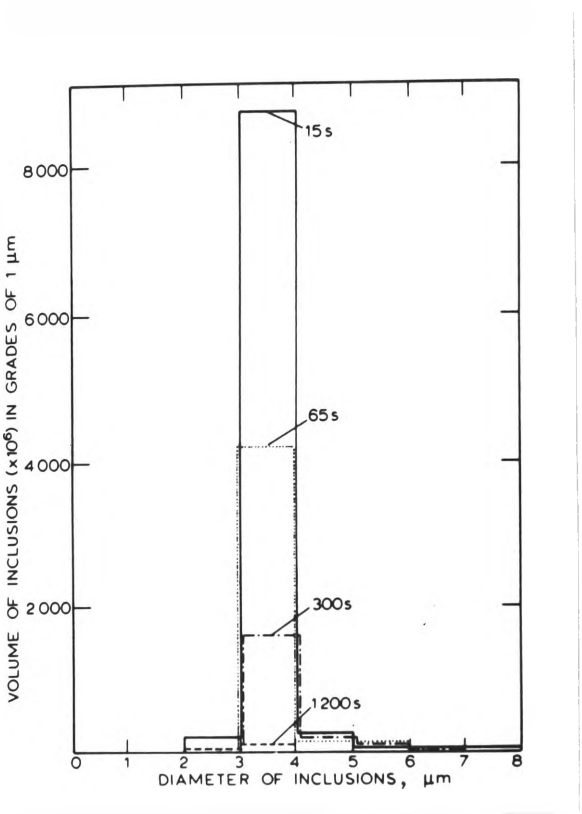

Fig. 2-5 Volume-size distribution resulting from aluminium deoxidation of a laboratory iron melt (63)

of alumina which has taxed the experimental and theoretical skills of many investigators is alumina clusters. The nucleation of this inclusion group is of prime importance for it is to a large extent responsible for the cleanness of the steel resulting from aluminium deoxidation.

This cluster type inclusion is generally composed of a large group of individual particles. With very few exceptions, these are of fairly uniform size (see Fig. 2-5), although the size of the inclusion cloud (or cluster) may vary considerably.

According to Baeyertz (2), the cloud type alumina inclusions are commonly found in steels killed with 0.23Kg or more of aluminium per ton of steel, (0.022%) and may occur in any location in the ingot, from the centre to the surface and from the top of the ingot to the bottom, without showing any clear relationship to the dendritic structure of the ingot. A single cloud of alumina often spans several branches of the same dendrite (2).

There is at present no generally accepted explanation for the formation of cloud-type inclusions. One attempt at providing an explanation was based on the premise that such inclusions are formed when alumina particles are pushed ahead of the advancing solidification front. This

explanation seems to be untenable in view of the observations made by Baeyertz (2) on a series of ingots deoxidized by mould addition of Al which indicated that the cloud-like inclusions were formed before the ingot solidified.

Of the many alternative hypotheses offered (2), the one which involved the oxidation of Al in the air during ladle or mould additions of the deoxidizer seemed quite reasonable. The aluminium was assumed to ignite as it entered the steel producing many alumina particles. Although these particles would be originally at the surface of the steel, they can be carried to some depth by the turbulence if Al is added to the ladle, or by the teeming stream if mould additions are made.

Another hypothesis which is similar to the above was based on the preferential oxidation of Al at the surface of the stream of metal during the teeming of the ingot. Many observations of inclusion distribution and deoxidation in steel (54, 55, 56) seem to support these hypotheses till Senda (57) found that air oxidation was not a necessary condition for cloud-like inclusion formation.

So other hypotheses need to be considered, one of which proposes that the reaction of aluminium with manganese

(a)

(b)

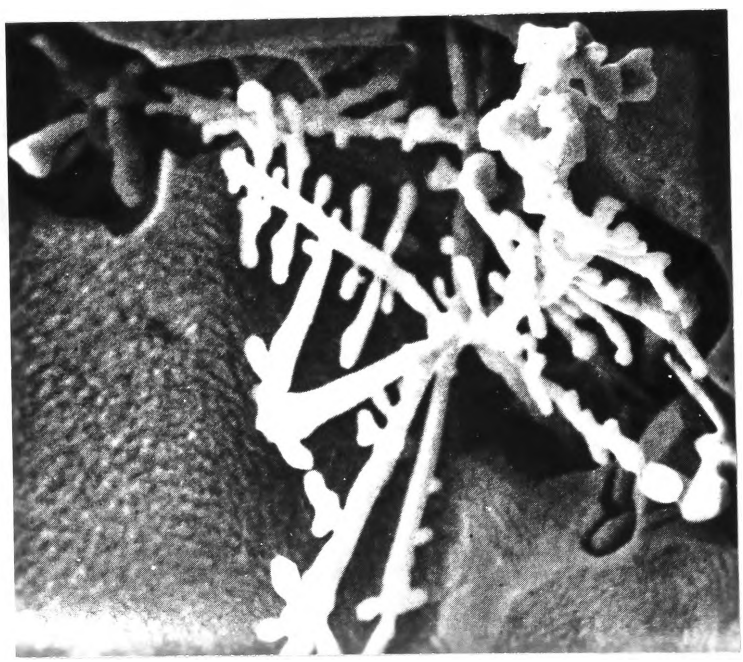

Fig. 2-6 (a) A planar view of alumina clusters in an as-cast steel (1500X).

(b) SEM image of an alumina cluster in as-cast steel (1500X) (from Rege et al (59)).

silicates would produce numerous small alumina particles which agglomerate together or with other reaction products (42). This mechanism, however, is far too restrictive and cannot explain all cases of cluster formation. The incomplete mixing model of Chipman seems to offer a better explanation. According to this model alumina clusters form from the precipitation of alumina along the boundary of an aluminium rich volume element.

The formation of the cluster whilst it is floating towards the surface of the melt is yet another variant of cluster formation by aggregation (49). This view has been supported by Torssell and Olette's investigations (58) which suggested that cluster formation was a result of collisions between small alumina particles.

The aggregation hypotheses appear to be disproved if the deep etched samples of Rege et al (59) are considered. In these samples the clusters are alumina dendrites (see Fig. 2-6)(59). On the other hand the dendritic morphology, appears to result only from specialized growth conditions (e.g. in static melts (60)), while from samples of their melts, Torssell and Olette (58) found that dendritic alumina amounted to less than 10% of the total alumina present. The aggregation hypotheses are, therefore, to be favoured with

the small particles forming in a small region of the melt from numerous nucleations, or by agglomeration through fluid motion or cluster flotation.

What is missing from the aggregation hypotheses however, is the cause of cluster stability. A possible cause is suggested from the recent work of Kozakevitch and Lucas (61). These authors showed that the conditions for particles to form a cluster are: $\Delta G < 0$ and $\theta > 90^{o}$, where ΔG is the change in surface free energy and θ is the contact angle of the inclusion/metal system. Using these criteria comparison of TiO_2 and Al_2O_3 (whose values of θ are 72 to 84^{o} and 140^{o} respectively, and ΔG values of 1112 to 378 erg/cm^2 and -2758 erg/cm^2 respectively) indicated that agglomerate formation would be very improbable for TiO_2 and very probable for Al_2O_3, which was in agreement with experimental observations (48, 62).

Though a large contact angle enables the formation of particle to particle contact, another phenomenon is needed to explain retention of contact. The retreat of the metal from the volume between the two alumina particles was considered by Kozakevitch et al (63) as sufficient to maintain the cluster, while Knuppel, Broztmann and Foster (64) propose the presence of a vacuum between the two particles as a necessary condition for cluster retention.

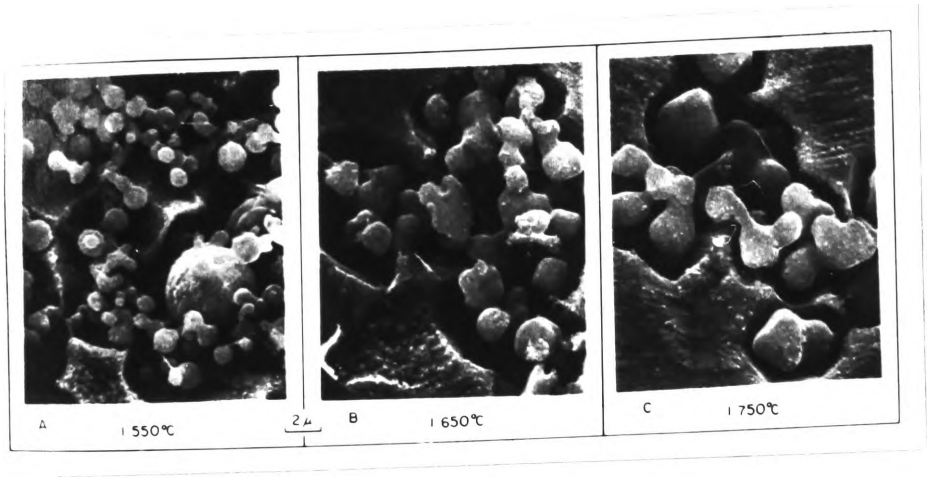

(a)

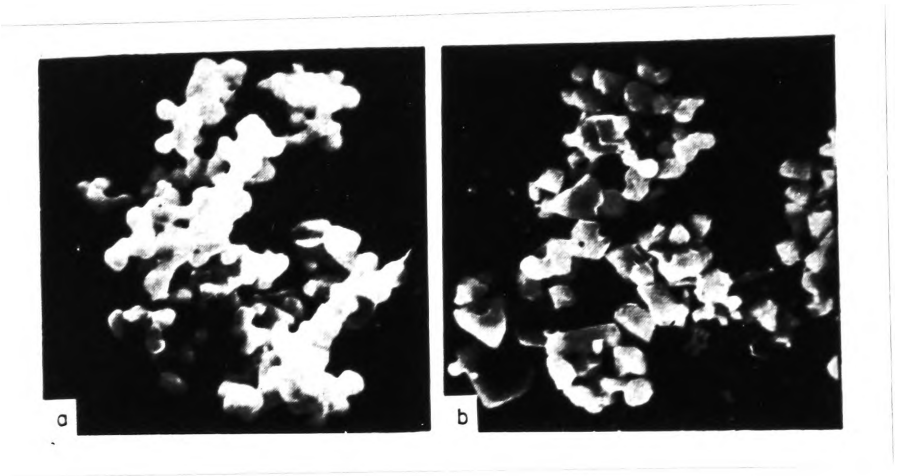

(b)

Fig. 2-7 SEM photographs of alumina clusters

(a) (60)

(b) (66)

The force holding two adhering inclusions together at different contact angles, θ, and under different ferrostatic pressures has been calculated by Baptismanski et al (65). It can be shown from their results that the force holding two alumina particles together is twice as great as that holding two silica particles together ($\theta = 115^{\circ}$) and is equal to 1×10^{-4}N for two alumina particles of radius 20μm and at a ferrostatic head of 30cm of iron plus 1 atm pressure. Whether the magnitude of such forces would be sufficient to prevent rupture during the turbulence of tapping and teeming was considered by Knuppel et al (64) who concluded that two adhering inclusions with wetting angles greater than 100° would not separate during tapping and teeming.

The need for such proposals seems unnecessary when some recent investigations are considered, for as can be seen from Fig. 2-7 the cluster has formed by agglomeration followed by sintering of the particles (60, 66).

2.2.4 Inclusion Growth Mechanisms

The growth of inclusions in iron melts and during solidification in ingots has received considerable interest

in recent years with many growth models being proposed to account for the many phenomena observed in these studies (19, 21, 30, 32, 41, 67). These growth models may be considered not as conflicting models of growth but rather as mechanisms which may occur only under specific conditions or only for a brief time during the total growth period of the inclusion.

As a consequence of this proposal, inclusions would grow by various mechanisms either simultaneously or more likely, progressively. The various growth mechanisms which have been proposed are listed as follows:

1. growth by diffusion of oxygen and deoxidizer in the melt;
2. growth of larger inclusions by diffusion of oxygen and deoxidizer from smaller inclusions, which are not in equilibrium with their surroundings;
3. growth by collisons resulting from Brownian movement, followed by coalesance;
4. growth by collisons resulting from different velocities followed by coalescence; and
5. growth by collisons due to the movement of inclusions in the melt, followed by coalesence.

The diffusional growth rate calculations of both von Bogdandy et al (32) and Sano et al (19) have been criticised by Torssell (21) for their failure to account for the extent of depletion of the melt, which depends on the number of nuclei present. When this factor is considered for silicon deoxidation, Torssell calculated that inclusions greater than 3-4μm could not be obtained even after a long period of time. Thus further growth of the inclusion must proceed by diffusion coalescence, or that resulting from Brownian movement or by coalescence resulting from collisons. The former two mechanisms have been regarded as contributing a negligible amount to the growth (21), because they are very slow once the number of inclusions per unit volume$_{(cm^3)}$ is reduced to 10^7 to 10^8 (30).

Growth of inclusions resulting from collisons followed by coalescence has been considered by a number of investigators (16, 19, 21, 30, 68). Such collisons can result from velocity gradients in the melt arising from turbulent stirring of the melt or from the inclusions rising in the melt at different rates. Both mechanisms depend on the melt containing a variable size distribution of inclusions.

The importance of coalescence as a growth mechanism

in aiding flotation and producing cleaner steels lead C.H. Herty over 30 years ago to introduce silico-manganese into steelmaking practice. Since then, coalescence in silico-manganese deoxidation has been investigated by many workers (19, 69, 70, 71, 20), who have explained the faster separation rates for melts deoxidized with higher Mn/Si ratios as resulting from coalescence of liquid manganese silicates.

The sequence of addition of the silicon and manganese also was found important in obtaining maximum growth by coalescence. If silicon is added after manganese, liquid silicates were observed to form and coalese and so were rapidly eliminated, but when silicon is added first, solid silica particles were formed which were slow to coalese (19) and so their elimination was sluggish.

A practical observation, which has been noted many times (16, 18, 19, 20, 67, 72), that inclusions have higher growth and flotation rates in the turbulent conditions of tapping and teeming is another indication of the importance of coalescence as a growth mechanisms. Clearly, if coalescence is the operative growth mechanism then disturbances which increase the rate of collisions of inclusions will also

increase the rate of growth of inclusions. Moreover, since work of adhesion is involved in coalescence then particle size must also be considered. This has been demonstrated by Popel' (30) who showed that the probability of collisions was greater between elongated than between spherical particles, and that there was an optimum size for best adhesion during coalescence.

It should be noted that the resistence to coalescence results from the viscosity of the inclusions, i.e., the more viscous the inclusions are the more difficult it is for the coalescence to occur between them.

In fact from studies of Mn-Si deoxidation, Grevillius (74) found that the viscosity of the inclusions was the only physical property of the inclusions which showed a large variation at different flotation rates. Thus it is not surprising that a more rapid growth of inclusions was observed when the inclusions were liquid rather than when they were solid (19, 26, 43, 69). In order to obtain coalescence between two particles the iron film surrounding the particles must be broken. This film tends to be easier to break up the higher the interfacial tension between the iron and the particles (73). It is significant to note that none of the mathematical models developed to predict growth

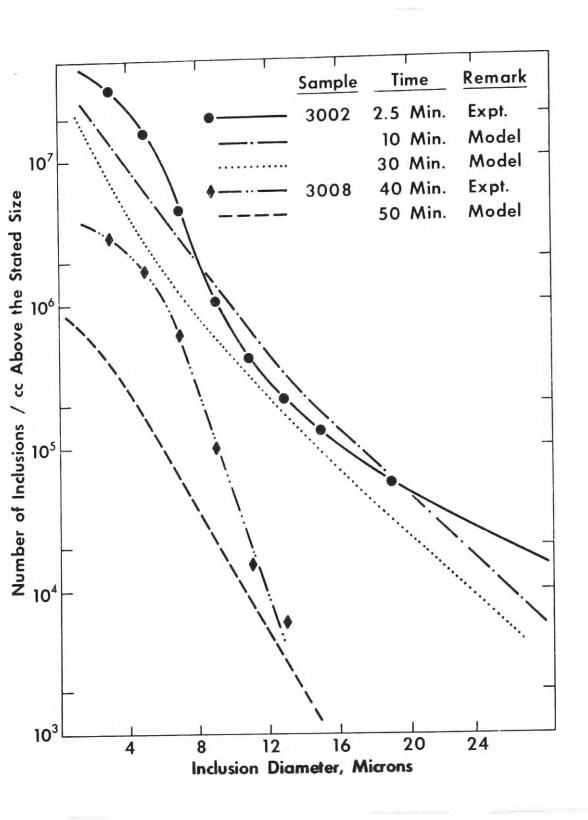

Fig. 2-8 Comparison of experimental and predicted inclusion size distributions (68).

(a)

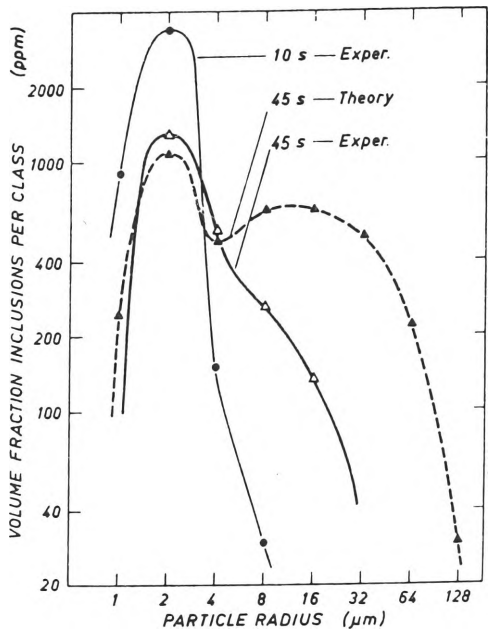

(b)

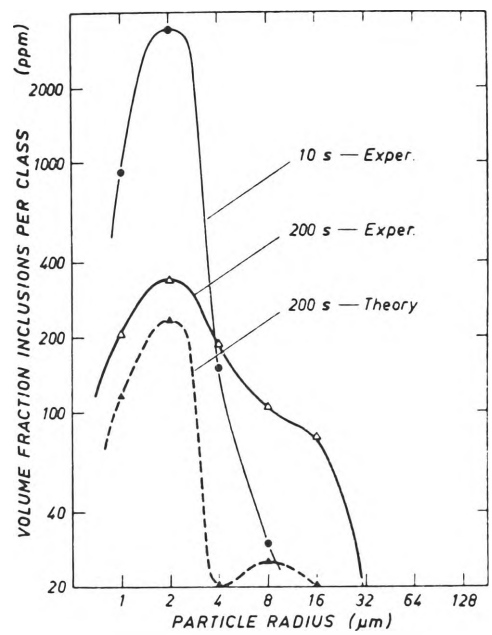

Fig. 2-9 Comparison of experimental and predicted inclusion size distributions

(a) 45 seconds and

(b) 200 seconds after deoxidant addition (73).

by collision and coalescence, considers the delaying effect caused by the inclusion's viscosity.

Mathematical treatments of inclusion growth by collision and coalescence have been derived by Lindborg and Torssell (73) and recently by Iyengar and Philbrook (68). Neither model is completely satisfactory as can be seen in Figs. 2-8 and 2-9 which show considerable deviations of the data from the expectations of the model for time greater than 30 seconds after deoxidant additions. The poor agreement of model with experimental data was explained by Iyengar and Philbrook as being a consequence of the difficulty of evaluating melt velocity profiles, while the assumption that every collision results in a coalescence made by Lindborg and Torssell is obviously an over-simplification and can lead to considerable errors.

In fact, Turkdogan (67) applied Hocking's equation for calculating the efficiency of collision between two spheres whose movement is subject to gravity and found that there was negligible probability of collision on flotation in quiescent melts. This lead him to conclude that growth by collision could only occur in turbulent melts, otherwise growth could be explained by diffusion and an uneven distribution of nucleating particles.

An unusual model of coalescence was used by Wahlster (48) to explain the formation of large inclusions during Si, Al and Ti deoxidation in very short times. The coalescence considered could be better termed sintering as local overheating in microscopically small areas was required to fuse the inclusionstogether. The high local temperatures which result from the large enthalpy of formation of the oxides provides the energy for the sintering. This mechanism was also proposed for silicon deoxidation (175). If this coalescence process occurs it obviously only lasts a few seconds in the case of high melting point oxides, but with lower melting point oxides it could possibly occur over a longer period of time.

Generally therefore, the growth of inclusions can be considered to be initially by diffusion and then by coalescence if they are liquid particles or by agglomeration followed possibly by sintering if they are solid particles.

The interpretation of the results of the many deoxidation studies reported in the literature require a dependence between the overall rate of deoxidation and either the nucleation rate and the distribution of potential nuclei or on the flotation and elimination of inclusions from the melt or ingot. The importance given to either of these view, at present seem to depend very much on personal opinion.

2.2.5 Inclusion Flotation and Separation

The flotation of inclusions in iron melts has been generally assumed to be in accordance with Stokes' Law, which is given as:

$$v = \frac{2}{9} g r^2 \frac{(\rho_{Fe} - \rho_{Ox})}{\sigma_{Fe}}$$

where v = velocity of inclusion at temperature T

g = gravitational constant

r = radius of the inclusion

ρ_{Fe} = density of liquid iron at temperature T

ρ_{Ox} = density of oxide at temperature T

σ_{Fe} = viscosity of iron at temperature T

Agreement of experimental flotation rates and those predicted by Stokes' Law have been reported for static melts (16, 19, 76, 77) while the rate of removal of silica (16, 78), alumina (16, 17, 79) and complex deoxidation products of Mn, Si and Al (16) in steel melts subjected to high frequency stirring were found to vary exponentially: i.e. of the form $C\ (\%) = C_o\ (\%) \exp(-kt)$, where t is in minutes, C_o (%) is the initial percent inclusion content (i.e. at $t = 0$) and (C%) is the percent inclusion content at time t.

This exponential rate equation was found by Kawawa and Ohkubo (16) to be operative only from about 30 seconds after deoxidation as there was a rapid flotation of inclusions immediately after the addition of Si, Al and their combined addition with Mn. The value of the separation rate constant, k, is generally larger with complex deoxidizers, especially if Mn is a constituent of the deoxidizer (80).

In another study Anderson (20) showed that the initial rate of removal of oxides was directly proportional to the amount of oxygen to be removed. Both the initial and final separation periods were again explained by the above equations, but the value of k for the initial period was found to depend on the inclusion volume to be removed.

It is important, however, not to be mislead into believing that because inclusions rise to the surface, then they must necessarily obey Stokes' Law. This law is valid for $N_{Re} < 0.1$ (22), but under steelmaking conditions $N_{Re} > 0.1$ (103). When $N_{Re} > 0.1$ the vertical motion of spherical particles can be studied by considering an intermediate region (N_{Re} 1 - 500) where the drag coefficient is approximated by $C_1 = \frac{12}{N_{Re}^{\frac{1}{2}}}$ (81).

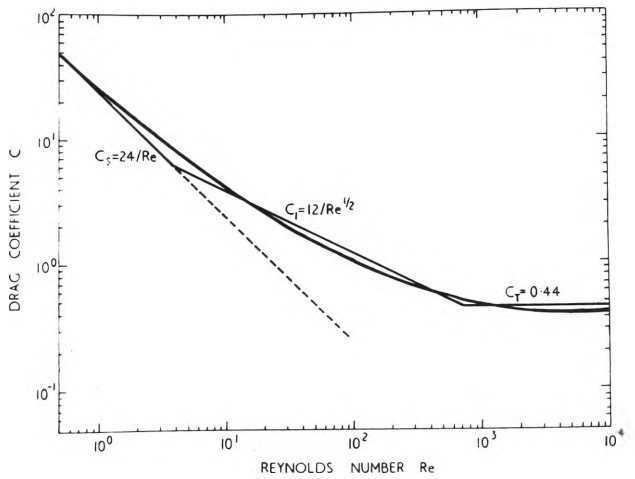

Fig. 2-10 A plot of the drag coefficient as a function of the Reynolds number for various types of fluid flow (81).

As the net force acting on a particle in a given direction is the vectorial sum of the frictional force and the external force then:

$$V_1 = k_1 \times D$$

where V_1 = the particle velocity in the intermediate region.

$$k_1 = \sqrt[3]{\frac{(\rho_{Fe} - \rho_{Ox})^2 \cdot g^2}{81 \cdot \sigma_{Fe} \cdot \rho_{Fe}}}$$

and D equals the particle diameter defined as a diameter equivalent to an Area A, (the particle area projected normal to the direction of motion) but in general depending on the definition of D used on obtaining N_{Re} for the drag coefficient vers N_{Re} plot.

For the intermediate region, the above approach would result in a better estimate of particle velocity than that of Stokes' Law. Unfortunately the latter is extended into the intermediate range and results in erroneous values as shown by the dashed line in Fig. 2-10.

Another approach to the applicability of Stokes' Law was examined by Iyengar and Philbrook (82) who used correcting functions to Stokes' Law to compensate for the deviations from the formulated conditions.

Their modified equation, however, would only be applicable to quiescent melts. If melt stirring, such as by induction or natural convection, were present the particles would be carried around in the fluid currents instead and the above approach would not apply.

From numerous observations and laboratory studies the flotation and elimination rate of inclusions from iron melts and probably other melts also have been found to result from a number of factors (16, 17, 19, 20, 21, 63, 67) viz;

1. the growth mechanism: coalescence or agglomeration
2. the number of nuclei present in the melt before deoxidation
3. the fluid flow pattern in the melt: turbulent, laminar or quiescent
4. the temperature of the melt
5. the melting point of the oxide inclusions
6. the deoxidant added: whether complex or not
7. surface properties of the melt, inclusions and the phase above the melt surface.

It has been reported by many observers (62, 72, 83, 84) that the flotation rate of alumina in molten steel or iron is faster than that of silica or silicates.

Rosegger (85), Muller and Plockinger (86) and Plockinger and Wahlster (84) all explained the difference in flotation rates by differences in the surface properties of the inclusions. Alumina has a higher interfacial tension than silica or silicates (17, 18, 35, 87) and hence was considered to be "wetted" by the steel to a lesser degree (62, 87).

Many experimental observations were said to support this correlation of flotation retardation due to inclusions "wetting" by the molten steel . Lindon and Billington (88) found that the separation rates for inclusions in a quiescent bath, increased as the interfacial tension between particles and the melt increased (i.e. Al_2O_3 SiO_2 Ca-Al-silicate), while investigations into deoxidation with complex deoxidants revealed that the separation rate of the resulting inclusions increased as the alumina content of additions increased (62, 88, 89).

A gradual decrease in the CaO : Al_2O_3 ratio of the inclusions with increasing distance from the bottom of the ingot was also reported (90) and interpreted as evidence of the greater flotability of the more aluminous inclusions. A higher flotation rate of the alumina-rich inclusions was also observed by Morgan et al (91) but they accorded importance to the retention of these particles in the slag layer.

If there is no "wetting" of the inclusion and there is "slip" between the inclusion and the iron then the maximum increase in Stokes flotation velocity would be 50% (82). This condition, however, is not approximated in alumina-iron system ($\theta > 140^{\circ}$) and so a more likely explanation for the difference in flotation rates should be sought in the different growth mechanisms of silica and alumina.

As was noted earlier alumina in stirred or turbulent flow melts agglomerate into clusters between 50 and 300 μm in size (58) and are rapidly removed from the melt, while silica particles, because of their high viscosity, are slow to coalesce and hence can have a slower flotation rate, unless liquid deoxidation products of low viscosity are formed.

The number of nuclei present after nucleation of the inclusions can also influence the rate of removal of oxygen from the melt. If the number is low, larger inclusions will form and be rapidly removed from the melt, whilst if the number is larger small particles will form and grow and hence removal from the melt will depend very much on the degree of fluid flow in the melt (67).

The influence of bath turbulence is evident in the

studies of Povolotskii et al (92) who found that in still melts small alumina inclusions ascended at a slower rate than the larger silicates, and that this effect was reversed when the melt was turbulent. The faster rate of alumina elimination compared with that of the silicates was said to be the result of absorption of the alumina by the slag and the ladle refractory walls, but the real cause is more probably a result of alumina agglomeration into clusters.

A temperature dependence of the flotation rates of silica and alumina was observed by Belyanchikov (93) and Kawawa et al (79). Their results showed the flotation of silica was greater at the lower temperatures, below 1570^{o}, while at higher temperatures there was a reversal. A possible reason for the increased flotation rate of alumina at the higher temperature is that the solubility of aluminium in steel decreases with increasing temperature (16) with the result that more inclusions would nucleate and rise to the surface.

The effects of surface phenomena occuring between inclusions, liquid metal, the atmosphere and a slag on the floating and elimination of solid inclusions have been examined by Kozakevitch et al (61, 63). The elimination of inclusions involved the formation of an

inclusion - gas or an inclusion - slag interface. This interface will always occur when the inclusion - gas or inclusion - slag interfacial tension is less than the inclusion - metal interfacial tension. This situation corresponds to contact angles greater than 90^{o}. The contact angles for some inclusions are given below (Data from Kozakevitch and Olette (63)).

Oxide	Liquid Metal	Gas	θ
Al_2O_3	Fe	Ar	141
"	Fe + 4.5%C		133
SiO_2	Fe	N_2	115
TiO_2	Fe	Vacuum	72
"	Fe	H_2	84

The higher θ for alumina ensures a greater tendency for it to remain on the surface of the melt and not be re-entrained in the fluid flow of the melt.

If deoxidation of the bath (to 0.07% oxygen) occurs the interfacial tension between oxide and the molten iron is decreased to a third of its value in pure iron (63). Also the contact angle was found to be about 80^{o}, indicating that flotation may be inhibited and reabsorbtion of the inclusion into the liquid steel likely. If a slag covered the molten metal surface, inclusions emerged from the melt and were

incorporated in the slag. The contact angle formed by the slag in contact with an inclusion was found to be always acute and if the inclusion was attacked by the slag the interfacial tension between slag and oxide (γ_{sl}) approached zero. Thus although the liquid metal - slag interfacial tension (γ_{ml}) was lower than the surface tension of the liquid metal, from the equation:

$$\Delta G = \gamma_{sl} - \gamma_{ml} - \gamma_{sm}$$

the small value of γ_{sl} was such as to ensure that ΔG was negative and the process was spontaneous.

There are of course other surface active elements besides oxygen e.g. (Group Vl of the Periodic Table) (61, 94, 96, 95) which influence the flotation and elimination of inclusions by decreasing the surface tension of iron. Sulphur is a good example of a surface active element as under these conditions the surface tension of iron drops from 1800 ergs/cm^2 to 1390 ergs/cm^2 at 1600^{o}C on the addition of 0.02% S to pure iron (74). Silicon also appears to act in a similar way, as found by Volkov et al (87). These authors showed that the surface tension of iron decreases from 1860 ergs/cm^2 to 1690 ergs/cm^2 on adding to the iron of 5.05% silicon.

SUMMARY

Nonmetallic inclusions entrapped in solid steel may originate from:

1. erosion of refractories (91, 97, 98, 99), entrapped slag (91, 97) and from alloy and deoxidant additions (100, 101) (Although Saunders et al (100) found no direct evidence relating inclusions in alloy additives to the inclusions in final steel product);
2. primary deoxidation products which are formed immediately after the addition of the deoxidizer; and
3. secondary deoxidation products which are formed during cooling and solidification.

Primary deoxidation products most probably form by heterogeneous nucleation, although nonhomogeneous dissolution of the deoxidizer may provide the supersaturation required for homogeneous nucleation.

The amount of primary products entrapped in the final ingot depends upon their rate of removal, which is influenced by turbulence in the liquid metal (72), the surface properties of the oxides, liquid metal and the slag

(61, 72, 88, 90) and nucleation and growth mechanisms. Collisions between inclusions result in their growth when they are liquid after the soluble oxygen content of the melt has been reduced to the equilibrium value with the dissolved deoxidizer.

The rate of flotation of inclusions, except in quiescent melts, does not agree with predictions from Stokes' Law, but seems to be of an exponential form. The contact angle can be used to predict successfully the tendency of inclusions to form agglomerates and to be eliminated from the melt. A slag covering can be beneficial to inclusion removal from the melt even if the inclusions are not dissolved by the slag.

The maximum amount of secondary products is determined by the residual oxygen content in equilibrium with the dissolved deoxidizer before cooling (88), but the actual amount should be less than this because some separation is likely to occur (91).

The inclusions found in ingots cannot be always clearly defined as being primary or secondary deoxidation products. The composition of the inclusions formed depends on the kinetics of the reactions, which in turn is influenced by several factors, such as the rate of mixing of the deoxidizer

(27), the number of suspended inclusions (41) and the solidification rate. The size of inclusions which are the product of deoxidation reactions proceeding during freezing, and precipitation due to the small solid solubility, varies with the rate of cooling and therefore position in the ingot (102).

3.0 NONMETALLIC INCLUSION ASSESSMENT METHODS

The first comprehensive investigation of inclusions by Benedicks and Lofquist in 1930 (102) included many methods for identifying and assessing the content of inclusions. Of these techniques; those for identifying inclusion types usually required the consideration of such physical properties of the particles as colour, shape and reflectance (103). The relative chemical inertness of the inclusions to various etchants was also an important distinguishing technique. Both of these methods employed the optical microscope as the examining instrument, using to full advantage many of its lighting variants (e.g. incident, polarized and dark field illumination).

The numerous developments in inclusion identification techniques which have occurred since 1930 have been extensively reviewed only recently (104). This major work of Konig and Ernst provides not only identification procedures but also examines the origins and chemical history of the inclusions. The techniques considered in this classic review, however, are both tedious and time consuming when compared to the speed and ease of in situ examination by the electron probe microanalyser. This

invaluable instrument has the added advantage of examining very small inclusions (105).

All existing identification methods are complemental as the encyclopaedical work of Kiessling and Lange reveals. They used optical microscopy, electron probe analysis, X-ray diffraction analysis and microhardness measurements simultaneously to provide a complete characterization of inclusions in steel.

Once inclusions were identified, the attention of both steelmaker and steeluser turned to the problem of measuring the quantity of inclusions present in a heat of steel or in the fabricated product. Out of the wranglings of maker and user the concept of steel cleanness and various means of quantifying it were evolved.

The many attempts made in numerous countries to obtain a reliable and reproducible estimate of inclusion content of steel samples have been reviewed by various investigators and committees (1, 6, 106, 107, 108, 109). Of the three basic categories of inclusion assessment methods, the one which incorporated the optical microscope has continuously had the dominant usage during the past 45 years. It is easy to understand why this is so when it is compared with other methods. The chemical methods

which involved inclusion isolation techniques were found to have a systematic bias (108, 109), resulting from the difficulty of completely isolating one phase. Moreover, as the end result of the chemical methods is a weight percent estimate of an element, these methods are obviously limited by their lack of information of the particle size distribution and dispersion.

The macroscopic methods which include such diverse procedures as ultrasonic testing, radiography, magnetic ink testing, step-turn test and radioactive tracer technique, have the great advantage of sampling a large volume of steel, thus producing a significant reduction in the sampling errors (1). The major limitation of these methods is their inability to determine inclusion compositions and, of course, they provide only a general indication of the inclusion dispersion as distinct from its size distribution.

On the other hand the many methods evolved employing the optical microscope (and to a limited extent the electron microscope) are able to determine all three basic features of inclusions in metals: namely size distribution, dispersion and content. Other important features such as shape and qualitative estimates of compostition can also be obtained and these enhance the universality of the microscopic method. The small sample size is its only

major limitation.

As the experimental work to be discussed in later sections was obtained using a microscopic method, only these methods will be discussed. Moreover, as the various microscopic methods have been extensively reviewed (6, 110-117) only those errors (both statistical and systematic) which limit the choice and area of application of the numerous optical methods will be considered. Even now, when automatic optical instruments are slowly replacing man as the assessor, the ever present unknown - human fallibility - has to be recognised, analysed and minimised.

However, before beginning such a discussion, the final aim of the assessment needs to be defined.

Inclusion content or "cleanness" as the British have parochially called it has no single definition but many. Cleanness of steel has been termed "freedom from oxide inclusions in killed steels" (89), or more generally as "the degree of absence of inclusions" (118).

Definitions have also been given in mensural terms, "in the form of direct volume fractions and numbers of intercepts for two separate inclusion phases present in the specimens" (119).

All of these definitions are essentially procedural in form and so miss an important consequence of poor cleanness, viz., its influence on the mechanical and

fabricating properties of the steel.

The observation that for some steel applications "a considerable quantity of dirt can be permitted", while for critical applications "too much dirt is undesirable, but the complete removal of inclusions from steel is impossible and unnecessary" was realized as early as 1929 (120), but it was not until 1969, that this realization was given a critical examination and some degree of quantification (5). What was needed in the interim was an increasing knowledge as to what parameters of the inclusions and their populations are important in modifying steel properties. The assessment methods available could only give a general measure such as "clean", "acceptably clean" or "unacceptably dirty" for a particular application, and in reality the final decision was based more on past experience than on any intrinsic interpretation of the value from the assessment method.

The correlation of cleanness with steel properties is even now an unresolved problem. The complexity of the relationship is exemplified by considering the ductility of structural steels. Sulphide inclusions of size greater than 0.5 μm (121) for example, significantly influence the ductility but as was shown by Kozasu (122) the final

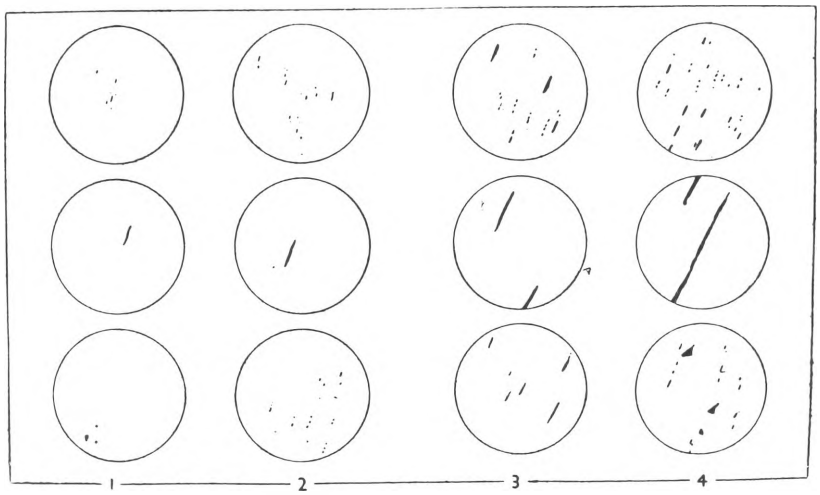

Fig. 3-1 Fox grading chart (125).

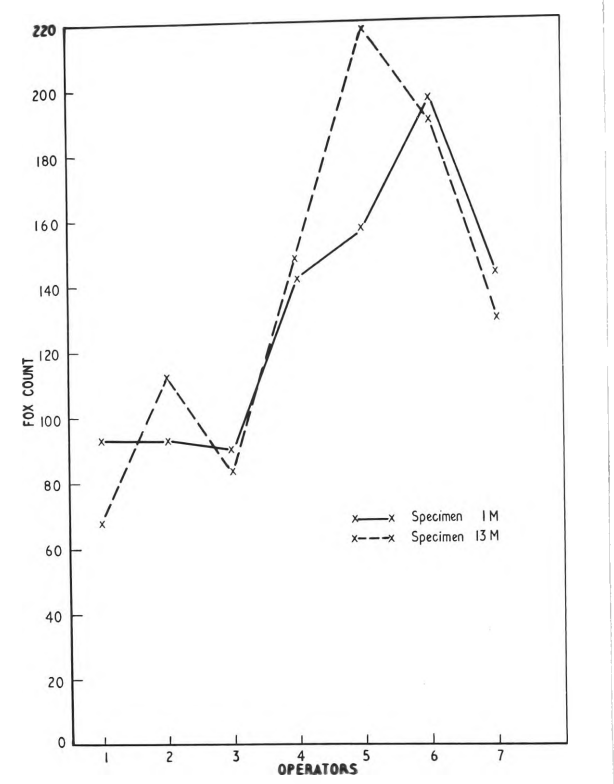

Fig. 3-2 Reproducibility of Fox count as reported by observers examining the same surface (125).

considered by Melford (111, 112) and Ridal and Cummins (113) and only a limited discussion of their respective errors is necessary.

3.1.1 Comparison Chart Methods

The poor reproducibility of the comparison chart methods needs no elaboration as this has been the overwhelming conclusion of many studies, (114, 115, 117, 124). This is perhaps unexpected when the simplicity of the Fox and JK counts is considered. The considerable between operator variability of the Fox count, as exhibited in Fig. 3-1, has been explained by the limited number of standard fields available (see Fig. 3-2(125)). The observer therefore has to guess when the sample field examined cannot be matched to a standard field (114). It is not surprising then that a variation between observers of more than 50% of the total assessment range can result as is shown in Fig. 3-2.

As the Fox method assesses only the total inclusion content, when a provision was made to assess separately different inclusion types (as in the JK method) yet another source of uncertainty was introduced and the final assessment value was considerably in error. The poor

agreement between observers, using the JK method as to the relative proportion of oxides and sulphids was found to contribute 50 to 60% to the total error (117). The causes of this large error were considered to be the tedium of the method which had increased as the complexity of the method increased as well as observer fatigue and pre-knowledge (115, 117, 124).

In their recommendations for the use of both JK and Fox counts, Blank and Allmand (117) considered that the value obtained as the average of single counts by a number of different observers would be a more reliable estimate than the average of the same number of counts made by one observer. There is a subtle fallacy in this conclusion for even the average value from the counts of a number of different observers cannot be regarded as an estimate of the "true" inclusion content (126). Therefore, whilst the average of one observer's counts will always give a biased estimate, for practical applications this will not be of much significance. This is because experience gained from numerous assessments, tempered by the knowledge of the subsequent performance of the material, will in most instances have a regulating influence on the interpretation of the significance of the assessment result. Thus, although these chart methods were an important means of quality

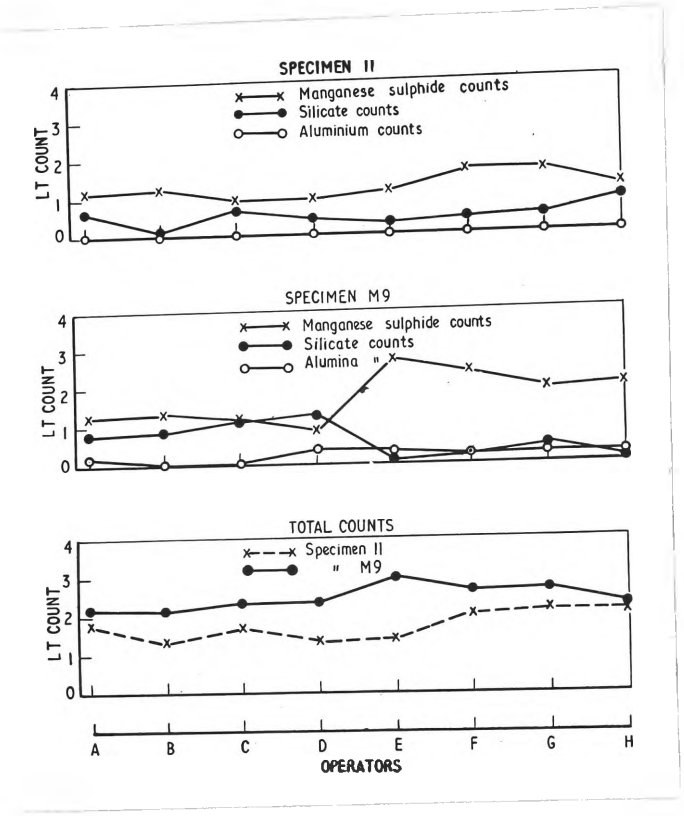

Fig. 3-3 Reproducibility of LT count as reported by different observers examining the same surface (123).

(b)

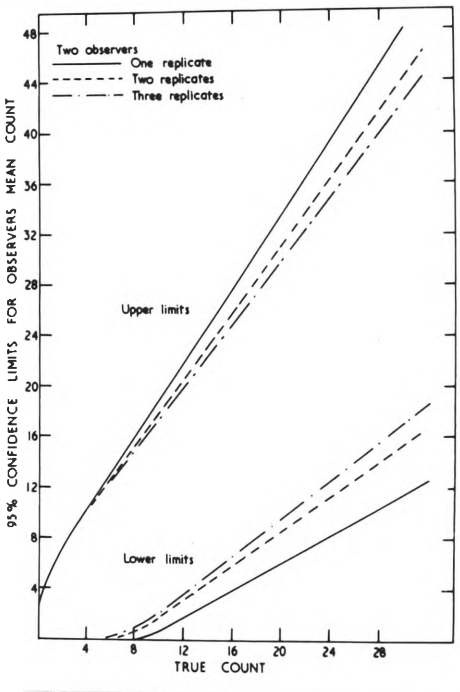
Two observers
One replicate
Two replicates
Three replicates
Upper limits
Lower limits
95% CONFIDENCE LIMITS FOR OBSERVERS MEAN COUNT
TRUE COUNT
4
8
12
16
20
24
28
32
36
40
44
48

(a)

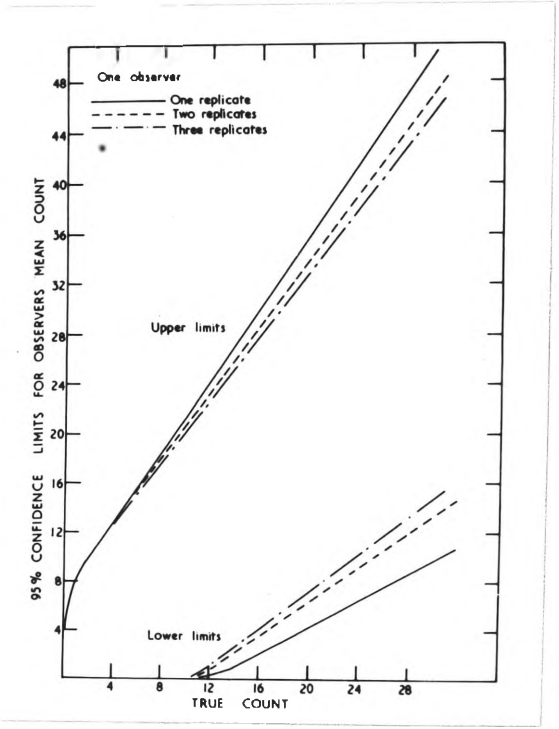
One observer
One replicate
Two replicates
Three replicates
Upper limits
Lower limits
95% CONFIDENCE LIMITS FOR OBSERVERS MEAN COUNT
TRUE COUNT
4
8
12
16
20
24
28
32
36
40
44
48

(c)

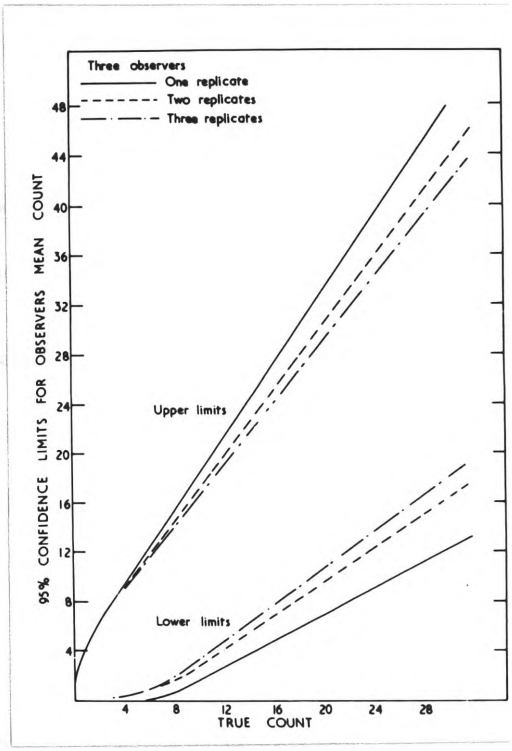

Fig. 3-4 Effect of total inclusion content on the accuracy of the LT count determined by:

(a) A single observer,

(b) Two observers, and

(c) Three observers

For MnS inclusions (117).

control for both steel maker and user, they are at best only an indication of gross differences in inclusion content. It is not surprising therefore, that a method giving a more precise measure of inclusion content was continually sought, particularly as specification requirements and fabricating and service conditions became more difficult to meet.

3.1.2 Direct Assessment Methods

A spate of quantitative and semi-quantitative methods were developed in the 1930's and 1940's (110) to assess inclusion contents of steels produced for specialised applications. These methods were generally extremely time consuming and so only a small number of samples could be examined. Consequently, the statistical accuracy of these methods was poor (110).

The lineal-traverse method developed by Hardy and Allsop (115) can be considered a "coup de grace". It was both simple to perform and had good reproducibility when the total number of inclusions was counted (see Fig. 3-3) (127). Like the comparison chart methods, however, the reproducibility between observers deteriorated when separate counts for various inclusion types were required (115, 127). Once again, as revealed in Fig. 3-4, Blank

(a)

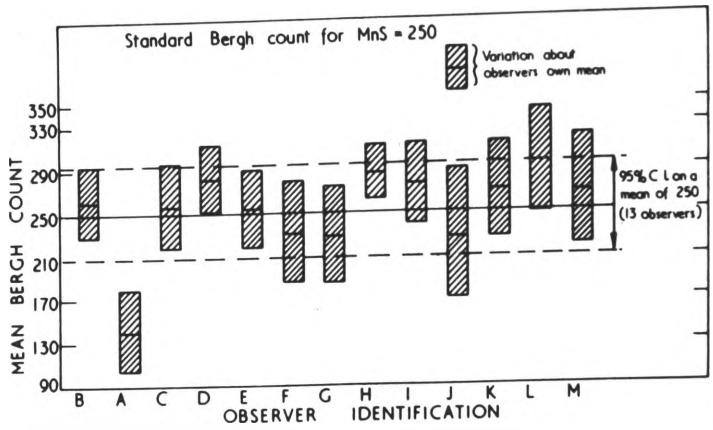

(b)

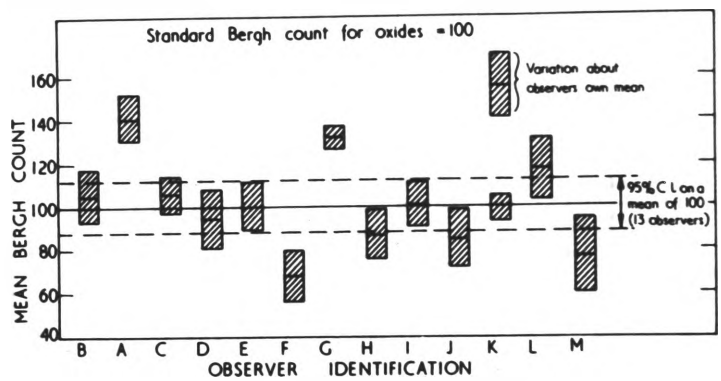

Fig. 3-5 Errors within and between observers due to variation in Bergh field assessment for

(a) MnS, and

(b) Oxides (117)

and Allmand (117) found greater accuracy was obtained (i.e. a narrower 95% C.L. band about the observers' mean) by a number of observers each counting the sample once than one observer counting the same number of replicates. The average value of the assessments of a number of observers, in this instance, could be considered a reasonable approximation to the actual number of inclusions present in the sample.

Another direct count method, which like the LT count has received considerable application, is the point count. In this method the observer estimates the volume fraction of the phase of interest by counting the number of points on a grid which appear to fall within the boundaries of the phase. The ratio of this value to the total number of grid test points provides an estimate of the area fraction of the inclusion sections present and hence, by Delesse's therem (128) is an estimate of the volume fraction of inclusions.

Even this simple procedure, when used to determine the volume fractions of various inclusion types has also been found to have poor between-observer reproducibility (117) as can be seen from the results of the Bergh count in Fig. 3-5.

Human fallability, however, is not the sole cause of the variations between observers seen in Fig. 3-5. The limited resolution of the optical microscope produces a systematic 10%

error in the volume fraction estimate, (129). This error in itself would only result in overall shift in the results of all observers, except that with small sized particles there is a greater probability of grid points being "observed" to fall on the particle's perimeter. Convention (130) decrees that this situation be assessed as a half to indicate the uncertainty of the observer. Therefore even in this seemingly objective method a judgement is required from the observer as to whether a grid point "appears" to be on a particle's perimeter or not. So once again a possible source of poor reproducibility between observers exists and the extent of the disagreement would increase the poorer the resolution of the microscope or the smaller the size of the particles.

The unsatisfactory reproducibility between observers using the LT method may also be explained by the limited resolution of the optical microscope used in the count. Some observers neglected to count very small inclusions (127), while variations in the reproducibility of the LT method from sample to sample were suggested to be a consequence of the varying distributions of small inclusions. The more probable cause for both these results, however, may be the difficulty experienced by observers in counting inclusions of size close to the resolution limit.

3.1.3 Automatic Cleanness Assessment

In recent years automatic instruments capable of carrying out quantitative metallographic assessments have been developed.

These instruments can assess a large number of samples in a relatively short time. Such a feature is of considerable importance as is indicated in the work of Mihaljev and Mironov (131). They found it was necessary to examine at least 100 samples from each cast before it was possible, with 95% confidence, to differentiate between casts of high and low inclusion contents. There is therefore a very great need for these instruments for use in industrial quality control, especially as the assessment results obtained are seemingly subject to little human error.

The earliest automatic counter used for inclusion studies was probably the Coulter counter (132). Although reliable results were obtained with this instrument (133, 134), problems with sample preparation and the inability of the instrument to separately assess oxides or sulphides or to assess the size of non-spherical

particles severely restricted its widespread use.

The automatic instruments which have lead the revolution in inclusion assessment practice have been those based on the optical microscope. The many instruments of this type and of those based on the principle of the electron microscope have been extensively discussed and tested (112, 113, 119, 135, 136), but only one has emerged, the Quantimet B, as the leader in this field. It is also a good representative of the optical automatic instruments. The Quantimet B (QTM) combines an optical microscope and a T.V. camera - the measurements being obtained electronically from the scanning electron beam. The optical part of the instrument of course, contributes its own inherent sources of error, whilst the electronic system introduces many others. The principal sources of errors which can arise may be summarised as follows: (137-143):

1. Non uniform detection throughout the blank frame,
2. errors in maintaining focus,
3. difficulties in setting the threshold,
4. sizing of inclusions when these are either small or elongated,
5. resolution of small inclusions,
6. separate detection of sulphides and oxides within the one field of view, and
7. orientation of inclusions in hot rolled product.

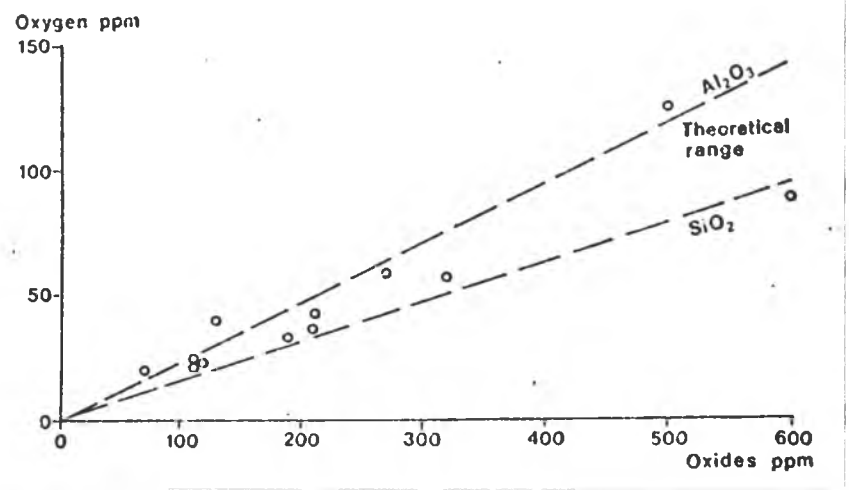
Oxygen ppm
150
100
50
0
0
100
200
300
400
500
600
Oxides ppm
Al_2O_3
Theoretical range
SiO_2

(a)

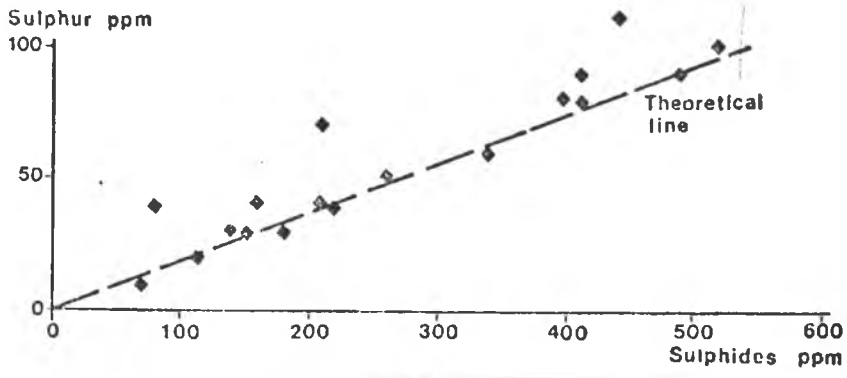
Sulphur ppm
100
50
0
0
100
200
300
400
500
600
Sulphides ppm
Theoretical line

(b)

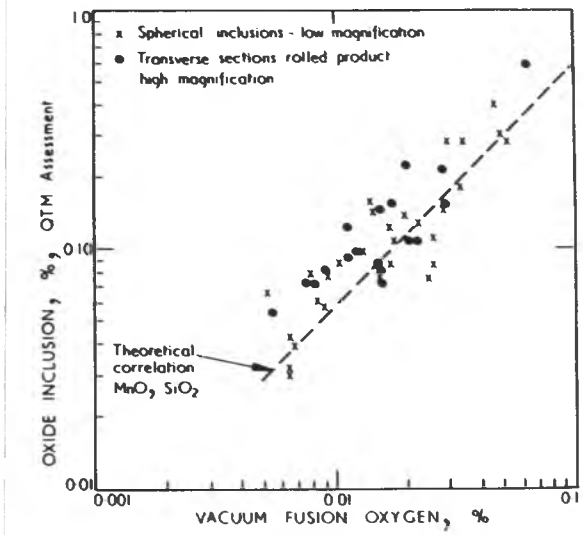

(c)

Fig. 3-6 Comparison of Q.T.M. inclusion assessment with chemical analysis:
(a) and (b) (138)
(c) (137)

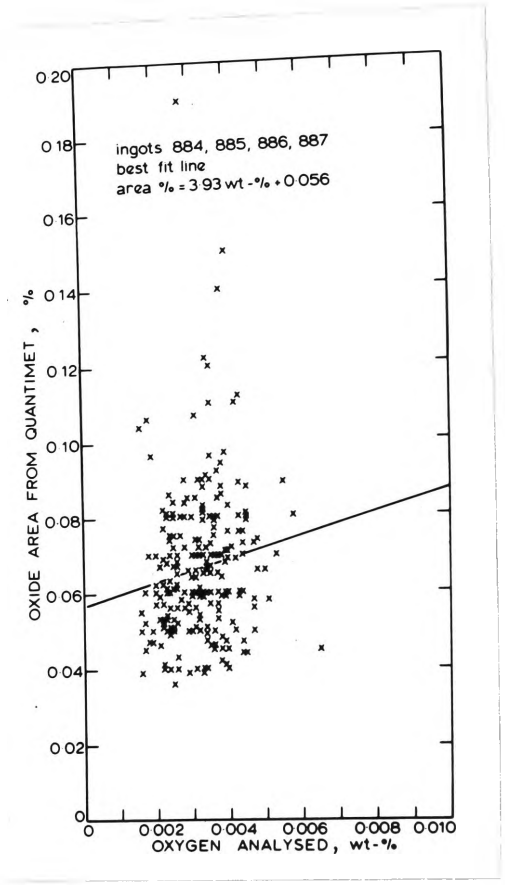

Fig. 3-7 Comparison of QTM area assessment with chemical analysis for oxides (and MnS) for 4 ingots of aluminium deoxidised steel (139).

The calibrations of volume fraction estimates of inclusions determined by the QTM with oxygen or sulphur contents obtained by chemical analysis were extremely good in many instances (as is given in Fig. 3-6), especially if all the possible sources of error are considered. For instance, each method examines different size samples, consequently there is a good possibility of errors from micro-segregation of inclusions. Also if both methods are to be compared using the same measure - volume fraction - then there is a need to assume a fixed chemical formula to calculate the volume fraction from the wt% value (137, 138).

The poor agreement obtained by Franklin (139) for alumina particles (see Fig. 3-7) was an exception and reveals the QTM's two major sources of error - threshold setting and resolution. The small size of the alumina particles, close to the resolution limit of the optics and the obtaining of a biased value (because a portion of the sulphides were included in the assessment) lead Franklin to conclude that alumina should not be assessed by the QTM. This conclusion is however too severe, as a corrective procedure developed by the Jernkontoret Committee (138) will allow some degree of statistical separation of oxide and sulphide counts, but the resolution problem still remains

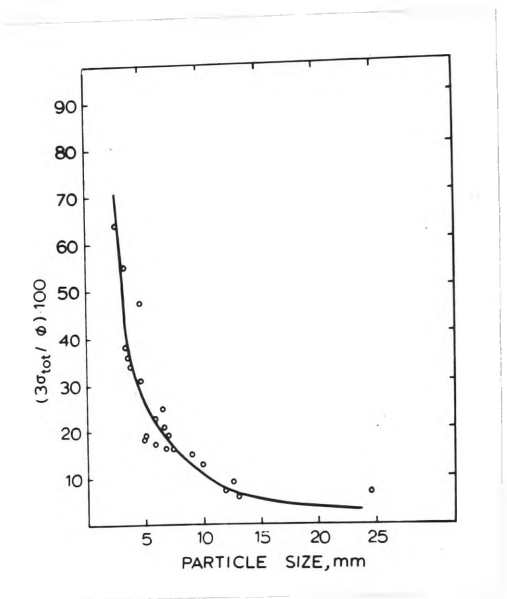

Fig. 3-8 Uncertainty in determination of particle size (138).

as Fig. 3-8 indicates.

A further example which explicitly shows the importance of having an accurate and reproducible method of setting the threshold is the comparison of the methods of Johansson (138) and Allmand and Coleman (140). Johansson obtained the "correct" setting when the light and dark coronas that surround the particle were of equal width, while Allmand and Coleman employed standard specimens of known size and area and so the threshold was adjusted until the instrument read the known area. The former method resulted in coefficients of variations between operators of approximately 15% and the latter only 2-4%. Thus it is again evident that if human judgement is involved in the technique (as it is in judging equal widths of coronas) human variability produces lower reproducibility. Furthermore, it has been shown (141) that if operators use their own methods and not a common one, coefficients of variation as high as 57% can result.

The errors arising from resolution and the threshold setting can be either overcome or at least minimised, but there is yet another source of error which considerably limits the assessment of rolled product by the QTM. When the shape of the inclusions is of an elongated form (as are sulphides and silicates in hot rolled steel plate) multiple

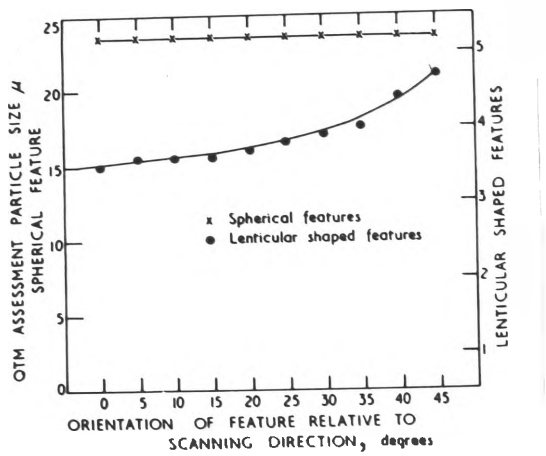

Fig. 3-9 The effect of particle shape and orientation on the accuracy of the sizing operation (137).

counting can occur if there are re-entrant angles in the deformed inclusion shape. The influence of both shape and orientation on the sizing operation are clearly shown in Fig. 3-9. It can be concluded from this graph that generally the greater the length to width ratio of the particle the greater will be the error. Adjustments to compensate for these errors can be made but they inevitably involve a compromise. In fact, the sizing of stringer inclusions can be so much in error (142) that recourse to manual methods is often necessary.

3.2 REPRESENTATIVE SAMPLING

Representative sampling of a heat of steel, an ingot, a plate, a billet or even a single "micro" specimen is still a major problem. The large number of samples required or the large sample area needed for the examination to give a value representative of the bulk material is exemplified by the work of Vero (144). Although he was able to decrease by 10% the number of piston pins rejected by examining 1200 cm^2 of sample surface in the step-turn test, he could not obtain a significant correlation between the total length of inclusions detected and the rejects per cast. How successful then is the common practice of examining 6 to 20

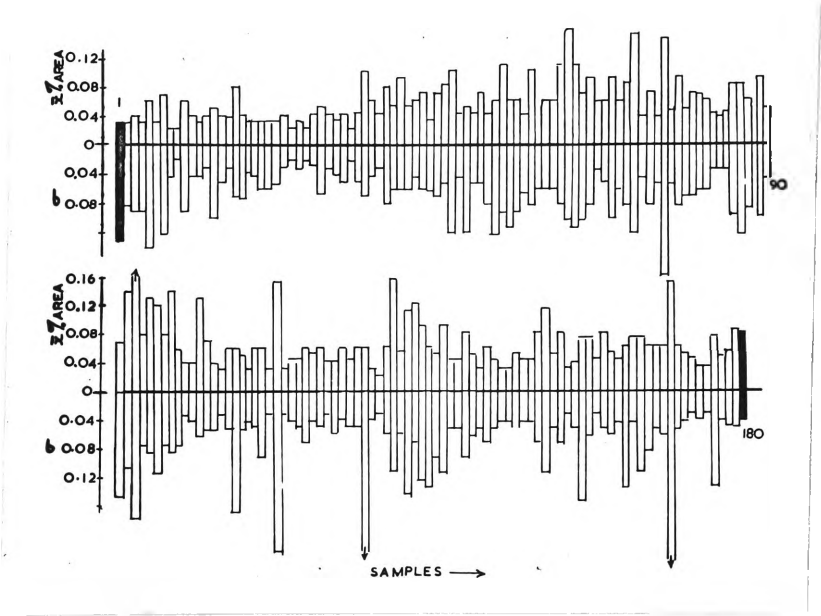

Fig. 3-10 Variation between determinations of mean percent area oxide inclusions (145).

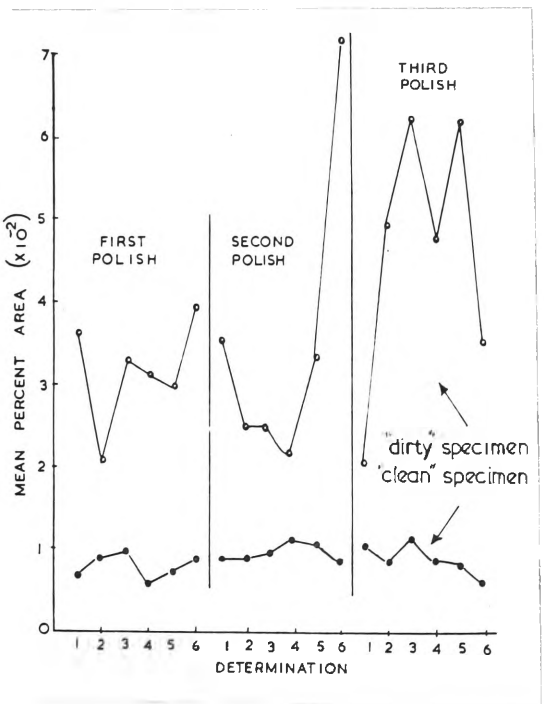

Fig. 3-11 Effect of repolishing the specimen on the mean area percent oxide estimate (145).

samples which results in an examined area of only 2 to 6 cm^2? And how representative is 6 cm^2 of a heat of steel? Yet the whole procedure of quantitative assessment of inclusions depends on a small sample being representative of the bulk.

These questions have been investigated by Allmand and Coleman (145) who considered the sampling of a single specimen and also that of a 14 to 15 foot long billet; the QTM B was employed in the assessments. It was found that the common practice of selecting 100 fields from one micro was inaccurate, as is shown in Fig. 3-10, and so they recommended the examination of at least 400 fields from four different polished surfaces.

Another source of error, which has been reported many times in the literature (114, 138, 146) is the large variations in inclusion assessments which can occur on re-examinations of the same sample after successive repolishes. Figure 3-11 from the work of Allmand and Coleman (145) shows how variable the results can be. Such a variation is not peculiar to any one assessment method but appears to be an orientation effect produced by the hot deformation process (129).

The practice of estimating the inclusion content of long billets from a single micro specimen obtained from the

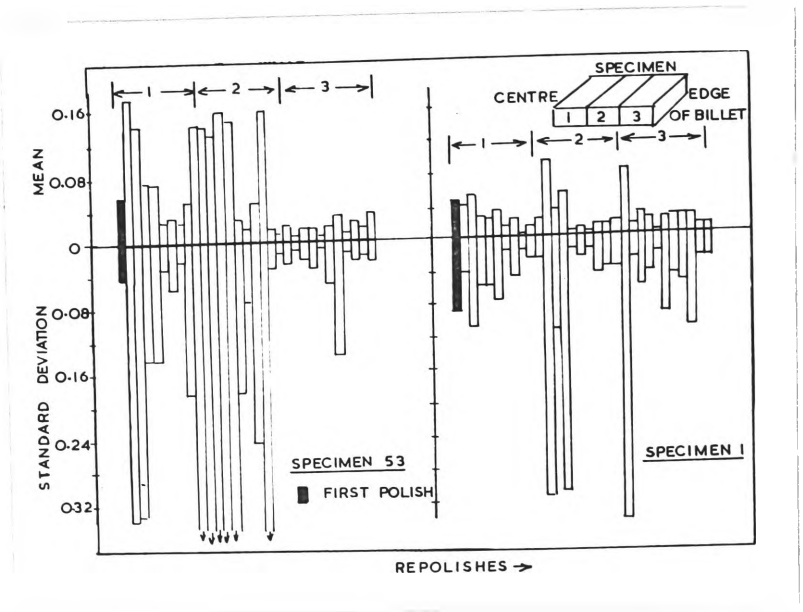

Fig. 3-12 Sampling error resulting from a single sample taken from a 14 foot long billet (145).

end of the billet can also result in large errors as can be observed in Fig. 3-12. Clearly there is a large variation between estimates and so Allman and Coleman (145) recommended an examination procedure involving at least 10 specimens per billet in order to obtain a statistically significant estimate.

It would appear from the sampling problems that if only an estimate of the volume fraction of oxides or sulphides is required a more reliable method for obtaining this would be the chemical analysis for oxygen or sulphur content. Then from the average composition of the inclusions (determined by EPMA) the respective volume fractions could be calculated (147).

SUMMARY

It is evident from the foregoing discussion that irrespective of whether a size or volume fraction estimate is required, the result will always be biased by the limited resolution of the microscope used and by the systematic and statistical errors inherent in the assessment procedure. The former error can only be minimised by employing instruments of greater resolving power, which in practice is not always possible. The latter errors may be reduced by

strictly defining the criteria required to include the inclusion in the count or sizing operation. But while these criteria are sloppily defined or slothfully adhered to, the assessments obtained will be measures of the variability of personal judgements rather than variations in inclusion contents.

Although the introduction of the automatic assessment instruments was hailed as the means whereby large numbers of samples could be examined to obtain representative estimates, the instruments brought with them new limitations and errors, many of which are as frustrating to the metallographer as those derived from manual procedures.

The assessment methods were born of the need to quantify the inclusion content of steel and so were in general estimates of the volume fraction, but now a new need has arisen as a consequence of the impracticable nature of producing completely clean steels. Steelmakers are gradually realising that it is more profitable to adjust the size, type and dispersion of inclusions than to completely remove them. No longer should it be necessary to unreservedly "legislate" (148) against inclusions, instead inclusions should be modified to suit the service required of the steel. To this end greater knowledge is

required as to how to ascertain accurately the size and shape distributions of inclusions in steel.

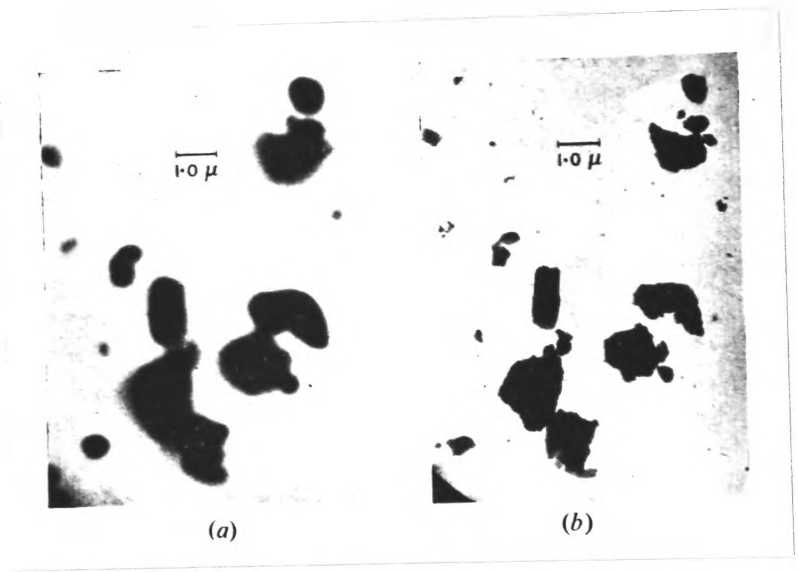

Fig. 4-1 Comparison of resolution of small (0.25 μm) particles by:
(a) Optical microscope (2mm oil immersion objective), and
(b) Electron microscope (151).

4.0 DEFINITION OF TERMS IN INCLUSION ASSESSMENT

The determination of the inclusion size distribution from a plane section is not an absolute process but one of estimation (149). The degree to which the estimate approaches the actual distribution depends to some extent on the physical principles employed and the assumptions and conventions involved. To prevent confusion such assumptions and conventions have to be set out and the terms defined. Hence definitions and procedures used in the inclusion assessment studies will now be considered.

4.1 PARTICLE (INCLUSION)

The American Society for Testing of Materials define a particle (150) as "the smallest discrete unit or a unit of matter whose size and shape depends on the forces of cohesion". For inclusion assessment, an individual inclusion can be either single-phase or multi-phase , and can be deemed an individual particle if within the resolution of the microscope it appears as one unit. Close to the resolution limit an individual inclusion so defined may in fact be resolvable into two or more (say) with the use of the electron microscope, see (Fig. 4-1) (151).

Irani and Callis (152) defined an ultimate particle of a substance as "the smallest state of subdivision which retains all the physical and chemical properties of that substance". In investigations of inclusion distributions in a silicon killed ingot using the electron microscope Bergh (135) could not detect inclusions smaller than 300-400Å, even though the resolution limit of the microscope was about 100Å. Therefore, if the replicating procedure used by Bergh was successful and as the critical nucleus size of silica is of the order of 10Å (19) it can be concluded that the ultimate inclusion size is very much dependent on the nucleation and growth conditions of the inclusions.

For optical microscope assessments the smallest inclusion size is determined by the resolution limit of the optical and illumination system. This artificial, lower size limit is between 0.2μm (150, 153) and 0.5μm (149, 152) using oil immersion objectives.

4.2 PARTICLE (INCLUSION) SIZE AND SHAPE

The size of a particle should be used in an unambiguous way. As the measurement of particle size, excepting spherical particles, is hardly ever an absolute process (149)

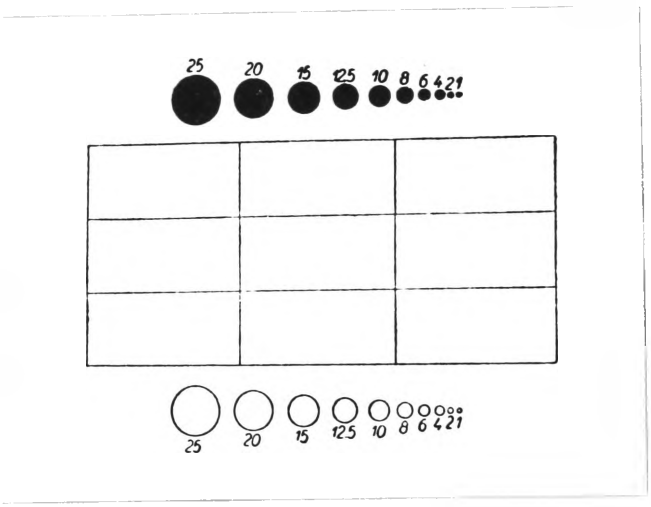

Fig. 4-2 Enlarged photograph of the Patterson-Cawood circular comparison graticules (149).

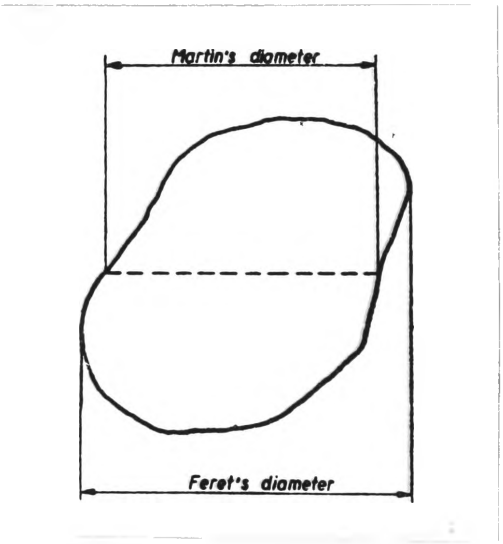

Fig. 4-3 Schematic sketch showing the measurements of Martin's and Feret's diameters (149).

but depends very much on the sizing technique used, a certain convention is required as to what will be regarded as the "size" of the particles.

A common method of representing the particle size is by the area of a circle having the same area as the observed section. Exact matching of the areas is not necessary as the particle sections would be grouped into various size intervals and only those with areas equivalent to the class boundaries will be subject to misclassification errors (154). The procedure is sufficiently accurate when the image of the particle is compared with calibrated circles on an eyepiece graticule (Fig. 4-2). Another technique is to estimate the statistical diameter according to methods devised by Martin and Ferret (Fig. 4-3) (149, 153).

Heywood (155) tested the various particle size methods and found that the "globe and circle" averages were within 5% of the actual diameters as the particle shape became more elongated (156).

The use of a circle for estimating the particle size is only a mathematical convention and so is seemingly no more advantageous than any other geometric shape when estimating either diameters or areas. Its real advantage comes when predictions of the distribution in the bulk material are

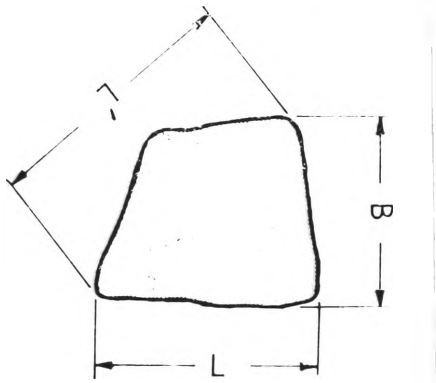

Fig. 4-4 Schematic presentation of the sizing of a particle according to Heywood (153).

required from the section distribution observed on the section plane. Other geometric shapes have also been used, as for example the use of ellipses to size non-spherical particles (157).

Another method for determining the size of the particle is that due to Heywood (153), who defined a particle's length and breadth as (Fig. 4-4.)

1. Breadth (B) - the maximum distance between two parallel lines tangent to the profile of the particle, and
2. Length (L) - the maximum distance between two parallel lines tangent to the outline and perpendicular to the lines defining the breadth.

The mean projected diameter can be determined from these measurements by the formula (153):

$$dp = \sqrt{\frac{4}{\pi} \phi . B . L} \qquad (4\text{-}1)$$

where ϕ is equal to 0.75 for angular particles and 0.77 for rounded particles.

According to the principle of geometrical similarity, particles whose two-dimensional images are of the same magnitude are also of the one size (153). That is, if the

particles have the same dp or BL then these particles can be grouped into the same class interval.

The accuracy of determining particle size was considered by Franklin (148). He concluded that the size of an inclusion which has an apparant diameter of 2R, i.e. twice the resolution of the optical system, will be underestimated by about one seventh and so its true diameter will be 2.3R. The apparent area of such an inclusion is three quarters that of the true area. For larger inclusions, however, the difference between the apparent area which is observed and the true area will be less; the difference decreasing as the inclusion area increases.

In inclusion assessment work the size of a particle may be defined in a direct manner or indirect manner, depending on the purpose of the assessment. The inclusions' size is defined in a direct manner if the purpose of the assessment is to provide a measurement which has a definite physical meaning or can be directly related to a physical measure of the size of the particle. Examples of such measurements are the diameter or area of circular sections throughspherical particles, or elliptical diameters, or areas of sections through ellipsoids. On the other hand the size may be defined indirectly if the purpose of the assessment is to

provide a measurement which is both quick and easy to make and requires little or no judgement on the part of the investigator. These measurements will, however, have only an indirect relationship to the size of the particle or perhaps only to some average, gross property of the particle distribution. Examples of such measurements are intercept chord, Martin and Feret's diameters and the mean intercept length.

The various statistical methods available for determining size distributions, recently reviewed by Underwood (158), have employed the sphere as the basic model. Other regular shapes such as ellipsoids have been treated under the spherical model with correcting shape factors (159), while cubes (160), triangular prisms (161) and lamellar structures (162) have received little attention due to their greater complexity of analysis compared with that of the spherical model. Use of equivalent sphere distributions to represent irregular shaped particle distributions have been proposed (163) and some success has been achieved (164). However, it should also be realised that if the particles have highly anisotropic shapes, their size distributions will differ considerably from that of the equivalent sphere distribution (161); e.g. ellipsoids with eccentricities greater than about 0.7 could not be

approximated by the spherical model (165).

A better shape model to the spherical one, therefore, would be one which can achieve reasonable approximations for elongated shapes. Such a model is one based on the general ellipsoid. With this model, of course, the sphere is a special case. Ideally then, the sections through particles would be ellipses and their size could be defined as either the geometric mean of the major and minor axes or as one or other of the axes if the particles are ellipsoids of revolution.

However, inclusion sections will not generally be ellipses but the measurements can still be made with the ellipsoidal model in mind. If the particle is assumed to be a general ellipsoid, then its particle size, can be defined as the geometric mean of the length of a line intercept which is the largest distance between two parallel tangents to the particle section and also the largest intercept between parallel tangents to the section normal to the first measurement. If the particle shape is assumed to be an ellipsoid of revolution then only one of the above measurements will be needed.

The ellipsoidal shape model was employed in the investigations discussed in Section 7 and so further discussion of it here is not necessary.

4.3 SECTION AND SPATIAL DISTRIBUTIONS

Most quantitative metallography using the optical microscope involves interpretation of a three dimensional opaque structure from various two dimensional sections through the structure. For particle size analysis one of the major problems is the determination of the relationship between the size of the particle sections seen on the two dimensional section plane and the actual size of the particles.

The distribution of particle sections on the section plane through the sample will be termed the "section distribution". This is the distribution which is assessed during the inclusion count. The distribution of particles in bulk of the sample will be termed the "spatial distribution". This is the distribution which is important with regard to any effect inclusions may have on the physical properties of the bulk material and is the distribution which is estimated from the section distribution.

5.0 EXPERIMENTAL

The ingots studied in this investigation can be divided into three groups:

1. Series 1 ingots which were preliminary copper ingots produced in a muffle furnace
2. Series 2 ingots which included both copper and iron ingots and were produced in a vacuum induction furnace
3. Series 3 ingot a copper ingot produced in an argon shielded muffle furnace

5.1 Ingot Production Apparatus

5.1.1 A Heraeus Vacuum Induction Furnace was used for the production of the majority of Series 2 ingots. The pumping equipment to evacuate the furnace consisted of a forepump (D.K.45) of pumping capacity 45 l/hr., and an oil diffusion pump(D1200) of pumping capacity 1200 l/sec.

Bourdon type vacuum gauge was used to measure the tank pressure in the range 760mm to 10mm Hg. The fore-vacuum between forepump and diffusion pump and the chamber pressure were measured by one gauge head, each on a Thermistor vacuum

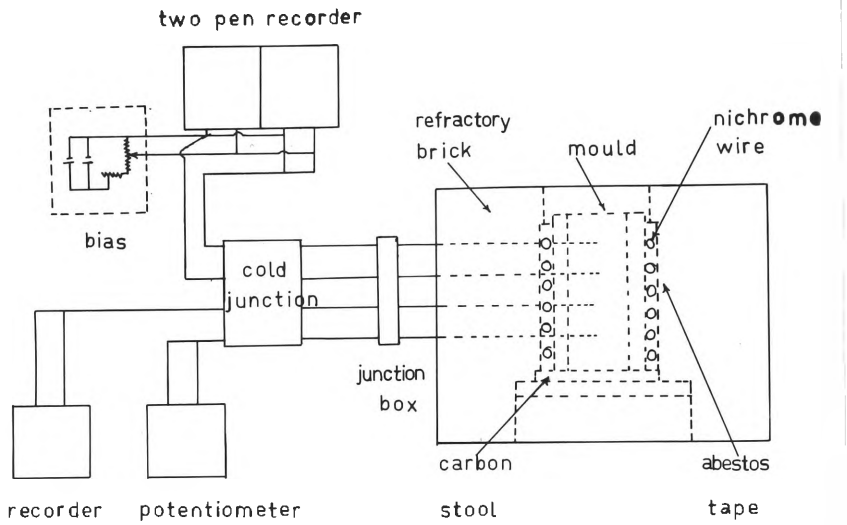

Fig 5-1 Experimental apparatus for Series 1 heats.

gauge (VMT - 3). A cold cathode vacuum gauge (VMP - 2) measured the high vacuum levels in the chamber in the range 10^{-3} to 10^{-6} mmHg.

5.1.2 A National Gas Fired Muffle Furnace was employed for some of the preliminary Series 1 copper melts, but control of oxidation, and deoxidation of the melt proved difficult. Hence most of the experimental copper melts (with the exception of ingot No. 30) were conducted in the Heraeus furnace, as a closer control could be maintained on the furnace atmosphere, the melt temperature and deoxidizer additions and recoveries. All the iron melts were conducted in the Heraeus furnace.

A melt (Series 3) was conducted in Morganite Mullite Crucible in the muffle furnace under an argon atmosphere. The apparatus for these melts are shown in Fig. (5-1). Ease and speed of sampling were the reasons for using this furnace in preference to the induction furnace.

5.1.3 The crucibles generally used in the Heraeus furnace were of two types, firstly of preformed zirconia with an approximate composition: 60% ZrO_2 and 40% SiO_2: and secondly of rammed fused magnesia with a composition as given in Table 5-1.

TABLE 5-1 COMPOSITION OF FUSED MAGNESIA (wt%)

MgO	SiO_2	Fe_2O_3	CaO	Na_2O	Al_2O_3	B_2O_3	TiO_2
96.31	2.00	0.10	1.50	0.01	0.07	0.00	0.00

The magnesia crucible was constructed by sintering rammed fused magnesia at 5KW for 5 minutes, 10KW for 10 minutes and 18KW for 30 minutes. The diameter of the crucible was approximately 10cm and the height was approximately 15cm.

The crucibles used for melting the charge material in the muffle furnace were salamander, zirconia or morganite mullite crucibles.

5.1.4 The thermocouple used to measure melt temperatures in the Heraeus furnace was a Pt - 20% Rh/Pt - 5% Rh in either silica or Morgan (grade 514) metamic sheaths. The silica sheaths were employed for the copper melts. The potential was measured by a Leeds and Northrop potentiometer.

For some melts, however, because of malfunctioning of the thermocouple it was necessary to use a Foster optical pyrometer.

A Pt 13% Rh - Pt thermocouple in a silica sheath was used in the series 3 melt in the muffle furnace. The thermocouple was calibrated using a standard couple at A.I.&S. The calibration results are given in Table 5-2.

5.1.5 The thermal analysis investigation of the solidification rate for copper ingots in both carbon and

TABLE 5-2 CALIBRATION OF Pt 13% Rh-Pt THERMOCOUPLE

Standard		Test Thermocouple		Difference	Comments
mV	°C	mV	°C	°C	
3.845	442.7	3.839	442.1	0.6	Tested at beginning of Series 3 melts
4.385	493.50	4.373	492.36	1.14	Tested at end of Series 3 melts

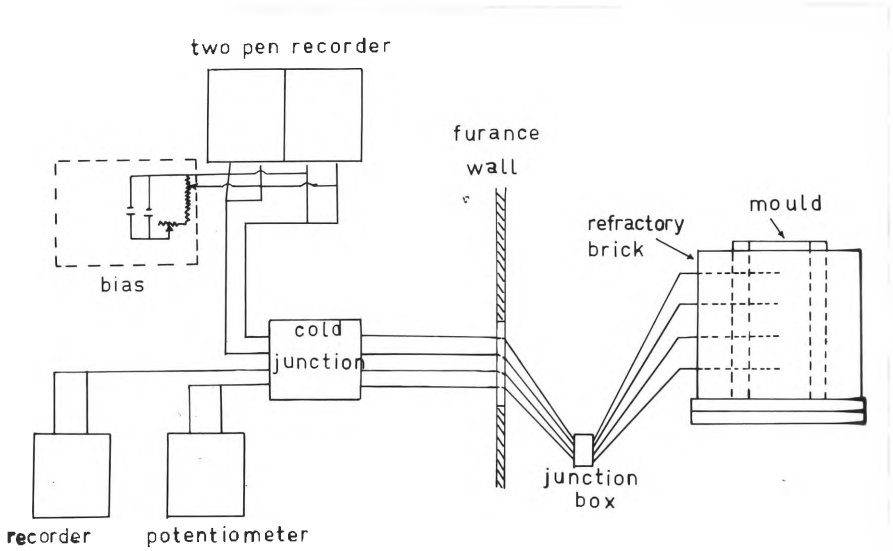

Fig. 5-2 Experimental apparatus for Series 2 heats.

cast iron moulds were investigated with the use of a two pen Texas "servo/ritter" recorder and a single pen Leeds and Northrop Speedomax H recorder. For series 3 melt a two pen Unicorder was used.

Four chromel-alumel thermocouples were positioned in the ingot mould as indicated in Fig. 5-1, calibration results for this batch are given in Table (5-3). When conducting the thermal analysis in the Heraeus furnace the thermocouple leads from the junction box then passed through a plate in the furnace wall to the recorders. A schematic diagram of the thermal analysis system used in the Heraeus furnace under vacuum is given in Fig. 5-2, while Fig. 5-1 gives the system when the melts were conducted in the gas fired furnace.

Silica sheaths covered the thermocouple wires in the vicinity of the mould, while the bead was coated with a thin layer of alumina cement.

Both recorders were biased to measure only a narrow temperature range about the melting point of copper. The value of the bias potential was progressively decreased during the solidification. The Speedomax H had an inbuilt bias, while a standard cell was required for the Texas recorder.

TABLE 5-3 CALIBRATION OF CHROMEL-ALUMEL THERMOCOUPLE

Standard		Test Thermocouple		Difference
mV	°C	mV	°C	°C
3.820	440.3	18.14	441.3	1.0

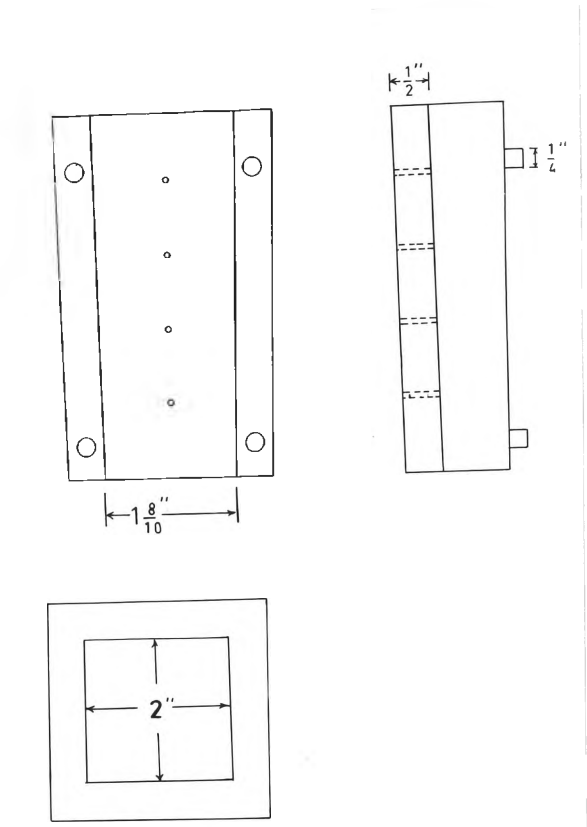

Fig. 5-3 Dimensions of cast iron mould.

A two way switch was initially employed with the Texas recorder, and switching was conducted manually every 10 seconds. However, a combination of rapid solidification rates and the necessity to continually alter the bias, because of the recorder's narrow span of 3mV, prevented a successful thermal analysis being obtained with this system. It was only at a later stage, when ingot No. 32 was produced, that an attenuator was obtained which enabled the span to be expanded to cover the required range and hence the standard cell was deleted from the circuit. This modification is, of course, accompanied by a loss of accuracy in determination of the temperature differences. Also in heat 32 the switch was deleted from the circuit and the thermocouple leads were connected direct to the recorders. The Unicorder was biased with two mercury batteries, allowing a one or two mV full span to be used.

5.1.6 The mould used in many of the preliminary melts was a round carbon mould, but for the majority of the heats a cast iron mould was employed. The dimensions of the moulds are given in Fig. 5-3.

Heats 1 to 3 involved no mould heating, however, with heats 4 to 9 the carbon mould was heated by wrapping

nichrome wire, firstly as the plain wire then secondly as the coiled wire to increase the resistance of the system. Insulation between the wire and the carbon mould was achieved by covering the outside of the mould with a layer of asbestos tape. With the coiled nichrome wire the carbon mould was heated to 900°C. This temperature was achieved by the further wrapping of the asbestos tape over the nichrome wire and the packing of insulation bricks around the mould. The mould arrangement for the preliminary heats with a carbon stool is shown in Fig. 5-1.

During heats 12 to 13 produced in the induction furnace it was observed that the cast iron mould, when placed on an alumina coated stool, began to induct. During melt down, with the power on 17KW, the mould temperature rose to 600°C. While after melt down, when the power was reduced to 10KW, the mould temperature dropped to 400°C. The mould temperature was measured using a chromel-alumel thermocouple. The mould arrangement for use in the Heraeus furnace is shown in Fig. 5-2.

5.2 MATERIALS

The copper charge for the experimental ingots was electrolytic grade Cu of average composition as given in Table 5-4. The iron charge for the production of the iron ingots was generally soft magnetic iron of an average composition as given in Table 5-5. However, one ingot was produced from a charge of plast-iron of average composition in Table 5-6.

The melt additions for the copper melts were:

1. CuO (laboratory grade)
2. Sn (electrolytic grade), and
3. aluminium (S2 grade)

The aluminium was cut into approximately 1/4" squares for addition to the melt, and laboratory grade aluminium turnings were added to the mould.

For the iron melts, the additions consisted of:

1. Fe_3O_4 (laboratory grade), and
2. Aluminium additions which were similar to that for the copper melts.

The experimental 12 ton ingot from which samples were taken was of the following composition; (Pit analysis):

TABLE 5-4 AVERAGE COMPOSITION OF COPPER (ppm)

As	Ag	Pb	Sb	Sn	Bi	Ni	Fe	O
1	8	5-12	2	2	0.1	10	10	250-300

TABLE 5-5 AVERAGE COMPOSITION OF SOFT MAGNETIC IRON (wt%)

C	P	Mn	Si	S	Ni
0.025	0.009	0.15	0.075	0.019	0.030

Cr	Mo	Cu	Al	Sn
0.040	0.005	0.050	-	0.010

TABLE 5-6

COMPOSITION OF PLAST-IRON

(wt %)

ELEMENT	AVERAGE	CHECK
C	0.010	0.0037
Cr	0.005	0.002
Mn	0.005	0.002
Ni	0.005	0.0012
O	0.08	0.047
P	0.005	0.005
Si	0.010	0.007
S	0.006	0.006

C	P	Mn	Si	S	Ti
0.19	0.013	1.27	0.30	0.015	0.026

Al
0.005

This ingot was produced at the Australian Iron and Steel Pty. Ltd.

5.3 INCLUSION ASSESSMENT EQUIPMENT

5.3.1 The optical microscope employed in the manual counting was a Reichert "MeF" microscope using 140/1.30 "Fluor O el" oil immersion objective lens. The ocular was of 8x magnification and the illumination was from a low-voltage quartz iodine lamp.

The sample was observed through a binocular with a magnification of approximately 1.3x. One of the oculars contained a graduated scale, an eyepiece micrometer, which was used to measure the inclusion's dimensions and which was calibrated using the standard stage micrometer supplied. The immersion oil was of n_d = 1.516.

Once calibration of the eyepiece micrometer was obtained, the arrangement of objective, eyepieces and separation of the binocular eyepieces were duplicated on each sample,

so that accuracy of the calibration was maintained in all samples.

For counting of the industrial samples, objectives 65/0.65 and 15/0.25 "Epi" were employed in the determination of the frequency of occurrence of the larger inclusions.

5.3.2 The Quantimet B (Q.T.M.) was used to count samples from both the laboratory ingot No. 28, and some industrial steels. A field size of 150 x 200 μm^2 was employed, and 500 fields were examined per sample.

The data obtained in these analysis were (per each field):

1. total projected length of inclusions,
2. number of inclusions in various size classes,
3. total projected area of inclusions, and
4. number of inclusions.

The counts were conducted with a Vickers "Microplan" 20/0.5 objective, the magnification changer was set on 1x and the step size 0.4mm. The electronic magnification was 67.5 giving a total television screen magnification of 1181.25x.

5.4 EXPERIMENTAL PROCEDURE

Heats 1 to 3 and 10 to 29 were produced in the Heraeus induction furnace, while the remaining were made in the gas fired muffle furnace.

A number of heats were unsuccessful because of premature cracking of the crucible, especially the ZrO_2 crucibles, which were initially used, and so ingots were not obtained. Those heats from which an ingot was cast are summarised in Tables 5-7, 5-8 and 5-9. Details of each of the Heraeus heats are given in Appendix 1. Similar progressive accounts of the muffle furnace heats were not recorded because:

(a) their inherently simpler procedure negated such specification and,

(b) all but 2 of the 8 heats made in the muffle furnace were preliminary melts whose aim was solely to see if a base cone of inclusions could be produced in small laboratory ingots.

TABLE 5-7 PRELIMINARY (SERIES 1) HEATS

Heat No	Charge Cu (Kg)	Additions Sn (g)	Additions Al (g)	Mould	Crucible	Furnace
1	3.7	37.02	48.1	Carbon	ZrO_2	Hereaus
3	3.7	37.00	48.0	"	Salamander	"
5	3.7	28.90	27.5	"	"	Muffle
6	3.7	81.30	54.8	"	ZrO_2	"
7	2.9	40.90	28.9	"	"	"

TABLE 5-8 SERIES 2 IRON INGOTS

Heat No	Charge (Kg)	Additions			Casting Temp (°C)	Pressure (Torr)
		Al (g)		Fe_3O_4 (g)		
		Melt	Mould			
22	3.09	11.1	5.0	52.5	1550	2×10^{-1}
23	2.98	23.2	5.0	59.9	1530	5
24	2.98	28.0	-	89.9 (a)	1540	2×10^{-1}
26 (b)	6.80	17.6	-	99.0	1560	20
28 (c)	3.09	--	-	-	1550	4×10^{-1}
29 (d)	4.54	40.3	-	56.9	1560	2×10^{-1}

(a) first vacuum degassed - oxide added to mould

(b) mould did not induct

(c) mould did not induct to same degree as Heat Nos 22-24

(d) melt solidified in crucible

TABLE 5-9 SERIES 2 AND 3 COPPER HEATS

Heat No	Charge (Kg)	Additions				Casting Temp (^{o}C)	Pressure (Torr)
		Sn (g)	Al(g)		CuO (g)		
			Melt	Mould			
14	4.00	-	22.8	4.6	69.5	1400	1.5×10^{-5}
17	3.54	-	34.4	5.1	69.5	1400	4×10^{-1}
18	3.40	35.1	34.4	5.0	35.0	1350	4×10^{-1}
19	3.52	35.2	34.2	5.1	35.0	1180	5×10^{-4}
20	2.92	-	34.3	-	35.0	1100	3×10^{-4}
21	3.43	35.3	18.1	-	70.0	1220	3.5×10^{-1}
30(a)	1.39	16.6	8.4	-	-	-	760
32(b)	3.86	34.5	39.0	-	-	1220	760
Series 3(a)	1.30	Sb - 23.43g				1230	760

(a) Muffle furnace used

(b) Temperature on solidification measured.

5.4.1 Series 1 Heats

Heats 4 to 9 were conducted by the melting of approximately 3.7Kg of copper in a salamander or zirconia crucible in a gas fired furnace. When molten, the tin and aluminium were added and the melt was cast into a carbon mould. It was found necessary to coat the inside of the carbon mould with alumina cement to prevent reaction of any remaining oxygen in the melt with the carbon. The determination of temperature variations during the solidification of various parts of the ingot was attempted in these heats. Thermal analysis results were successfully obtained for Heat 3.

5.4.2 Series 2

The experimental procedure for Heats 14 to 31 (excepting 24, and 30, 32) consisted of:

1. The metal charge and oxide additions were placed in the crucible and the camber was evacuated using the forepump to a pressure of 10^{-1} torr.

2. Heating of the charge was then begun initially at

5KW, and then progressively increased by steps of 5KW to 20KW.

3. When the charge was molten the power was reduced to 5 to 10KW., depending on the temperature required of the melt and the particular mould.

4. On adjusting the temperature to the required level, addition of aluminium or tin followed by aluminium were made from the alloy hopper, under the required pressure level.

5. On re-adjusting the temperature to the required casting temperature and clearing any oxide skull which may have formed after deoxidation of the melt, the melt was cast under an argon atmosphere of 100mmHg. pressure.

6. The ingot was allowed to solidify and cool before removal from the chamber. During the solidification of Heat 32, the temperature variations in four positions in the ingot were continuously recorded.

5.4.3 Series 3 Heat

The muffle furnace was again used but the crucible had a refractory lid. Two silicon tubes, one containing the thermocouple and the other argon gas were passed through

a hole in the lid. Argon gas was employed to maintain an inert atmosphere above the melt surface. Deoxidant additions were made by wrapping the Anitmony (laboratory grade) in copper foil and plunging this package, which was attached to a copper rod, into the melt.

Samples from the melt were taken using evacuated silica tubes attached to silica or copper rods. As soon as possible after sampling the tubes were quenched in water. After all samples had been taken the heat was cast into an iron mould. The melt temperature throughout the sampling period was recorded with a Unicorder two pen recorder.

5.5 Macro and Micro-Examination

The ingots were sectioned in half, one half being used for chemical analysis and microscopic examination while the other half was macroetched.

5.5.1 Chemical Analysis

Copper ingots were analysed for aluminium, tin and oxygen from drillings by the Electrolytic Refining and Smelting Co. Pty. Ltd. The analysis for aluminium and tin

were performed on the atomic absorption spectrograph, and oxygen by vacuum fusion analysis.

Iron ingots were analysed by Australian Iron and Steel Pty. Ltd. Analysis for aluminium was conducted using the spectrograph as well as a complete analysis at various points in the ingot to check for the presence of any segregation of other elements.

Vacuum fusion analysis was used to obtain the oxygen contents. The oxygen samples were taken from the same sample positions that were sparked for aluminium content.

5.5.2 Macro Etching

The surface was prepared for etching on a linisher with 600 grade paper. Copper ingots were etched in 50% nitric acid for half an hour, while the iron ingots were etched in dilute nitric acid for 20 minutes. The ingots halves, after completion of etching, were washed in water followed by an ethanol wash.

5.5.3 Microexamination

Both iron and copper samples for microscopic examination were polished using the usual procedure, wet grinding on papers to 600 mesh, wax lap, 4-8 μm Diamond and 0-1 μm Diamond. The copper specimens after polishing on the 0-1 μm diamond wheel were successively polished with alumina paste and etched in a solution of: 1 part NH_4ON, 1 part H_2O and 2 parts 2.5% $(NH_4)_2 S_2O_8$.

The micro-samples were prepared for inclusion counting and for observation of inclusion types and morphologies. Microphotographs were obtained using the Reichert "MeF" microscope with either green or yellow filters. The photographic films used were Ilford "G5-52" or "Orthoset" and Kodak "Commercial Ortho". The high contrast film, "G5-52", was found necessary for photographing inclusions at high magnifications, because of the lower contrast of the higher power objectives.

5.6 The Manual Inclusion Count Procedure

The technique used was a modification of the lineal traverse method of Hardy and Allsop (115) and that suggested by the Nonmetallic Inclusions Group of the

Rolling Ingots Sub-Committee (127). The laboratory ingot samples were examined at 1450x magnification and the industrial samples at 64x, 120x and 650x depending on the sample, using a Reichert "MeF" microscope.

The polished section was traversed until a given area of sample had been covered. All inclusions in the field of view of the microscope were counted and sized. However, when sizing alumina clusters, because of the large number of inclusions per field, the iris diaphram was closed down and only the inclusions in the reduced field of view were counted.

The dimensions of the inclusion particles measured were as defined and discussed in Section 4-2. Each individual inclusion (as defined in Section 4-1), was sized and counted in order to overcome operator variation which was present in earlier LT. counts (127), where some operators included the very small inclusions and others neglected them.

For the laboratory ingot sample counts, approximately 10 traverses and a total traversed length of 10cm was the proposed standard procedure for each sample to cover the required area of 3 sq. mm. However, the procedure was varied depending on the inclusion distribution and numbers present. The procedure for the counting of the samples

from the industrial ingots and rolled products involved approximately 20 traverses and a total traversed length of 20cm. These two procedures are similar to the recommendations given in references (127, 166). The reproducibility of this method with varying inclusion distributions, on recounting and on repolishing are discussed in Section 7-1.

5.6.1 Calibration of Graticules for Optical Assessment

The eyepiece graticule used to determine the size of inclusions had a scale of a hundred units with every ten units numerically marked. At each magnification used in the inclusion assessments the scale was calibrated using the standard 1mm scale supplied with the Reichert microscope.

For the 1450x magnification, using the 140x oil immersion objective, the following calibration was obtained:

39 eyepiece graticule units	=	0.03 mm
90 eyepiece graticule units	=	0.07 mm
90.5 eyepiece graticule units	=	0.07 mm
26 eyepiece graticule units	=	0.02 mm

Therefore:

1 eyepiece graticule unit = 0.77243 ± 0.00180 μm

Also for the 675x magnification, using the 65x objective the following calibration was obtained:

64 eyepiece graticule units = 0.11 mm

70 eyepiece graticule units = 0.12 mm

35 eyepiece graticule units = 0.06 mm

Therefore:

1 eyepiece graticule unit = 0.0017158 ± 0.0000026 mm

At the 470x magnification, using the 45x objective, the following calibration was obtained:

40 eyepiece graticule units = 0.20mm

20 eyepiece graticule units = 0.10mm

Therefore:

1 eyepiece graticule unit = 0.005mm

5.6.2 Electron Microscopy

Replicas for examination with the electron microscope were initially prepared as for optical examination, ending with a light etch in a polish attack solution of one

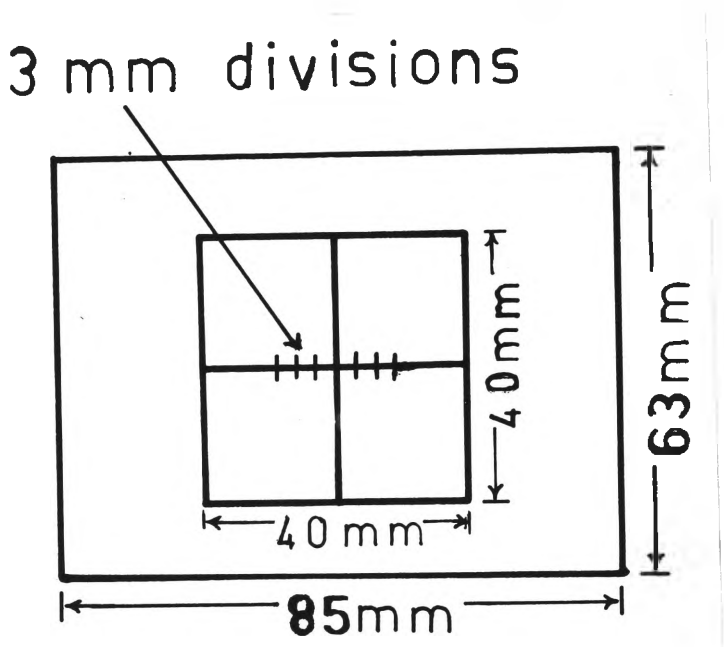

Fig. 5-4 Grid used for sizing inclusions on the electron microscope.

part ammonium hydroxide, one part 2.5% solution of ammonium persulphate and one part water. The sample was shadowed with Au-Pd and coated with carbon. The replica was extracted in a solution of 5 g of ammonium persulphate in 90ml of water. Care was needed to avoid bubble formation and as soon as the replicas were freed (between 5 and 10 minutes) they were washed in distilled water.

The inclusion counts using a JEOL electron microscope were at 8,300x nominal magnification. Four fields per grid square (at each corner) were systematically chosen for assessment, between 5 and 7 replicas per sample were examined.

The grid employed for sizing is schematically represented in Fig. 5-4. As it was not possible to rotate either the sample or the grid only the horizontal diameter could be measured, the vertical diameter had to be estimated. However, as the inclusion sections counted with the electron microscope were almost circular the difficulty and error in estimating the diameters of the particles were minimised.

5.6.3 Calibration of Grid and Magnification of Electron Microscope

In order to calibrate the magnification used a 1152 lines per mm graticule was photographed with the electron microscope at the nominal setting of 8300x. An average line spacing was measured at 0.7659 ± 0.0057 cm. on the negative.

An attempt was also made to photograph the same graticule through a cover glass using the oil immersion 140x lens on the Reichert microscope. Although interference contrast and a 12x occular was used neither clarity (small depth of focus) nor sufficient contrast was obtained on the negative to enable accurate measurement of the line spacing. When an 80x objective was used, however, a good negative was obtained and the line spacing was determined as: 0.03911052 x 2.54 ± 0.0002204 x 2.54 cm.

The magnification of the Reichert was then calibrated by photographing the standard 1 mm scale. The line spacing on the negative was then determined as 0.46339552 x 2.54 ± 0.0003642444 x 2.54 cm using the 80x objective.

Therefore:

$$1 \text{ EM grid spacing} = \frac{0.03911052}{0.46339552} \times 0.01 \text{ mm}$$

$$1 \text{ unit of EM screen scale at 8300X} = \frac{3}{7.6594 \times R.R.}$$

Where R.R. = reduction ratio from film plane to screen on the electron microscope

$$= \frac{\text{length of centre of projection lens pole Piece to the plate}}{\text{length of centre of projection lens pole piece to the screen}}$$

$$= \frac{360.5}{289.5}$$

Therefore:

$$1 \text{ unit of EM screen scale at 8300x} = \frac{3 \times 360.5}{7.6594 \times 289.5}$$

Or

$$1 \text{ unit of EM screen scale at 8300x} = \frac{3 \times 360.5}{7.6594 \times 289.5} \times$$

$$\frac{0.03911052 \times 0.01}{0.46339552 \text{ mm}} = 0.00041164 \text{ mm}$$

As 1 eyepiece graticule unit of the O.M. at 1450X

= 0.00077243 mm

Then:

1 eyepiece graticule unit of the O.M. at 1450X

$$= 0.00077243 \Big/ \frac{0.03911052 \times 0.01 \times 3 \times 360.5}{0.46339552 \times 7.6594 \times 289.5}$$

= 1.8764 units on the EM screen at 8300X

The magnification on the screen of the electron microscope is given as:

$$= 7.6594 \times 1152 \times \frac{289.5}{360.5}$$

= 7086X

5.7 COMPUTER PROGRAM FOR DETERMINATION OF A LOGNORMAL DISTRIBUTION

The program is written so that a two, three or four parameter lognormal distribution can be fitted to a set of experimental data. The data obtained from the assessment is organised into classes with class widths usually in a geometric progression (modulus $\sqrt{2}$). The upper and lower boundaries of each size class and the frequency of inclusions whose size falls within each class are the imput data for the program. A definition of "falls within" and the structuring of the classes are discussed fully in Appendix 4.

A first estimate of y_u is also required and is obtained either from an examination of the sample at a lower magnification or from a log-probability plot of the data.

Successive estimates of the parameters are then made and calculations of the theoretical frequencies using the estimated parameters are obtained. The chi-square test for goodness of fit was used to assess the validity of the fit of the theoretical distribution to the observed frequencies. Usually about 50 iterations were sufficient to obtain a good fit, although with a few samples 100 iterations were necessary.

The first four moments were calculated from the moment generating equation given by Johnson (192) using a quadrature formula to evaluate the integral. Further details of this method and the program in general are given in Appendix 4.

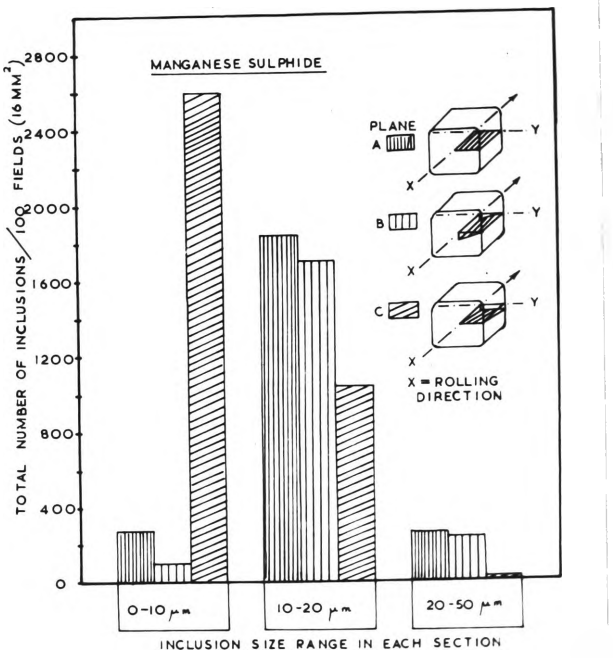

Fig. 6-1 Distribution of the total number of MnS inclusions for the size range, 0 - 50 μm, for the same sample but from different angled sections (140).

6.0 DEVELOPMENT OF THE MATHEMATICAL MODELS

6.1 SIZE DISTRIBUTIONS IN THE SECTION PLANE AND IN THE VOLUME OF THE SAMPLE

Studies of the influence of inclusions on the mechanical properties of steel (168, 169, 170) have revealed a need for information on the shape and size distribution of inclusions. The cleanness indices obtained by existing assessment techniques do not supply this data and are usually only relevant to the two dimensional section plane but it is the distribution of inclusions in the steel volume which influences the mechanical properties of the steel.

Significant differences can exist between the distribution seen on the polished section and that in the bulk of steel, and so the relationship between the two needs to be carefully examined.

An example to illustrate the considerable variation in size distributions of inclusions which can be obtained from various sections from a sample of hot rolled steel is given in Fig. 6-1. The section distribution of manganese sulphides in 3 size ranges can be seen to show considerable variation depending on the relationship of the section plane to the rolling direction and plane.

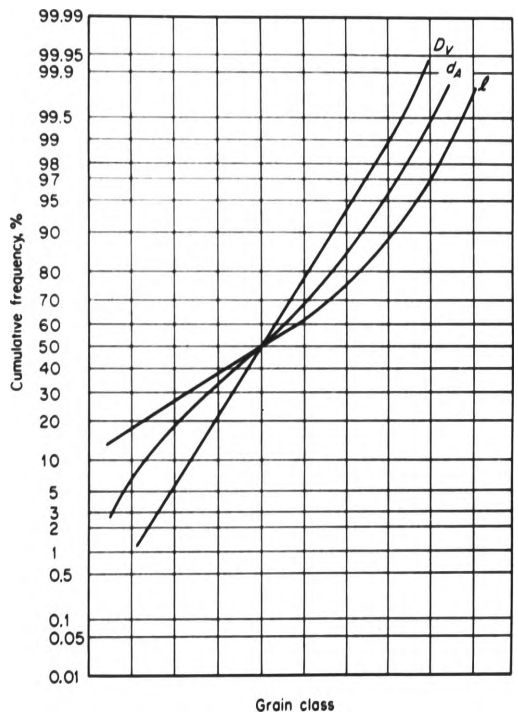

Fig. 6-2 Schematic sketch of the distribution curves (171),

l - linear intercept distribution

d_A - Section diameter distribution

D_V - Spatial diameter distribution

Type 11 MnS in rolled product form a linear orientated system (158) and so a random section through the sample will not supply accurate information of the particle size and shapes, rather in this special case systematic sampling is required.

Another example presented in Fig. 6-2 is a schematic representation of the distributions of chord lengths (l), section diameters (d_A) and the actual (3-D) diameter (D) of spherical "grains". The spatial distribution given by D can be seen to be clearly different from the section distribution d_A.

These examples illustrate that great care is required in interpreting the size distributions obtained from planar sections through a sample volume. The causes of the differences seen in Fig. 6-2 between section and spatial distributions can be expressed as:

(1) Particles are very rarely sectioned through their centroid and hence their section size is smaller than their true size.

(2) The larger particles tend to be sectioned with a greater frequency than the smaller particles. Exner (172) has termed these two effects as the "truncation" and "sampling" effects respectively, while Nicholson (173) discussed

these effects in terms of a statistical two stage sampling procedure.

The measurements taken of the particle sections on a plane cut through the composite material can be of three types (158).

(1) l, the length of a line intercept with the section, or

(2) d_A, the diameter of a circular section, the length of a side, diagonal or major or minor diamensions of non-circular sections, or

(3) A, the area of the section.

The distribution of sizes, X, where X is defined as one of the above parameters, is usually grouped into a number of classes. There are several reasons for this procedure, ease of calculation and presentation as well as simplification of data acquisition (174, 175).

The class groupings are chosen in either an arithmetic or geometric progression. The class size in the former case is usually determined as a fraction of the maximum particle size (154, 158, 159, 174), while the latter usually with a modulus of 2 or $10^{-0.1}$ for area distributions or $\sqrt{2}$ and $10^{-0.2}$ for d_A and l distributions (154, 158, 174).

The data so grouped can be presented in any one of

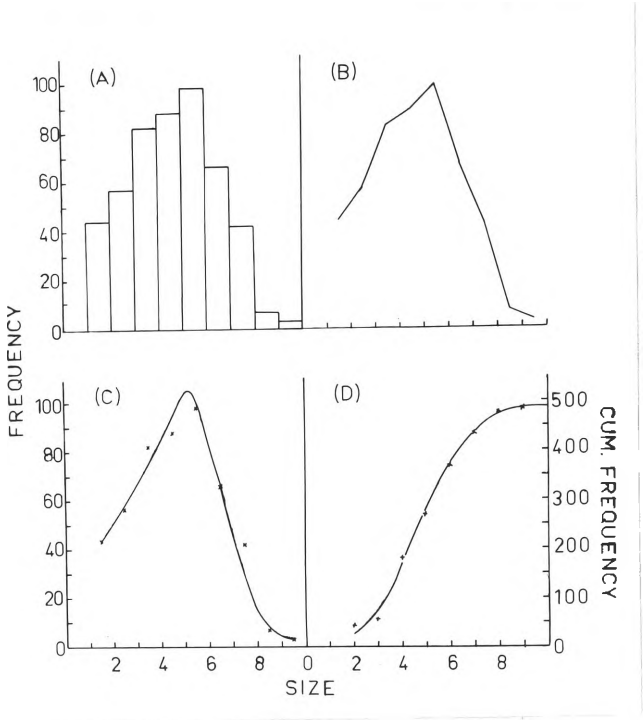

Fig. 6-3 Various ways of plotting grouped distribution data:

(a) Frequency histogram

(b) Frequency polygon

(c) Frequency curve

(d) Cumulative frequency curve

the following ways:

(1) as a histogram where the frequencies in each class are plotted with the class upper or lower limits;

(2) as a frequency polygon where the frequencies divided by the class width are plotted against the class mid points (arithmetic or geometric);

(3) as a relative frequency curve where a smooth curve is drawn through the points of the frequency polygon

(4) as a cumulative frequency curve where the cumulative frequency, greater or lesser than a given size class limit is plotted against that class limit.

An example of each of these presentations for one sample is given in Fig. 6-3.

Each presentation has its advantages and disadvantages. The shape of the first three graphs is dependent on the class grouping employed while the fourth, the cumulative frequency curve, has no such limitation (174).

This fact as well as the linearity of the cumulative frequency curves of the normal and log-normal functions when plotted on probability paper, has enhanced the popularity of this presentation mode for both spatial

and section distributions. For many investigators the representation of the section distribution as a histogram or cumulative frequency curve was the end point of their data analysis. In reality, however, it should have been the beginning, with the estimation of the spatial distribution as their goal.

The complexity of the relationship between the two distributions was the major inhibiting factor and so most investigators were content to only report what they observed on a polished section. The estimation of the spatial distribution from the section distribution in fact has only been achieved for particles of simple geometric shapes, e.g. spheres, ellipsoids, circular plates and cubes (154, 158, 159, 165, 176).

Only one method has been proposed which can be applied to any particle shape. This is the section area method of Saltykov (154) but in addition to assessing the section area distribution from the polished plane, knowledge is also required of the distribution of sections which can be expected when a particle of the given shape is intersected by random planes. Computer simulation (177) or the pioneering empirical approach of Hull and Houk (178) can be used to obtain the required section area distribution for the given particle shape.

The commonest method used for determining inclusion size distributions, however, is the LT method which although giving a simple formula for estimating the spatial distribution of spheres (163, 174) results in very complex expressions for the distribution of intercept lengths through randomly oriented particles of the next simplest geometric shape, cubes (177) and presumably for more complex polyhedra.

If the particles cannot be assumed to be represented by a simple geometric shape, Bockstiegel (163) using the linear intercept method of assessment, has shown that the calculated distribution from the chord lengths distribution is equivalent to the intercept length distribution resulting from spheres; and further that the volume fraction (V_v), the surface area per unit volume (S_v), and the mean "diameter" are the same for both spherical and non-spherical spatial distributions.

The basic problem of the chord or intercept length distribution, however, is the large number of small chord lengths obtained during assessment. Thus for size distribution determinations the area or "diameter" are the prefered parameters.

Intuitively implied in the previous discussion is that the estimation of the spatial distribution from the

section distribution requires knowledge of the shape of the particles (171, 179). This problem as well as ways of simplifying the description of inclusion shapes is discussed in the following section.

6.2 SPHERICAL OR ELLIPSOIDAL SHAPE PARTICLES

6.2.1 Spherical Particles

The assumption of a spherical shape and to some extent an ellipsoidal shape has been basic to almost all investigations of particles or grain size distributions (158).

The first and by far the most significant contribution to the estimation of the spatial distribution from the section size distribution came from Wicksell in two articles published in 1925 and 1926 (165, 180). This comprehensive work both for spheres and ellipsoidal particles has generally been unknown to the metallurgist with the consequence that his results have been re-derived many times by other investigators (159, 174, 181, 182, 183).

The two major results of Wicksell's analysis for spherical particles are:

$$g(x) = \frac{x\, f(x)}{\bar{x}} \qquad \text{(6.2.1)}$$

and

$$m(y) = \frac{y}{\bar{x}} \int_{y}^{X\,max} \frac{f(x)\, d\, x}{\sqrt{x^2 - y^2}} \qquad \text{(6.2.2)}$$

where:

$f(x)$ = the relative frequency distribution of spheres in the composite material - this is the function to be estimated

$g(x)$ = the relative frequency distribution of spheres which are intersected by the sectioning plane.

X_{max} = maximum size of the spherical particles in the sample.

x = the diameter of the spherical particles

$\bar{x}$ = the mean diameter of the spherical particles

$m(y)$ = the relative frequency distribution of the circular section diameters - the distribution determined in the assessment

y = the diameter of the circular sections

The assumptions inherent in Eqs. (6-2-1) and (6-2-2) are:-

(a) the spheres are uniformly and independently distributed throughout the matrix (173)

(b) $F(x) = \int f(x)dx$ is a continuous function (184).

If f(x) cannot be equated with a standard mathematical frequency curve; e.g. one of Pearson's functions, the log-normal or the gamma frequency functions; then the computing of f(x) accurately from m(y) is very complex (172).

The complexity of this problem may be seen from Wicksell's (180) three methods of establishing the spatial size distribution from the intersection distribution:

(1) a combined graphical and analytical method which is both time consuming and dependent on accuracy of the graphical plotting.

(2) matching the moments calculated from the intersection data with those of the spatial distribution, and

(3) multiplying both sides of Eq. (6-2-2) by $A_A N_V \bar{x}$ and integrating with respect to x. The result of the integration can be expressed as:

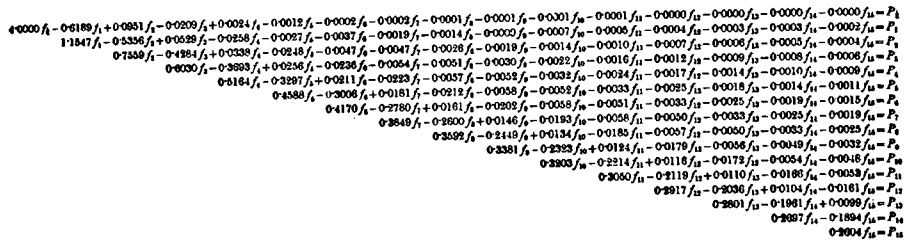

Table 6-1 Wicksell's table of coefficients for calculating spatial size distribution from section size distribution for spheres (size = Diameter) (180).

$$(N_A)_i = \sum_{n=o}^{k-i} (N_V)_{j=n+i} \Delta x \; a_{ij} \qquad (6\text{-}2\text{-}3)$$

where $(N_A)_i$ = the observed number of circular sections in the $i\Delta x$ th class per unit area

$(N_V)_j$ = the number of spherical particles per unit volume of size $j\Delta x$

Δx = class interval size both for circular sections and the sphere distribution

a_{ij} = the probability of sectioning a spherical particle of size $j\Delta x$ to obtain a section of diameter between $i\Delta x - \frac{\Delta x}{2}$ and $i\Delta x + \frac{\Delta x}{2}$

However, as $(N_A)_i$ are the known values and $(N_V)_j$ are the quantities to be evaluated, these simultaneous linear equations had to be solved. Wicksell did this and also supplied a table of coefficients to aid the computation of $(N_V)_j$. It should be noted that his solution is similar to that independently derived by Saltykov (183) some 33 years later.

Saltykov's equation for spherical particles sized by their diameters can be expressed as (158):

	Coefficients, a(i,j)														
	$N_A(1)$	$N_A(2)$	$N_A(3)$	$N_A(4)$	$N_A(5)$	$N_A(6)$	$N_A(7)$	$N_A(8)$	$N_A(9)$	$N_A(10)$	$N_A(11)$	$N_A(12)$	$N_A(13)$	$N_A(14)$	$N_A(15)$
$N_V(1)$	+1.0000	0.1547	0.0360	0.0130	0.0061	0.0033	0.0020	0.0013	0.0009	0.0006	0.0005	0.0004	0.0003	0.0002	0.0001
$N_V(2)$		+0.5774	0.1529	0.0420	0.0171	0.0087	0.0051	0.0031	0.0021	0.0015	0.0010	0.0009	0.0006	0.0006	0.0004
$N_V(3)$			+0.4472	0.1382	0.0408	0.0178	0.0093	0.0057	0.0037	0.0026	0.0018	0.0013	0.0010	0.0007	0.0007
$N_V(4)$				+0.3779	0.1260	0.0386	0.0174	0.0095	0.0058	0.0038	0.0027	0.0020	0.0016	0.0012	0.0009
$N_V(5)$					+0.3333	0.1161	0.0366	0.0168	0.0094	0.0059	0.0040	0.0028	0.0021	0.0016	0.0013
$N_V(6)$						+0.3015	0.1081	0.0346	0.0163	0.0091	0.0058	0.0041	0.0028	0.0022	0.0018
$N_V(7)$							+0.2773	0.1016	0.0329	0.0155	0.0090	0.0057	0.0040	0.0029	0.0022
$N_V(8)$								+0.2582	0.0961	0.0319	0.0151	0.0088	0.0056	0.0039	0.0028
$N_V(9)$									+0.2425	0.0913	0.0301	0.0146	0.0085	0.0055	0.0039
$N_V(10)$										+0.2294	0.0872	0.0290	0.0140	0.0083	0.0054
$N_V(11)$											+0.2182	0.0836	0.0280	0.0136	0.0080
$N_V(12)$												+0.2085	0.0804	0.0270	0.0132
$N_V(13)$													+0.2000	0.0776	0.0261
$N_V(14)$														+0.1925	0.0750
$N_V(15)$															+0.1857
N_V	1.0000	0.4227	0.2583	0.1847	0.1433	0.1170	0.0988	0.0856	0.0753	0.0672	0.0610	0.0553	0.0511	0.0472	0.0441

Table 6-2 Saltykov's table of coefficients for calculating spatial size distribution from section size distribution for spheres (size = Diameter) (183).

$$(N_V)_j = \frac{1}{\Delta x} \sum_{i=j}^{k} \alpha_i (N_A)_i \qquad (6\text{-}2\text{-}4)$$

where α_i is a series of coefficients as in Table 6-2.

This equation represented an improvement on Schwartz's solution (182) which in turn was a considerable improvement over Scheil's so called "pioneering" solution of 1931 (181). Scheil's method began with the assumption that the largest sections observed were great circles through the largest spheres in the sample. The number of particles in the spatial distribution with the largest size could then be calculated as well as the contribution by these spheres to smaller intersect diameters. The latter values had to be subtracted from the observed values class by class, working from the largest size class to the smallest. This recursive method however tended to accumulate errors in the smaller size classes. Errors in these classes, which were the result of observational misclassification of the data, were therefore inflated by the calculation "round-off" errors.

The advantages of the methods of Schwartz, Saltykov and Wicksell over Scheil's method are that the calculation is made using observed sectional data and

not values calculated from this data. Moreover, the number of particles per unit volume can be determined for any size group without it being necessary to determine the number in the larger size groups. Also Wicksell's and Saltykov's methods have an advantage over Schwartz's method, in that a new table of coefficients does not have to be calculated if a different number of classes is required.

Hyam and Nutting (185) avoided the latter problem by classifying the data into geometric ($\sqrt{2}$) rather than arithmetic grouping; thus only one set of coefficients was required for any number of class groups. Their method involving sequential calculations, however, still suffered from the disadvantages of accumulating errors. This was overcome by Exner (174) who expressed the sphere frequencies as an explicit function of the frequencies of the diameters of the circle of intersection:

$$(N_V)_i = \frac{1}{i\Delta x}\left(Co\,(N_A)_i - \sum_{j=1}^{k-i} C_j\,(N_A)_{i+j}\right)$$

Exner supplied a table of coefficients (C_o,C_j) for a modulus of the geometric grouping of $\sqrt{2}$ as shown in Table 6-3.

TABLE 6-3 EXNER'S TABLE OF COEFFICIENTS FOR CALCULATING THE SPATIAL DISTRIBUTION FROM THE SECTION DISTRIBUTION FOR SPHERES WHEN THE SECTION DATA IS GROUPED IN A GEOMETRIC SERIES (174)

C_o	C_1	C_2	C_3	C_4	C_5	C_6
1.4142	0.3178	0.0673	0.0193	0.0063	0.0022	0.008

C_7	C_8
0.0003	0.0001

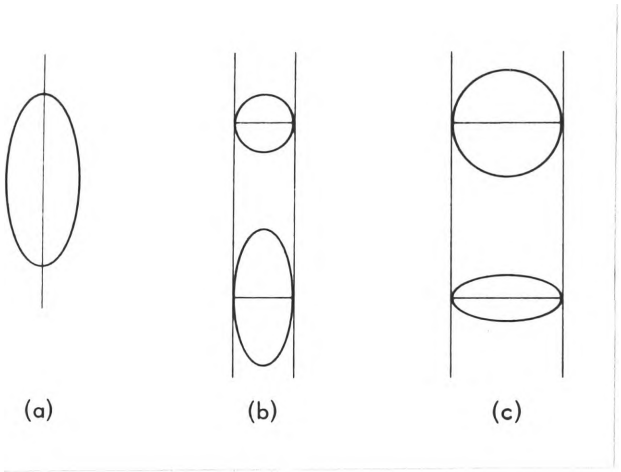

Fig. 6-4 System for identifying elliptical sections, (a) as prolate (b) and oblate (c) by their largest equiaxed and non-equiaxed sections (159).

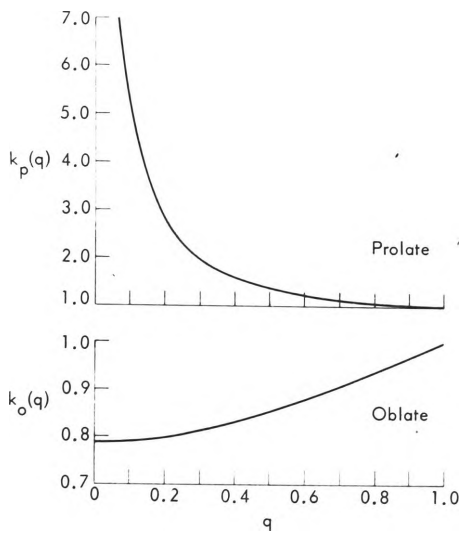

Fig. 6-5 Shape factors $k_p(q)$ and $k_o(q)$, for prolate and oblate sheroids, respectively, plotted versus q, the axial ratio of the generating ellipse (159).

6.2.2 Ellipsoidal Particles

By multiplying the right hand side of Saltykov's equation, Eq (6-2-4), by a shape factor $\frac{1}{k(q)}$, DeHoff enabled the number of ellipsoidal particles per unit volume to be calculated from the intersection distribution, employing the same table of coefficients as used for spherical particles (159). The major assumption required for this procedure was that the particles had to be prolate or oblate ellipsoids of constant axial ratio. The ellipsoid type and axial ratio were estimated from the largest equiaxed and elongated sections. If the largest sections observed were those of (a) in Fig. 6-4 then the particles were assumed to be prolate ellipsoids, while if they were like those of (b) they were assumed to be oblate ellipsoids.

The axial ratio, q, the ratio of the minor to the major axis, is determined from these two sections and the shape factor $k(q)$ is determined from graphs given by DeHoff, as in (Fig. 6-5).

The "size" of the prolate ellipsoid is defined as the length of its minor axis; while the "size" of an oblate ellipsoid equals the length of its major axis.

Although this is a simple procedure to use, the assumption of ellipsoids of constant axial ratio severely limits the applicability of the analysis to real systems. Wicksell's (165) treatment of general ellipsoids is a better approximation to real particles, though lack of knowledge of its existence, and when known, the complexity of the analysis, have limited its application. A simplification of his analysis will be considered in a later section.

6.3 LOG-NORMAL DISTRIBUTION FUNCTION

As was noted in the previous section if a functional form for f(x) can be assumed the estimation of the spatial distribution from the section distribution can be considerably simplified.

The distributions which have been considered frequently in studies of small particles are empirical functions such as the Rosin-Rammler distribution and the Roller distribution (149), or statistical functions such as the normal (149), log-normal (171, 174, 175, 186, 187), gamma and Pearson distributions (149, 172, 188).

The distribution which has attracted considerable

attention is the log-normal function. The size range of zero to infinity, the skewness of the function (the positive skewness form receiving the majority of use) and ease of determining its parameters approximately by graphical analysis (149, 174, 189) have been the significant reasons for its popularity.

The relationship between the normal or Gaussian distribution and the log-normal distribution (L-N distribution) can be defined as (190): "Consider an essentially positive variate X ($0 < x < \infty$) such that $Y = \log X$ is normally distributed with a mean μ and variance σ^2. We then say that X is lognormally distributed...."

The distribution function of the L-N function has been expressed in many forms (174, 187, 190, 191, 192). For the subsequent discussion it is given here as:

$$f(x) = \frac{1}{\sqrt{2\pi}\,\sigma x} \cdot e^{\frac{-\frac{1}{2}(\ln x - \ln \mu)^2}{\sigma^2}}, \quad x > 0 \qquad (6\text{-}3\text{-}1)$$

where μ and σ are the parameters of the distribution:

μ = geometric mean of x or the median of x (50% of the distribution being less than or greater than $x = \mu$)

$\ln \mu$ = arithmetic mean of $\ln x$

σ = arithmetic standard deviation of lnx

$$= \sqrt{\ln \left[E(X^2)\right] - 2\ln \left[E(X)\right]} \qquad (6\text{-}3\text{-}2)$$

and $$E(X^i) = \int_0^\infty x^i f(x)\, dx$$

$$= e^{i\ln x + \frac{i^2\sigma^2}{2}} \qquad (6\text{-}3\text{-}3)$$

A property of the L-N distribution which is important to particle studies is its reproductive property; that is, if the random variate X is log-normally distributed with parameters $\ln\mu$ and σ^2, then X^n is also log-normally distributed with parameters $n\ln\mu$ and $n^2\sigma^2$ (190). Thus from the diameter-frequency distribution the surface area, volume and weight distributions can be determined (149).

The log-normal distribution has found wide application in small particle systems; examples of the diversity of the fields of study involved are:

1. The size-frequency distribution of subsieve particles that are formed by precipitation or comminution (193).
2. The size-frequency distribution of particles of photographic emulsions (175, 194).
3. In examining Bacillus Subtilis the frequency of fluorescence levels for a given pH level were found to be described by the log-normal

function (195)

4. A log-normal distribution approximately describes the particle size distribution of samples of power station boiler flyash (196).

While in metallurgical particulate systems; the size-frequency distributions of carbide particles (187, 197), of silica particles in copper (186), of oxide inclusions in steel (137) and the planar grain size (198) and spatial grain size distributions (171) have been represented by the log-normal distribution.

Thus in the domain of small particle statistics the log-normal distribution has become well established In the majority of studies the use of this distribution has been justified on the empirical grounds of successful curve fitting. No satisfactory theoretical explanation has been proposed for its description of size distributions in metallurgical microstructures (172). Although Drapal and Horalek (187) have given a qualitative discussion, invocking the law of proportionate effect (190) to justify the use of the L-N distribution as a description of the size distribution of carbide particles.

If the size distribution of nonmetallic inclusions formed by various growth mechanisms can be theoretically shown to be of the log-normal distribution form, then

the spatial distribution can be more easily and accurately determined from the measured section distribution by the use of the method of moments.

6.4 DERIVATION OF LOG-NORMAL DISTRIBUTION OF NON-METALLIC INCLUSION SPATIAL SIZE-FREQUENCY DISTRIBUTION

The derivation of the log-normal distribution of inclusion sizes is similar to that given by Aitchison and Brown (199) and Epstein (200) for the distribution of incomes and particle sizes resulting from a breakage process respectively. The notation used is similar to that of Aitchison and Brown.

Let $F_t(V_t)$ denote the distribution function of particle size at time t, that is, the probability of a particle size being equal to or less than V_t at time t is $F_t(V_t)$. The size of the particle is defined as its volume. The transition probabilities $dGt(V_{t+1}, Vt)$ are defined as the probability that a particle with a size in the interval $(V_t, V_t + dV_t)$ at time t will have a size in the interval $(V_{t+1}, V_{t+1} + dV_{t+1})$ by time $t+1$.

The theory of proportionate effect is equivalent to the proposition that $dG_t(V_{t+1}, V_t)$ depends only on

the ratio V_{t+1}/V_t. That is:-

$$dG_t(V_{t+1}, V_t) = d\,H_t\,(V_{t+1}/V_t)$$

Then $$dF_{t+1}(V_{t+1}) = \int_0^1 d\,Ht(V_{t+1}/V_t)\,dF_t(V_t)$$

Therefore:

$$F_{t+1}\,(V_{t+1}) = \int_0^1 Ht\,(V_{t+1}/V_t)\,dF_t\,(V_t)$$

If V_t and T_t are the variates associated with the distribution functions $F_t(V)$ and $H_t\,(V_{t+1}/V_t)$ respectively then the above equation implies that

$$V_{t+1} = T_t\,V_t$$

so that $$V_n = V_o \prod_{i=1}^{n-1} T_i$$

where V_o is the variate associated with the initial distribution function $G(V)$.

Subject to certain assumptions of the central limit theorem (190) $\log V_n$ is asymptotically normally distributed and hence V_n is asymptotically log-normally distributed in a two-parameter form.

It may be of interest to note a similar log-normal distribution has also been derived by Kottler (175) for

particles undergoing diffusional growth. The rate of growth was given by:-

$$\frac{dx}{dt} = kx \qquad (6\text{-}4\text{-}1)$$

where k was defined as the velocity constant of growth.

On integrating equation (6-4-1) the equation relating time, t, and size, x, was given as:-

$$t = a_1 + b \ln x$$

In deriving the log-normal distribution of particle sizes Kottler assumed that:

1. growth was isotropic
2. each particle began to grow at an individually different random time. The times, t, were assumed to be normally distributed. Thus by this assumption the function of sizes, x, was shown to be log-normally distributed.

This derivation is similar to that derived here for inclusions in that equation (6-4-1) states that the rate of growth is proportional to the momentary value of its size. Thus if a particle during growth is subjected to a large number of impulses each of which causes a certain increase in its size, then the distribution of particle sizes will approach a log-normal distribution as the number of impulses becomes larger.

If the size of the particles needs to be expressed

as a linear dimension (as will be necessary when determining the distribution of inclusions in 3 dimensions from the section sizes in a 2 dimensional plane) the log-normal distribution of volumes of the particles will present no problems, as has already been noted if a variate X is log-normally distributed then X^n is also log-normally distributed (190).

The inclusion size distribution will be bounded at a lower limit, the critical nucleus size or the minimum size resulting from diffusion and Browian growth, and at an upper limit, the maximum size the operative growth mechanism permits for the time of growth. In order to simplify the mathematics involved, a two parameter distribution can be assumed for the particle size distribution. This assumption in practice should not introduce significant error into the results as the smallest particle size will be near zero size, while the assumption of particles of infinite size will only cause slight increases in the 3rd and 4th moments.

6.5 EXAMPLES OF SPATIAL SIZE DISTRIBUTIONS OF PARTICLES UNDERGOING GROWTH WHICH ARE OF A LOG - NORMAL FORM

1. Wojcik, Raybeck and Paliwoda (137) extracted inclusions from a silicon killed tube steel and measured the spatial size distribution using a Coulter counter. Table 6-4 includes their observed data from six counts, and the calculated frequencies of the computer fitted L-N distribution together with the χ^2 value for goodness of fit.

   As the calculated χ^2 value is not only less than the tabulated value of χ^2 at the 5% significance level but also the 30% level, the representation of the data by the model of Section 6.4 can be considered extremely satisfactory.

2. Kottler (201) measured the projected area distribution of silver halide grains in a photographic emulsion which had grown by diffusion. He obtained a significant fit to a two parameter log-normal distribution with a $\chi^2 = 0.91$ for three degrees of freedom. As the tabulated value of χ^2 for the 10%

TABLE 6-4 ANALYSIS OF WOJCIK ET AL'S (137) DATA USING L-N MODEL

OBSERVED FREQUENCY	L-N PREDICTED FREQUENCY	CLASS LIMITS (μm)
1305.6	1296.95	7.6 - 9.7
484.2	509.83	9.7 - 12.0
307.8	280.02	12.0 - 15.0
148.5	157.93	15.0 - 19.0
80.4	83.66	19.0 - 24.0
48.6	43.75	24.0 - 30.0
25.38	25.14	30.0 - 38.0
13.44	13.79	38.0 - 49.0
4.44	6.28	49.0 - 62.0
1.08	3.00	62.0 - 78.0
2.34	1.44	78.0 - 99.0

$X^2 = 7.6635$

$\chi^2_{05} = 14.07$

D.F. = 7

significance level and three degrees of freedom is 6.25 the L-N description of the spatial distribution is highly significant.

Other examples and further discussions of the representation of the spatial distribution of inclusions by the two parameter log-normal model are given in subsequent sections.

6.6 THE RELATIONSHIP OF THE LOG-NORMAL SPATIAL DISTRIBUTION OF SPHERE DIAMETERS TO THE SECTION DISTRIBUTION OF CIRCULAR DIAMETERS

If a definite functional form is used to represent the spatial distribution then the form of the section distribution can be determined mathematically rather than by using tables of coefficients as discussed in Section 6-1. An illustration of this can be found in the work of Drapal and Horalek (187) who examined spheroidized cementite. They assumed the spatial distribution to be from the log-normal "family" and expressed the cumulative frequency distribution of section diameters, M(y) as:

$$M(y) = 1 - \frac{1}{\sqrt{2\pi}\,\sigma\, E(X)} \cdot \int_{y}^{\infty} \left[\int_{t}^{\infty} \frac{t}{x\sqrt{x^2 - t^2}} \cdot e^{-\frac{1}{2}\frac{(\ln x - \ln \mu)^2}{\sigma^2}} dx \right] dt \qquad (6\text{-}6\text{-}1)$$

After solving this double integral, M(y) was given in the form:

$$M(y) = \phi\left(\frac{\ln y - \ln \mu - \sigma^2}{\sigma}\right) + \sum_{j=1}^{\infty} \frac{y^{2j} \cdot e^{2j(j-1)\sigma^2}}{\mu^{2j}} \cdot \frac{\Gamma\left(\frac{2j-1}{2}\right)}{2\,\Gamma\left(\frac{1}{2}\right)\Gamma(j+1)} \cdot \left[1 - \phi\left(\frac{(\ln y - \ln \mu + (2j-1)\sigma^2)}{\sigma}\right)\right] \qquad (6\text{-}6\text{-}2)$$

where $\phi(z) = \frac{1}{\sqrt{2\pi}} \cdot \int_{-\infty}^{x} e^{-\frac{1}{2}t^2} dt$

The section diameter distribution of "spherical" cementite particles was measured on three planes of polish and was tested for goodness of fit with the theoretically calculated distribution M(y). A significant fit was obtained at the 5% level using the Kolmogorov-Smirnov test of goodness of fit. The assumption of a log-normal spatial distribution was, therefore, empirically justified.

The weaknesses of Drapal and Horalek's approach are that each set of data has to be tested for goodness of fit to a complex series calculation of M(y) and the estimates of μ and σ used will inevitably be biased as they are obtained from the sample moments of a truncated section distribution.

A better approach would be to show theoretically that M(y) can be described by one of the many families of statistical distribution curves, namely the log-normal distribution family.

6.7 DERIVATION OF THE LOG-NORMAL DISTRIBUTION OF SECTION SIZES

The derivation of the log-normal law of section sizes resulting from particles which have been intersected

by a random plane is again similar to that derived previously for particle size distributions resulting from a breakage process (200) or the distribution of incomes (199).

The derivation involves a restatement of the theory of proportionate effect in terms of distribution functions rather than in terms of random variables.

The basic concept required for the derivation is that the sampling process of section sizes from a given area A can be subdivided into n steps - each step involving the determination of the sizes of sections within a given area of the section plane, ΔA (where $n\Delta A = A$).

Let $G(x)$ denote the initial distribution function, that is, the probability of a section size being less than or equal to x is $G(x)$.

Also let each sampling step give a distribution function $F(Z_i)$, $i = 1$ to n.

Now denote the distribution function resulting from the first sampling step, $F_1(x)$.

Then $X_1 = X_o Z_1$ where X_1, X_o, Z_1 are random variables having distribution functions $F_1(x)$, $G(x)$ and $F(Z_1)$ respectively. That $X_1 = X_o Z_1$ is a result of the assumption that X_o and Z_1 are independent random variables.

Similarly $F_2(x)$, the result of two sampling steps, is the distribution function of a random variable X_2 which is the product of two independent random variables X_1 and Z_2 having distribution functions $F_1(x)$ and $F(Z_2)$ respectively. However, as the random variable X_1 is a product of the two independent random variables X_o and Z_1, $F_2(x)$ is the distribution function of a random variable X_2 which is the product of three independent random variables X_o, Z_1 and Z_2. Thus after n steps in the sampling process Fn(x) will be the distribution function of a random variable X_n which is the product of (n+1) indpendent random variables X_o, Z_1, Z_2 ...., Z_n.

Therefore:

$$\ln Xn = \ln X_o + \sum_{i=1}^{n} \ln Z_i$$

Now as Z_n is independent of the number of steps and that $E\left\{\ln Z_n\right\}$ and $E\left\{(\ln Z_n)^2\right\}$ both exist the central limit theorem of statistics can be applied. The multiplicative form of this theorem indicates that the random variable X_n tends to be lognormally distributed as $n \rightarrow \infty$

The initial distribution G(x) can be determined on

a small portion of the section plane.

The dimension of the section area chosen as a measure of "size" will depend on the shape assumed for the particles. In the case of ellipsoidal particles the square root of the product of the major and minor axes can be regarded as the measure of "size" of the section area. As the definition of the size variate is to some extent arbitrary (but subject to shape requirements) and as the size variate in practice will have a range of say zero to X_u, an upper limit equal to the size of the largest particle in the sample, then Y, defined as

$$Y = \frac{X}{X_u - X}$$

by the above derivation can also be shown to be asymptotically log-normally distributed in a two parameter form. The variate X is therefore asymptotically log-normally distributed in a three parameter form.

The area sampled at each step in the process and also the total area to be examined can also be stated in general terms. This allows different sampling techniques to be included in the range of definition. For example the area A of the sampling process as a whole can be defined as the total length of traverse multiplied by a

standard width or as a number of fields of a given area.

With both section and spatial distributions belonging to the same "family" of distributions the calculations of one from the other is greatly simplified and quickly obtained. Also because the log-normal distribution can be easily transformed into a normal distribution, all the significance tests derived for the normal distribution can be used. The importance of this comparison of distributions will be discussed in latter sections.

6.8 EXAMPLES OF THE LOG-NORMAL DISTRIBUTION OF SECTION DISTRIBUTIONS OF PARTICLES USING DATA OBTAINED FROM METALLURGICAL LITERATURE

1. Drapal and Horalek (18) examined three random planes of a steel specimen for which they sized spheroidized particles of cementite. As shown in Table 6-5 the section distribution for each plane is significantly described by a L-N distribution. The L-N Pred. Frequencies stated in this table were determined using the computer program given in Appendix 4. By reference to the original paper and Table 6-5 the L-N distribution is, in fact,

TABLE 6-5 ANALYSIS OF DRAPAL AND HORALEK (187) DATA USING L-N MODEL

PLANE 1		PLANE 2		PLANE 3	
Obs Freq	L-N Pred Freq	Obs Freq	L-N Pred Freq	Obs Freq	L-N Pred Freq
51	49.8	48	48.7	50	49.4
101	104.9	104	102.1	99	103.3
90	79.6	82	79.3	88	80.8
31	40.1	43	41.7	40	41.5
20	16.6	14	18.3	15	16.9
3	6.2	4	7.3	5	5.9
3	2.1	5	2.7	2	1.8
1	0.7			1	0.5
X^2 =	6.43	X^2 =	4.61	X^2 =	1.84
χ^2_{05} =	9.49	χ^2_{05} =	7.82	χ^2_{05} =	9.49
D.F. =	4	D.F. =	3	D.F. =	4

a better fit to the empirical data of Drapal and Horalek's than their theoretically derived function for M(y). For example, for plane 2 the goodness of fit test for their calculated distribution to the data was $X^2 = 23.12$, which is greater than the tabulated χ^2 at 0.01% probability for 4 degrees of freedom. As a consequence of this very little confidence can be attributed to their fitting of the observed data.

2. Lindon and Billington (17) using the QTM determined the size distribution per mm^2 of non-metallic inclusions resulting from Mn-Si-Al deoxidation. The size distributions determined from samples taken at various times after deoxidation in experiment number 7 were used and fitted to a log-normal distribution again using the computer program in Appendix 4. The calculated results of the chi-square goodness of fit test are as follows:

SAMPLE TIME	X^2	χ^2_{05}	DEGREES OF FREEDOM
½ MIN	0.46	5.99	2
1 MIN	1.82	3.84	1
2 MIN	1.65	3.84	1
4 MIN	5.01	5.99	2
7 MIN	3.27	3.84	1

As all X^2 are less than the corresponding χ^2_{05} values, it is evident that all the samples can be significantly fitted by the L-N distribution. As a representation of the form of the empirical distribution data given in these two examples from the metallurgical literature, the three parameter model derived in section (6-7) can be considered adequate. Further justifications of it are given in subsequent sections.

7.0 RESULTS AND DISCUSSION

The findings of the preliminary solidification investigations are summarised below, detailed considerations of the results are given in Appendix 3.

Generally both iron and copper ingots solidified at a rapid rate, although the moulds had been induction heated to approximately 400°C. The iron ingots were essentially equiaxed in structure while the copper ingots were predominately columnar. The presence of 0.5 to 1.0 wt% Sn in the copper ingots resulted in the formation of an equiaxed zone. The grain size of both columnar and equiaxed grains in both metal ingots and also the number of grains as expected were found to be related to the degree of superheat and nucleants present.

7.1 REPRODUCIBILITY OF SAMPLING AND ASSESSMENT METHODS

The significance given to the size-frequency distribution assessment depends on the confidence placed on the reproducibility of sample preparation, the amount of sample examined and whether a random or orientated sample is examined. Recommendations given in the

literature (123, 130, 166) for total traverse length, number of traverses, area or number per field are attempts to generalise from experience gained on particular types of inclusion distributions and so not surprisingly bear little agreement with each other and are of little help for a different assessment technique or inclusion population. A more rational approach would be to use statistical techniques to indicate the degree of significance which can be attributed to the sample. This is the philosophy which is employed in the following sections.

7.1.1 Representative Sampling

For the randomly occurring alumina inclusion distribution, studied in Series 2 ingots, two samples were examined and the results for each independent and different traverse were recorded separately.

A χ^2 contingency test was employed to test reproducibility between traverses. This test detects errors arising from nonrepresentative or improper techniques in sampling, and as non-representative sampling is the major source of error in V_V, P_L, and N_L counts (158) it may also be considered the major source of error in size-frequency determinations.

Tables 7-1 and 7-2 give the between traverse comparisons for samples 5 and 8 from copper ingot No. 18.

As the values of $\bar{X}^2$ in Table 7-1 and 7-2 are less than χ^2_{05} for both samples, any difference between traverses for each sample can be attributed to chance variation which can be expected in such a sampling procedure. It can also be concluded that for either sample one traverse of 11mm in length is sufficient to give a representative sample of the size-frequency distribution of alumina.

When a distribution of inclusions having a higher N_A is examined the traverse length to give a representative sample was found to be less than 11mm, as can be noted from Tables 7-3 and 7-4.

Again, as in both samples X^2 is less than the corresponding χ^2_{05} for the respective degrees of freedom, no significant difference between the three traverses on each sample can be assumed. Moreover, for this sample a traverse of length 3mm would give a representative sample.

The conclusion to be made from these results is obvious - no general statement can be made of how large a sample area should be without reference to the frequency of occurrence of the particles, N_A.

TABLE 7-1 SAMPLE 5 INGOT 18 (SERIES 2)

1ST TRAVERSE		2ND TRAVERSE	
Obs Freq	Exp Freq	Obs Freq	Exp Freq
14	11.1853	8	10.8147
20	23.8959	27	23.1041
45	49.8254	53	48.1746
78	65.0781	50	62.9219
82	87.4487	90	84.5513
71	66.0949	59	63.9051
19	24.4043	29	23.5957
3	4.0674	5	3.9326
332		321	

Traverse Length = 11.04mm

X^2 = 13.34

X^2_{05} = 14.07

Traverse Length = 11.05mm

D.F. = (8-1)(2-1)

= 7

TABLE 7.2 SAMPLE 8 INGOT 18 (SERIES 2)

1ST TRAVERSE		2ND TRAVERSE		3RD TRAVERSE	
Obs Freq	Exp Freq	Obs Freq	Exp Freq	Obs Freq	Exp Freq
26	20.5466	17	19.7247	15	17.7287
19	18.0668	21	17.3441	11	15.5891
32	29.0486	25	27.8866	25	25.0648
33	31.1741	32	29.9271	23	26.8988
38	35.0709	35	33.6680	26	30.2611
16	24.0891	21	23.1255	31	20.7854
10	14.5243	14	13.9433	17	12.5324
1	2.4798	3	2.3806	3	2.1397
175		168		151	

Traverse Length = 11.36mm

Traverse Length = 11.16mm

Traverse Length = 10.90mm

X^2 = 19.05

D.F. = (8-1)(3-1)
= 14

χ^2_{05} = 23.685

TABLE 7-3 BOTTOM INGOT 10% AREA 1 (SERIES 3)

1ST TRAVERSE		2ND TRAVERSE		3RD TRAVERSE	
Obs Freq	Exp Freq	Obs Freq	Exp Freq	Obs Freq	Exp Freq
10	12.8504	13	17.4488	41	33.7008
37	33.1299	43	44.9852	85	86.8848
58	52.6063	68	71.4311	136	137.9626
41	43.3701	60	58.8898	115	113.7402
25	24.8976	40	33.8071	59	65.2953
12	13.8543	21	18.8120	36	36.3337
13	13.0512	15	17.7215	37	34.2274
8	10.2402	17	13.9045	26	26.8553
204		277		535	

Traverse Length = 3.11mm

Traverse Length = 4.89mm

Traverse Length = 6.69mm

X^2 = 8.94

D.F. = (8-1)(3-1)
= 14

X^2_{05} = 23.685

TABLE 7.4 SAMPLE BOTTOM INGOT 10, AREA 2 (SERIES 3)

1ST TRAVERSE		2ND TRAVERSE		3RD TRAVERSE	
Obs Freq	Exp Freq	Obs Freq	Exp Freq	Obs Freq	Exp Freq
225	209.3639	191	202.3695	37	41.2666
265	262.0515	243	253.2969	59	51.6516
160	164.9954	167	159.4833	30	32.5214
115	109.5347	99	105.8754	23	21.5898
49	58.6958	63	56.7349	15	11.5692
31	33.7385	39	32.6114	3	6.6500
23	22.6464	23	21.8899	3	4.4637
10	11.0921	13	10.7216	1	2.1863
8	8.3191	9	8.0412	1	1.6397
12	17.5625	21	16.9758	5	3.4617
898		868		177	

Traverse Length = 6.21mm

X^2 = 17.59

Traverse Length = 6.13mm

D.F. = (10-1)(3-1)

= 18

Traverse Length = 1.17mm

χ^2_{05} = 28.87

7.1.2 Uniformity of Distribution and Experimental Errors

The experimental errors discussed in this section are sample preparation, fatigue and lack of consistence in sizing by the operator. These errors appear as the error which can be measured by repeating the assessment on a sample.

Large variations in size-frequency distributions have been reported (147) when the assessments were conducted both before and after sample repolishing. Non-random inclusion distributions and resolution problems were given as reasons for this variability, but undoubtedly the experimental errors mentioned above should have also been considered.

In the present work, three samples were examined - two contained randomly occuring alumina particles and the other contained grain boundary films of Type 11 sulphides. After assessment the samples were repolished and re-assessed. The results of χ^2 contingency tests for the samples containing alumina inclusions are given in Tables 7-5 and 7-6.

The conclusions which emerge from these two statistical significance tests are that there is probably

TABLE 7-5 SAMPLE: INGOT 18 NUMBER 4 (SERIES 2)

TRAVERSE LENGTH = 90.27mm

1ST ASSESSMENT

Obs Freq	Exp Freq	X^2
28	18.8	4.5
17	15.8	0.09
10	22.4	6.88
23	28.0	0.89
33	34.8	0.09
36	30.9	0.84
16	14.3	0.20
8	6.2	0.52
171		

$X^2 = 17.9$

$\chi^2_{05} = 14.1$

$\chi^2_{01} = 18.5$

TRAVERSE LENGTH = 98.29mm

ASSESSMENT AFTER REPOLISHING

Obs Freq	Exp Freq	X^2
60	69.3	1.42
57	58.3	0.02
95	82.7	1.83
108	103.1	0.23
130	128.1	0.00
109	114.0	0.17
51	52.8	0.06
21	22.8	0.14
631		

D.F. = (8-1)(2-1)

= 7

TABLE 7-6 SAMPLE: INGOT 30, BOTTOM (SERIES 2)

TRAVERSE LENGTH = 34.23mm

1ST ASSESSMENT

Obs Freq	Exp Freq	X^2
178	153.9431	3.7594
108	115.0984	0.4378
87	82.4695	0.2489
68	70.9238	0.1205
51	61.0274	1.6476
26	36.2866	2.9161
11	10.4461	0.0294
7	6.5976	0.0245
7	5.4980	0.4103
543		

$X^2 = 21.31$

TRAVERSE LENGTH = 44.52mm

ASSESSMENT AFTER REPOLISHING

Obs Freq	Exp Freq	X^2
102	126.0569	4.5911
101	93.9016	0.5366
63	67.5305	0.3039
61	58.0762	0.1472
60	49.9726	2.0121
40	29.7134	3.5612
8	8.5539	0.0359
5	5.4024	0.0300
3	4.5020	0.5011
443		

D.F. = (9-1)(2-1)

= 8

$\chi^2_{05} = 15.5$

$\chi^2_{01} = 20.09$

a difference in the distributions obtained before and after repolishing for ingot 18 sample number 4 and more definitely a difference for ingot 30 bottom sample. However, if the chi-square values for each size class interval are examined, in both cases the first class interval is seen to contribute a disproportionately large value to X^2. This interval has class limits of 0.386 - 0.546 μm, where detection and sizing errors are quite large (148) as the resolution limit for an oil immersion objective is between 0.2 μm (150, 153) and 0.5 μm (149, 152). The detection of particles in this size interval would also be expected to be very sensitive to polishing differences.

If this size interval is neglected in both samples and the χ^2 contingency tests again calculated, then the results presented in Tables 7-7 and 7-8 are obtained.

The significance tests now suggest no grounds for inferring a difference between distributions for the two samples examined. Thus decisions on non-reproducible sampling have to be moderated with a knowledge of the experimental errors inherent in the assessment technique.

When a different inclusion type and distribution was examined there was again an uncertainty in assessment of the first class interval frequencies for assessments

TABLE 7-7 INGOT 18, NUMBER 4, (SERIES 2)

1ST ASSESSMENT		ASSESSMENT AFTER REPOLISHING	
Obs Freq	Exp Freq	Obs Freq	Exp Freq
17	14.8207	57	59.1793
20	21.0294	95	83.9706
23	26.2367	108	104.7633
33	32.6457	130	130.3543
36	29.0406	109	115.9594
16	13.4188	51	53.5812
8	5.8081	21	23.1919
143		571	

$X^2 = 11.879$

D.F. = (7-1)(2-1)
= 6

$\chi^2_{05} = 12.592$

TABLE 7-8 INGOT 30, BOTTOM (SERIES 2)

1ST ASSESSMENT		ASSESSMENT AFTER REPOLISHING	
Obs Freq	Exp Freq	Obs Freq	Exp Freq
108	108.0524	101	100.9476
87	77.5496	63	72.4504
68	66.6926	61	62.3074
51	57.3867	60	53.6133
26	34.1218	40	31.8782
11	9.8229	8	9.1771
14	11.3739	8	10.6261
365		341	

X^2 = 9.459 D.F. = 6

χ^2_{05} = 12.59

before and after repolishing. The remainder of the distribution, however, showed no significant difference between the two assessments as can be seen from the Table 7-9.

As the distribution in this sample was a pseudo-distribution on a section plane of grain-boundary Type 11 sulphides, differences between one section and another, a few microns below, can be quite different. However, as this analysis reveals the section distributions obtained before and after repolishing will agree provided a large sample area is examined.

For representative assessments, therefore, both the area examined on the plane section and the frequency of occurrence of inclusions (i.e. N_A) need to be considered. The specification of a minimum number of inclusions to be examined or a minimum number of traverses to be conducted cannot be given. Instead, the particle distribution for each sample has to be initially determined (say after n traverses or mm^2) and adequate sampling then determined by testing this distribution against that obtained after n+1 traverses or mm^2, using a test such as the chi-square contingency test. When the calculated X^2 is not significant at the decision criterion (usually 5%) level, a representative sample can be

TABLE 7-9 8A2 (INDUSTRIAL)

TRAVERSE LENGTH = 192.18mm 1ST ASSESSMENT			TRAVERSE LENGTH = 98.93mm ASSESSMENT AFTER REPOLISHING		
Obs Freq	Exp Freq	X^2	Obs Freq	Exp Freq	X^2
14	19.7005	1.6495	20	14.2995	2.2725
60	58.5219	0.0373	41	42.4781	0.0514
34	33.6067	0.0046	24	24.3933	0.0063
86	89.8109	0.1617	69	65.1891	0.2228
34	39.4009	0.7403	34	28.5991	1.0199
81	77.6430	0.1451	53	56.3570	0.2000
36	30.7095	0.9114	17	22.2905	1.2557
25	22.5976	0.2554	14	16.4024	0.3519
13	11.0091	0.3600	6	7.9909	0.4960
383			278		

X^2 = 10.142 D.F. = 8

χ^2_{05} = 15.507

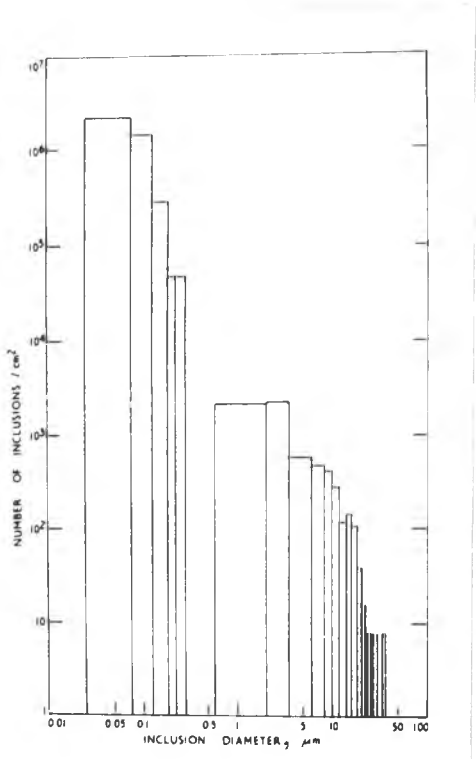

Fig. 7-1 Size distribution curve for the oxide inclusions in a Si - killed steel ingot (135).

considered to have been obtained. If the distribution of particle sizes has a broad range, assessment at a number of magnifications may be necessary to reduce resolution and sampling errors. It is obvious that this conclusion is of great practical significance in any assessment work and provides ground rules by which results can be compared with much greater confidence than was hitherto possible.

7.2 MATHEMATICAL REPRESENTATION OF SIZE-FREQUENCY DISTRIBUTION DATA

In a pioneering study of inclusion size distribution Bergh (135) showed that in seven samples out of ten from a 6 ton silicon killed ingot, between 90 and 119% of the chemically determined oxygen could be represented as particles in a size-frequency distribution such as in Fig. 7-1.

In such a distribution 98% (by number) of the inclusions are less than 0.2 μm in diameter, but these small particles, measurable only with the electron microscope, represent only 1 to 2% of the total oxygen content (ppm) in the steel.

Examination of Fig. 7-1 shows that the size-frequency

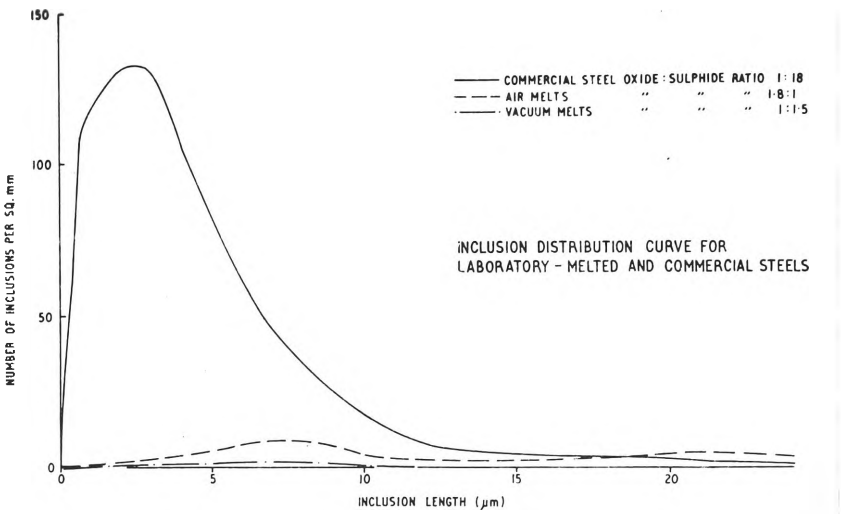

Fig. 7-2 Size-frequency distribution of stringer inclusions in hot rolled strip (202).

data measured with the optical microscope is the tail portion of a highly positively skewed distribution or hyperbolic curve. Sometimes the portion of the distribution sized with the optical microscope includes the mode of the distribution, as is shown in Fig. 7-2 which gives the size distribution of stringer sulphides and oxides in hot rolled strip (202). However, more often, as with Bergh's data, only the tail of the distribution is determined as shown in Table 7-10 taken from the work of Banks (142). This table gives the results of an assessment of two samples obtained at the billet stage from a semi-killed steel.

These distributions are section distributions as are most others discussed in inclusion studies (17, 57, 166, 203, 204) and have a range of $0 \leqslant y \leqslant y_u$; where y_u is the maximum section size $\leqslant x_u$, the maximum particle size in the sample. Most investigators (154, 159, 181, 182, 185, 205) who have studied spherical or ellipsoidal shaped particles have assumed $y_u = x_u$. This need not necessarily be so, as such equality will depend to some extent on the sampling technique. This is because large particles have a low frequency of occurence but a high probability of being sectioned. If the particles are non-spherical some orientations of the particle relative to the section plane will be such that although

TABLE 7-10 SIZE DISTRIBUTIONS OF TWO BILLET SAMPLES

Sample	Number of Inclusions in Size Ranges (μm)					
	1-15	15-30	30-45	45-60	60-75	>75
IK 49 (Dirty)	380	56	14	3	11	9
IK 57 (Clean)	166	13	8	1	3	0

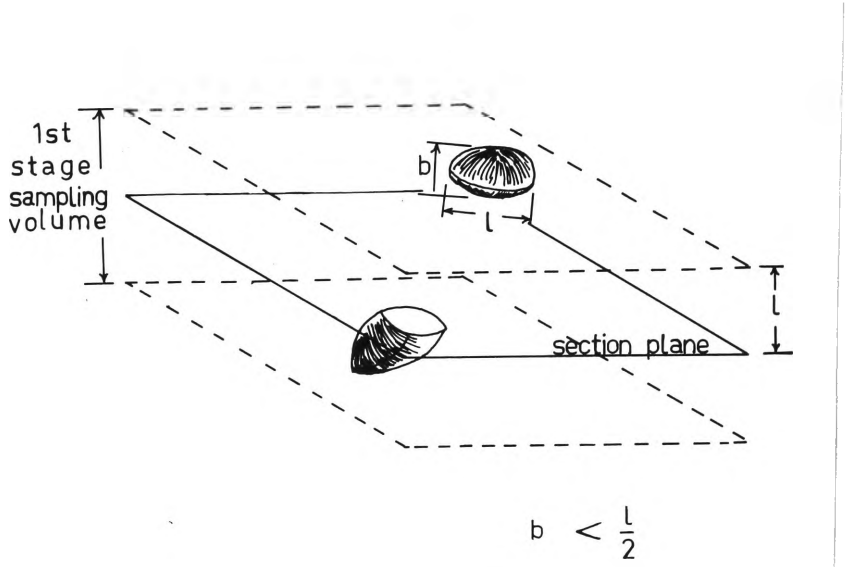

Fig. 7-3 Two pictorial examples of the influence of orientation on the probability of sectioning of oblate ellipsoids.

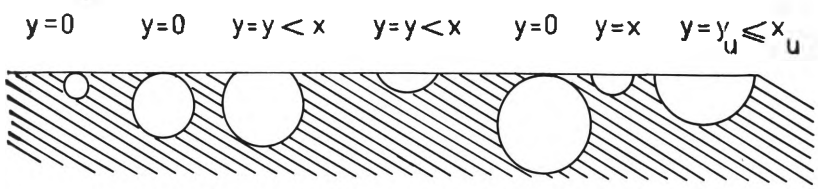

Fig. 7-4 Examples of possible sections obtained from a number of differently sized spheres.

these particles are within the first stage sampling volume, they may be orientated in such a way that they are not intersected. The other possibility is that they may be sectioned away from the plane of largest size. (Fig. 7-3)

The limits of the section distribution for spherical particles can be seen in Fig. 7-4. The lower limit of zero corresponds to the section plane where the particle is tangential to it.

If, as is common practice, inclusion section size distributions are to be assessed by the optical microscope, usually at one magnification (though procedures for using two magnifications have been proposed (124, 141)), the estimation of the spatial size distribution from this truncated data can be extremely poor unless a mathematical function is assumed to represent f(y) (206).

In accordance with the model derived in Section (6-7), the log-normal frequency function which has this range is:

$$f(y) = \frac{y_u}{y(y-y_u)\sigma\sqrt{2\pi}} \cdot \exp\left[-\frac{1}{2\sigma^2}\left\{\ln\left(\frac{y}{y-y_u}\right) - \ln\mu\right\}\right], \qquad (7\text{-}1\text{-}1)$$

$$0 < y < y_u$$

$$f(y) = 0, \qquad y \leq 0 \quad \text{or} \quad y \geq y_u$$

Equation (7-1-1) can be readily obtained from equation (6-3-1) if the variable X is replaced by $\frac{Y}{Y-y_u}$.

7.3 TESTING THE PROPOSED MODEL AND THE ASSUMPTION OF INCLUSION SHAPE

Both the lognormal section and spatial models proposed in sections 6-7 and 6-4 respectively were tested using size distributions obtained from samples from three ingots (of Series two heats) which had been deoxidized by aluminium. The shape approximation which best represents the shape of alumina particles was also determined. The size distribution was assessed by the technique given in Section (5-6). Once this is known the volume fraction (V_v) and surface area per unit volume (S_v) of the particles can then be determined if an appropriate shape is assumed. S_v and V_v were also determined using standard quantitative metallographic techniques (159) which do not depend on particle shape. The shape assumption was then adjusted to give agreement between the two sets of S_v and V_v values.

As both the section distributions and spatial distributions are defined as members of the family of

log-normal distribution functions an appropriate method of estimating the parameters of the spatial distribution from the section distribution is to use their moments. Although, as shown by Heyde (207) the log-normal distribution is not determined by its moments; other distributions having the same moments as that of the log-normal distribution are for most practical purposes indistinguishable from that of the log-normal.

The general equation relating the moments of both distributions can be expressed as (180, 187, 206)

$$E(Y^i) = \frac{k_i \, E(X^{i+1})}{E(X)} \qquad (7\text{-}3\text{-}1)$$

For the case of spherical particles (208):

$$k_i = \tfrac{1}{2}\sqrt{\pi} \cdot \frac{\Gamma\left[\tfrac{1}{2}(i+2)\right]}{\Gamma\left[\tfrac{1}{2}(i+3)\right]} \qquad (7\text{-}3\text{-}2)$$

and for the general ellipsoidal case (165):

$$k_i = \frac{\tfrac{1}{2}\sqrt{\pi}\,\Gamma\left[\tfrac{1}{2}(i+2)\right]}{\Gamma\left[\tfrac{1}{2}(i+3)\right]} \cdot \frac{\lambda_i}{\lambda_o} \qquad (7\text{-}3\text{-}3)$$

where λ_i and λ_o are functions of the eccentricities, e_2 and e_3.

As variate X is log-normally distributed with parameters μ and σ, Equation (7-3-1) becomes:-

$$E(Y^i) = k_i \frac{\mu^{i+1} e^{\frac{1}{2}(i+1)^2\sigma^2}}{\mu e^{\frac{\sigma^2}{2}}}$$

$$= k_i \mu^i e^{\frac{i(i+1)}{2}\sigma^2} \qquad \text{(7-3-4)}$$

The parameters (μ, σ) of the spatial distribution can thus be estimated from the first two moments of the section distribution. Solving simultaneously the two equations obtained from (7-3-4) for i = 1 and 2, the following equations are obtained:

$$\ln \hat{\mu} = 2.3025851\ (4 \log E(Y) - 3/2 \log E(Y^2) + 0.1555035)$$
$$\hat{\sigma}^2 = 2.3025851\ (\log E(Y^2) - 2 \log E(Y) - 0.0337289) \qquad \text{(7-3-5)}$$

Then using estimates $\hat{\mu}$ and $\hat{\sigma}$, the estimates of $E(Y^3)$ and $E(Y^4)$ can be calculated and compared with those determined assuming the variate, Y, to be log-normally distributed with parameters μ, σ, and y_u.

7.4 TESTING L-N MODELS FOR SECTION AND SPATIAL DISTRIBUTIONS

The adequacy of the log-normal model as a description of the section distribution can be tested with the well known chi-square goodness of fit test. The computer program described in Appendix 4 yields the "best fit" three parameter log-normal distribution by minimizing the chi-square value. If this value is less than the chi-square tabulated value for the specified degrees of freedom and criterion level, the model can be considered adequate.

The results of the computer analysis of a number of samples from Series 2 ingots are given in Table 7-11.

All samples (with the exception of I18 No.5 and I30B) have X^2 values which are not only less than the tabulated value of chi-square at the 5% level but are also less than the tabulated value at the more stringent level of 10%. Thus it can be concluded that the three parameter log-normal distribution provides a very adequate representation of the inclusion section distributions in these samples.

The first four moments of these best fit three parameters log-normal distributions are also calculated

TABLE 7-11 RESULTS OF COMPUTER FIT FOR SERIES 2 SAMPLES

INCLUSION TYPE (SAMPLE CODE)	MOMENTS OF FITTED DISTRIBUTION 1ST	2ND	3RD	4TH
Random Alumina				
(I22 No 1)	1.2527	2.1279	4.6809	12.760
(I22 No 6 Ob)	1.1862	2.9538	12.057	67.463
(I18 No 5R)	2.5317	8.5886	37.752	207.62
(I18 No 4)	2.5238	9.3095	43.098	230.30
(I18 No 8R Ob)	2.8125	14.162	97.836	811.37
(I22 No 6 Ob)	1.1862	2.9538	12.057	67.463
(I30 M)	0.15502	0.25835	1.3674	11.870
(I30 T)	0.70923	1.6402	7.5177	50.048
(I30 B)	0.14938	0.30931	2.2781	28.338
Alumina Clusters				
(I22 No 1C)	1.3682	2.3077	4.5917	10.408
Oxy-Sulphide				
(20 & 2T)	3.4939	15.974	93.562	685.52
Type 111 Sulphides				
(I27 Top Ob)	1.7120	4.8965	19.348	93.949

MOMENTS CALCULATED FROM β AND α				GOODNESS OF FIT OF SECTION DISTRIBUTION		
1ST	2ND	3RD	4TH	X^2	χ^2_{05}	DEGREES OF FREEDOM
1.2527	2.1279	4.7207	13.465	4.872	7.815	3
1.1863	2.9538	14.8723	149.017	5.796	9.488	4
2.5317	8.5886	37.603	209.171	10.783	11.070	5
2.5239	9.3093	48.340	347.844	4.217	5.991	2
2.8125	14.162	122.97	1812.5	8.666	14.067	7
1.1863	2.9538	14.872	149.017	5.796	9.488	4
0.15502	0.25835	4.4582	784.18	10.426	14.067	7
0.70923	1.6402	11.9131	267.516	4.524	11.070	5
0.14938	0.30931	8.5506	3106.603	9.324	11.070	5
1.3682	2.3077	4.6212	10.818	0.862	5.991	2
3.4938	15.974	92.046	658.057	2.445	7.815	3
1.7120	4.8965	22.532	164.24	8.031	11.070	5

with the aid of the computer. The first two moments are then substituted in Equ. (7-3-5) to calculate parameters $\hat{\mu}$ and $\hat{\sigma}$. The estimates, $\hat{\mu}$ and $\hat{\sigma}$, are the mean and standard deviation respectively of the spatial distribution of spheres which When intersected by a random plane would give the observed section distribution.

For ellipsoidal shaped particles these parameters do not define the two parameter log-normal function which describes their spatial distribution. Nevertheless these parameters can be used to determine the required function as the moments of the spherical spatial distribution are proportional to the moments of the spatial distribution of ellipsoids, i.e. Equ. (7-5-8). In this equation the shape factor, $\frac{\lambda_{n-1}}{\lambda_{n-1}}$, is a constant for the estimated values of the eccentricities e_2 and e_3.

To examine the adequacy of the fit of the two parameter log-normal model for the spatial distribution it is only necessary to show that the moments of the section distribution calculated from $\hat{\mu}$ and $\hat{\sigma}$ using Equ. (7-3-4) are equal to those of the best fit section distribution.

The moments determined from the fitted distribution and those calculated from $\hat{\mu}$ and $\hat{\sigma}$ are also given in Table 7-11 for a number of Series 2 ingot samples.

Four of the eleven samples listed in the table show very good matching of the 3rd and 4th moments, and so confirm the two parameter log-normal distribution as an adequate representation of the spatial distribution of inclusions. The remaining seven samples, however, show varying degrees of mismatch especially in the 4th moment.

These differences in the moments can be shown simply to result from the adoption of an infinite upper size limit to the inclusion spatial distribution when in reality the distribution has a finite limit. This is so because the value of third, fourth and higher moments of asymmetrical long-tailed distributions such as the two parameter log-normal, may depend very much on contributions from the tail of the distribution (210).

In order to assess the magnitude of the decrease in the third and fourth moments which can be expected when the upper limit of the distribution has a finite value, two studies were conducted.

Firstly data from plane 3 of Drapal and Horalek's assessment of cementite particles was computer fitted to three parameter log-normal distributions with upper size limits of 54.817 and 5000 μm. The moments calculated by the computer are as follows:

MOMENTS	DISTRIBUTION $y_u = 5000\ \mu m$	DISTRIBUTION $y_u = 54.817\ \mu m$
1ST	9.2806	9.2250
2ND	100.85	98.883
3RD	1283.0	1212.5
4TH	19104	16754

It is clear from these results that the 12% increase in the fourth moment of the longer tailed distribution has come from the 55 to 5000 tail portion of the distribution. However, some of the differences in the moments recorded in Table 7-11 are considerably more than 12%. To assess the magnitude of these differences, the third and fourth moments of two parameter log-normal distributions which have the same first two moments of the fitted section distributions were determined. These values are given in Table 7-12. It is clearly evident from this table that a finite upper limit to the size range decreases the magnitude of both the third and fourth moments. Also if the values of the third and fourth moments of the two parameter distribution in Table 7-12 are compared with those of the distribution calculated from $\hat{\mu}$ and $\hat{\sigma}$ in Table 7-11, they can be seen to be of similar magnitude.

TABLE 7-12 MOMENTS OF THE SECTION DISTRIBUTION IN A TWO OR THREE PARAMETER FORM

SAMPLE CODE	MOMENTS OF FITTED 3 PARAMETER L-N DISTRIBUTION				MOMENTS OF 2 PARAMETER L-N DISTRIBUTION			
	1ST	2ND	3RD	4TH	1ST	2ND	3RD	4TH
I22 No 1	1.2527	2.1279	4.6809	12.760	1.2527	2.1279	4.9012	15.309
I18 No 5R	2.5317	8.5886	37.752	207.62	2.5317	8.5886	39.043	237.81
I18 No 4	2.5238	9.3095	43.098	230.30	2.5238	9.3095	50.192	395.5
I18 No 8 Ob	2.8125	14.162	97.836	811.37	2.8125	14.162	127.66	2060.6
I22 No 6 Ob	1.1862	2.9538	12.057	67.463	1.1862	2.9538	15.439	169.39
I30 M	0.15502	0.25835	1.3674	11.87	0.15502	0.25835	4.6291	891.7
I30 T	0.70923	1.6402	7.5177	50.048	0.70923	1.6402	12.368	304.16
I27 T Ob	1.7120	4.8965	19.348	93.949	1.7120	4.8965	23.472	188.37

Thus the large mismatching of moments observed in Table 7-11 can be attributed, not to a defect in the general model, but to the restrictions placed in the number of parameters used to specify the spatial distribution.

In reality the size range of the spatial distribution is limited at both ends, however, as the moments of such a distribution cannot be expressed analytically (192, 199) the upper limit was assumed infinite in order to obtain a more tractable analysis.

7.5 ESTIMATION OF INCLUSION SHAPE

As was noted earlier, the volume fraction, V_v, and surface area per unit volume, S_v, of inclusions in a volume of metal can be calculated from the section distribution providing the shape of the inclusions are known. Furthermore as V_v and S_v can be determined independently by quantitative metallographic methods, these two parameters can be used to determine estimates of the shapes of non-spherical inclusions.

As the relationship between V_v and S_v and the moments of the spatial distribution have already been determined (165), it only remains to derive from these expressions the relationship with the moments of the

section distribution.

The relationship between V_v and the third moment of the spatial distribution is as follows (165):

$$V_v = \frac{\pi}{6} \cdot N_v \cdot E(X^3) \qquad (7\text{-}5\text{-}1)$$

and as (165):

$$N_v = \frac{N_A}{E(X)\,\lambda_o} \qquad (7\text{-}5\text{-}2)$$

Then:

$$V_v = \frac{\pi}{6} \cdot N_A \cdot \frac{E(X^3)}{\lambda_o\, E(X)} \qquad (7\text{-}5\text{-}3)$$

The problem, therefore, is to express the ratio $\frac{E(X^3)}{E(X)}$ in terms of the moments of the section distribution, $E(\gamma^i)$.

Initially, if the particle size is defined as the geometric mean of the diameters of an ellipse which best fits the section, or the ellipsoid which best fits the particle, such a relationship can be obtained via

an intermediate relationship.

Wicksell (165, 180) showed that the distribution of the geometric mean diameters of the elliptical sections cut by a plane passing through the centre of the ellipsoids and also parallel to the section plane, could be obtained from the distribution of the geometric mean section diameters using Equ. (7-3-1) for spherical particles. Also this relationship is valid irrespective of the form of the distribution of eccentricities and the directions of the axes of the ellipsoids (165).

Thus, if z is the geometric mean diameter of the section through the particle centre parallel to the section, then:

$$E(\gamma^i) = \frac{E(Z^{i+1})}{E(Z)} \cdot k_i \qquad (7\text{-}5\text{-}4)$$

and:

$$E(\gamma^{-1}) = \frac{k_{-1}}{E(Z)} \qquad (7\text{-}5\text{-}5)$$

As $E(Z^o) = 1$

Whilst from Equ (7-3-1):

$$E(Y^{-1}) = \frac{k_{-1}\,\lambda_{-1}}{E(X)\,\lambda_o} \qquad (7\text{-}5\text{-}6)$$

Equating Equ. (7-5-5) and (7-5-6) gives:

$$E(X) = E(Z)\,\frac{\lambda_{-1}}{\lambda_o} \qquad (7\text{-}5\text{-}7)$$

Substituting Equ. (7-5-7) and (7-5-4) into Equ. (7-3-1) and rearranging yields:

$$E(X^{i+1}) = E(Z^{i+1}).\,\frac{\lambda_{-1}}{\lambda_i} \qquad (7\text{-}5\text{-}8)$$

Thus:

$$\frac{E(X^3)}{E(X)} = \frac{E(Z^3).\,\dfrac{\lambda_{-1}}{\lambda_2}}{E(Z).\,\dfrac{\lambda_{-1}}{\lambda_o}} = \frac{E(Z^3).\,\lambda_o}{E(Z).\,\lambda_2} \qquad (7\text{-}5\text{-}9)$$

Also, from Equ. (5-12-4):

$$\frac{E(Z^3)}{E(Z)} = \frac{E(Y^2)}{k_2} \qquad (7\text{-}5\text{-}10)$$

Thus the relationship sought becomes:

$$\frac{E(X^3)}{E(X)} = \frac{E(\gamma^2)}{k_2} \cdot \frac{\lambda_o}{\lambda_2} = \frac{3.\ E(\gamma^2)}{2} \cdot \frac{\lambda_o}{\lambda_2} \quad \text{(7-5-11)}$$

And as $\lambda_2 = 1$, then:

$$V_v = \frac{\pi}{4} \cdot N_A \cdot E(\gamma^2) \quad \text{(7-5-12)}$$

The extression relating S_v to the moments of the section distribution are similarly derived, as (165):

$$S_v = N_v \cdot \pi \cdot E(X^2)\,\lambda \quad \text{(7-5-13)}$$

$$\text{or, } S_v = N_A \cdot \pi \cdot \frac{E(X^2)}{E(X)} \cdot \frac{\lambda}{\lambda_o}$$

Thus, the problem is again to express the ratio $\frac{E(X^2)}{E(X)}$ in terms of the moments $E(\gamma^i)$. So again from Equ. (7-5-8) the following is obtained.

$$\frac{E(X^2)}{E(X)} = \frac{E(Z^2)\cdot \frac{\lambda_{-1}}{\lambda_1}}{E(Z)\cdot \frac{\lambda_{-1}}{\lambda_0}}$$

$$= \frac{E(Z^2)\cdot \lambda_0}{E(Z)\cdot \lambda_1} \qquad \text{(7-5-14)}$$

And from Equ. (7-5-4):

$$E(\Upsilon) = \frac{E(Z^2)\cdot k_1}{E(Z)}$$

$$= \frac{E(Z^2)\cdot}{E(Z)} \frac{\pi}{4} \qquad \text{(7-5-15)}$$

Thus substituting $\frac{E(X^2)}{E(X)}$ in Equ. (7-5-13)

using Equs. (7-5-14) and (7-5-15) yields:

$$S_v = \frac{4\cdot N_A \cdot E(\Upsilon)\cdot \lambda}{\lambda_1} \qquad \text{(7-5-16)}$$

where λ is a function of the eccentricities and is defined as (165):

$$\lambda(e_2, e_3) = \left[(1 - e_2^2)\ (1 - e_3^2)\right]^{\frac{1}{6}} \int_0^1 \int_0^{\sqrt{1-y^2}} \frac{\sqrt{1 + e_3^2 y^2 + e_3^2 d^2}}{\sqrt{1 - y^2 - d^2}}\ dy\,dd$$

(7-5-17)

Thus from Equ. (7-5-12) the volume fraction of ellipsoidal shaped particles can be determined without any specification of axial lengths, only the second moment of the section distribution and the number of particles per unit area of the section are required. Only when the surface area per unit volume is sought does the shape of the particles need specification and hence only with this parameter can shape assumptions be assessed.

7.6 ELLIPSOIDAL APPROXIMATION OF THE SHAPE OF ALUMINA

The method of equating the quantitative metallographically determined parameters S_v and V_v to the moments of the section distribution discussed in the previous section, involving Equs. (7-5-12) and (7-5-16), can be used to determine an ellipsoidal shape approximation for alumina particles providing that the shape factors λ_n can be

evaluated. These factors are functions of the eccentricities e_2 and e_3 of the ellipsoids.

If only oblate ellipsoids of revolution are considered ($e_2 = e$ and $e_3 = o$) but of varying axial ratios, then the calculation of λ_ns are greatly simplified. Now all that is required are the determinations of the average values of λ_ns from the distribution of e. The problem thus is to determine the distribution of e from the apparent distribution of eccentricities, ϵ, of the section ellipses. Fortunately, the relationship between these two distributions has been derived by Wicksell (165), which for oblate ellipsoids is:

$$g(\epsilon') = \frac{1}{\delta_o} \epsilon' \sqrt{1+\epsilon'^2} \int_{\epsilon'}^{\infty} \frac{F(e')(1+e'^2)^{-\frac{1}{3}}\, de'}{e' \sqrt{e'^2 - \epsilon'^2}} \qquad (7\text{-}6\text{-}1)$$

where:

$g(\epsilon') = f(\epsilon)(1+\epsilon'^2)^{\frac{3}{2}}$

$F(e') = F(e)(1+e'^2)^{\frac{3}{2}}$

$f(\epsilon)$ = distribution of apparent section eccentricities

$F(e)$ = distribution of eccentricities and

$$\epsilon' = \frac{\epsilon}{\sqrt{1-\epsilon^2}} \quad , \quad e' = \frac{e}{\sqrt{1-e^2}}$$

An example of the proceedure for obtaining F(•) from f(ϵ) is given in Appendix 5.

The samples assessed for the section distributions of alumina particles were from ingots of the Series 2 heats. These heats involved both copper and iron melts deoxidized with aluminium. Heat details are given in Appendix 1. The values for the average or gross properties of the particle distribution, V_v and S_v, calculated by both methods are given in Table 7-13.

It can be seen from this table that the mean eccentricities of the samples varied between 0.82 and 0.91. The S_v values calculated employing the mean values of λ_n in Equ. (7-5-16) are in good agreement with those values of S_v determined from the P_L count.

The volume fractions calculated using Equ. (7-5-12), however, showed some disagreement with the quantitative metallographically determined values. Also these differences in the two determinations seem to be independent of the goodness of fit of the section distribution or the percentage of the fitted distribution which covers the assessed size range. As the V_v value for sample I_{22} No. 1 was more than twice the standard error from the mean of the point count, it can be concluded that the inclusion distribution in this sample was not

TABLE 7-13 ESTIMATES OF S_v AND V_v AS OBTAINED BY QUANTITATIVE METALLOGRAPHY AND FROM SIZE-FREQUENCY DATA ASSUMING PARTICLES ARE OBLATE ELLIPSOIDS OF REVOLUTION WITH VARYING AXIAL RATIO

QUANTITATIVE METALLOGRAPHY							e = 0.85	e=0.87	e=0.90	GOODNESS OF FIT		% EXP.	SAMPLE CODE	INGOT POSITION *
V_v %		S_v		V_v	$\bar{e}$	S_v	S_v	S_v	S_v	X^2	$\chi^2_{.05}$			
MEAN	Sd ER	MEAN	Sd ER	%										
0.0529	0.0157	1.493	0.223	0.0545	0.833	1.305	1.261	1.276	1.307	4.524	11.070	45.9	I30	TOP
0.0662	0.0142	1.919	0.246	0.0599	0.838	1.974	1.916	1.944	1.992	10.426	14.067	8.7	I30	MIDDLE
0.1266	0.0288	2.887	0.332	0.0869	0.913	2.997	2.749	2.768	2.836	4.872	7.815	94.9	I22	1
0.0417	0.0143	0.551	0.095	0.0383	0.816	0.569	0.554	0.560	0.575	4.217	5.991	92.8	I18	4
0.0625	0.0131	1.279	0.161	0.0661	0.884	1.115	1.040	1.052	1.079	10.783	11.070	99.6	I18	5R

NOTE: S_v IN mm^2/mm^3

* SEE FIG. 7-5 TO 7-7, PAGE 158

uniform. The distribution of inclusions has differed from one plane of polish to another. An observation which has been noticed by other investigators (114, 146).

The surface area per unit volume for three particular values of e, 0.85, 0.87 and 0.90, are also given in Table 7-13, to show the variation of S_v with e.

From the results present in Table 7-13 it can be concluded that a reasonable approximation for the hexagonal plate morphology of alumina (106, Fig. A-7 , Appendix 3) would be an oblate ellipsoid of revolution having a mean eccentricity of 0.85 (the mean value of e).

The general overall agreement for both V_v and S_v calculated by both methods is in itself significant, as other attempts recorded in the literature have not been so successful (211). Most probably this has been so because all previous analyses have employed another assumption to aid computation, namely that all inclusions assessed have the same axial ratio. Also this ratio was determined only by an approximate procedure (159).

7.7 SIMPLIFIED APPROACH FOR ESTIMATING THE SPATIAL DISTRIBUTION

As the assumption of oblate ellipsoids of revolution for alumina particles was found to be adequate in the previous section, the "size" of the inclusions can also be defined as the major length of the section. With this definition the transformation of moments of the section distribution to that of the spatial distribution is achieved without requiring any knowledge of the distribution of eccentricities of the ellipsoids.

In other words the shape factors required (k_is) are those used for transforming moments of a distribution of spheres, and Equ. (7-3-1) can be redefined as:

$$\frac{E(S^{i+1})}{E(S)} = \frac{E(Y_o^i)}{k_i} \qquad (7\text{-}7\text{-}1)$$

where S = major diameter of oblate ellipsoid

and Y_o = major diameter of section ellipse

The relationship between S_v and V_v and the moments $E(Y_o^i)$ can be readily derived from Equs. (7-7-1), (7-5-12) and (7-5-16). In order to complete these derivations the following relationships are also required:

Equ. (7-5-2) is redefined as:

$$N_v = \frac{N_A}{E(S)E(k_o)} \qquad \text{(7-7-2)}$$

where, for oblate ellipsoids in which e varies independently of S:

$$E(k_o) = E\left(\tfrac{1}{2}\left[\sqrt{1-e^2} + \frac{1}{e} \cdot \arcsin e\right]\right) \qquad \text{(7-7-3)}$$

and the relationship between the moments of the geometric mean diameter of the ellipsoids and the moments of the major diameter of oblate ellipsoids (165):

$$E(X^i) = E(S^i)\, E\left[(1-e^2)^{\frac{i}{2}}\right] \qquad \text{(7-7-4)}$$

When the ellipsoids have a constant form Equ. (7-7-4) becomes:

$$E(X^i) = E(S^i)(1-e^2)^{\frac{i}{2}} \qquad \text{(7-7-5)}$$

Using Equs. (7-7-1) to (7-7-4) together with Equs. (7-5-1) and (7-5-13) the following relationships

can be derived:

$$V_v = \frac{\pi N_A E(Y_o^2) E(1-e^2)^{\frac{1}{2}}}{4 \cdot E(k_o)} \qquad (7-7-6)$$

for the volume fraction of inclusions and:

$$S_v = \frac{4N_A E(Y_o) E(1-e^2)^{\frac{1}{3}} E(\lambda)}{E(k_o)} \qquad (7-7-7)$$

for the surface area per unit volume of inclusions.

If the particles are approximated by ellipsoids of revolution of constant form, then $(1-e^2)^{\frac{1}{2}}$, $(1-e^2)^{\frac{1}{3}}$, λ and k_o replace the mean values listed in the above equations.

To examine the adequateness of this analysis, the samples previously discussed in section (7-6) were re-examined accordingly. A best fit three parameter log-normal distribution wasobtained to the distribution of largest section lengths. The results of the goodness of fit tests and calculated values of V_v and S_v for various values of e are given in Table 7-14.

It is again evident that the three parameter

TABLE 7-14 ESTIMATES OF S_v AND V_v AS OBTAINED BY QUANTITATIVE METALLOGRAPHY AND FROM SIZE-FREQUENCY DATA ASSUMING PARTICLES ARE OBLATE ELLIPSOIDS OF REVOLUTION AND CONSTANT AXIAL RATIO

SAMPLE CODE	POSITION *	QUANTITATIVE METALLOGRAPHY V_v	QUANTITATIVE METALLOGRAPHY S_v (mm^2/mm^3)	e	V_v	S_v (mm^2/mm^3)	GOODNESS OF FIT X^2	GOODNESS OF FIT $\chi^2_{.05}$	% EXPLAINED
I30	TOP	0.000529	1.493	0.833	0.000526	1.185	4.646	12.592	35.01
	Sd ER	0.000157	0.223						
I30	MIDDLE	0.000662	1.919	0.838	0.000546	2.079	9.002	12.592	0.32
	Sd ER	0.000142	0.246						
I22	1	0.001266	2.887	0.913	0.001211	3.066	14.894	12.592	84.17
	Sd ER	0.000288	0.332						
I22	6	0.000208	0.505	0.884	0.000194	0.591	5.796	9.488	74.95
	Sd ER	0.000087	0.086						
I18	4	0.000417	0.551	0.816	0.000397	0.533	2.923	7.815	95.52
	Sd ER	0.000143	0.095						
I18	5R	0.000625	1.279	0.884	0.000799	1.170	13.196	18.307	99.31
	Sd ER	0.000131	0.161						

* SEE FIG. 7-5 TO 7-7, PAGE 158

TABLE 7-14 (CONT)

SAMPLE CODE	POSITION	e = 0.85 V_v	e = 0.85 S_v (mm^2/mm^3)	e = 0.87 V_v
I30	TOP	0.000540	1.164	0.000511
I30	MIDDLE	0.000558	2.051	0.000527
I22	1	0.00159	3.231	0.001498
I22	6	0.000221	0.606	0.000209
I18	4	0.000391	0.517	0.000369
I18	5R	0.000949	1.196	0.000897

	e = 0.90		SPHERICAL (e = 0)	
S_v (mm^2/mm^3)	V_v	S_v (mm^2/mm^3)	V_v	S_v (mm^2/mm^3)
1.143	0.000458	1.109	0.000883	1.421
2.015	0.000473	1.954	0.000911	2.505
3.175	0.001345	3.079	0.002592	3.946
0.595	0.000188	0.577	0.000362	0.739
0.508	0.000331	0.493	0.000639	0.632
1.167	0.000805	1.139	0.001551	1.461

log-normal function is a good representation of the section distribution, as all samples, except I22 No 1, have X^2 less than the tabulated value of chi-square at the 10% significance level. Even for I22 No 1, X^2 is less than $\chi^2_{0.02} = 16.622$ and hence smaller than the tabulated χ^2 for the 1% significance criterion level.

It should be noted that considerable disagreement exists amongst statisticians as to what level of significance should lead to a rejection of the hypothesis that there is no difference between the two distributions being tested. For example, Kottler (201) used the conservative 10% level, while Hald (212) recommended the more commonly employed criterion level of 5%, but the less stringent level of 1% is also in common use (201, 213).

It can be concluded therefore that the log-normal distribution model is also a possible description of sample I22 No 1, but the confidence to be put on the fit will obviously need to be gauged from other tests such as the relative agreement between distribution and quantitative metallographic estimates of S_v and V_v.

A comparison of the S_v and V_v values calculated from both methods indicate that the agreement between these estimates for sample I22 No 1 is as good as that

obtained for the other samples listed in Table 7-14. In this table the V_v and S_v values are calculated from Equs. (7-7-6) and (7-7-7) respectively, using mean values of the shape factors calculated from the distribution of eccentricities.

Also included in Table 7-14 are the values of V_v and S_v calculated assuming oblate ellipsoids of constant form, e = 0.85, 0.87 and 0.90, as well as for the case of spherical particles, e = o. From the inspection of these results it is obvious that the assumption of spherical shaped particles would result in large systematic errors in both S_v and V_v for the samples studied.

As Equs. (7-7-6) and (7-7-7) both contain terms involving e, then both S_v and V_v can be used to determine the ellipsoid shape which best fits the alumina particles. If the various values of S_v and V_v are compared in Table 7-14 it can be concluded that good estimates of S_v and V_v were obtained from Equs. (7-7-6) and (7-7-7) using shape parameters calculated from the distribution of eccentricities. The results of these calculations and those of Section (7-6), therefore, support the representation of alumina by oblate ellipsoids of revolution.

Thus in subsequent calculations of samples containing alumina particles the shape approximation used will be

oblate ellipsoids of revolution with $\bar{e} = 0.85$.

7.8 EXAMINATION OF DIFFERENCES BETWEEN ALUMINA DISTRIBUTIONS

The usefulness of expressing the spatial distribution of inclusions in a given volume of metal by a distribution function becomes readily apparent when comparisons of distributions are required. The two parameter log-normal function is completely described by its parameters μ and σ, and so testing for similarity between two such distributions requires only the parameters to be tested.

This testing procedure is both simpler and more efficient than any method involving visual comparisons of tabulated data or graphs. It should be noted that contemporary investigators (68, 114, 135, 136, 144, 166) still employ these latter methods, in spite of the fact that none of these methods can measure the degree of difference between distributions or determine whether the apparent difference, if present, is a real difference or only resulting from random variability in the sampling technique.

The significance tests for comparing normal distributions can also be employed for comparisons of log-normal distributions, since the former distribution can be

obtained from the latter by a simple transformation (212). This is yet another advantage of employing the log-normal function for describing the spatial distribution of inclusions.

The parameters of the transformed normal distribution which are used in the significance tests are $\ln \mu$ and σ^2, the mean and variance respectively. Naturally, before the standard t-test for comparison of means can be applied, the equivalence of variances must be tested, which involves the application of the F test. As both of these tests are standard procedures in statistical analysis they will be dealt with as such. However, as the analysis of some samples in the present work required modifications of these tests, and since such modifications are not common practice they will be given special mention.

7.8.1 Testing Variances of Spatial Distributions

The variances to be tested are those of the normal distributions obtained from the transformation of the log-normal spatial distributions, assuming the alumina particles to be oblate ellipsoids with $\bar{e} = 0.85$, and the particle size defined by the major axes of the ellipsoid.

In order to apply the F test some measure of the

sample size is required for each distribution tested. The original number of particles sized in each assessment cannot be used for this purpose as this is only a measure of the number of particles per unit area of section. Rather the sample size that is required for testing spatial distributions is the number of particles per unit volume, N_v. This quantity was calculated for each sample to be tested by using Equ. (7-6-2), where k_o was determined for $e \simeq 0.85$.

The calculated values of F, F_{CAL}, together with the tabulated values of F at the 5% significance level for the samples tested are given in Table 7-15. When both f_1, and f_2 were greater than 30 the approximate formula was used (212) to estimate $F_{0.05}$:

$$\log F_{0.05} \approx \frac{1.4287}{\sqrt{h - 0.95}} - 0.681 \left[\frac{1}{f_1} - \frac{1}{f_2} \right] \qquad (7\text{-}8\text{-}1)$$

where $\frac{1}{h} = \frac{1}{2}\left[\frac{1}{f_1} + \frac{1}{f_2} \right]$

The large value of the degrees of freedom

TABLE 7-15 RESULTS OF F TEST

SAMPLE CODES	INGOT POSITIONS	F_{CAL}
I18 No 4 - I18 No 5R	Bottom - Bottom	1.443
I18 No 8R - I18 No 4	Top - Bottom	1.180
I18 No 8R - I18 No 5R	Top - Bottom	1.702
I22 No 6 - I22 No 1	Top - Bottom	1.079
I22 No 1 - I22 No 1C	Bottom - Bottom	1.652
I30 B - I30 T	Bottom - Top	1.267
I30 M - I30 T	Middle - Top	3.535
I30 M - I30 B	Middle - Bottom	2.791
I27 T - I27 B	Top - Bottom	7.810

$F_{0.05}$	DEGREES OF FREEDOM		TEST OF MEANS REQUIRED
	f_1	f_2	
1.871	22	31	t
1.773	325	22	t
1.609	325	31	Modified t
1.225	153	594	t
1.314	594	93	Modified t
1.063	2364	3636	Modified t
1.039	1,995,311,529	3636	Modified t
1.049	1,995,311,529	2364	Modified t
1.116	7684	281	Modified t

for sample I30 M evident in Table 7-15 is a result of the large magnitude of N_A from which N_V and the degrees of freedom are estimated. The basic cause, however, is that only a small proportion of the fitted section distribution falls within the size range of the assessed data. The mode, median and mean of the estimated spatial distribution for sample I30 M, 0.0001, 0.03 and 0.4 Å respectively, are all less than the critical nucleus size of approximately 12Å calculated from Equ. (1-3). As the critical nucleus size is calculated from the homogeneous nucleation theory it should represent the smallest size possible in the Cu-Al_2O_3 system. The fitted section size distribution is, therefore, considered to be in error. Problems experienced in the fitting of the three parameter log-normal distribution to assessment data are discussed fully in Appendix 4.

In only three comparisons of variances in Table 7-15 was a non-significant result obtained, and hence only in these cases can the t test be applied. For the remaining comparisons a modification of the t test was required.

7.8.2 Comparison of Means of Spatial Distribution

To test for equivalence of means when the variable, t^1 given as (212):

$$t^1 = \frac{X_1 - X_2}{\sqrt{\frac{S_1^2}{n_1} + \frac{S_2^2}{n_2}}} \qquad (7\text{-}8\text{-}2\text{-}1)$$

is distributed approximately as t with degrees of freedom, f, given by:

$$f = \frac{f_1 f_2}{f_2 C^2 + f_1 (1-C^2)} \qquad (7\text{-}8\text{-}2\text{-}2)$$

where

$$C = \frac{\frac{S_1^2}{n_1}}{\frac{S_1^2}{n_1} + \frac{S_2^2}{n_2}} \qquad (7\text{-}8\text{-}2\text{-}3)$$

When f_1 and f_2 are both greater than 30 Equ. (7-8-2-1) is a good approximation to the t test (212).

The results of tests for equivalence of means are

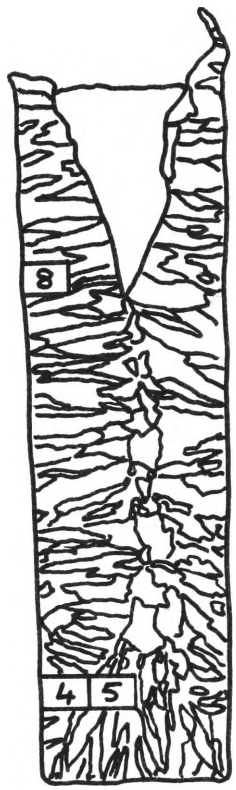

Fig 7-5 Diagrammatic representation of the macrostructure and sampling positions in Ingot 18 (copper).

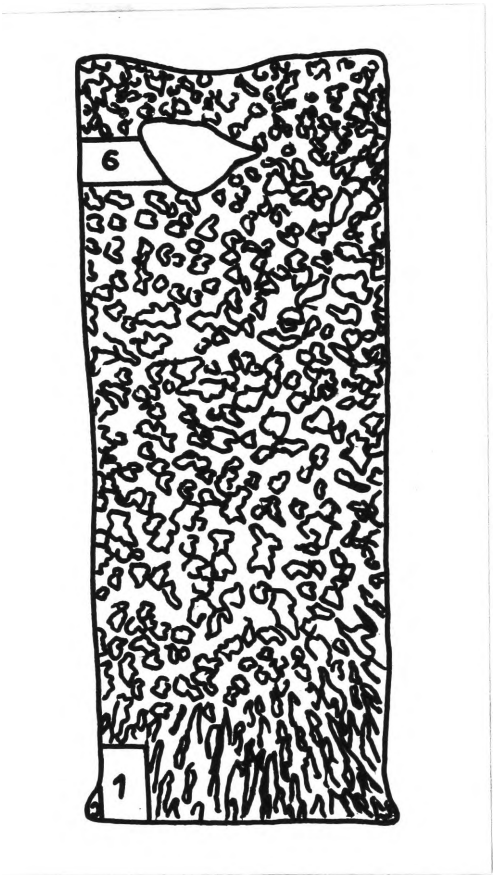

Fig. 7-6 Diagrammatic representation of the macrostructure and sampling positions in Ingot 22 (iron).

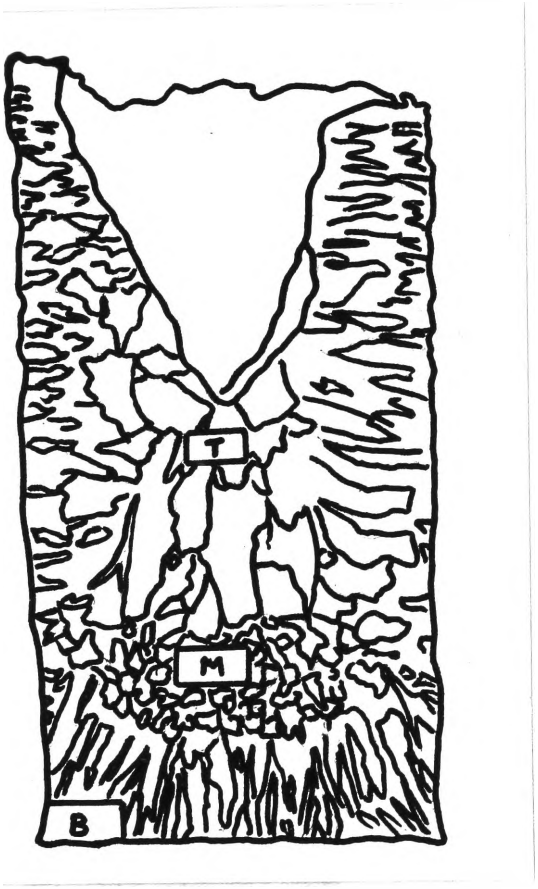

Fig 7-7: Diagrammatic representation of the macrostructure and sampling positions in Ingot 30 (copper).

given in Table 7-16, which shows that only one test gave a non-significant result (I18 No. 4 - I18 No 8R). In all the other tests the distributions were found to have different means. The results of the comparisons involving I30 M can be considered meaningless, again because of its large value of N_v.

7.8.3 Discussion of Tables 7-15 and 7-16

A diagrammatic representation of the sampling positions and grain structures for ingots 18, 22 and 30 are given in Figs. 7-5 to 7-7. Photographs of their macro-etched structure are given in Appendix 1.

Examination of Figs. 7-5 to 7-7 shows that the transformed distributions tested for $\sigma_1^2 = \sigma_2^2$ and $\ln \mu_1 = \ln \mu_2$ in Tables 7-15 and 7-16 are in reality comparisons of inclusion distributions in different ingot positions and in different ingot grain strucutures

The top and bottom side samples from both ingots 18 and 22 compare inclusion distributions from similar grain strucures and only differ in ingot position. The remaining comparisons, however, involve both differences in ingot position and grain structure.

TABLE 7-16 RESULTS OF t TEST

SAMPLE CODE	INGOT POSITION	t_{CAL} or t_{CAL}	$t_{0.05}$	DEGREES OF FREEDOM	test
I18 No4 - I18 No 5R	Bottom - Bottom	2.334	1.675	53	t
I18 No4 - I18 No 8R	Bottom - Top	1.406	1.65	349	t
I18 No5R- I18 No 8R	Bottom - Top	5.721	1.683	43	Modified t
I22 No 1- I22 No 6	Bottom - Top	5.839	1.647	749	t
I22 No1 - I22 No 1C	Bottom - Bottom	5.821	1.657	146	Modified t
I30 T - I 30 B	Top - Bottom	25.063	1.645	4622	Modified t
I30 T - I30 M	Top - Middle	497.74	1.645	3636	Modified t
I30 B - I30 M	Bottom - Middle	325.79	1.645	2364	Modified t
I27 T - I27 B	Top - Bottom	215.82	1.652	281	Modified t

7.8.3.1 Distributions Differing Only with Ingot Position

An examination of the F tests for variances of samples I18No 4 and No 8R and samples I22 No 1 and No 6 reveal that in both cases a non-significant result was obtained. This result for each ingot indicates that the variation of inclusion sizes about the mean size is similar for samples from both ingot positions and hence grain growth structures.

The non-significant results of tests for both $\sigma_1^2 = \sigma_2^2$ and $\ln \mu_1 = \ln \mu_2$ for samples I18 No 4 and No 8R indicates that the alumina distributions of both samples are the same and hence must have formed under similar conditions of nucleation and growth. Primary deoxidation products in ingot 18, as in all the ingots studied, were mainly of the clustered morphology and were found, on macro etching, to be present around the primary pipe (See Appendix 1). The inclusions present in the side columnar grains, therefore, must be either isolated primary deoxidation particles or secondary precipitation particles which formed during ingot solidification.

As ingot 18 was tapped at 1350°C into a mould insulated with refractory brick, the time before

solidification was completed can be expected to be at least similar and probably greater than the thermal arrest measurement of 18 seconds determined for ingot 32. The latter ingot was cast at 1220°C into a mould at a temperature of 500°C. Assuming Stokes' Law is applicable and an ingot height of approximately 18cms, a time of 20 seconds would allow inclusions of size greater than 120 μm to rise to the surface of the ingot from its base while inclusions of size 20 μm would only rise by 0.4cm.

The inclusion distribution in both samples No 4 and No 8R, therefore, can be considered to be randomly distributed isolated, primary deoxidation particles. The principal reasons for this conclusion are:

1. no section sizes larger than 16 μm were observed,
2. the rapid solidification from the mould walls trapped and fixed the existing inclusion distribution, and
3. rapid solidification allowed little or no time for inclusion cluster formation and flotation.

Any secondary precipitation of alumina during solidification could be considered to have similarly affected the distributions in both samples as the dendritic regions and the segregation of oxygen into

the remaining liquid would be expected to be similar for both ingot positions.

The results of the statistical tests comparing these two distributions with that from sample 5R, indicate that the latter distribution, although having a similar variance, has a significantly different mean. If the median, mean and mode of each distribution (see Table 7-17) are considered it can be concluded that the distribution from ingot position 5 was subject to the longest period of growth as its parameters are the largest. Entrappment in the columnar dendrites from the base would have occurred after the distributions at ingot positions 4 and 8 had been fixed, and so growth by continual precipitation on existing particles would have increased the size of all particles without altering significantly the distribution of sizes about the mean size.

The transformed spatial distributions from samples 6 and 1 of the iron ingot 22 can be considered to have equal variances but significantly different means (Tables 7-15 and 7-16). The larger spatial distribution parameters of sample 6, as can be noted from Table 7-17, suggests that either the inclusions were not randomly distributed in the melt prior to tapping or

TABLE 7-17 PARAMETERS OF SPATIAL DISTRIBUTION OF MAJOR AXES OF OBLATE ELLIPSOIDS (e = 0.85)

Sample Code	Ingot Position	Mode (μm)	Median (μm)	Mean (μm)	Variance
I18	4	1.3577	2.0824	2.5789	0.4277
I18	5R	2.2565	3.0354	3.5205	0.2965
I18	8R	1.0139	1.6795	2.1617	0.5047
I22	1	0.4577	0.8467	1.1516	0.6151
I22	1C	0.8808	1.2780	1.5395	0.3723
I22	6	0.2872	0.5579	0.7776	0.6639
I30	Top	0.0181	0.0829	0.1775	1.5225
I30	Middle	1.44×10^{-8}	3.13×10^{-6}	4.62×10^{-5}	5.3818
I30	Base	0.004997	0.03438	0.09016	1.9285

that local solidification times were different for the two ingot positions.

As ingot 22 was cast from a melt at 1550°C, solidification was completed within 10 seconds. The almost complete equiaxed grain structure and internal pipe observed in this ingot are physical indications of the rapid solidification rate. The observed columnar growth from the ingot base resulted from the rapid heat extraction of the steel base plate. As the solidification rate was rapid for both ingot positions, therefore the differences in inclusion size distributions can be considered to mainly result from prior heterogeneity of the inclusion distribution in the melt.

7.8.3.2 Distributions Differing in Both Ingot Position and Grain Structure

The samples from top and bottom positions of copper ingot 30 have transformed spatial distributions whose means and variances are both significantly different at both 5% and 1% significance levels. The slower local solidification time of the upper portions of the ingot can be qualitatively inferred from the greater interdendritic spacing in this region compared with the

base columnar spacing (see Fig. 7-7 and Appendix 1). The larger spatial distribution parameters for the top sample, therefore, can be correlated with the local solidification time as Kawabara has already noted. (214).

7.8.3.3 Distributions of Inclusions Differing in Morphology and Growing by Different Mechansisms

As discussed in Appendix 3 the clusters of alumina form in both copper and iron ingots by random collisions followed by sintering at the corners of the hexagonally shaped particles followed by a gradual spheroidization. It is not surprising then, that the individual inclusions in the cluster have a different size distribution (e.g. No 1c) to that of the randomly occurring alumina particles (e.g. No 1).

Whenever possible the particles in the cluster were sized as if they were individual particles, i.e. as if they were not sintered together. The resulting spatial distribution is more closely sized than that of the randomly occurring inclusions as can be seen from the smaller variance (Table 7-17) of sample No 1c. The larger mode, mean and median of No 1c is a consequence of the spheroidization of the particles in the cluster and

the greater probability of the larger size particles joining the cluster. The smaller particles would tend to slipstream around the particles in the cluster.

The operative growth mechanisms therefore are diffusion of the solutes Al and O to the existing alumina particles during solidification and Ostwald ripening in the melt whilst the cluster is carried in the liquid metal currents resulting from the induction heating and during flotation in the ingot.

7.8.4 Summary

The log-normal model not only adequately describes the size distribution of alumina particles but also allows standard statistical techniques to be used to determine subtle differences in the size distributions in various regions of small 3 Kg ingots. Not only can differences in mean sizes be examined and assessed against random perturbations but also differences in the variances.

Small variations in the growth conditions of particles in the melt, or at different ingot positions, or in various grain structures are incorporated in the parameters of the spatial distribution and so only a study of the complete distribution and not its average or gross

properties (i.e. V_v or S_v) will reveal these influences, and allow them to be quantified.

7.9 EXAMINATION OF SAMPLES CONTAINING VARIOUS INCLUSION TYPES

In the previous sections the log-normal model has been applied to the distribution of alumina particles is small laboratory ingots. These distributions were formed under special conditions and so the agreement between model and data could possibly be a unique one. Also the testing of the model was complicated by the need to ascertain a simple geometric shape which adequately represents the shape of the inclusions.

It is obvious, therefore, that inclusion distributions resulting from other deoxidation practices and deoxidants as well as other particle shapes need to be examined. Moreover, if the statistical model presented is to have practical applications, then the inclusion size-frequency distributions in hot rolled material need also to be considered. Consequently samples containing MnS, samples from a 12 ton industrial ingot and samples from hot rolled plate were examined and the distributions of inclusion sizes so obtained were tested for agreement with

Fig. 7-8 Type III MnS inclusion in Ingot 27. (2100X)

the proposed log-normal model.

7.9.1 Distribution of Type III MnS

Ingot 27 was produced by carbon deoxidation of the melt under vacuum to a level of 10ppm oxygen followed by an addition of electrolytic maganese, aluminium and iron sulphide. The inclusions in the ingot as a consequence of the low concentration of oxygen were type III sulphides as shown in Fig. 7-8.

These inclusions have been found to have an octahedral shape (209), As a sphere or oblate ellipsoid would be a suitable approximation to this shape the section distribution was formed by grouping the major axes of the sections. The result of the chi-square goodness of fit test for the best fit three parameter log-normal function was given previously in Table 7-11 (Section 7-4). The fit was adequate as X^2 was less than tabulated value of χ^2 at the 10% level.

The values of V_V and S_V determined by quantitative metallographic methods were 0.00163 and 3.8018 respectively

If the particles in sample 127 TOP were assumed to be spherical then Equs (7-7-6) and (7-7-7) reduce to:

$$V_v = \frac{\pi}{4} \cdot N_A . E(Y^2)$$

and

$$S_v = 4. \; N_A . E(Y)$$

Substituting $E(Y^2) = 4.8965$

$E(Y) = 1.712$

$N_A = 523.3645$

in the above equations then

$$V_v = 0.002013$$

and $S_v = 3.5839$

which is not very different than those values determined by quantitative metallography.

However, a better match of V_v and S_v values is obtained if the particles are assumed to be oblate ellipsoids of revolution with $e = 0.6$

That is:

$$V_v = 0.00172$$

and $S_v = 3.329$

Fig. 7-9 Oxide (or oxy-sulphide) inclusions in 3.5cm thick plate.
(1000X)

(a)

(b)

(c)

Fig. 7-10 Oxy-sulphide (a) (b) and sulphide (c) inclusions in 3.5cm thick plate. (1000 X)

7.9.2 Samples from Hot Rolled Plate

The samples were obtained from 3.5cm thick plate. Check analyses indicated, an average composition of (wt%):

C	P	Mn	Si	S	Al	O
0.20	0.031	1.30	0.44	0.008	0.045	0.004

The heat had been deoxidized in a 50 ton electric furnace, initially with aluminium after the first slag-off, and then just before tap with a complex calcium containing deoxidant called "Hypercal" (215). A further addition of Hypercal was made to the ladle during tapping. The total Hypercal addition amounted to 4.54Kg per ton, while the aluminium furnace addition was 1.36Kg per ton.

A description of the shape and the composition (determined by electron probe microanalysis) of the inclusions observed in the samples are given in Table 7-18. Optical microscope examination of the oxides revealed a generally circular section shape as shown in Fig. 7-9, while the sulphides and oxy-sulphides were of an elliptical shape (see Fig. 7-10). General conclusions which can be made from the EPMA results in Table 7-18 are:

1. the oxides were of the composition $CaO.6\ Al_2O_3$

TABLE 7-18 NORMALISED ELECTRON PROBE MICROANALYSIS OF INCLUSIONS

INCLUSION SHAPE	SPEC. No.	POSITION	ELEMENTS ANALYSED Ca (%)	Mn (%)	S (%)	Al (%)
Long Thin Inclusions	2S		0.3	62	38	
	"		2.2	61	37	
	"		2	60	38	
	"		0	64	36	
	2T		0.8	61	39	
	"		0.5	62	38	
	2V		1.5	59	40	
Elliptical-teardrop shaped inclusions	2S		4	53	43	
	"		4	52	44	
	2T		4-5	56	39	
	"		2-6	58	40	
	2V		2	59	39	

Table 7-18 C'tued

Round	2S	Outer sulphide
duplex	"	" "
inclusions	"	Centre oxide
	"	Outer sulphide
		Centre Oxide
	"	Outer sulphide
		Centre oxide
	"	Outer sulphide
		Centre oxide
	2V	Outer sulphide
		Centre oxide

49	24	27	
25	40	35	
17 CaO			83 Al_2O_3
56	21	23	
14 CaO			86 Al_2O_3
46	24	30	
60 CaO			40 Al_2O_3
41	34	25	
12 CaO			89 Al_2O_3
55	22	23	
27 CaO			73 Al_2O_3

$CaO.\ 2\ Al_2O_3$ or $3\ CaO.\ Al_2O_3$ enveloped to a varying degree with a rim of sulphide which contained 20 - 60% Ca and 20 - 40% Mn.

2. the calcium content of the sulphides increased from a range of 0.3 to 2.2% in the elongated shape to 2 to 5% in the ellipsoidal form.

The samples were examined for the size distribution of oxides and oxy-sulphides only, as the sulphides were too infrequent in occurrence. The count was done at 675 X magnification and an area of 24.84 sq mm was examined. Table 7-19 summaries the results of the fitting of the three parameter log-normal model to the data.

The results of the chi-squared tests for both oxides and oxy-sulphides in Table 7-19 show a very good representation of the data by the three parameter log-normal distributions.

The disagreement in 3rd and 4th moment estimations for the oxide distribution can again be accounted for by the short tail of the fitted three parameter log-normal distribution, $Y_u \simeq 25.67$, (which is within the last class interval) and the assumption of a two parameter log-normal distribution for the spatial distribution (see Section 7-4)

TABLE 7-19 MOMENTS OF THE FITTED SECTION DISTRIBUTIONS OF OXIDES AND OXY-SULPHIDES

Inclusion Type (Sample Code)	Moments of Fitted Distribution				Moments Calculated from $\hat{\mu}$ and $\hat{a}$				Goodness of Fit of Section Distribution		
	1ST	2ND	3RD	4TH	1ST	2ND	3RD	4TH	X^2	$\chi^2_{0.05}$	Degrees of Freedom
Oxy-sulphide (20 & 2T)	3.4939	15.974	93.562	685.52	3.4938	15.974	92.046	658.057	2.445	7.815	3
Oxide (20 & 2T)	9.0024	121.58	1975.7	35508	9.0024	121.58	2372.5	65852	1.734	7.815	3

7.9.2.1 Oxides

As the section shapes for most oxides observed were almost circular their spatial shape was assumed to be a sphere. To test the applicability of the log-normal model, the volume fraction of inclusions was calculated from the size-distribution using Equ. (7-5-12). The volume fraction was calculated to be 0.0001732.

The point count method was then used to supply a shape-independent estimate of V_v, which was found to be 0.0001733 $\pm$ 0.0000703.

The excellent agreement between the two V_v estimates supports the lognormal representation of the spatial distribution.

7.9.2.2 Oxy-sulphides

These inclusions showed some deformation in the direction of rolling (Fig. 7-10).

Obviously they would have had an approximately spherical shape in the ingot, but during rolling these inclusions would have tended to deform to an oblate ellipsoidal shape.

To examine this shape assumption and the log-normal

model as a description of the spatial distribution, the volume fraction and surface area per unit volume were calculated from the distribution data using Equs (7-5-12) and (7-5-16) and compared with estimates from point and intercept counts.

The volume fraction determined from the Equ (7-5-12) was 0.00014029, whilst that determined from point counting was 0.0001721 ± 0.0000494. As the value calculated from the distribution data is within one standard error of the mean, the two estimates can be considered to be in agreement.

In order to ascertain the eccentricity of the ellipsoid which best represents the oxy-sulphide shape the surface area per unit volume was determined from Equ (7-5-16) and independently by the intercept count. For the latter assessment, as the oxy-sulphides showed some deformation due to hot rolling, the system of inclusions in the steel matrix was considered as a partially orientated system. Consequently P_L counts were determined both parallel and normal to the rolling direction and the total surface area per unit volume was calculated from (158):-

$$S_v = 1.571\ (P_L)_{\perp} + 0.429\ (P_L)_{11}\ mm^2/mm^3$$
$$= 0.1815 \pm 0.0155\ mm^2/mm^3$$

S_v was calculated from Equ (7-5-16) using the

following mean values of the shape parameters calculated from the distribution of e:

$$M(\lambda(e,o)) = 1.1118$$

$$M(\lambda_1) = 1.0371$$

giving $S_v = 0.1675$

Again as this value is within one standard error of the mean of the metallographic count, it can be concluded that an oblate ellipsoid of revolution with $\bar{e} = 0.803$ is an adequate description of the shape of these oxy-sulphide inclusions.

7.9.3 12 Ton Experimental Ingot

The ingot examined was a titanium killed steel of composition as given in Section 5-2, that had been teemed into a 50" x 22" BEUmould. After stripping the ingot was sectioned to obtain a complete vertical plane and horizontal sections at 1.4, 12.4, 22.1, 46.2, 57.8, 70.3, 82.0 and 94.5% ingot height positions. Fifty-four samples from selected positions were examined both optically and with the electron probe. Additionally four samples from top and bottom columnar and equiaxed

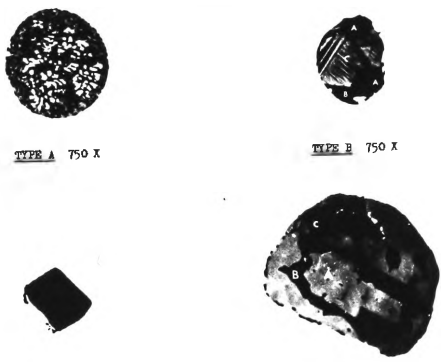

TYPE A 750 X

TYPE B 750 X

TYPE C 750 X
with edge of MnS

TYPE D 500 X

Inclusion	Al_2O_3	SiO_2	CaO	TiO_2	MnO	FeO
Type A (av. comp.)	28	11	0.3	44.2	15	1.5
Type B						
Phase A	100	-	-	-	-	-
Phase B	28	0.6	-	68.6	1.1	1.7
Phase C	3	-	-	75	20	2
Type C	14	-	-	81	2.5	2.5
Type D						
Phase A	15	7	0.8	61	5	1.2
Phase B	28	53	2	10	5	3
Phase C	100	-	-	-	-	-

Fig. 7-11 Oxide inclusion types found in 12 ton experimental ingot with EPMA results.

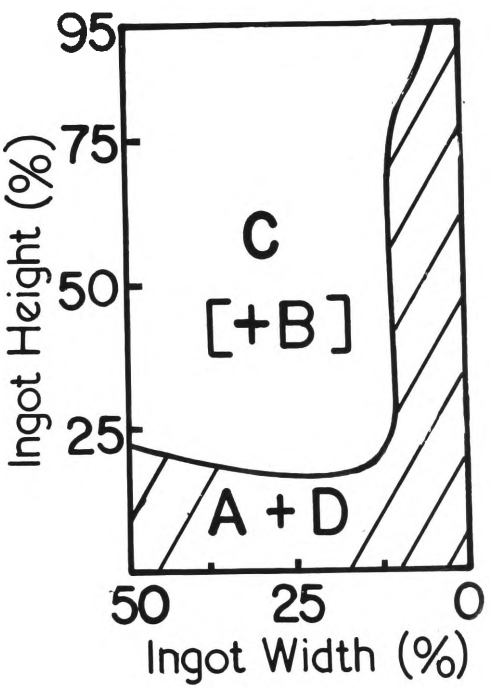

Fig. 7-12 Regions of predominance of the various inclusion types in the 12 ton experimental ingot.

regions were assessed to determine the oxide section distributions. The counting procedure was the same as for samples from the laboratory ingots except that it was performed at 650x. The lower magnification was necessary so that a large sample area could be examined, The large size of inclusions observed in the ingot allowed such a magnification to be employed without significant loss of information (see percentage explained for samples examined in Table 7-20).

Initial microscopic and EPMA examination of the samples revealed a mixture of exogeneous and endogenous oxide inclusions of differing composition and morphology as shown in Fig. 7-11.

The EPMA indicated that inclusions with high concentrations of silica and up to 2% calcium oxide, tended to be found at the edge and in the bottom ingot positions. The axial region above approximately 22% of the ingot height contained predominantly inclusions of type C, and did not contain any phases of possible exogenous origin. Figure 7-12 summarises the areas in which these oxide types were observed.

The inclusion dispersion shown in Fig. 7-11 may be explained by a combination of the two following phenomena:

TABLE 7-20 RESULTS OF THE COMPUTER ANALYSIS OF THE SECTION DISTRIBUTIONS

SAMPLE CODE	% EXP.	MOMENTS OF FITTED DISTRIBUTION				MOMENTS CALCULATED FROM $\hat{\mu}$ AND $\hat{\alpha}$				GOODNESS OF FIT OF SECTION DISTRIBUTION		
		1ST	2ND	3RD	4TH	1ST	2ND	3RD	4TH	X^2	$\chi^2_{0.05}$	DEGREES OF FREEDOM
52	88.1	2.8464	15.926	125.25	1187.0	2.8464	15.926	168.70	3330.7	6.952	9.488	4
59	99.7	4.4189	29.702	277.98	3350.9	4.4189	29.702	292.49	4154.0	8.029	11.070	5
8A9	98.7	3.8228	27.177	337.91	6760.5	3.8228	27.177	346.06	7770.0	8.141	11.070	5
8A2	99.7	5.8664	76.922	192.83	7482.5	-	-	-	-	28.814	11.070	5

(1) the trapping of the primary deoxidation products, some of which may have been of exogeneous origin, because of the initial rapid solidification rate; and

(2) the flotation from the central region of the larger primary and exogeneous oxides with the consequent depletion of the latter type of inclusions from this zone. The remaining liquid core thus contained idiomorphic TiO_2 rich inclusions of primary and secondary origin.

The TiO_2 particles, because of their inability to aggregate into stable clusters (63) (as alumina does), were not eliminated from the liquid core as quickly as the larger heterogeneous inclusions (e.g. types A, B and D).

This general explanation of the macroscopic oxide distribution enables meaningful interpretations to be made of the microscopic inclusion assessment distributions. The samples which were examined were from the 22.1% and 94.5% ingot height planes and were from approximately 12.5% and 42% ingot width positions.

The results of the goodness of fit tests and the comparison of calculated and fitted moments of the section distributions for the four samples are given in Table 7-20.

The interesting observation which emerges from this table is the non-significant result obtained for sample 8A2. Before the implications of this result are discussed, the other three samples, which are adequately represented by the three parameter section distribution model, need to be considered.

The "size" of the inclusions in all four samples was defined as the greatest distance between two parallel tangents to the section, which for most sections amounted to a diameter measurement. The definition of the particle size in this manner has, of course, the advantage of also providing the distribution of major diameters of oblate ellipsoids - the shape which next to the sphere would also be a reasonable approximation to the shape of the inclusions. Only the single phase, type C inclusions (see Fig. 7-11) had irregular shape sections, but as they were all approximately equiaxed in form, the assumption of spherical shape was also considered a reasonable representation. The greater simplicity inherent in this assumption for all inclusion types was another reason for its adoption.

Table 7-21 gives the parameters of the spatial distributions of spheres for samples 52, 59 and 8A9. To test for agreement between the distributions of the three

TABLE 7-21 PARAMETERS OF SPATIAL DISTRIBUTIONS

SAMPLE CODE	INGOT POSITION (%)		MODE	MEDIAN	MEAN	VARIANCE
	IH	IW	(μm)	(μm)	(μm)	
52	94.5	42	0.8123	1.4775	1.9926	0.5982
59	94.5	12.5	2.3942	3.3696	3.9976	0.3418
8A9	22.1	12.5	1.2532	2.1564	2.8287	0.5427

NOTE: IH - Ingot Height

IW - Ingot Width

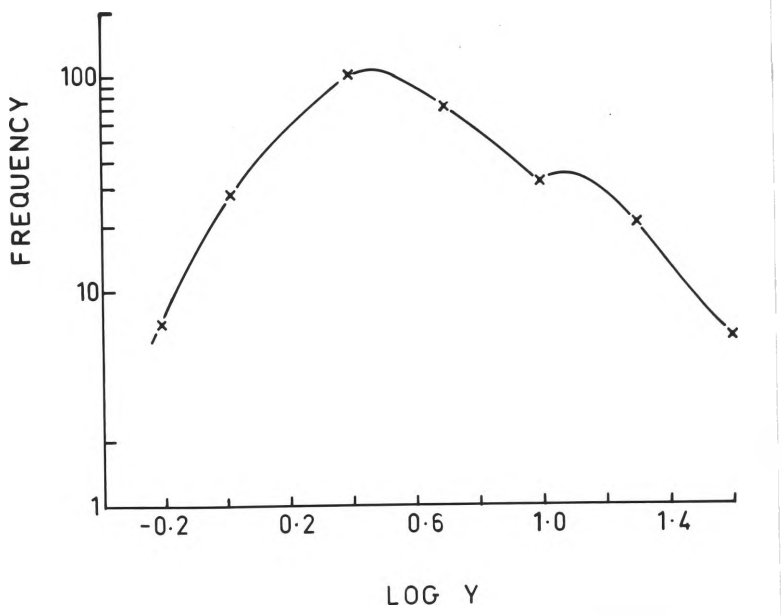

Fig. 7-13 Section distribution of sample 8A2.

samples, both F and t tests were performed on the transformed normal distributions in the manner outlined earlier. The results of these statistical tests are given in Tables 7-22 and 7-23.

For each comparison of the distributions given in Table 7-23 a significant difference in the means was obtained both at the 5% and 1% significance levels. A discussion of the practical significance of these differences, however, also requires an understanding of sample 8A2.

The position of sample 8A2 is just on the border of the region of predominance of A and D type inclusions as is schematically shown in Fig. 7-12. Thus when the poor fit to the section distribution was obtained, a logical extension of the analysis was to look for a heterogeneity in the section distribution.

A simple graphical technique of testing for heterogeneity is to plot the data on log-log paper and look for two or more parabolas (212). An examination of the relevant plot in Fig. 7-13 strongly indicates that the section distribution of sample 8A2 is the sum of two parabolas.

In order to estimate the parameters of the two distributions, each distribution (after transformation to

TABLE 7-22 RESULTS OF F TEST

SAMPLE CODES	INGOT POSITIONS	F_{CAL}	$F_{0.05}$	DEGREES OF FREEDOM f_1	DEGREES OF FREEDOM f_2	TEST OF MEANS REQUIRED
52 - 8A9	TM - BE	1.102	1.36	82	162	t
59 - 8A9	TE - BE	1.588	1.44	162	63	modified t
52 - 59	TM - TE	1.750	1.49	82	63	modified t

NOTE: TM - 94.5% ingot height and 42% ingot width position

TE - 94.5% ingot height and 12.5% ingot width position

BE - 22.1% ingot height and 12.5% ingot width position

TABLE 7-23 RESULTS OF t TEST

SAMPLE CODE	INGOT POSITIONS	t_{CAL} or t'_{CAL}	$t_{0.05}$	DEGREES OF FREEDOM	test
52 - 8A9	TM - BE	3.737	1.651	244	t
59 - 8A9	TE - BE	4.800	1.656	145	modified t
52 - 59	TM - TE	7.355	1.656	145	modified t

NOTE: TM - 94.5% ingot height and 42% ingot width position

TE - 94.5% ingot height and 12.5% ingot width position

BE - 22.1% ingot height and 12.5% ingot width position

a normal distribution) was considered as a truncated distribution. Both the distributions to the left and to the right hand side in Fig. 7-13 were considered to be truncated at log y which is equal to 0.8365267. The distribution to the left (8A2L) is truncated in its right tail, whilst the distribution to the right (8A2R) is truncated in its left tail.

The assumption of truncation is only a procedural technique so that each distribution can be treated separately using Hald's method of parameter estimation for truncated normal distributions (212). The first estimates of parameters for the left distribution in Fig. 7-13 were $\ln\hat{\mu} = 0.3817728$ and $\hat{\sigma} = 0.269804$ and a percentage truncation of 7.85. The frequencies in each of the class intervals were then calculated using these estimates and the total frequency which is given by the summation of the observed frequencies divided by 1-0.078535. The results of these calculations are given in column (3) of Table 7-24. The frequencies of right distribution in Fig. 7-13 for the classes of size greater than the truncation point 0.8365267 are obtained by the subtraction of column (3) from column (2) (column (4)) in Table 7-24. The parameters of the right

TABLE 7-24 ESTIMATED FREQUENCIES OF 8A2L

CLASS MID-POINT (log y) (1)	OBSERVED FREQUENCY (2)	CALCULATED FREQUENCY-LEFT DISTRIBUTION (3)	FREQUENCY FOR RIGHT DISTRIBUTION (4) = (2) - (3)
-0.2173315	7	10.14	
0.0839517	29	54.35	
0.3849817	99	94.12	
0.6860117	70	53.05	
0.9870417	31	9.66	21.34
1.2880590	20	0.55	19.45
1.5890890	6	-	6

distribution were then estimated from these frequencies, again using Hald's method for truncated distributions. The results of these calculations are given in column (3) of Table 7-25.

Then again by subtraction from the observed frequencies the left distribution is obtained in column (4) of Table 7-25. A check is then made to see if the estimation process can be terminated at the first approximations. Table 7-26 gives the details of the chi-square goodness of fit test, whereby the adequacy of the estimation is examined. As the value of X^2 exceeds the tabulated value of chi-square at the 5% and 1% levels of 5.99 and 9.21 respectively, the new set of frequencies for the left distribution given in column (4) of Table 7-25 are used to supply new estimates of the left distribution parameters, $\ln \mu$ and σ.

The results of these calculations and those of the chi-square test for the combined calculated frequencies are given in Table 7-27. As the value of X^2 is less than the tabulated value of χ^2 at the 5% level then the section data for sample 8A2 can be considered to be bi-modal, with the parameters of both section distributions being as follows:

TABLE 7-25 ESTIMATED FREQUENCIES OF 8A2R

CLASS MID-POINT (log y) (1)	OBSERVED FREQUENCY (2)	CALCULATED FREQUENCY-RIGHT DISTRIBUTION (3)	FREQUENCY FOR LEFT DISTRIBUTION (4) = (2) - (3)
-0.2173315	7	-	7
0.0839517	29	-	29
0.3849817	99	0.47	98.53
0.6860117	70	5.94	64.06
0.9870417	31	20.67	10.33
1.2880590	20	18.98	1.02
1.5890890	6	6.25	-

TABLE 7-26 GOODNESS OF FIT TEST FOR FIRST APPROXIMATION

CLASS MID-POINT (log y)	CALCULATED FREQUENCY-LEFT DISTRIBUTION	CALCULATED FREQUENCY-RIGHT DISTRIBUTION	COMBINED CALCULATED FREQUENCY (LEFT AND RIGHT)	OBSERVED FREQUENCY	CLASS CONTRIBUTIONS TO X^2
-0.2173315	10.1353	-	10.1353	7	0.9699
0.0839517	54.3456	-	54.3456	29	11.8206
0.3849817	94.1164	0.4688	94.5852	99	0.2061
0.6860117	53.0450	5.9430	58.9880	70	2.0557
0.9870417	9.6555	20.6677	30.3232	31	0.0151
1.2880590	0.5511	18.9768	19.5279	20	0.0114
1.5890890	-	6.2497	6.2497	6	0.0099
			TOTAL X^2 =		15.0888

TABLE 7-27 GOODNESS OF FIT TEST FOR SECOND APPROXIMATION

CLASS MID-POINT (log y)	CALCULATED FREQUENCY LEFT DISTRIBUTION	CALCULATED FREQUENCY RIGHT DISTRIBUTION	COMBINED CALCULATED FREQUENCY (LEFT AND RIGHT)	OBSERVED FREQUENCY	CLASS CONTRIBUTIONS TO X^2
- 0.2173315	5.0581	-	5.0581	7	0.7455
0.0839517	36.4120	-	36.4120	29	1.5088
0.3849817	85.1777	0.4688	85.6465	99	2.0819
0.6860117	65.5167	5.9430	71.4597	70	0.0298
0.9870417	16.5052	20.6677	37.1729	31	1.0251
1.2880590	1.3229	18.9768	20.2998	20	0.0044
1.5890890	0.0501	6.2497	6.2998	6	0.0143
				TOTAL X^2 =	5.4099

left distribution: $\ln \hat{\mu} = 1.0693667$

$\hat{\sigma} = 0.389994$

TOTAL FREQUENCY ≈ 210

right distribution: $\ln \hat{\mu} = 2.6062886$

$\hat{\sigma} = 0.336902$

TOTAL FREQUENCY ≈ 53

The parameters of both spatial distributions of 8A2 are given in Table 7-28. It can be seen from a comparison of this table with that of Table 7-21 that the left spatial distribution of 8A2 has both a median and a variance of similar magnitude to those of the spatial distribution from position 59. Thus both F and t tests were calculated for this comparison (and also for the comparions of spatial distribution 8A2L with the spatial distributions from the other ingot positions). The results of these calculations are given in Tables 7-29 and 7-30, and from these it is obvious that the spatial distribution 8A2L is not identical to any of the other distributions. Thus all 5 spatial distributions specified in Tables 7-21 and 7-28 are statistically significantly different distributions.

In order that a practical interpretation can be

TABLE 7-28 PARAMETER OF SPATIAL DISTRIBUTIONS

SAMPLE CODE	MODE (μm)	MEDIAN (μm)	MEAN (μm)	VARIANCE
8A2 - LEFT DISTRIBUTION	2.0649	2.8219	3.2989	0.3123
8A2 - RIGHT DISTRIBUTION	10.6783	13.8384	15.7536	0.2592

TABLE 7-29 RESULTS OF F TESTS

SAMPLE CODES	INGOT POSITIONS	F CAL	F 0.05	DEGREES OF FREEDOM f 1	DEGREES OF FREEDOM f 2	TEST OF MEANS REQUIRED
8A2L - 8A9	BM - BE	1.738	1.45	162	63	MODIFIED T
8A2L - 52	BM - TM	1.915	1.50	82	63	MODIFIED T
8A2L - 59	BM - TE	1.094	1.53	63	63	t
8A2L - 8A2R	BM - BM	1.205	19.5	63	2	t

NOTE:

TM - 94.5% ingot height and 42% ingot width position

TE - 94.5% ingot height and 12.5% ingot width position

BM - 22.1% ingot height and 42% ingot width position

BE - 22.1% ingot height and 12.5% ingot width position

8A2L - left distribution of 8A2

8A2R - right distribution of 8A2

TABLE 7-30 RESULTS OF T TESTS

SAMPLE CODE	INGOT POSITIONS	t_{CAL} or t^1_{CAL}	$t_{0.05}$	DEGREES OF FREEDOM	TEST
8A2L - 8A9	BM - BE	2.966	1.657	150	MODIFIED t
8A2L - 52	BM - TM	5.872	1.657	144	MODIFIED t
8A2L - 59	BM - TE	1.754	1.658	126	t
8A2L - 8A2R	BM - BM	5.128	1.669	65	t

NOTE:

TM - 94.5% ingot height and 42% ingot width position

TE - 94.5% ingot height and 12.5% ingot width position

BM - 22.1% ingot height and 42% ingot width position

BE - 22.1% ingot height and 12.5% ingot width position

8A2L - left distribution of 8A2

8A2R - right distribution of 8A2

given to these differences, an optical examination of the samples was conducted to ascertain the predominant and minor inclusion types in each sample. The results of this examination are given in Table 7-31. The inclusion phases which were described in this table by colour were also analysed by the electron probe and the results of that investigation are given in Table 7-32.

Considering Tables 7-31 and 7-28 and Fig. 7-12 together, the heterogeneity of sample 8A2 can be attributed to a mixture of the distributions of type C and Type D inclusions. The left distribution consists of type C inclusions and the right distribution (with its much larger median) describes the type D inclusions. Also the distributions of samples 52 and 59 can be seen to be those of the predominant inclusions types E and A respectively.

Sample 8A9 at first glance presents a conflict. It contains two predominant inclusion types, as does sample 8A2, yet it is not bimodal like sample 8A2 (i.e. the section distribution of 8A9 can be represented by a single three parameter lognormal distribution). To explain this apparent paradox the conditions whereby a mixture of two normal distributions will exhibit a bimodal relative frequency curve need to be examined.

TABLE 7-31 PREDOMINATE INCLUSION TYPES IN THE SAMPLES ASSESSED

SAMPLE CODE	PREDOMINATE INCLUSION TYPE (MINOR CONSTITUENT)	COMMENTS FROM OPTICAL EXAMINATION
8A2	C, D (E)	Predominately types C and D Some type E and duplex (light grey and brown coloured phases)
8A9	C,A	>10 μm type C <10 μm type A Some duplex (blue and cream coloured phases)
52	E (C)	Predominately type E, sometimes with an alumina particle Some type C and a few duplex enveloped by MnS
59	A (C)	type A and some type C and duplex (blue and cream coloured phases)

TABLE 7-32 ELECTRON PROBE ANALYSIS OF INCLUSION PHASES

PHASE	PERCENTAGE COMPOSITION					
	Al_2O_3	SiO_2	CaO	TiO_2	MnO	FeO
Bluish Grey*	2	-	-	74	22	2
Light Grey	2	0.3	0.5	59.5	36	1.7
Cream	33	0.5	-	60.5	4	2

* Major phase of Type E Inclusions.

This is done by considering, as Eisenberger has shown (216), what is the sufficient condition for a relative frequency curve to be bimodal. For two log-normal distributions this is:

$$(\ln \mu_2 - \ln \mu_1)^2 > \frac{8 \sigma_1^2 \sigma_2^2}{\sigma_1^2 + \sigma_2^2} \qquad (7\text{-}9\text{-}1)$$

Substituting the appropriate values from the two distributions of sample 8A2 in Equ (7-9-1), the following result is obtained:

$$2.5282 > 1.1331$$

This result again confirms the bimodal nature of the spatial distribution of 8A2.

As the left distribution of sample 8A2 is of type C inclusions and the spatial distribution of 59 is of Type A inclusions, the condition given in Equ (7-9-1) can be calculated for these distributions. The result is given below:

$$0.03146 \not> 1.3055$$

As the inequality is negated, a mixture of distributions of these two inclusions types would not exhibit a bimodal relative frequency curve.

The sufficient condition that the relative frequency curve of the spatial distributions of 59 and 8A2L are unimodal is that (216):

$$(\ln \mu_2 - \ln \mu_1)^2 < \frac{27 \sigma_1^2 \sigma_2^2}{4(\sigma_1^2 + \sigma_2^2)} \qquad (7\text{-}9\text{-}2)$$

The substitution of the appropriate parameters in Equ (7-9-2) gave the following result:

$$0.03146 < 1.1055$$

Thus although sample 8A9 contains two separate inclusion types with their own individual spatial distributions the medians of the two distributions are not sufficiently separated for the relative frequency curve (of log x) to exhibit two modes. In fact, the difference $\ln \mu_2 - \ln \mu_1$ has to be at least three times the standard deviation before the relative frequency curve will exhibit two modes (212). For the case under consideration $\ln \mu_2 - \ln \mu_1$ is only equal to approximately half either standard deviations.

The assumptions which are implicit in the above discussion are that the spatial distribution of type A inclusions does not significantly vary from position 59 to position 8A9, and that the spatial distribution of Type C inclusions is similar in both 8A2 and 8A9 ingot positions.

Firstly, type A inclusions (from Fig. 7-11) have high concentrations of SiO_2 and MnO and small quantities of FeO and CaO all of which are in finely divided forms intermixed with each other. These facts imply this inclusion type had an early origin, partly exogenous,

during steelmaking and underwent considerable compositional changes during titanium ladle deoxidation. Also as this inclusion type was not found in the central ingot region but only in the outer (columnar) region and in the ingot base (below approximately 22% ingot height) it can be concluded that any further growth to that which had already occurred in the ladle was quickly terminated by the rapid solidification from the ingot walls and ingot base. This being so, the spatial distributions in positions 59 and 8A9 would not be expected to differ significantly.

Secondly, type C inclusions found in both 8A2 and 8A9 ingot positions were probably a mixture of primary inclusions which could not float out and secondary precipitation products. As this inclusion type is predominately titanium oxide (81%) with a small proportion of alumina (14%), and also is of angular shape, it was probably not liquid at steelmaking temperatures and so considerable growth during solidification was unlikely. Furthermore, as inclusions in positions 59 and 8A2 would be subject to longer growth times than those in position 8A9, the difference between medians of the two distributions from positions

59 and 8A2 should represent an extreme case. The difference for the two distributions in 8A9 should be less and certainly not the three standard deviations required for the appearance of the bimodal frequency curve.

Thus it has been shown above that a combination of both EPMA, optical microscopy and inclusion size distribution assessment, together give a clearer interpretation of the inclusions in this experimental industrial size ingot than any other one method applied in isolation. It is also shown that both the three parameter log-normal section distribution model and the two parameter lognormal spatial distribution model can be successfully applied to the diverse inclusions formed with industrial deoxidation practice.

8.0 CONCLUSIONS

Two statistical models for describing inclusion size-frequency distributions have been formulated in this thesis. One represents the relative frequency distribution of inclusions observed on a polished section and the other, the spatial relative frequency distribution, of inclusions which when intersected by a section plane would produce the former distribution. Unlike many previous investigators who were content with assessing only the section distribution, this investigation involved a study of both section and spatial distributions.

The log-normal distribution, both in its three and two parameter forms, is presented as the distribution function which best represents the size distributions of the many inclusion types studied in this research. The size distributions assessed were not only of inclusions formed under laboratory controlled conditions but also of those formed in the variable conditions of industry. The log-normal function, however, adequately described samples from either situation, as well as representing deformed inclusions in hot rolled plate.

The adequacy or significance of the fit of the log-normal distribution function to the distribution

data was tested analytically by the chi-square goodness of fit test, as other testing methods, such as graphical analysis, are often open to erroneous conclusions. In most samples examined the fit was significant at the 10% confidence level or at the very least the 5% level. Any data which could not be represented by the log-normal distribution on further examination were found to be heterogenous in either inclusion type or shape.

The advantage obtained from the log-normal formulation of the spatial relative frequency distributions was that standard statistical techniques developed for the normal distribution could also be used. All that is required for this application is that the F and t tests be applied to the normal transforms of the relative frequency distributions. So that in this study, not only were the difference in means of two inclusion distributions examined by these statistical tests, but also the difference in variances (dispersion of sizes about the mean).

The importance of being able to examine these parameters of the spatial distributions can only be fully appreciated when it is realized that small variations in the growth conditions of particles in the melt or at different ingot positions during solidification

will affect these parameters. Thus only by employing a model for the inclusion distributions, such as given in this thesis, can more thorough studies of inclusions and their influences on the steel matrix and stresses incorporated in the matrix be successfully conducted. Previous investigators have been content to assess only average or gross parameters of the inclusion distribution (i.e. V_v or S_v) and as a consequence were only able to report gross or major changes in inclusion content, the smaller perturbations in the distributions going unnoticed.

As both section and spatial distributions are formulated as mathematical functions for which moments are readily calculated, the estimation of the spatial distribution from measured section distribution is very quickly, simply and accurately obtained. This procedure circumvents previous tabular methods which are longer and more tedious to perform, as well as being inherently less accurate.

To achieve an estimate of the spatial distribution from assessed data, unfortunately the shape of the inclusions needs also to be known. The usual procedure for this situation, as employed by most investigators, was to assume that the inclusions were all spherical in shape.

In most instances however, the inclusions resulting from the various deoxidation practices employed in industry are not spheres. This fact was immediately apparent when alumina sections were observed in samples from the laboratory ingots in this study. Thus another shape model was developed which gives a better representation of the irregular shaped inclusions, as well as those of more spherical morphology. This model used the general ellipsoid as its basic form.

The mathematical techniques required to use this ellipsoidal shape model were already developedsome 50 years ago by Wicksell (165), but the complexity of his analysis was very prohibitive to widespread application.

It was shown in this investigation that for most applications the assumption of ellipsoids of revolution for the shape of the inclusions examined resulted in reasonable approximations with little error. That is, for example, alumina particles were approximated by oblate ellipsoids of revolution with a mean eccentricity of 0.85.

Though the assessment procedure and analysis presentation in this thesis is more comprehensive than any method so far proposed, at this stage of development

a manual method is unfortunately necessary for assessing the inclusion section distribution. Recourse to manual methods, when there were automatic instruments available, was unavoidable as the latter were found to be extremely inaccurate.

This was especially evident when attempts were made to assess deformed inclusions in hot rolled product. Also the sizing of inclusions (defined in this thesis as the geometric mean of major and minor diameters of the section) could not be obtained with the present commercially available instruments.

The long times required to obtain one assessment using the manual method, together with the somewhat complex calculations required, may limit the application of this technique in industrial quality control. Consequently for these purposes another procedure was developed which involves the assessing of the area of inclusions in each of 500 fields on the QTM and representing their frequency of occurrence by the Rosin-Rammler law. The logic of this approach is that quite often in volume fraction estimates one or a few fields will contain more than half the final volume fraction, the other 400 odd fields contributing the other half. A procedure which allows an examination of

the relative proportion each field makes to the final result, obviously aids the metallographer in assessing the overall cleanness of the steel examined. The representation of the data by a mathematical function allows the metallographer to express not only the cleanness of the steel quantitatively but also allows him to compare the cleanness of different steels quantitatively.

Although this study has been concerned mainly with inclusion size-frequency distributions the results of studies of the laboratory ingots reveal the need in kinetic studies to give more consideration to the rate and extent of mixing of the deoxidizer in the melt. The presence of non-equilibrium inclusion phases and of occlusions in the ingots examined, even though the deoxidants were added to induction stirred melts, support the incomplete mixing hypothesis of Chipman (27). Also examination of the alumina clusters present mainly in the top of the laboratory ingots support the mechanism of formation which involves the aggregation of small particles soon after deoxidation due to surface energy requirements followed by a gradual sintering of the tips of the hexagonal alumina plates.

Possible future developments and extensions of the

statistical analysis of distributions proposed in this thesis can be divided into three categories, namely the analysis of heterogeneous populations, the use of a four parameter log-normal function as a more realistic representation of the spatial distribution and the use of size-frequency parameters in kinetic and mechanical property studies.

1. As most inclusion size-frequency distributions in steel ingots or rolled products are heterogeneous, quicker and easier methods of analysi ng these distributions than the trial and error method used in this study are required. This is especially so when three or more separate distributions are compounded, or when the modes of the individual distributions are not graphically discernible.
2. All spatial distributions of inclusions have finite upper and lower limits to the size range and so a four parameter log-normal distribution function would be an obvious improvement to the two parameter function used in this thesis. However, as there are no simple analytical expressions for the first four moments of a four parameter log-normal distribution, the

fitting of such a distribution is difficult when all parameters are unknown.

3. The statistical analysis developed in this thesis enables a new approach to be made to the analysis of kinetic data. Rather than report overall decreases in oxygen content of the melt or plot the change in inclusion size-frequency curves, the form of these curves and their alteration with time can be quantified as parameters of the log-normal function. Thus, for example, Torssell's studies (21) could be analysed as revealing the formation of a second distribution during the growth and flotation period.

To be able to quantify inclusion shape and size distributions is an initial requirement in the study of the influence of inclusions on the mechanical properties of the metal-inclusion composite. This fact was particularly emphasised by Pickering (217) in a recent review of this topic. However, before any major work can be conducted in this field there is firstly a need for rapid automatic inclusion assessment instruments which will perform sizing operations in two mutually perpendicular directions and which will accurately count

different coloured and shaped inclusions. Once such data can be obtained and is statistically analysed the parameters of the spatial distributions would be the fundamental data required for the investigation of the influence of inclusions on mechanical properties.

REFERENCES

1. G.W. Giles, "Clean Steel", Spec. Rep. 77, ISI, Percy Lund and Humphries, London, 1963, pp 1-4.
2. M. Baeyertz, "Nonmetallic Inclusions in Steel", ASM, Cleveland, 1947.
3. C.E. Sims, Trans. AIME, 215, 1959, pp 367-393.
4. R. Kiessling et al, "Nonmetallic Inclusions in Steel", Parts 1,2,3, ISI Spec. Rep. 90, and Pub. 100 and 115, London, 1964, 1966 and 1968.
5. R. Kiessling, J of Metals, 21, (10), 1969, pp 48-54.
6. H.B. Bell, Iron and Steel, 1954, (Oct), pp 44-50, (Nov), pp 51-57.
7. A.M. Samarin, "Prod. and Appl. of Clean Steels", ISI Spec. Rep. 134, ISI, London, 1970, pp 17-23,
8. O. Repetylo, M. Olette and P. Kozakevitch, J. of Metals, 19, (5), 1967, pp 45-49.
9. V.P. Luzgin et al, Izvest. VUZ Chern. Met., 9, 1963, p50.
10. L. von Bogdandy et al, Stahl u Eisen, 89, 1969, p704.

11. E. Forster and H. Richter, "Prod. and Appl. of Clean Steels", ISI Spec. Rep. 134, ISI, London, 1970, p 24-28.

12. R.J. Fruehan, Met. Trans., 1, 1970, pp 3403-3410.

13. A.M. Samarin, Jernkont. Ann., 151, (3), 1967, pp 181-196.

14. J.C. D'Entremont et al, Trans AIME, 227, 1963, p 14.

15. H. Wentrup and G. Hieber, Tech. Mitt. Krupp A Forschungsberichte, 2, 1939, pp 47-53.

16. T. Kawawa and M. Ohkubo, Trans. ISIJ, 8, 1968, pp 203-219.

17. P.H. Lindon and J.C. Billington, Trans. AIME, 245, 1969, pp 1775-1783.

18. G.C. Duderstadt and R.D. Weller, J of Metals, 18, (6), 1966, pp 714-718.

19. N. Sano, S. Shiomi and Y. Matsushita, Trans. ISIJ, 7, (5) 1967, pp 244-253.

20. J. Andersson, Jernkont. Ann. 154, 1970, pp 429-455.

21. K. Torssell, Jernkont. Ann. 151, 1967, pp 890-949.

22. Y. Kojima, K. Takahaski, H. Sakao and K. Sano, Trans ISIJ, 7, (4), 1967, pp 172-179; Y. Miyashita, Tetsu-to-Hagane, 50, 1964, pp 507-511.

23. E. Grethen and L. Phillippe, "Prod. and Appl. of Clean Steels", ISI Spec. Rep. 134, ISI, London, 1970, pp 29-34.

24. L. Luyckx , J of Metals, 20 , (6), 1968, pp 61-68.

25. M. Olette et al, B H M, 113, (11), 1968, pp 484-492.

26. Discussion by R.G. Ward to reference 18, pp 117-8.

27. J. Chipman, Trans. AIME, 224, 1962, pp 1288-1289.

28. M. Volmer and A. Weber, Z. Phys. Chem ., 119, 1926, pp277-301; R. Becker and W. Doring, Ann. Phys., 24, (5), 1935, pp719-752.

29. L. von Bogdandy, W. Meyer and I.N. Stranski, Arch fur das Eisenhuttenw., 32, 1961, pp 451-460.

30. S.I. Popel', Fiz-Khim Osnovy Proiz Stali, Moscow, 1964, pp 15-23.

31. F.H. Woehlbier and G.W.P. Rengstorff, J of Metals, 19, (5), 1967, pp 50-53.

32. L. von Bogdandy, W. Meyer and I.N. Stranski, Arch fur das Eisenhuttenw., 34, (4), 1963, pp 235-241.

33. G.K. Sigworth and J.F. Elliott, Met. Trans., 4, 1973, pp 105-113.

34. V. Hopp and R. Troschke, Hoesch. Ber. Fosch. Entwickl, 1, 1968, p20.

35. M.L. Turpin and J.F. Elliott, JISI, 204, 1966, pp 217-225.

36. G. Pomey and B. Trentini, "Prod. and Appl. of Clean Steels," ISI Spec. Rep. 134, ISI London, 1970, pp 1-14.

37. G. Forward and J.F. Elliott, J of Metals, 17, (5) 1967, pp 54-59.

38. A. McLean, J of Metals, 20, (3), 1968, pp 96-100.

39. G. Forward and J.F. Elliott, Met. Trans., 1, 1970, pp 2889-2898.

40. E.T. Turkdogan, Electric Furnace Proc., 1966, pp 22-26.

41. E.T. Turkdogan, JISI, 204, 1966, pp 914-919.

42. F.B. Pickering, Jernkont. Ann., 148, (11), 1964, pp 845-872.

43. H. Straube et al, Arch fur das Eisenhuttenw, 38, 1967, p 509.

44. H. Straube et al, ibid, 38, 1967, p 607.

45. R. Saliagami, Tetsu-to-Hagane, 48, 1962, p 401.

46. Y. Miyashita and K. Nishikawa, ibid, 52, 1966, p 552.

47. T. Kawawa and R. Okubo, ibid, 53, 1967, p 1567.

48. M. Wahlster, Frieberger Forschungshefte, B68, June, 1962, pp 47-70.

49. I. Uchiyama and T. Saito, Tetsu-to-Hagane, 51, 1965, pp 1956-1958.

50. K. Mukai, H. Sakao and K. Sano, Trans. ISIJ, 9, 1969, pp 203-215.

51. P.J.H. Maunder and J.A. Charles, JISI, 206, 1968, pp 1039-1040.

52. E.T. Turkdogan and J. Pearson, JISI, 176, 1954, pp 59-63.

53. S.L. Case and K.R. Van Horn, "Aluminium in Iron and Steel", John Wiley and Sons, New York, 1953.

54. J.H.S. Dickenson, JISI, 45, 1925, pp 373-381.

55. B.M. Larsen and T.E. Brower, United States Steel Corp., Research Laboratory Rep. No. 444, Jan. 1942.

56. W.A. Hare and G. Solar, Trans. ASM, 26, 1938, pp 903-928.

57. K. Senda, Tetsu-to-Hagane Overseas, 5, (4), 1965, pp 303-316.

58. K. Torssell and M. Olette, Rev. Met., (Dec), 1969, pp 813-822.

59. R.A. Rege et al, Met. Trans., 1, 1970, pp 2652-2655.

60. H. Ooi, T. Sekine and G. Kasai, Tetsu-to-Hagane, 59, 1973, pp 1078-1088.

61. P. Kozakevitch and L.D. Lucas, Rev. Met., 65, 1968, pp 589-598.

62. Kuang An-Min, V.A. Mchedlivili and A.M. Samarin, Russian Met. and Fuels, (4), 1962, pp 10-20.

63. P. Kozakevitch and M. Olette, "Prod. and Appl. of Clean Steels", ISI Spec. Rep. 134, ISI, London, 1970, pp 42-49.

64. H. Knuppel, K. Brotzmann and N.W. Forster, Stahl u. Eisen, 85, 1965, pp 675-688.

65. V.I. Bapstizmanskii, N. Bakhmann and Yu. V. Minishreiv, Izvest. VUZ Chern. Met, 12, (3), 1969, pp 42-45.

66. K. Okohira, N. Sato and H. Mori, Tetsu-to-Hagane, 59, 1973, pp 1166-1173.

67. E.T. Turkdogan, JISI, 210, 1972, pp21-36.

68. R.K. Iyengar and W.O. Philbrook, Met. Trans., 3, 1972, pp 1823-1830.

69. F. Korber and W. Oelsen, Mitt Kaiser Wilhelm Inst., Eisenforsch., 15, 1933, p 271.

70. A.D. Kramarov and S. Ya Reznikova, Stal', (9), 194 -, p775.

71. V.A. Mchedlishvili and A.M. Samarin, Pub. ANSSSR, 1953.

72. E. Plockinger, "Clean Steel", Spec. Rep. 77, ISI, Percy Lund and Humphries, London, 1963, pp 51-56.

73. U. Lindborg and K. Torssell, Trans. AIME, 242, (1), 1968, pp 94-102.

74. N.F. Grevillius, Jernkont. Ann., 153, 1969, pp 547-572.

75. R. Scimar, Rev. Universelle des Mines, 106, (Oct), 1963, pp 403-418.

76. M. Kawai and S. Kobayaski, Tetsu-to-Hagane, 52, (4), 1966, pp 546-549.

77. M. Kawai, S. Kobayaski, H. Yonezawa and Y. Adachi, Tetsu-to-Hagane, 52, (4), 1966, pp 549-551.

78. T. Kawawa, M. Okubo and M. Ihida, Tetsu-to-Hagane, 50, (11), 1964, pp 1859-1862.

79. T. Kawawa, M. Okubo, Y.Sasajima and K. Gunji, Tetsu-to-Hagane, 51, (4), 1965, pp 777-780.

80. M. Okubo, T. Kawawa, Y. Sasajima and H. Tokunaga, Nippon Kokan Techn. Rep., (37), 1966, pp 161-172.

81. B.E. Lindblom, JISI, 206, (6), 1968, p 609.

82. R.K. Iyengar and W.O. Philbrook, International Conf. on Kinetics of Met. Processes in Steelmaking, Institut. fur Eisenhuttenw., Aachen, 1970.

83. V.I. Korokhov, V.I. Glazo, G.A. Klemeshov, B.G. Ryabinin and V.D. Rostorgnev, Russian Metallurgy, (6), 1967, p 6.

84. E. Plockinger and M. Wahlster, Stahl u. Eisen, 80, 1960, pp 659-669.

85. R. Rosegger, Radex-Rundschau, 1958, pp 738-753.

86. C.A. Muller and E. Plockinger, Radex-Rundschau, 1957, pp 738-753.

87. S.E. Volkov, V.A. Mchedlishvili and A.M. Samarin, "Wettability of Corundum and Quartz Glass by Ferrosilicon Melts".

88. P.H. Lindon and J.C. Billington, JISI, 207, (3), 1969, pp 340-347.

89. N. McCallum and J.R. Wynne, "Clean Steel", Spec. Rep. 77, ISI, Percy Lund and Humphries, London, 1963, pp 40-50.

90. W.J.M. Salter and F.B. Pickering, JISI, 207, (7), 1969, pp 992-1002.

91. E.L. Morgan, J.R. Blank, W.J.M. Salter and F.B. Pickering, JISI, 206, (10), 1968, pp 987-1001.

92. D. Ya Povolotskii et al, Izvest. VUZ Chern Met., 10, (11), 1967, pp 20-24.

93. L.N. Belyanchikov, Izvest VUZ, Chern Met., (7), 1965, pp 74-77.

94. P. Kozakevitch and G. Urban, Mem. Sci. Rev. Met., 58, 1961, pp 517-534.

95. W.D. Kingery, "Physical Chemistry of Steelmaking",

95. Proc. Conf. Endicott House, Mass., (May), 1956, pp 33-34.

96. P. Kozakevitch and G. Urban, "The Physical Chemistry of Steelmaking", J.F. Elliott ed., John Wiley and Sons, New York, 1959, pp 27-34.

97. D.H. Houseman, Steel Times, 193,(May 27), 1966, pp 689-695.

98. P. Logi and L. Mattcoli, La Metallurgia Italiana, 56, (9), 1964, (Sept), pp 443-449.

99. D.C. McCarter, S. Ramachandran and J.C. Fulton, Proc. Electric Furnace Conf., 18, AIMME, 1960, pp 24-36.

100. E.R. Saunders, W.D. Forgeng and J.W. Farrell, Proc. Electric Furnace Conf., 18, AIMME, 1960, pp 93-111.

101. B.B. Gulyayev, Izvest Akad Nauk SSSR, (3-4), 1942, p 57.

102. C. Benedicks and H. Lofquist, "Nonmetallic Inclusions in Iron and Steel", Chipman and Hall, 1930.

103. R.B. Snow, J of Metals, 20, (10), 1968, pp 55-62.

104. G. Konig and T. Ernst, Radex-Rdsch., (1), 1970, pp 45-63; (2), 1970, pp 67-98.

105. R. Kiessling and N. Lange, JISI, 201, (12), 1963 pp 1016-1024

106. F.B. Pickering, "Clean Steel", Spec. Rep. 77, ISI, Percy Lund andHumphries, London, 1963, pp 1-24.

107. K.A. Ridal, Iron and Steel, Special Issue, 1970, pp 93-98.

108. K. Segawa, Trans, ISIJ, 7, (4), 1967, pp 163-171.

109. Fourth Report of the Oxygen Sub-Committee of the Committee of the Heterogeneity of Steel Ingots, JISI, 148, 1943, pp 231p - 428p.

110. T.R. Allmand, JISI, 190, 1958, pp 359-372.

111. D.A. Melford, "Automatic Cleanness Assessment of Steel", ISI Pub 112, London, 1968, pp 14-23.

112. D.A. Melford, "Prod. and Appl. of Clean Steels", ISI Spec. Rep. 134, 1SI London, 1970, pp 229-234.

113. K.A. Ridal and R. Cummins, ibid, pp 248-254.

114. W.H. Hatfield and G.W. Giles, JISI, 142, (2), 1940, pp 237p - 256p.

115. J.V. Hardy and R.T. Allsop, JISI, 1960, 195, pp 302-306.

116. S. Bergh and U. Lindborg, Jernkont Ann., 146, 1962, pp 862-868.

117. J.R. Blank and T.R. Allmand, "Automatic Cleanness Assessment of Steel", ISI Pub. 112, 1968, pp1-11.

118. R. Whittaker, "clean Steel", Spec. Rep. 77, ISI, Percy Lund and Humphries, London, 1963, pp 36-39.

119. D.M. Cottingham et al, "Automatic Cleanness Assessment of Steel", ISI Pub 112, London, 1968, pp 31-39.

120. R.H. Sherry, "Steel Treatment Practice", McGraw Hill Book Co., 1929, p 224.

121. W. Dahl, H. Hengstenberg and C. Duren, Stahl u. Eisen, 86, 1966, p 796.

122. I. Kozasu, T. Shimizu and H. Kubota, Trans. ISIJ, 13, 1973, pp 20-28.

123. D.A. Melford, Discussion 1, "Clean Steel", Spec. Rep. 77, ISI, Percy Lund and Humphries, London, 1963, p 30.

124. F.D. Bridge, Steel Times, Jan. 24, 1964, pp 118-125.

125. Eighth Report Heterogeneity of Steel Ingots, ISI, Spec. Rep. 25, 1939.

126. G.R. Bolsover, Discussion to reference 114, p 265p.

127. BISRA Nonmetallic Inclusion Group, JISI, 204, 1966, pp 146-151.

128. A. Delesse, Annales Des Mines, 13, 4th Series, 1848, pp 379-388.

129. S.M. El-Soundani and R.M. Pelloux, Metallography, 6, 1973, pp 37-64.

130. J.E. Hilliard, "Quantitative Microscopy", R.T. De Hoff and F.N. Rhines ed., McGraw Hill Book Co., New York, 1968.

131. M.S. Mihaljev and L.U. Mironov, Stahl', 20, 1960, p 647.

132. S. Bergh, Jernkont. Ann., 146, 1962, pp 748-762.

133. Y. Mujashita and K. Nishikawa, Trans. ISIJ, 8, 1968, pp 181-185.

134. W.M. Wojcik, R.M. Raybeck and E.J. Paliwoda, J of Metals, 19, 1967, pp 36-40.

135. C. Fisher, "Automatic Cleanness Assessment of Steel", ISI Pub 112, 1968, pp 24-30.

136. K.A. Ridal, ibid, pp 40-46.

137. T.R. Allmand and J.R. Blank, "Automatic Cleanness Assessment of Steel", ISI Pub 112, 1968, pp 47-71.

138. S. Johansson, Scand. J. Metallurgy, 2, 1973, pp 24-28.

139. A.G. Franklin, "Prod. and Appl. of Clean Steels", ISI Spec. Rep. 134, ISI, London, 1970, pp 241-247.

140. T.R. Allmand and D.S. Coleman, Metals and Materials, 5, 1971, pp 32-41.

141. H. Martensson, "Prod. and Appl. of Clean Steels", ISI Spec. Rep. 134, ISI, London, 1970, pp 235-240.

142. E. Banks, BHP Technical Bulletin, 13, (2), 1969, pp 20-23.

143. S. Johansson, Jernkont. Ann., 154, 1970, pp 425-426.

144. J. Vero, "Prod. and Appl. of Clean Steels", ISI Spec. Rep. 134, ISI London, 1970, pp 273-277.

145. T.R. Allmand and D.S. Coleman, The Microscope, 20, 1972, pp 57-81.

146. S. Epstein, Metals and Alloys, 2, 1931, pp 186-191.

147. A.G. Franklin, JISI, 207, 1969, pp 181-186.

148. J.F. Sewell and R. Wilcock, "Clean Steel," Spec. Rep. 77, ISI, Percy Lund and Humphries, London, 1963, p 5.

149. G. Herdan, "Small Particle Statistics", Butterworth, London, 1960, pp 73-105.

150. ASTM Standards, Part 30, E20-68, Am.Soc. Testing Mats., 1969, pp 106-118.

151. J. Cartwright, "The Physics of Particle Size Analysis", Brit. J. of App. Phys., Supplement No. 3, Paper E4, 1954, pp 5109-5120.

152. R.R. Irani and C.F. Callis, "Particle Size: Measurement, Interpretation and Application", John Wiley and Sons, New York, 1963.

153. H. Heywood, "Symposium on Particle Size", Instit. of Chem. Eng. and Soc. of Chem. Ind., 1947, pp 14-24.

154. S.A. Saltykov, "STEREOLOGY - Proceedings of the Second International Congress for Stereology", H. Elias ed, Springer Verlag, New York, 1967, pp 163-173.

155. H. Heywood, "The Physics of Particle Size Analysis", Brit. J. Of App. Phys, Supplement No. 3, Discussion to paper E2, 1954, p5104.

156. B.H. Kaye, Powder Technology, 2, (2), 1968, pp 97-110.

157. K. Kasai, Scientific Papers, Inst. Phys. and Chem. Research, Tokyo, No. 242, 1930, pp 135-183.

158. E.E. Underwood, "Quantitative Stereology", Addison-Wesley, Mass., 1970.

159. R.T. DeHoff, Trans. AIME, 224, 1962, pp 474-477.

160. H.E. Exner and H.L. Lukas, Metallography, 4, 1971, pp 325-338.

161. T.W. Butler, Metallography, 2, 1969, pp 289-292.

162. J.W. Cahn and R.L. Fullman, Trans. AIME, 206,

1956, pp 610-612.

163. G. Bockstiegel, Zeitschr f. Metallhunde, 57, (8), 1966, pp 647-652.

164. F.A.L. Dullien and P.N. Mehta, Powder Technology, 5, 1971/72, pp 179-193.

165. S.D. Wicksell, Biometrika, 18, 1926, pp 151-172.

166. B.V. Guellard, "A microscopic technique suitable for determining size/frequency relationships of inclusions. A note prepared for the inclusions assessment group", 27th Jan., 1966, Steel Company of Wales.

167. Yu. A. Shul'te, E.I. Tsivirko, A.I. Garevskikh and A.A. Shalomeev, Zavodskaya Laboratoriya, 33, (6), 1967, pp 730-733.

168. P.A. Thornton, J. of Material Science, 6, 1971, pp 347-356.

169. M. Wahlster, "Prod. and Appl. of Clean Steels", ISI Spec. Rep. No. 134, ISI, London, pp 205-214.

170. I. Kozasu, T. Shimizu and H. Kubota, Trans. ISIJ., 13, 1973, pp 20-28.

171. F. Schuckher, "Quantitative Microscopy", McGraw-Hill Book Co., R.T. DeHoff and F.N. Rhines ed, 1968, pp 201-265.

172. H.E. Exner, International Met. Reviews, Review 159

17, 1972, pp 25-42.

173. W.L. Nicholson, Biometrika, 57, (2), 1970, pp 273-297.

174. H.E. Exner, Z. Metallkunde, 57, (10), 1966, pp 753-763.

175. F. Kottler, J. Franklin Instit., 250, 1950, pp 339-356, pp 419-441.

176. R.L. Fullman, J. of Metals, 5, 1953, pp 447-452.

177. H. Itoh, Metallography, 3, 1970, pp 407-417.

178. F.C. Hull and W.J. Houk, Trans. AIME, 197, 1953, pp 565-572.

179. J.E. Hilliard, Trans. AIME, 242, 1968, pp 1373-1380.

180. S.D. Wicksell, Biometrika, 17, 1925, pp 84-99.

181. E. Scheil, Z. Anorg.u.allg. Chem., 201, 1931, p 259.

182. H.A. Schwartz, Metals and Alloys, 5, (6), 1934, pp 139-140.

183. S.A. Saltykov, "Stereometric Metallography", 2nd ed., Moscow: Metallurgizdat, 1958.

184. G.M. Tallis, Biometrics, 26, 1970, pp 87-103.

185. E.D. Hyam and J. Nutting, JISI, 184, 1956, pp 148-165.

186. M.F. Ashby and R. Ebeling, Trans. AIME, 236, 1966, pp 1396-1404.

187. S. Drapal and V. Horalek, Act. Technica, 4, (6), 1959, pp 474-493.

188. G. Bach, "STEREOLOGY - Proceedings of the Second International Congress for Stereology", H. Elias ed., Springer Verlag, New York, 1967, pp 174-185.

189. J.M. DallaValle, "Micromeritics", 2nd ed., Pitman Pub. Co., New York, 1948, Chapter 5.

190. J. Aitchison and J.A.C. Brown, "The Lognormal Distribution", Cambridge Uni Press, 1966, Chapter 2.

191. F. Binder, Radex-Rdsch., (2), 1962, pp 82-105.

192. N.L. Johnson, Biometrika, 36, 1949, pp 149-176.

193. E.W. Meyer, "The Physics of Particle Size Analysis", Brit. J. of App. Phys., Supplement No. 3, Discussion to Paper E3, 1954, p 5108; T. Hatch and A.P. Choate, J. Franklin Instit., 31, (2), 1929, p 99.

194. R.P. Loveland and A.P.H. Trivelle, J. Phys. and Coll. Chem., 51, 1947, p 1004.

195. H.C. Schwartz and E.A. Botan, The Microscope, 17, (4), 1969/1970, pp 277-285.

196. T.Tuma, The Microscope, 17, (2), 1969, pp 105-110.

197. W.E. Stumpf and C.M. Sellars, Metallography, 1, 1968, pp 25-34.

198. D.A. Aboav and T.G. Langdon, Metallography, 2, 1969, p 171.

199. J. Aitchison and J.A.C. Brown, Metroeconomica, 6, 1954, pp 88-96.

200. B. Epstein, J. of Franklin Instit., 244, 1947, pp 471-477.

201. F. Kottler, J. Franklin Instit., 251, 1951, pp 499-514, pp 617-641.

202. R.F. Dewsnap, R. Pearce and J.R. Branson, private communication.

203. K. Asano, T. Saeki and T. Nakano, Proc. Interm Conf. Science and Technology of Iron and Steel, Section 3, 2, 1971, pp 584-587.

204. M. Frohlke, The Microscope, 19, 1971, pp 403-414.

205. W.A. Johnson, Metal Progress, 49, 1946, pp 87-92.

206. G.S. Watson, Biometrika, 58, (3), 1971, pp 483-490.

207. C.C. Heyde, J. Royal Statist. Society, Series B, 25, 1963, pp 392-393.

208. M.G. Kendall and P.A.P. Morgan, "Geometrical Probability", Griffin, London, 1963, p 88.

209. T.J. Baker and J.A. Charles, JISI, 210, 1972, pp 702-706.

210. E.S. Pearson, Biometrika, 50, 1963, pp95-112.

211. R.W. Heckel et al., Trans AIME, 233, 1965, pp 1798-1799; 233, 1965, pp 2001-2011.

212. A. Hald, "Statistical Theory with Engineering Applications", John Wiley and Sons, New York, 1962.

213. M.R. Spiegel, "Theory and Problems of Statistics", Schaum Pub. Co., New York, 1961.

214. H.D. Brody and M.C. Flemings Trans. AIME, 236, 1966, pp 615-624; T.Z. Kattamis and M.C. Flemings, Trans. AIME, 236, 1966, pp 1523-1532.

215. D.C. Hilty and V.T. Popp, Electric Furnace Proceedings, 1969, pp 52-66.

216. I. Eisenberger, Technometrics, 6, (4), 1964, pp 357-362.

217. F.B. Pickering, Steel Times Annual Review, 1973, pp 99-110.

218. S.A. Main, JISI, 142, 1940, p 270.

219. J.E. Russell, "Clean Steel", ISI Spec. Rep. 77, 1963, p 33.

220. R.W. Ruddle, "The Solidification of Castings", Inst. of Metals, Monograph and Rep. Series No. 7, London, 1950.

221. S. Oya and U. Honma, (Waseda Univ Tokyo) Rept. Castings Research Lab., Waseda Univ, (11), 1960, pp 36-60.

222. C. Benedicks, disc. of 1st Rept. of Heterogeneity Committee, JISI, 113, 1926, pp 169-171.

223. B. Chalmers, J. Aust. Inst. Metals, 8, 1963, p 255.

224. K.A. Jackson, J.D. Hunt, D.R. Uhlmann and T.P. Seward 111, Trans AIME, 236, 1966, pp 149-158.

225. H. Biloni and B. Chalmers, J. of Mat. Sci., 3, (2), 1968, pp 139-149.

226. J.A. Spittle, G.W. Dellamore and R.W. Smith, "The Solidification of Metals", ISI, Pub. 110, London, 1968, pp 318-322.

227. A. Ohno and H. Soda, Trans ISIJ, 10, 1970, pp 13-20.

228. W.C. Winegard and B. Chalmers, Trans ASM, 46, 1954, p 214.

229. R.T. Southin, Trans AIME, 239, 1967, p 220.

230. L.M. Hogan and R.T. Southin, AFS Cast. Metals Research J., March, 1968, pp 1-4.

231. L. Northcott, J. Inst. of Metals, 62, 1938, pp 101-120.

232. S. Ya Skoblo, Stal' in English, (3), 1962, pp 185-189.

233. J.A. Charles, "The Solidification of Metals",

ISI Pub 110, London, 1968, pp 309-312.

234. M. Wahlster and H. Brocher, Techn. Mitt. Krupp, 20, (3), 1962, pp 73-82.

235. M. Hasegaw and T. Mori, Trans ISIJ, 8, (2), 1968, pp 61-67.

236. A. Adachi, N. Iwamoto and M. Ueda, Trans ISIJ, 6, (1), 1966, pp 24-30.

237. D.C. Hilty, disc. to G.C. Dunderstadt and R.D. Weller, Open Hearth Proceedings, 1966, p 117.

238. G. Beveridge and R. Schechter, "Optimisation Theory and Practice", McGraw Hill, 1970.

239. J. Draper, Biometrika, 39, 1952, pp 290-301.

240. J.A. Lambert, Austral. J. Statist., 12, 1970, pp 33-43.

241. A. Fisher, Discussion, p 80, Trans ASCE, 101, 1936.

242. R. Rosin and E. Rammler, J. Instit. of Fuel, 7, 1933, pp 29-36.

243. J.G. Bennett, J. Instit. of Fuel, 10, 1936, pp 22-39.

244. L.R. Kittleman, J. of Sedimentary Petrology, 34, (3), 1964, pp 483-502.

245. H.A. Vogels and F. Bruening, Arch Eisenh., 35, 1964, p 115.

246. K.J. Irvine, JISI, 208, 1970, pp 717.

247. T.J. Baker and J.A. Charles, JISI, 211, 1973, pp 191.

APPENDIX 1

(a) - HEAT DETAILS

HEAT 14

TIME hr min	MELT TEMPERATURE °C	CHAMBER VACUUM LEVEL Torr	COMMENTS
0			diff heater on
5			power on
30			10KW
45			16KW - diff pump off - forepump on chamber
50		4×10^{-1}	pressure increasing
1 05			chamber opened to adjust mould
1 20			pump down begun
2 00		1.5×10^{-5}	17½KW
2 08		1.5×10^{-5}	charge molten - power reduced to 12KW
2 15	1400		Al addition made
2 20		1.5×10^{-5}	Cast

CHARGE:	4 Kg Copper.
ADDITIONS:	69.5g of Copper (11) Oxide to melt.
	22.8g of Aluminium to melt.
	4.6g of Aluminium to mould.
CRUCIBLE:	ZrO_2
MOULD:	Cast iron Surrounded by refractory bricks.
STOOL:	Carbon.

HEAT 17

TIME	MELT TEMPERATURE ^{o}C	CHAMBER VACUUM LEVEL Torr	COMMENTS
hr min			
0			diff heater on - generator on
40			15KW
42		8×10^{-1}	18KW pressure increasing
55		5×10^{-1}	pressure decreasing - 20KW
1 10		8×10^{-1}	charge molten - power reduced to 12KW - air introduced into chamber
1 14			samples taken for oxygen content
1 15		4×10^{-1}	chamber evacuated - 11KW
1 33	1400	4×10^{-1}	power reduced to 7KW
1 38			chamber opened to remove silica sheath which broke
1 44			Al addition made - oxide layer formed on surface
1 50			back fill to 100mmHg of argon
1 52			cast

CHARGE:	3.54Kg Copper.
ADDITIONS:	69.5g of Copper (11) Oxide to melt.
	34.4g of Aluminium to melt.
	5.1g of Aluminium to mould.
CRUCIBLE:	Magnesia.
MOULD:	Cast Iron.
STOOL:	Carbon

HEAT 18

TIME	MELT TEMPERATURE °C	CHAMBER VACUUM LEVEL Torr	COMMENTS
hr min			
0			diff heater on - generator on
30		2×10^{-5}	diff pump on - power on 10KW
42		6×10^{-4}	power 17KW
45		2×10^{-4}	power 20KW
55		2×10^{-5}	charge molten - 7KW
1 00			CuO plus Sn additions placed in feeder and evacuated
1 10	1200		CuO plus Sn additions made
1 15			evacuating feeder on forepump on placing Al addition
1 18	1240		
1 19			diff pump on
1 20		4×10^{-4}	
1 25	1310	2×10^{-5}	Al addition made - oxide layer formed on surface
1 27	1350	10^{-5}	7KW

HEAT 18 C'tued

1	33	back fill to 100mmHg of argon and cast

CHARGE:	3.40 Hg Copper
ADDITIONS:	35g of Copper (11) Oxide to melt
	35.1 of Tin to melt
	34.4 of Aluminium to melt
	5g of Aluminium to mould
CRUCIBLE:	Magnesia
MOULD:	Cast Iron surrounded by refractory bricks
STOOL:	Carbon

HEAT 19

TIME	MELT TEMPERATURE °C	CHAMBER VACUUM LEVEL Torr	COMMENTS
hr min			
0			diff heater on - generator on
39			power on 7KW
44		5.5×10^{-1}	9 KW
49		1	19KW
1 00		4×10^{-1}	charge molten - 15 KW reduced to 10KW - oxide layer on surface from previous heat
1 04		2.4×10^{-1}	7.5KW
1 09	1170	1.7×10^{-1}	6 KW
1 22	1180		4 KW
1 28	1130	3×10^{-4}	diff pump on
1 32	1140	5×10^{-4}	
1 34			CuO plus Sn additions
1 42		5×10^{-4}	5KW
1 44	1150	6×10^{-4}	
1 49	1180		
1 50			Al addition made -

HEAT 19 C'tued

				remained on oxide layer until molten
1	54		2×10^{-5}	
1	56	1180	10^{-4}	thick oxide layer
1	59			cast under pressure of 100mmHg of argon

CHARGE: 3.52Kg Copper

ADDITIONS: 35g of Copper (11) Oxide to melt
35.2g of Tin to melt
34.2g of Aluminium to melt
5.1g of Aluminium to mould

CRUCIBLE: Magnesia

MOULD: Cast Iron surrounded by refractory bricks

STOOL: Steel

HEAT 20

TIME	MELT TEMPERATURE °C	CHAMBER VACUUM LEVEL Torr	COMMENTS
hr min			
0			diff heater on - generator on
50		10^{-5}	power on 5KW
53		2×10^{-4}	10KW
55		3×10^{-1}	diff pump off 14KW
1 00		5×10^{-1}	20 KW
1 09		3.5×10^{-1}	charge molten - power reduced to 7KW
1 15			power off - thermocouple will not clear crucible
1 23			pump down - 5KW
1 28		2×10^{-1}	starting to remelt
1 37		1.4×10^{-1}	5KW
1 39			diff pump on
1 43	1070		
1 47	1130	1.2×10^{-1}	5KW
1 55	1200		3KW
2 00	1110	10^{-1}	
2 01			3KW
2 03	1080	5×10^{-5}	

HEAT 20 C'tued

2	07	1100	4×10^{-4}	
2	11	1110	6×10^{-5}	
2	13			power off - pressure dropped as temperature dropped
2	14	1070	2×10^{-5}	thermocouple added to partially molten Cu melt pressure increased as power was applied
2	19		3×10^{-4}	
2	20		5×10^{-4}	Al addition made - oxide surface layer formed - some Al pieces remained on layer until molten
2	25	1100	3×10^{-4}	
2	29			cast under pressure of 100mmHg of argon

CHARGE:	2.92Kg Copper
ADDITIONS:	35g of Copper (11) Oxide to melt
	34.3g of Aluminium to melt
CRUCIBLE:	Magnesia
MOULD:	Cast Iron surrounded by refractory bricks
STOOL:	Steel

HEAT 21

TIME hr min	MELT TEMPERATURE °C	CHAMBER VACUUM LEVEL Torr	COMMENTS
0			diff heater on - generator on
3		IT	power on 15KW
8		1.5T	18KW
15		1.5T	19KW
21		2T	19KW
34		1.2	charge molten - power reduced to 6KW - small oxide layer near crucible wall about $\frac{1}{4}$" thick
40	1020	7×10^{-1}	4.5KW
43	1070	5×10^{-1}	4.5KW
46	1070	4×10^{-1}	5KW
50	1050	4×10^{-1}	5KW
53			Sn addition made - oxide layer formed
1 00	1150	3.5×10^{-1}	oxide layer cleared
1 02			Al addition made - oxide layer formed on melt surface

HEAT 21 C'tued

1	06	1120	3.8×10^{-1}	5KW
1	10	1150	3.5×10^{-1}	5.5KW
1	13	1220	3.5×10^{-1}	
1	17			Cast

CHARGE: 3.43Kg Copper

ADDITIONS: 70g of Copper (11) Oxide to melt

35.3g of Tin to melt

18.1g of Aluminium to melt

CRUCIBLE: Magnesia

MOULD: Cast Iron surrounded by refractory bricks

STOOL: Steel

HEAT 22

TIME hr min	MELT TEMPERATURE °C	CHAMBER VACUUM LEVEL Torr	COMMENTS
0			diff heater on - generator on
6		3	5KW
10		1	10KW
16		1.5	15KW
18		1.2	19KW
35		2.5	19.5KW
1 00		3×10^{-1}	19KW
1 15			Al addition made - boil was proceeding until Al addition - power reduced - surface froze
1 25			11KW
1 30	1550	1.5×10^{-1}	backfilled to 100mmHg of argon - cast

CHARGE:	3.09Kg Soft Magnetic Iron
ADDITIONS:	52.5g of Fe_3O_4 to melt
	11.1g of Aluminium to melt
	5g of Aluminium to mould
CRUCIBLE:	Magnesia
MOULD:	Cast Iron surrounded by refractory bricks
STOOL:	Steel

HEAT 23

TIME	MELT TEMPERATURE °C	CHAMBER VACUUM LEVEL Torr	COMMENTS
hr min			
0			generator on - diff heater on
8		3.2×10^{-1}	5KW
10		8×10^{-1}	10KW
16		1.5	15KW
20		1.4	20KW
28		2	20KW
36		5×10^{-1}	21KW
45			starting to melt - partial boil - pumps shut off 15KW
56			back fill to 100mmHg of argon
1 00			pressure increased to 200mmHg of argon
1 10			opened chamber to remove hang up
1 15			back fill to 100mmHg of argon
1 18			charge molten

HEAT 23 C'tued

1	19	1450	Al addition made
1	30	1530	Cast

CHARGE: 2.98Kg Soft Magnetic Iron

ADDITIONS: 59.9g of Fe_3O_4 to melt

23.2g of Aluminium to melt

5g of Aluminium to mould

CRUCIBLE: Magnesia

MOULD: Cast Iron surrounded by refractory bricks

STOOL: Steel

HEAT 24

TIME	MELT TEMPERATURE °C	CHAMBER VACUUM LEVEL Torr	COMMENTS
hr min			
0			generator on - diff heater on
15		1.5×10^{-1}	5KW
17		3.5×10^{-1}	10KW
25		1	15KW
28		20	15KW
30		20	20KW
35		3	19KW
41		1.5	20KW
1 15			charge molten - charge open twice during period to remove hang ups - C boil
1 30	1440	2.5×10^{-1}	boil ceased
1 33		2.8×10^{-1}	Al addition made
1 35	1540	2×10^{-1}	
1 37			back fill to 100mmHg of argon then cast

CHARGE:	2.98Kg Soft Magnetic Iron
ADDITIONS:	89.9g of Fe_3O_4 added to mould
	28g of Aluminium added to melt
CRUCIBLE:	Magnesia
MOULD:	Cast Iron surrounded by refractory cricks
STOOL:	Cast Iron

HEAT 26

TIME	MELT TEMPERATURE °C	CHAMBER VACUUM LEVEL Torr	COMMENTS
hr min			
0			generator on
19		10^{-1}	back fill to 60mmHg of argon
20			6KW
25			25KW
45		120	19KW
1 00		200	charge molten - carbon boil
1 10	1700	55	boil ceased
1 30	1530	60	Al addition made - thick oxide layer formed on surface
1 40		20	surface layer removed
1 45	1560		cast mould did not induct

CHARGE:	6.80Kg Soft Magnetic Iron
ADDITIONS:	99g of Fe_3O_4 to melt
	17.6g of Aluminium to melt
CRUCIBLE:	Magnesia
MOULD:	Cast Iron surrounded by refractory bricks
STOOL:	Steel

HEAT 28

TIME	MELT TEMPERATURE °C	CHAMBER VACUUM LEVEL Torr	COMMENTS
hr min			
0			generator on - diff heater on
7		2.5×10^{-1}	
12			5KW
18		9×10^{-1}	15KW
20		1.5	20KW
35		1.5	20KW
40		4×10^{-1}	20KW
1 10			back fill to 80mmHg of argon - forepump off
1 15			20KW
1 30			Chamber opened to remove hang up
1 35			melt complete - carbon boil
1 45	1500		9KW - boil ceased
1 46		4×10^{-1}	10KW
1 49	1550		back fill to 100mmHg cast - ingot took ≈ 10 sec to solidify

CHARGE:	3.09Kg Soft Magnetic Iron
ADDITIONS:	None
CRUCIBLE:	Magnesia
MOULD:	Cast Iron surrounded by refractory bricks
STOOL:	Steel

HEAT 29

TIME	MELT TEMPERATURE °C	CHAMBER VACUUM LEVEL Torr	COMMENTS
hr min			
			half the charge melted - chamber opened - Fe_3O_4 addition made and other half of charge added - pumped down to 2.5×10^{-1}T - then back fill to 20T with argon - FeO layer formed on suface when chamber was opened to obtain sample - sample not obtained - evacuated chamber - melt completed under pressure of 50T of argon
0			FeO layer removed
			power reduced from 25to
5			10KW - sample cast
7	1400		

HEAT 29 C'tued

13	1510	
14		Al addition made - oxide layer formed on surface - surface cleared
16		samples taken from melt
18	1560	power off
20	1480	
22.5	1410	
24	1410	
26	1380	
28.5	1310	
29	1280	
30	1240	
34	1140	

CHARGE: 4.54Kg Soft Magnetic Iron

ADDITIONS: 56.9g of Fe_3O_4 to melt

40.3g of Aluminium to melt

CRUCIBLE: Magnesia

MOULD: None

STOOL: None

APPENDIX 1

(b) INGOT DETAILS

MACROSTRUCTURES

INGOT 3

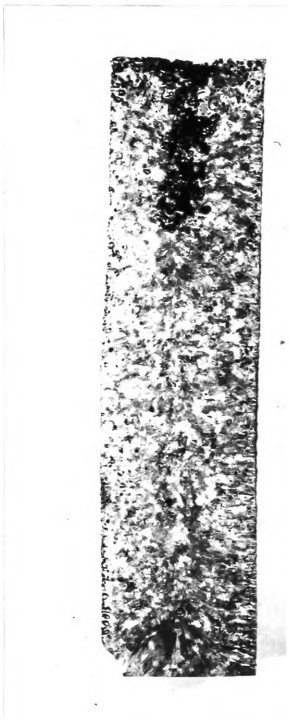

INGOT 18

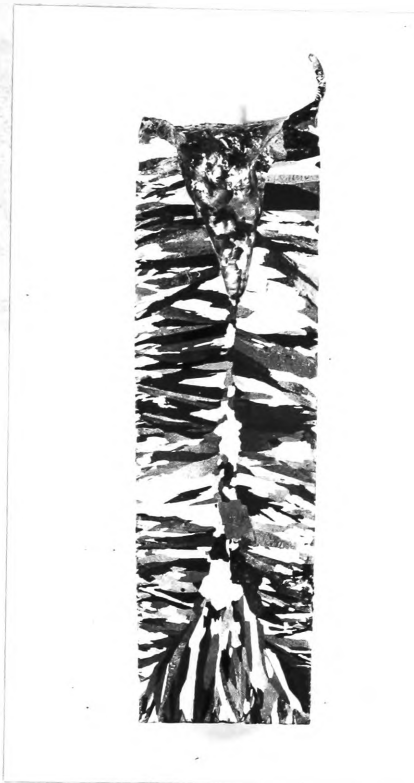

MACROSTRUCTURES

INGOT 27

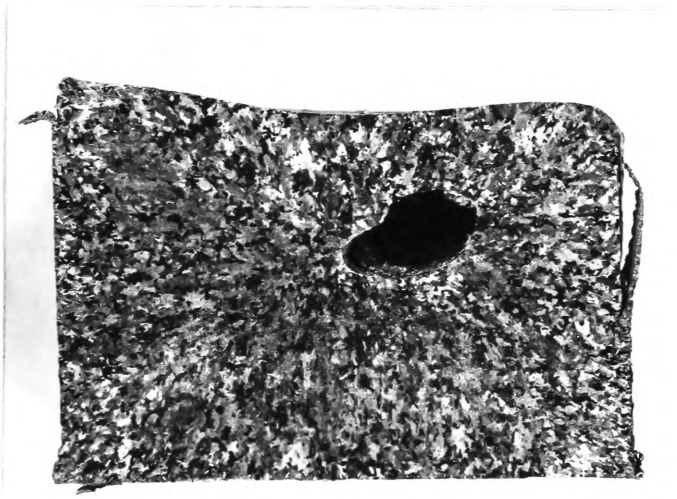

INGOT 29

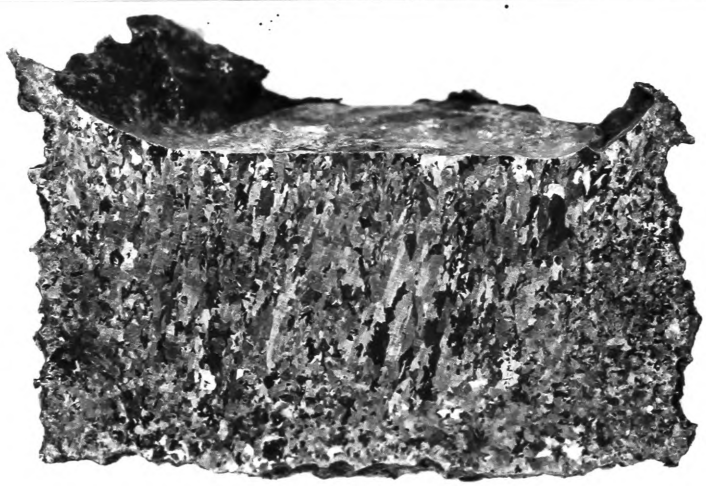

MACROSTRUCTURES

INGOT 30

INGOT 5

(ppm)

0

520	550	930
	270	
	260	
560	480	480
160	1000	990
1180	410	640
	230	
160		120
	210	
340	500	210
460	420	
200	410	180

MACROSTRUCTURE

(wt %) Al		
1.51	1.45	1.37
	1.35	
	1.38	
1.37	1.18	1.20
1.30	1.07	1.21
1.08	1.05	1.06
	0.91	
0.68		0.67
	0.70	
0.70	0.70	0.70
0.66	0.66	
0.63	0.62	0.62

(wt %) Sn		
1.12	1.15	1.20
	1.19	
	1.19	
1.12	1.10	0.96
1.15	1.15	0.79
1.14	1.21	0.81
	1.29	
1.15		0.93
	1.13	
1.26	1.13	0.92
1.30	1.13	
1.33	1.21	0.88

INGOT 6

O
(ppm)

130	360	270
30	70	40
280	60	70
35	100	70
	190	

MACROSTRUCTURE

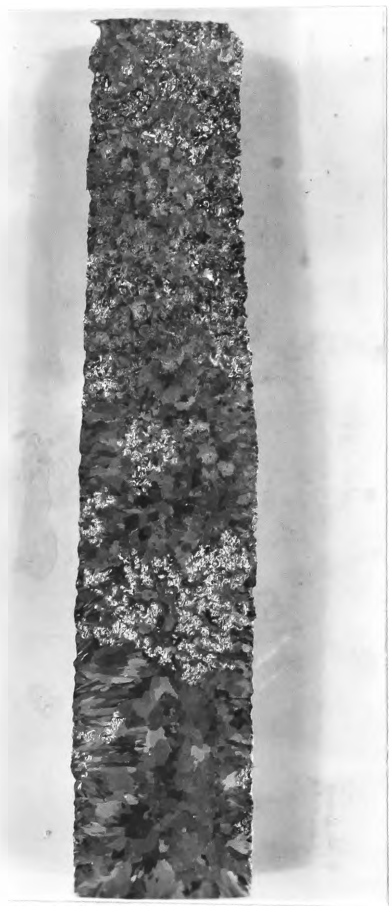

(wt %) Al		
	0.91	
	0.97	
	0.99	
	0.89	
	0.81	
	0.66	
0.61	0.62	0.59
0.59	0.59	0.59
0.56	0.53	0.52
0.57	0.56	0.56
	0.55	

(wt %) Sn		
	0.78	
	0.79	
	0.84	
	0.77	
	0.91	
	0.76	
0.36	0.41	0.36
0.37	0.36	0.39
0.34	0.34	0.38
0.36	0.37	0.36
	0.41	

INGOT 14

MACROSTRUCTURE

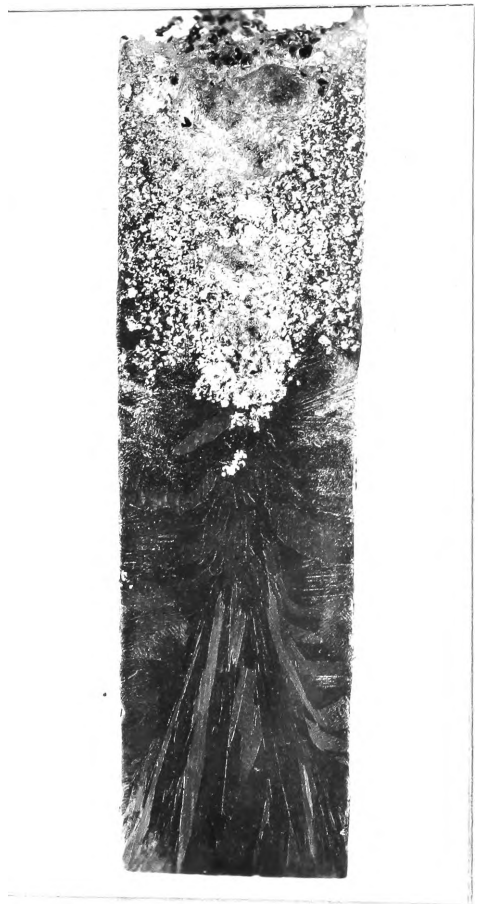

(wt%) Al			(ppm) O		
0.33		0.36	2600		2100
0.32		0.37	1500		1300
0.32		0.36	200		1900
0.32		0.35	110		60
0.36	0.36	0.36	70	280	80
	0.36			120	
0.37	0.35	0.37	40	80	70
0.37	0.36	0.37	2	270	100
0.38	0.29	0.36	60		200

INGOT 17

MACROSTRUCTURE

(wt%) Al		
1.04		0.99
	0.98	
1.02	0.97	1.00
0.98	0.98	0.98
0.98	0.95	1.01
0.95		0.94
	0.91	
0.91	0.92	0.91
0.94	0.89	0.96

(ppm) O		
1790		2460
	2660	
1590	2210	1830
1580	1900	1840
30	40	1780
35		40
	120	
50	55	60
85	60	50

INGOT 19

MACROSTRUCTURE

(wt%) Al		
1.14		1.18
0.94		1.12
1.08		
1.06		1.09
	1.03	
1.07		1.12
	1.06	
1.02	1.07	1.05
1.08	1.04	1.04
1.07	1.06	1.03

(wt%) Sn		
0.40		0.36
0.35		0.37
0.38		
0.35		0.42
	0.34	
0.36		0.35
	0.40	
0.38	0.40	0.36
0.40	0.34	0.34
0.37	0.39	0.36

INGOT 20

MACROSTRUCTURE

(wt%) Al		
	0.92	
1.00	0.70	1.26
	1.15	1.26
	1.12	
1.02	0.92	0.28
0.72	0.35	0.10
1.25	0.96	1.35

(ppm) O		
	1190	
1230	1180	1000
	1170	1000
	1640	
1440	1220	1130
1060	1270	2110
1010	980	2030

INGOT 21

MACROSTRUCTURE

INGOT 22

MACROSTRUCTURE

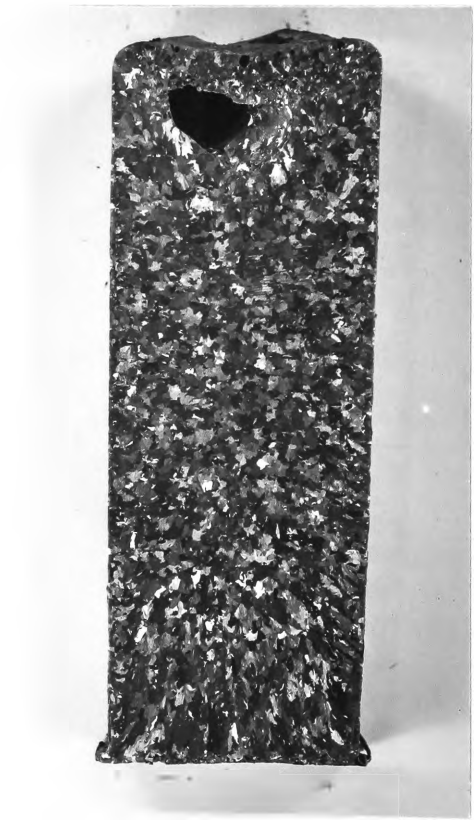

	(wt%) Al			(ppm) O		
	0.25		0.24	90		224
2	0.49	0.24	0.24	300	70	85
	0.25	0.25	0.23	20	75	90
	0.24		0.23	75		105
5		0.25			55	
	0.36	0.23	0.25	40	37	95
	0.26	0.23	0.24	46	50	65
8	0.26	0.25	0.24	30	65	70
	0.26	0.25	0.24	60	40	40

Sparks at levels 2, 5, 8, showed no segregation in other elements mean values are:

C	P	Mn	Si	S	Ni	Cr	Mo
<0.03	0.010	0.06	0.055	0.022	0.025	0.020	<0.005
Cu	Sn						
0.045	0.011						

INGOT 23

MACROSTRUCTURE

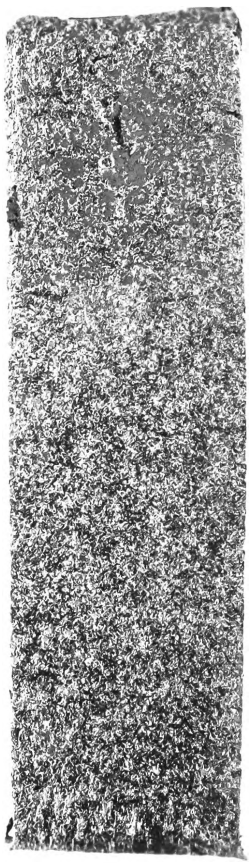

	(wt%) Al			(ppm) O			4 successive sparks
	*		0.70	1000		670	* 0.52, 0.63, 0.48
2	+		>1.0	190		1770	0.36
	0.63		>1.0	425		1625	+ 0.74, 0.84, 1.0
	0.48		0.57	110		195	0.81
5		0.47			50		
	●		0.47	940		90	● 0.46, 0.72, 0.73
		0.45			70		0.54
8	X	0.45	0.49	60	65	85	X 0.62, 0.72, 0.45
	0.47	0.47	0.46	60	80	45	0.49
	0.48	0.47	0.46	195	70	60	
	0.50	0.48	0.47	410	80	85	

Sparks at levels 2,5,8 showed no segregation in other elements

Apparent high C(0.07) and S (0.043) were probably due to matrix effect of high Al at level 2.

Mean analysis.

C	P	Mn	Si	S	Ni	Cr	Mo	Cu	Sn
<0.03	0.014	0.065	0.06	0.023	0.025	0.012	<0.005	0.050	0.013

INGOT 24

MACROSTRUCTURE

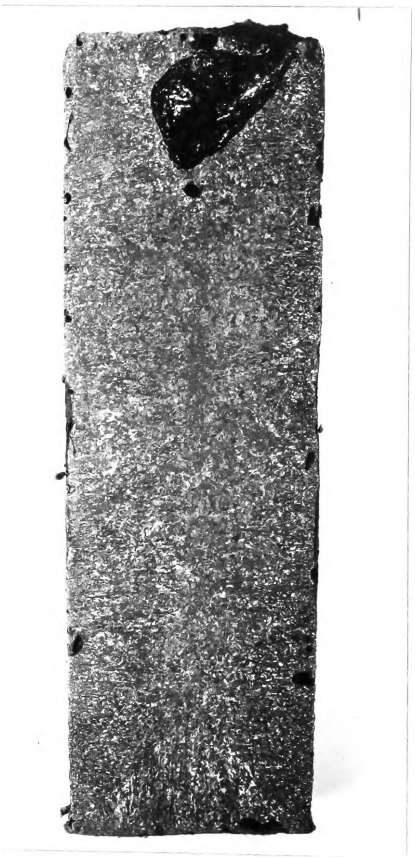

	(wt %) Al			(ppm) O		
	0.48		0.44	340		360
2	0.45	0.46	0.46	280		250
	0.48		0.46	270		280
		0.47			270	
5	0.44		0.46	350		485
		0.46			515	
	0.46	0.45	0.46	370	220	280
8	0.46	0.47	0.45	320	310	300
	0.46	0.46	0.45	360	350	

Sparks at levels 2,5, and 8 showed no segregation in other elements except, possibly C at 0.037 at level 2.

Mean analysis

C	P	Mn	Si	S	Ni	Cr	Mo	Cu	Sn
<0.03	0.012	0.055	0.075	0.022	0.025	0.012	<0.005	0.047	0.012

APPENDIX 2 - INCLUSION ASSESSMENT DATA

A2-1 SERIES 2 SAMPLES

Magnification = 1450x

B = Minor axis of section ellipse

A = Major axis of section ellipse

A and B are expressed in graticule units

1 graticule unit = 0.7724 μm

I22 No 1 (TRAVERSE LENGTH = 57.33mm)

B x A	FREQUENCY	B x A	FREQUENCY
1 x 1	172	2 x 10	1
1 x 2	154	2 x 11	1
1 x 3	68	2 x 12	1
1 x 4	34	2 x 15	3
1 x 5	37	3 x 3	6
1 x 6	14	3 x 4	4
1 x 7	7	3 x 5	4
1 x 8	5	3 x 6	2
1 x 9	3	3 x 7	1
1 x 10	1	3 x 10	1
1 x 11	1	3 x 13	1
1 x 15	1	4 x 4	1
2 x 2	42	4 x 5	2
2 x 3	43	4 x 7	1
2 x 4	25	4 x 8	1
2 x 5	15	5 x 6	2
2 x 6	7	5 x 7	1
2 x 7	7		
2 x 8	2		
2 x 9	1		

I22 No 1C (TRAVERSE LENGTH = 57.33mm)

1 x 1	34	2 x 5	1
1 x 2	39	2 x 6	1
1 x 3	12	2 x 7	1
1 x 4	10	2 x 8	2
1 x 5	3	2 x 12	1
1 x 6	1	3 x 3	4
1 x 7	2	3 x 4	2
1 x 11	1	3 x 5	2
2 x 2	35	3 x 8	1
2 x 3	23	3 x 9	1
2 x 4	12	4 x 4	2

I22 No 6 (TRAVERSE LENGTH = 87.645mm)

B x A	FREQUENCY	B x A	FREQUENCY
1 x 1	86	2 x 6	2
1 x 2	126	2 x 7	1
1 x 3	33	2 x 8	1
1 x 4	3	3 x 3	6
1 x 5	5	3 x 4	6
1 x 6	4	3 x 6	3
1 x 9	4	4 x 4	2
1 x 10	1	4 x 5	1
2 x 2	21	4 x 7	2
2 x 3	28	4 x 17	1
2 x 4	10	5 x 8	1
2 x 5	7	6 x 13	1

I18 No 4R (TRAVERSE LENGTH = 98.295)

B x A	FREQUENCY	B x A	FREQUENCY
½ x ½	48	2 x 2	16
½ x 1	18	2 x 3	38
½ x 2	11	2 x 4	29
½ x 3	4	2 x 5	35
½ x 4	5	2 x 6	22
½ x 5	2	2 x 7	9
½ x 7	1	2 x 8	9
1 x 1	49	2 x 9	6
1 x 2	43	2 x 10	7
1 x 3	46	2 x 11	4
1 x 4	30	2 x 12	5
1 x 5	10	2 x 13	2
1 x 6	15	2 x 14	3
1 x 7	5	2 x 15	2
1 x 8	6	3 x 3	13
1 x 9	1	3 x 4	18
1 x 10	5	3 x 5	14
1 x 11	1	3 x 6	12
1 x 13	1	3 x 7	13
1 x 14	1	3 x 8	7

I18 No 4 R (C'tued)

B x A	FREQUENCY	B x A	FREQUENCY
3 x 9	3	5 x 9	3
3 x 10	3	5 x 10	6
3 x 11	3	5 x 11	3
3 x 12	2	5 x 13	4
3 x 15	2	5 x 14	2
4 x 4	9	5 x 15	1
4 x 5	14	5 x 16	1
4 x 6	4	6 x 6	1
4 x 7	8	6 x 8	6
4 x 8	2	6 x 10	1
4 x 9	3	6 x 11	2
4 x 10	5	6 x 12	2
4 x 11	2	6 x 13	1
4 x 12	3	6 x 14	1
4 x 13	2	7 x 8	1
4 x 15	2	7 x 10	1
5 x 5	7	7 x 12	1
5 x 6	2	7 x 15	1
5 x 7	4	8 x 9	1
5 x 8	1	8 x 12	1
		10 x 13	1

I18 No 4 (TRAVERSE LENGTH = 90.27mm)

1 x 1	28	3 x 9	2
1 x 2	17	3 x 10	1
1 x 3	1	3 x 16	1
1 x 4	1	4 x 4	6
1 x 5	3	4 x 5	10
2 x 2	8	4 x 6	2
2 x 3	15	4 x 7	3
2 x 4	5	4 x 8	2
2 x 5	4	4 x 11	1
2 x 6	1	4 x 20	1
2 x 9	1	5 x 5	6
2 x 10	1	5 x 7	2
2 x 11	1	5 x 8	1
2 x 19	1	5 x 10	1
3 x 3	8	5 x 13	1
3 x 4	8	5 x 18	1
3 x 5	6	5 x 19	1
3 x 6	3	6 x 6	1
3 x 7	3	6 x 7	2
3 x 8	1	6 x 8	1

I18 No 4 (C'tued)

B x A	FREQUENCY	B x A	FREQUENCY
6 x 9	1	8 x 9	1
6 x 10	2	8 x 11	1
7 x 9	1	9 x 12	1
8 x 8	1	11x 11	1

I18 No 8R (TRAVERSE LENGTH = 33.42mm)

½ x ½	86	2 x 5	22
½ x 1	8	2 x 6	11
½ x 2	11	2 x 7	7
½ x 3	8	2 x 8	4
½ x 4	3	2 x 9	3
½ x 5	3	2 x 10	3
½ x 6	1	2 x 11	1
1 x 1	41	2 x 12	2
1 x 2	46	2 x 15	2
1 x 3	33	3 x 3	14
1 x 4	14	3 x 4	14
1 x 5	7	3 x 5	16
1 x 6	3	3 x 6	12
1 x 7	3	3 x 7	6
1 x 9	1	3 x 8	7
1 x 11	1	3 x 9	5
1 x 12	1	3 x 10	6
2 x 2	31	3 x 11	3
2 x 3	42	3 x 12	3
2 x 4	33	3 x 13	1

I18 No 8R (C'tued)

B x A	FREQUENCY	B x A	FREQUENCY
3 x 14	1	5 x 9	2
3 x 15	2	5 x 10	5
4 x 4	8	5 x 12	1
4 x 5	6	5 x 15	1
4 x 6	5	6 x 6	2
4 x 7	1	6 x 7	1
4 x 8	3	6 x 8	1
4 x 9	1	6 x 9	1
4 x 10	3	6 x 12	1
4 x 11	3	7 x 7	1
4 x 14	1	7 x 12	1
5 x 5	3	8 x 10	1
5 x 6	3	9 x 10	1
5 x 7	3	9 x 15	1
5 x 8	6	10 x 12	1

I30 TOP (TRAVERSE LENGTH = 47.36mm)

½ x ½	112	1½ x 2½	5
½ x 1	54	1½ x 3	8
½ x 1½	27	1½ x 4	5
½ x 2	14	1½ x 12	1
½ x 2½	2	2 x 2	26
½ x 3	6	2 x 2½	12
½ x 4	4	2 x 3	20
½ x 5	1	2 x 4	17
½ x 6	1	2 x 5	4
½ x 7	1	2 x 6	3
1 x 1	129	2 x 8	2
1 x 1½	49	2 x 9	1
1 x 2	27	2 x 10	1
1 x 2½	7	2½ x 2½	1
1 x 3	9	2½ x 3	2
1 x 4	2	2½ x 4	2
1 x 5	1	2½ x 5	2
1 x 6	3	2½ x 7	1
1½ x 1½	26	3 x 3	13
1½ x 2	30	3 x 4	20

I30 TOP (C'tued)

B x A	FREQUENCY	B x A	FREQUENCY
3 x 5	7	5 x 8	1
3 x 6	3	5 x 9	2
3 x 7	1	5 x 10	1
3 x 8	2	5 x 11	1
3 x 10	2	5 x 13	1
3 x 11	2	6 x 8	1
4 x 4	3	6 x 9	1
4 x 5	11	6 x 12	1
4 x 6	3	7 x 16	1
4 x 8	3	8 x 15	1
4 x 11	1	9 x 14	1
4 x 12	1	10 x 16	1
5 x 5	1	11 x 11	1
5 x 6	4	8 x 20	1
5 x 7	2		

I30 MIDDLE (TRAVERSE LENGTH = 37.39mm)

½ x ½	184	1½ x 4	4
½ x 1	47	1½ x 5	3
½ x 1½	25	2 x 2	26
½ x 2	10	2 x 2½	8
½ x 2½	4	2 x 3	16
½ x 3	3	2 x 4	8
½ x 4	3	2 x 5	4
½ x 5	1	2 x 6	4
½ x 8	1	2 x 7	3
1 x 1	149	2 x 9	1
1 x 1½	58	2½ x 3	2
1 x 2	34	2½ x 4	1
1 x 2½	3	2½ x 5	4
1 x 3	2	2½ x 6	1
1 x 4	2	3 x 3	5
1 x 6	1	3 x 4	7
1½ x 1½	28	3 x 5	10
1½ x 2	27	3 x 6	3
1½ x 2½	4	3 x 7	3
1½ x 3	5	3 x 8	2

I30 MIDDLE (C'tued)

B x A	FREQUENCY	B x A	FREQUENCY
3 x 9	2	5 x 11	1
3 x 10	2	5 x 12	1
4 x 4	3	5 x 15	1
4 x 5	6	6 x 7	1
4 x 6	3	7 x 10	2
4 x 7	1	7 x 14	1
4 x 8	1	7 x 15	1
4 x 9	1	9 x 15	1
4 x 12	1	12 x 44	1
5 x 7	1	7 x 23	1
5 x 9	1	5 x 21	1

I30 BOTTOM (TRAVERSE LENGTH = 34.23mm)

½ x ½	141	1½ x 3	7
½ x 1	38	1½ x 4	1
½ x 1½	20	1½ x 5	3
½ x 2	6	1½ x 8	1
½ x 2½	2	2 x 2	14
½ x 3	3	2 x 2½	6
½ x 4	3	2 x 3	27
½ x 7	1	2 x 4	4
1 x 1	82	2 x 5	4
1 x 1½	49	2 x 6	1
1 x 2	30	2 x 7	1
1 x 2½	8	2 x 9	1
1 x 3	5	2 x 10	1
1 x 4	4	2½ x 3	1
1 x 5	1	2½ x 6	1
1 x 7	1	3 x 3	4
1 x 9	1	3 x 4	8
1½ x 1½	14	3 x 5	3
1½ x 2	17	3 x 6	1
1½ x 2½	4	3 x 7	1

I30 BOTTOM (C'tued)

B x A	FREQUENCY	B x A	FREQUENCY
4 x 4	2	6 x 7	1
4 x 5	3	6 x 12	1
4 x 6	2	7 x 7	1
4 x 11	1	7 x 15	1
5 x 5	1	8 x 11	1
5 x 8	2	9 x 9	1
5 x 12	1	13 x 40	1
5 x 14	1	6 x 18	1
5 x 15	1	9 x 30	1
6 x 6			

I30 BOTTOM R (TRAVERSE LENGTH = 55.65mm)

½ x ½	70	2 x 3	26
½ x 1	32	2 x 4	12
½ x 1½	24	2 x 5	4
½ x 2	9	2 x 6	1
½ x 2½	3	2½ x 2½	2
½ x 3	2	2½ x 3	3
½ x 8	1	2½ x 4	3
1 x 1	68	2½ x 5	1
1 x 1½	30	2½ x 8	1
1 x 2	28	3 x 3	5
1 x 2½	2	3 x 4	10
1 x 3	2	3 x 5	13
1 x 5	3	3 x 6	2
1½ x 1½	16	3 x 7	1
1½ x 2	18	3 x 9	1
1½ x 2½	3	4 x 4	3
1½ x 3	7	4 x 5	1
1½ x 4	1	4 x 11	1
2 x 2	19	5 x 5	1
2 x 2½	6	5 x 6	1

I30 BOTTOM R (C'tued)

5 x 7	1	12 x 15	1
5 x 10	1	6 x 20	1
6 x 6	1	2 x 25	1
6 x 7	1	15 x 18	1
6 x 15	1	15 x 25	1
7 x 10	1	14 x 19	1

I27 TOP (TRAVERSE LENGTH = 35.21mm)

B x A	FREQUENCY	B x A	FREQUENCY
½ x ½	47	1½ x 2½	5
½ x 1	4	1½ x 3	13
½ x 1½	12	1½ x 4	11
½ x 2	19	1½ x 5	3
½ x 2½	2	1½ x 6	3
½ x 3	9	2 x 2	31
½ x 4	4	2 x 2½	2
½ x 5	1	2 x 3	36
½ x 7	1	2 x 4	25
1 x 1	53	2 x 5	8
1 x 1½	14	2 x 6	5
1 x 2	44	2 x 7	3
1 x 2½	5	2 x 8	1
1 x 3	13	2 x 12	1
1 x 4	11	2½ x 3	1
1 x 5	4	2½ x 4	2
1 x 6	2	2½ x 5	1
1 x 7	2	2½ x 7	1
1½ x 1½	9	2½ x 8	1
1½ x 2	10	3 x 3	7

I27 TOP (C'tued)

3 x 4	8	4 x 7	3
3 x 5	6	4 x 8	2
3 x 6	4	4 x 12	1
3 x 7	1	5 x 5	1
3 x 8	2	5 x 6	1
3 x 9	1	5 x 7	3
4 x 4	6	6 x 10	1
4 x 5	2	8 x 10	1
4 x 6	3		

I27 BOTTOM (TRAVERSE LENGTH = 59.34mm)

B x A	FREQUENCY	B x A	FREQUENCY
½ x ½	162	2 x 5	6
½ x 1	39	2 x 6	1
½ x 1½	11	2 x 7	1
½ x 2	19	2½ x 2½	1
½ x 2½	1	2½ x 4	1
½ x 3	7	3 x 3	7
½ x 4	3	3 x 4	8
½ x 6	1	3 x 5	2
1 x 1	132	4 x 4	1
1 x 1½	42	4 x 5	1
1 x 2	22	4 x 6	1
1 x 2½	4	6 x 6	1
1 x 3	17	7 x 8	1
1 x 4	3	9 x 11	1
1 x 5	2	40 x 20	1
1 x 6	1		
2 x 2	23		
2 x 2½	4		
2 x 3	17		
2 x 4	3		

A2-2 INDUSTRIAL SAMPLES

Magnification = 675X

1 Graticule Unit = 1.7158 μm

20 & 2T OXIDE (TRAVERSE LENGTH = 108 mm)

B x A	FREQUENCY	B x A	FREQUENCY
1 x 1	3	5 x 8	4
1 x 2	2	5 x 9	1
2 x 2	4	6 x 9	1
3 x 4	1	7 x 9	1
4 x 4	3	7 x 12	1
4 x 5	2	8 x 10	1
4 x 6	1	9 x 13	1
4 x 7	3	14 x 15	1
5 x 5	2		

20 & 2T OXY-SULPHIDES (TRAVERSE LENGTH = 108mm)

1 x 1	13	2 x 5	5
1 x 2	2	2 x 9	2
1 x 3	2	2 x 12	1
1 x 5	1	3 x 3	15
1 x 6	1	3 x 4	10
2 x 2	39	3 x 5	3
2 x 3	21	3 x 6	3
2 x 4	4	3 x 7	2

20 & 2T OXY-SULPHIDES (C'tued)

4 x 4	8	5 x 7	1
4 x 5	4	5 x 8	1
4 x 8	1	6 x 8	1
4 x 10	1	6 x 9	1
4 x 13	1	8 x 10	1
5 x 5	2	2 x 31	1
5 x 6	4	2 x 33	1

59 (TRAVERSE LENGTH = 147.94 mm)

B x A	FREQUENCY	B x A	FREQUENCY
½ x ½	10	2 x 3	19
½ x 1	4	2 x 4	6
½ x 1½	3	2 x 5	3
½ x 2	1	2 x 7	2
½ x 2½	1	2 x 9	1
½ x 3	1	2 x 10	1
1 x 1	24	2 x 19	1
1 x 1½	12	2½ x 2½	4
1 x 2	13	2½ x 3	4
1 x 3	2	3 x 3	31
1 x 4	1	3 x 4	10
1 x 5	1	3 x 5	2
1 x 6	1	3 x 6	1
1½ x 1½	7	3 x 7	2
1½ x 2	9	3 x 8	1
1½ x 3	4	3 x 10	1
1½ x 4	4	4 x 4	14
1½ x 5	2	4 x 5	2
2 x 2	31	4 x 6	3
2 x 2½	3	5 x 5	4

59 (C'tued)

5 x 6	3	6 x 10	1
6 x 6	2	7 x 8	1
6 x 8	2	7 x 10	1

8A2 (TRAVERSE LENGTH = 192.18mm)

B x A	FREQUENCY	B x A	FREQUENCY
½ x ½	7	4 x 6	2
½ x 1	2	4 x 8	1
½ x 2	2	5 x 5	12
½ x 3	1	5 x 10	1
1 x 1	27	5 x 11	1
1 x 2	18	5 x 13	1
1 x 3	10	6 x 6	3
1 x 4	3	6 x 8	1
2 x 2	79	6 x 9	1
2 x 3	7	6 x 15	1
2 x 4	3	7 x 7	1
2 x 5	2	7 x 9	1
2 x 6	1	7 x 12	3
2 x 10	1	7 x 15	1
3 x 3	20	8 x 8	1
3 x 4	2	8 x 10	1
3 x 5	4	8 x 11	1
3 x 6	1	9 x 9	1
4 x 4	23	9 x 10	1
4 x 5	2	9 x 12	1

8A2 (C'tued)

10 x 17	1	19 x 19	1
12 x 17	1	4 x 20	1
13 x 13	1	21 x 27	1
14 x 14	1	22 x 24	1
14 x 15	1	22 x 27	1

8A2 R (TRAVERSE LENGTH = 98.93mm)

½ x ½	197	3 x 4	4
½ x 1	5	4 x 4	10
½ x 1½	5	4 x 5	3
½ x 2	4	4 x 6	3
1 x 1	689	4 x 9	1
1 x 1½	22	5 x 5	4
1 x 2	11	5 x 7	1
1 x 2½	4	6 x 6	1
1 x 3	3	6 x 7	2
1 x 4	1	6 x 8	3
1½ x 1½	65	6 x 9	1
1½ x 2	21	7 x 7	1
1½ x 3	1	7 x 10	1
1½ x 4	2	8 x 11	1
2 x 2	22	8 x 12	1

8A2 R (C'tued)

B x A	FREQUENCY	B x A	FREQUENCY
2 x 2½	3	9 x 10	1
2 x 3	4	10 x 10	1
2 x 4	2	10 x 12	1
2 x 5	3	11 x 14	1
3 x 3	7	12 x 12	1

8A2 R (c'tued)

12 x 13	2	11 x 18	1
12 x 14	1	17 x 23	1
12 x 16	1	17 x 34	1
15 x 15	1	22 x 24	1

52 (TRAVERSE LENGTH = 183.78mm)

½ x ½	25	2 x 7	1
½ x 1	17	2½ x 3	1
½ x 1½	1	3 x 3	13
1 x 1	18	3 x 4	2
1 x 1½	9	4 x 4	4
1 x 2	11	4 x 6	1
1 x 3	6	4 x 7	1
1 x 6	1	5 x 5	6
1½ x 1½	3	5 x 6	1
1½ x 2	2	6 x 6	2
2 x 2	7	6 x 7	1
2 x 2½	1	8 x 8	1
2 x 3	8	8 x 10	1

8A9 (TRAVERSE LENGTH = 168.53mm)

B x A	FREQUENCY	B x A	FREQUENCY
½ x ½	44	5 x 6	1
½ x 1	13	5 x 7	1
½ x 2	3	5 x 11	1
1 x 1	63	6 x 6	10
1 x 2	33	6 x 7	1
1 x 3	5	6 x 8	1
1 x 4	1	7 x 7	6
1 x 5	2	7 x 8	3
2 x 2	132	7 x 10	1
2 x 3	12	8 x 8	2
2 x 4	8	8 x 9	1
2 x 5	4	8 x 10	1
2 x 6	1	10 x 10	1
3 x 3	51	11 x 17	1
3 x 4	5	12 x 12	1
3 x 5	1	13 x 14	1
4 x 4	33	15 x 24	1
4 x 5	4		
4 x 6	1		
5 x 5	7		

A2-3 QUANTITATIVE METALLOGRAPHIC DATA

P_p and P_L (or N_L) counts are per 10 fields unless otherwise stated.

I30 TOP

P_a	$P_p = \frac{P_a}{10 \times 80}$	N_L	$S_v = \frac{4N_L}{10 \times 1.36}$
0	0	0	0
0	0	2	0.5882
1	0.00125	4	1.1765
1	0.00125	5	1.4706
1	0.00125	9	2.6471
0	0	1	0.2941
0	0	6	1.7647
0	0	2	0.5882
2	0.0025	13	3.8235
0	0	0	0
0	0	4	1.1765
0.	0	3	0.8824
0	0	2	0.5882
0	0	3	0.8824
0	0	2	0.5882
0	0	10	2.9412
0	0	1	0.2941
1	0.00125	8	2.3529
0	0	6	1.7647
1	0.00125	13	3.8235

I30 TOP (C'tued)

1	0.00125	3	0.8824
0	0	10	2.9412
2	0.0025	11	3.2353
0	0	5	1.4706
0	0	4	1.1765
1	0.00125	5	1.4706

$V_v = \bar{P}_p = 0.000529$

$\sigma = 0.000804$

$\frac{\sigma}{\sqrt{26}} = 0.000158$

$S_v = M\left(\frac{4N_L}{10 \times 1.36}\right)$

$= 1.493$

$\sigma = 1.1374$

$\frac{\sigma}{\sqrt{26}} = 0.2231$

INGOT 30 MIDDLE

P_a	$P_p = \frac{P_a}{10 \times 80}$	N L	$S_v = \frac{4N}{L}$ 10×1.36
2	0.0025	15	4.4117
0	0	22	6.4706
0	0	15	4.4118
1	0.00125	17	5.0
1	0.00125	4	1.1765
1	0.00125	9	2.6471
1	0.00125	7	2.0588
2	0.0025	8	2.3529
0	0	6	1.7647
0	0	3	0.8824
0	0	6	1.7647
0	0	2	0.5882
1	0.00125	3	0.8824
1	0.00125	7	2.0588
0	0	4	1.1765
1	0.00125	5	1.4706
0	0	1	0.2941
0	0	4	1.1765
0	0	4	1.1765
0	0	1	0.2941
0	0	2	0.5882
0	0	7	2.0588
0	0	1	0.2941
0	0	6	1.7647
2	0.0025	12	3.5294
0	0	2	0.5882
1	0.00125	8	2.3529
0	0	5	1.4706
1	0.00125	8	2.3529
0	0	1	0.2941
0	0	11	3.2353
1	0.00125	4	1.1765
1	0.00125	6	1.7647
1	0.00125	10	2.9412

$V_v = \bar{P}_p = 0.000662$

$\sigma = 0.000828$

$\frac{\sigma}{\sqrt{34}} = 0.000142$

$S_v = M\left(\frac{4N}{10 \times 1.36}\right)$

$= 1.9197$

$\sigma = 1.4342$

$\frac{\sigma}{\sqrt{34}} = 0.246$

I18 No 4

P_a	$P_p = \frac{P_a}{10 \times 80}$	P_L	$S_v = \frac{2P_L}{10 \times 1.11}$
0	0	6	1.0811
1	0.00125	4	0.7207
0	0	2	0.3604
0	0	5	0.9009
0	0	2	0.3604
1	0.00125	4	0.7207
0	0	2	0.3604
1	0.00125	2	0.3604
0	0	6	1.0811
0	0	4	0.7207
0	0	0	0
0	0	0	0
1	0.00125	2	0.3604
1	0.00125	8	1.4414
1	0.00125	4	0.7207
0	0	0	0
0	0	2	0.3604
0	0	2	0.3604

$V_v = \bar{P}_p = 0.000417$ $\quad S_v = M\left(\frac{2P_L}{10 \times 1.11}\right) = 0.5506$

$\sigma = 0.000606$, $\frac{\sigma}{\sqrt{18}} = 0.000143$ $\quad \sigma = 0.4028$, $\frac{\sigma}{\sqrt{18}} = 0.0949$

I18 No 5

1	0.00125	2	0.6452
1	0.00125	4	1.2903
1	0.00125	9	1.2903
0	0	1	0.3226
1	0.00125	9	2.9032
0	0	4	1.2903
1	0.00125	2	0.6452
1	0.00125	8	2.5806
1	0.00125	8	2.5806
1	0.00125	4	1.2903
0	0	4	1.2903
1	0.00125	4	1.2903
0	0	3	0.9677
1	0.00125	4	1.2903
1	0.00125	1	0.3226

I18 No 5 (C'tued)

P_a	$P_p = \frac{P_a}{10 \times 80}$	P_L	$S_v = \frac{2P_L}{10 \times 0.62}$
0	0	3	0.9677
2	0.0025	4	1.2903
0	0	8	2.5806
0	0	3	0.9677

I18 No 5 (C'tued)

0	0	2	0.6452
1	0.00125	6	1.9355
1	0.00125	2	0.6452
0	0	3	0.9677
0	0	4	1.2903
0	0	7	2.2581
0	0	0	0
0	0	0	0
0	0	2	0.6452
0	0	8	2.5806
0	0	0	0

$V_v = \bar{P}_p = 0.000625$

$S_v = M\left(\frac{2P_L}{10 \times 0.62}\right)$

$= 1.279$

$\sigma = 0.000715$

$\sigma = 0.882$

$\frac{\sigma}{\sqrt{30}} = 0.000131$

$\frac{\sigma}{\sqrt{30}} = 0.161$

I22 No 1

No of Fields	P_a	$P_p = \frac{P_a}{N \text{ of } F \times 80}$
27	4	0.001852
25	3	0.0015
26	0	0
25	5	0.0025
23	2	0.001087
22	3	0.001705
19	1	0.000658
18	1	0.000694
14	1	0.000893

No of Fields	P_a	$P_p = \frac{P_a}{N \text{ of } F \times 80}$
14	1	0.000893
11	0	0
11	3	0.003409

$V_v = \bar{P}_p = 0.001266$

$\sigma = 0.000996$

$\frac{\sigma}{\sqrt{12}} = 0.000288$

I22 No 1

P_L	$S_v = \frac{2 P_L}{N \text{ of } F \times 0.62}$
6	3.87097
8	3.22581
18	5.80645
13	3.49462
13	3.81232
14	3.22581
6	1.20968
20	3.39559
12	1.84332
11	1.61290
18	1.71429
29	4.25220
20	1.66667
28	3.76344
6	0.87977
15	2.41936

$S_v = M\left(\frac{2P_L}{N \text{ of } F \times 0.62}\right) = 2.887$

$\sigma = 1.3285$

$\frac{\sigma}{\sqrt{15}} = 0.3321$

I22 No 6

P_a	$P_p = \frac{P_a}{80 \times 10}$	P_a	$P_p = \frac{P_a}{80 \times 10}$
0	0	0	0
0	0	0	0
0	0	0	0
0	0	1	0.00125
0	0	0	0
0	0	0	0
1	0.00125	0	0
0	0	0	0
1	0.00125	0	0
0	0	0	0
1	0.00125	0	0
0	0	0	0
1	0.00125	0	0
0	0	0	0
0	0	0	0

$V_v = \bar{P}_p = 0.000208$

$\sigma = 0.000474$

$\frac{\sigma}{\sqrt{30}} = 0.0000865$

I22 No 6

P_L	$S_v = \frac{2P}{L}$ / 10×1.11	P_L	$S_v = \frac{2P}{L}$ / 10×1.11
2	0.3604	2	0.3604
8	1.4414	4	0.7207
2	0.3604	2	0.3604
2	0.3604	4	0.7207
4	0.7207	2	0.3604
0	0	2	0.3604
4	0.7207	4	0.7207
0	0	4	0.7207
4	0.7207	2	0.3604
2	0.3604	0	0
8	1.4414	6	1.0811
0	0	2	0.3604
10	1.8018	0	0
0	0	0	0
4	0.7207	0	0

$$S_v = M\left(\frac{2P}{10 \times 1.11}\right) = 0.5045$$

$\sigma = 0.4694$

$\frac{\sigma}{\sqrt{30}} = 0.0857$

20 & 2T OXY-SULPHIDES

P_a	$P_p = \frac{P_a}{20 \times 80}$	P_a	$P_p = \frac{P_a}{20 \times 80}$
0	0	0	0
0	0	0	0
0	0	0	0
0	0	2	0.00125
0	0	0	0
0	0	3	0.001875
3	0.001875	0	0
0	0	0	0
0	0	0	0
0	0	1	0.000625
0	0	1	0.000625
0	0	1	0.000625
0	0	0	0
1	0.000625	0	0
0	0	0	0
1	0.000625	0	0
0	0	0	0
0	0	1	0.000625
1	0.000625	0	0
0	0	0	0
0	0	0	0
0	0	0	0
0	0	0	0
0	0	0	0
0	0	0	0
0	0	1	0.000625
0	0	0	0
0	0	0	0
0	0	0	0

20 & 2T OXY-SULPHIDES (CONT)

0	0	0	0
0	0	2	0.00125
0	0	0	0
0	0	1	0.000625
0	0	0	0
		0	0

$V_v = \overline{P}_p = 0.000172$

$\sigma = 0.000411$

$\frac{\sigma}{\sqrt{69}} = 0.000049$

0	0	2	0.0901
4	0.1802	2	0.0901
4	0.1802	0	0
8	0.3604	2	0.0901
0	0	4	0.1802
6	0.2703	0	0
2	0.0901	0	0
8	0.3604	8	0.3604
8	0.3604	4	0.1802
0	0	4	0.1802
8	0.3604	8	0.3604
2	0.0901	2	0.1802
2	0.0901	6	0.2703
2	0.0901	4	0.1802
0	0	0	0
4	0.1802	12	0.5405
4	0.1802	0	0
0	0	2	0.0901
4	0.1802	10	0.4505
2	0.0901	2	0.0901

20 and 2T

P_L $S_v = \frac{2P_L}{20 \times 1.11}$ P_L $S_v = \frac{2P_L}{20 \times 1.11}$

20 and 2T (Cont)

P_L	$S_v = \frac{2P_L}{20 \times 1.11}$	P_L	$S_v = \frac{2P_L}{20 \times 1.11}$
2	0.0901	0	0
14	0.6306	0	0
2	0.0901	4	0.1802
0	0	0	0
4	0.1802	4	0.1802
4	0.1802	2	0.0901
4	0.1802	10	0.4505
6	0.2703	2	0.0901
6	0.2703	2	0.0901
2	0.0901	6	0.2703
6	0.2703	14	0.6306
4	0.1802	0	0
6	0.2703	2	0.0901
2	0.0901	4	0.1802
0	0	2	0.0901
4	0.1802	4	0.1802
2	0.0901	0	0
0	0	2	0.0901
10	0.4505	0	0
2	0.0901	2	0.0901

20 and 2T (Cont)

P_L	$S_v = \frac{2P}{L}$ / 20 x 1.11	P_L	$S_v = \frac{2P}{L}$ / 20 x 1.11
3	0.1351	4	0.1802
4	0.1802	10	0.4505
2	0.0901	4	0.1802
12	0.5405	0	0
7	0.3153	10	0.4505
10	0.4505	0	0
6	0.2703	10	0.4505
11	0.4955	8	0.3604
2	0.0901	8	0.3604
2	0.0901	8	0.3604
4	0.1802	4	0.1802
4	0.1802		

$$M\left(\frac{(2P)}{20 \times 1.11}\right) = 0.1815$$

$$\sigma = 0.1572$$

$$\frac{\sigma}{\sqrt{103}} = 0.0155$$

APPENDIX 3

SEGREGATION AND MACROSTRUCTURE STUDIES

Details of experimental heats including macrostructure, segregation and inclusion assessment of the resulting ingots are given in Appendix 1. Salient features of these results are discussed in the following sections.

A3-1 SOLIDIFICATION

Examination of the macrostructures and the segregation patterns of selected ingots were conducted as an aid to the interpretation of the inclusion assessment and statistical results.

A3-1-1 Copper Ingots

In general all the copper ingots exhibited a tendency towards columnar growth, confirming the observations of Ruddle (220), who showed this to be the result of the high freezing rates of these alloys.

Ingots 14 and 17, which contained 0.8 to 1.2wt% aluminium as the major solute, were completely columnar in structure (Appendix 1). This finding is similar to that reported by Oya and Honma (221) for Cu-Al alloys of 0.3 to

1.0% aluminium. The large columnar growth from the base of ingots 14 and 17 can be explained by the greater heat extraction of the carbon base plate, compared with that of the heated mould walls (which were at approximately 400°C). By contrast, ingot 19 which was cast on an alumina coated steel base plate had a smaller base columnar cone (Appendix 1). The smaller cone most probably was the result of the lower heat extraction of the alumina coated steel base plate.

The presence of a chill zone in ingots 17, 19 and 30 (Appendix 1) can be related to the degree of superheat at which these ingots were cast. Heat 17 was cast at approximately 1400°C, while heat 19 was cast at 1180°C. The presence of a chill zone in ingot 19 and its almost complete absence in the similar size ingot 17 suggests that the greater superheat of the latter prevented a chill zone forming. This is in agreement with the observations of Benedicks (222) and with numerous other investigations. Similarly the absence of the chill zone in ingot 21 (Appendix 1) cast at 1220°C, compared with the same size ingot 30, cast at about 1150°C, can also be related to the degree of superheat of each.

At higher superheats there is less chilling of the melt by the mould with a corresponding lower number of crystallites forming from which columnar grains grow. This

can be observed in the coarser columnar structure of ingots 17 and 21 compared with 19 and 30 respectively. An equiaxed zone was observed in ingots 3, 5, 6, 21 and 30 (Appendix 1). These ingots all contained 0.3 to 1.3wt% tin, in addition to 0.5 to 1.0wt% aluminium. Ingots 3, 5 and 6 which were cast atlow superheats ($< 1150^{\circ}C$), substantiate the findings of Chalmers (223) for laboratory scale ingots, namely that the length of the columnar zone and the equiaxed grain size decreased as the pouring temperature was lowered.

In fact, in ingot 6 very little columnar growth was present as an appreciable fraction of the liquid undercooled immediately after casting and nucleation would have occurred rapidly while the liquid was still in motion induced by casting. The obvious nucleation from a "big-bang" mechanism (223) in this ingot could also have been enhanced by the operation of the crystal multiplication mechanisms, proposed by Jackson et al (224).

Ingot 20, which was cast at $1100^{\circ}C$ with approximately $50C^{\circ}$ superheat, exhibited complete inhomogeneity of structure and of solute distribution (Appendix 1) particularly that of oxygen. During casting of this ingot, the stream was quite viscous and hence the ingot is an extreme example of copious nucleation in the liquid during casting and on contact with the mould.

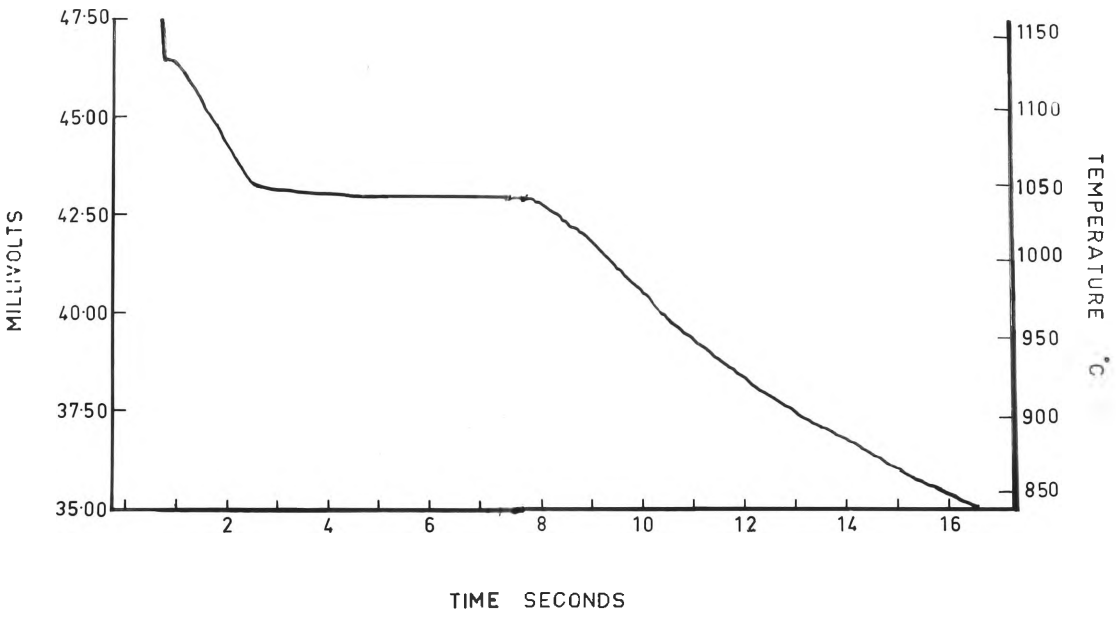

Fig. A-1 Trace from thermocouple positioned in the central-top region of Ingot 3.

The origin of the crystallites from which the equiaxed zone in ingots 21 and 30 formed would appear to be different. For small ingots such as the above, Biloni and Chalmers (225), Spittle et al (226) and Ohno et al (227) suggested that the nuclei for the equiaxed zone form in the initial stages of solidification. Results presented here confirm that this mechanism was operative in the ingots studied.

Figure A-1 gives the thermal analysis of the central upper part of ingot 3. The observed lack of recalescence in the solidification of this ingot can be interpreted (225) as negating the operation of the theory of Winegard and Chalmers (228) of nucleation in the melt ahead of the solidification front. Thus for equiaxed grains to be present in the copper ingots nuclei must have formed at the beginning of solidification or remelted from the solidification fronts and then carried by currents to the central region.

In ingot 21, the higher casting temperature, the lack of a chill zone and the coarse columnar grains suggest that the origin of the equiaxed zone could have resulted largely from crystallites which have fallen from the surface layer during its initial formation (i.e. Southin's mechanism (229)) and also by remelting from the lateral solidification fronts (i.e. Jackson et al's mechanism (224)).

However, the lower casting temperature of ingot 30,

the presence of a chill zone and the finer columnar grains, suggest that the origin of the lower equiaxed zone in this ingot came more from crystallites nucleating during chilling of the melt by the mould (i.e. Chalmer's mechanism (223)).

In the examination of these ingots the presence of 0.5 to 1.0 wt% tin must also be considered. Tin increases the undercooling of the central liquid region and as such would increase the probability of equiaxed zone formation (230). The loss of half the tin addition in ingot 21 as tin oxide resulted in only 0.5 wt% tin remaining in solution. This together with the high casting temperature would not produce a large undercooling of the liquid core and hence there would not be rapid growth of the crystallites circulating in the currents. Thus columnar growth would continue for a relatively long period of time before the numerous crystallites have grown to a sufficiently large size to form a barrier for further columnar growth. Furthermore, the observed columnar length of 15.24 to 17.78mm in ingot 21 is in reasonable agreement with Northcott's (231) findings of 20.32mm for a Cu - Sn alloy containing 0.5 wt% Sn.

In ingot 30, the higher solidification rate and the higher tin content, would have resulted in greater constitutional undercooling of the liquid core and the crystallites would have thus been able to grow to the size

sufficient to act as a barrier sooner; this is clearly evident if the corner columnar growth in both ingots are compared, (i.e. Appendix 1). The re-introduction of columnar growth above the equiaxed zone in ingot 30 can be explained in terms of the greater directional solidification of this ingot because of its H:D ratio of 1.56. Skoblo (232) has shown that ingots of small H:D ratios tend to complete solidification vertically. Thus it is probable that after the crystallites during the early period of solidification have grown and precipitated, some grains which were favourably oriented have grown in a columnar form because of the directional heat extraction.

A3-1-2 Iron Ingots

All iron ingots were characterised by an almost complete equiaxed structure, with some tendency in ingots 22 and 28 (Appendix 1) for columnar growth from the ingot base. The low casting temperature of the iron ingots (1530 - 1550^{o}C) and their small size suggest that an appreciable fraction of the liquid would have frozen soon after casting. Confirmation of this comes from the observation that approximately 10 seconds was required to complete solidification.

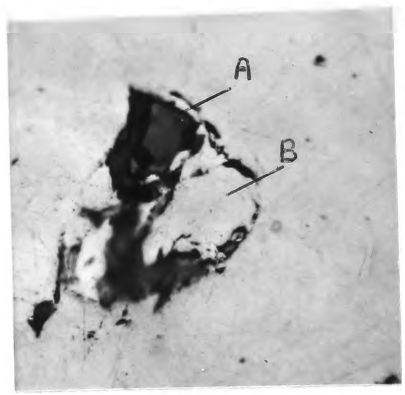

Fig. A-2 Large two phase inclusion present in Ingot 28, magnification 500X

Phase A 0.3% Al_2O_3

98.7% Fe_2O_3

Phase B 99.0% Al_2O_3

0.6% Fe_2O_3

As the nucleation of steel during solidification usually occurs heterogeneously on foreign particles, the possibility of heterogeneous nucleation on alumina particles can be concluded from observations such as:

(1) the presence of inclusions (Fig. A-2) similar to those reported by Charles (233) which he showed were acting as nuclei.

(2) ingot 27 exhibited a larger equiaxed grain size than the majority of other iron ingots. This was inspite of the ingot's greater solidification rate resulting from the large chilling effect of the cold mould. After vacuum degassing to 10ppm of oxygen, aluminium was added to this ingot to produce type III manganese sulphides. Thus a lower number of alumina particles can be expected in this ingot and therefore fewer nucleating centres. The equiaxed grains were thus able to grow to larger sizes before interacting with neighbouring grains.

A3-2 Segregation

Only some of the experimental ingots were investigated for possible segregation of elements used. Observation of

many of the macrostructures, as in Appendix 1, revealed the flotation of alumina towards the top of the ingot. Analysis for oxygen content (with the exception of the specially cast ingots 20 and 24) were in agreement with the observed flotation. The amount of oxygen at the top of the ingots was greater by a factor of 2 to 9 compared with that at the ingot base.

The anomalous behavour of ingots 20 and 24, in that the alumina distribution was irregular throughout the ingot, can be accounted for by the low casting temperature and by the formation of alumina only after teeming.

Microscopic examination of the inclusion distributions in the upper regions of ingots 14, 17, 23 and 30 revealed the presence of numerous alumina clusters and these clusters could be related to the macro-effect observed on etching as in Appendix 1.

The segregation of aluminium in both copper and iron ingots was not as marked as that of oxygen, and, in the majority of ingots there was little difference in aluminium contents between the upper and the lower ingot positions. This can be clearly seen from the average values given in Table A-1. The immediate conclusion suggested by these observations is that the major portion of the aluminium was present in solid solution in the metal, while only a small

TABLE A-1 AVERAGE CONTENTS OF Al, O AND Sn IN THE TOP AND BASE REGIONS OF SERIES 2 INGOTS

Ingot No.	Al (wt %)		O (ppm)		Sn (wt %)	
	Top	Base	Top	Base	Top	Base
5	1.256	0.688	602	286	1.091	1.138
6	0.914	0.568		131	0.818	0.370
14	0.340	0.358	1221	114		
17	0.990	0.939	1984	202		
18	2.325	2.146	217	111	0.978	1.029
19	1.080	1.059			0.371	0.371
20	1.059	0.772	1235	1361		
21	0.020	0.0275	3003	1828	0.523	0.500
22	0.266	0.256	113	53		
23	0.697	0.494	670	105		
24	0.463	0.458	293	336		

Fig. A-3 Large occlusion in sample from Ingot 20, magnification 100X.

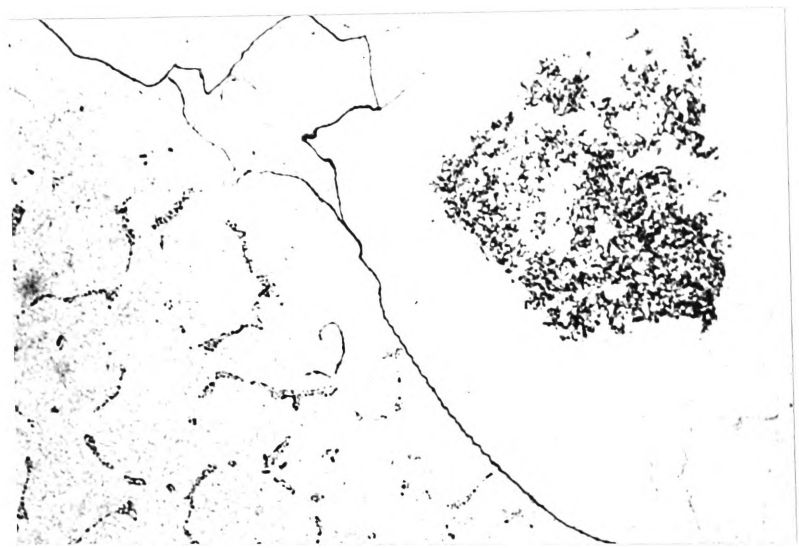

Fig. A-4 Large occlusion in sample from Ingot 20, magnification 100X.

portion was combined as alumina.

There was little segregation of tin in the copper ingots, and as tin oxide was observed only in ingot 21, the tin in the other ingots must have been present in solid solution. The small ingot size and fast solidification rate obviously prevented significant inverse segregation. The presence of some segregation, in these ingots is similar to that observed by Wahlster and Brocker (234) in their small ingots.

A3-3 INCLUSIONS

A3-3-1 Copper Ingots The microstructures of ingots 6, 20 and 30 revealed the presence of the Cu - Cu_2O eutectic. Large occlusions, optically different from the copper matrix, as in Figs. A-3 and A-4 were also observed. These occlusions, containing sometimes thin alumina films, are similar in form to those reported by Luyckx (24).

The large excess (between 0.3 to 0.9 wt%) of aluminium added to these ingots, above that required for deoxidation, should have converted all other oxide forms to alumina provided, (as has been assumed in the past (19)), that the rate of solution of the deoxidizer was not rate determining. The sharp demarkation between an area containing eutectic and an area free of eutectic in Fig. A-4, however disproves

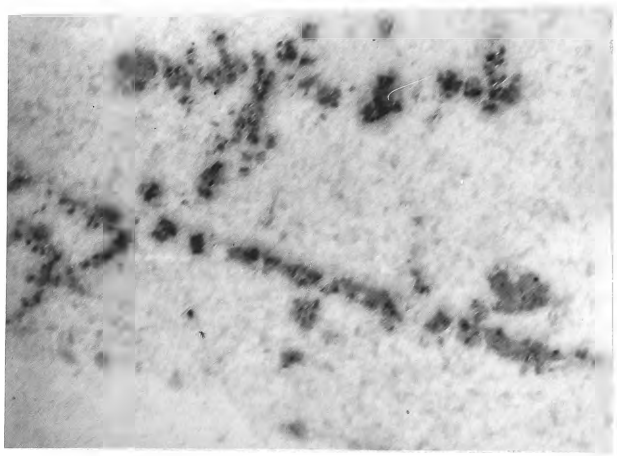

Fig. A-5 Grain boundary film of CuO and Cu_2O particles within the occlusion. (55,000X).

this assumption even for induction stirred melts.

It, therefore, appears that regions with high aluminium content form a thin film of alumina around them which prevents further dissolution and oxidation of the deoxidizer. This proposal made initially by Chipman (27) has also been confirmed by the experiments of Hasegaw and Mori (235). These investigators levitated ferroaluminium and found that an alumina film formed on heating which although very thin, was able to resist the surface tension of the molten metal.

Further examination of ingot 20 indicated the presence of grain boundary precipitates within the occlusion (Figs. A-3 and A-4) which were identified by the electron probe microanalysis as copper oxides. The grain boundary film was identified by electron diffraction as a mixture of CuO and Cu_2O particles as shown in Fig. A-5. (The diffraction data, on which this conclusion is based, are given in Table A-2).

Ingots cast at approximately 1400^{o}C did not contain any eutectic. However, in ingot 17 large copper oxide particles were identified by EPMA.

All these observations, considered together, support the hypothesis of Chipman (27), that considerable time is required for complete mixing of the deoxidant in the melt. The influence of higher superheats in aiding dissolution can be seen by comparing ingots 20 and 30 with ingots 14 and 17.

TABLE A-2 d SPACINGS FROM ELECTRON DIFFRACTION PATTERNS OF THE GRAIN BOUNDARY FILM IN SAMPLE FROM INGOT 20.

DIFFRACTION PATTERNS					ASTM XRAY POWDER DATA FILE	
1	2	3	4	5	50661 CuO	50667 Cu_2O
3.37	3.04	2.76	2.79	2.35	2.75	3.02
2.91	2.76	2.47	2.12	1.69	2.53	2.47
2.79	2.48	2.41	2.06	1.265	2.52	2.14
2.49	2.26	2.29	1.90	1.18	2.32	1.74
2.26	2.14	2.06	1.70	1.09	2.31	1.51
2.16	1.94	2.03	1.55	0.97	1.96	1.29
1.74	1.53	2.00	1.29		1.87	1.23
1.51		1.96	1.10		1.78	1.07
		1.42	1.04		1.71	0.98
		1.39	1.03		1.58	
		1.37			1.51	
		1.25			1.42	
		1.15			1.41	
		1.08			1.38	
					1.30	
					1.27	
					1.26	
					1.20	

TABLE A-2 (CONT)

ASTM XRAY POWDER DATA FILE 50661 CuO
1.17
1.16
1.12
1.09
1.07

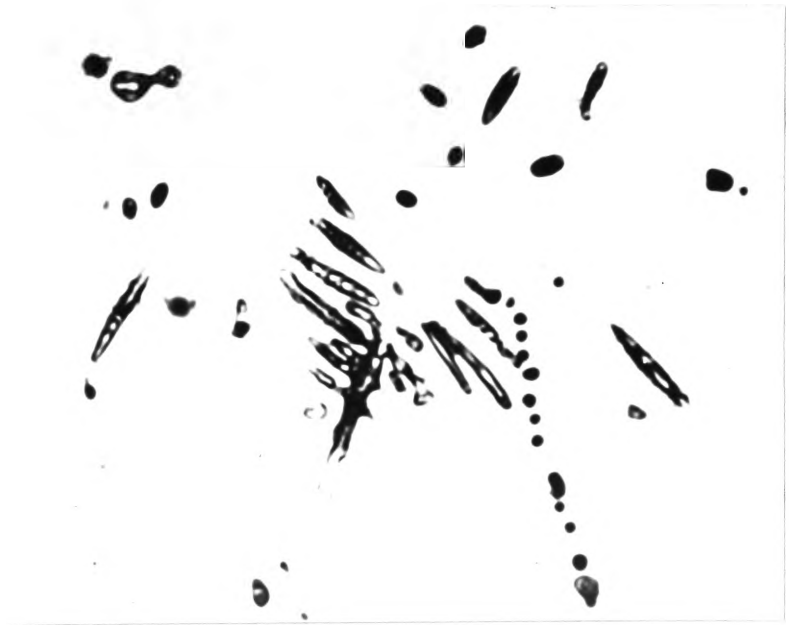

(a)

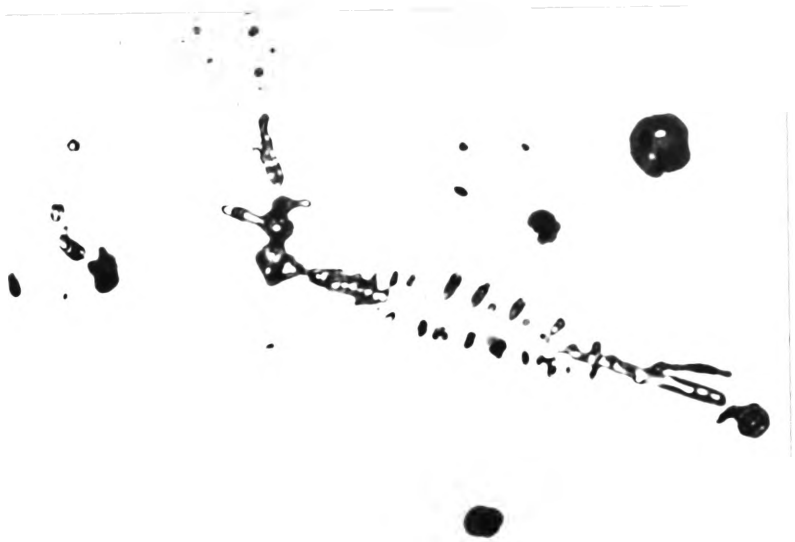

(b)

Fig. A-6 Dendritic alumina inclusions in slow cooled ingot 29.

(a) 1000X

(b) 1240X

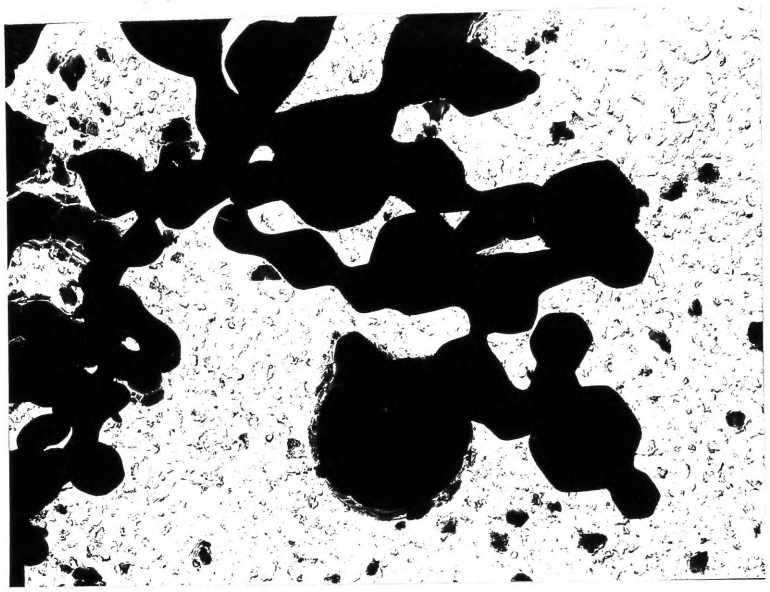

(a)

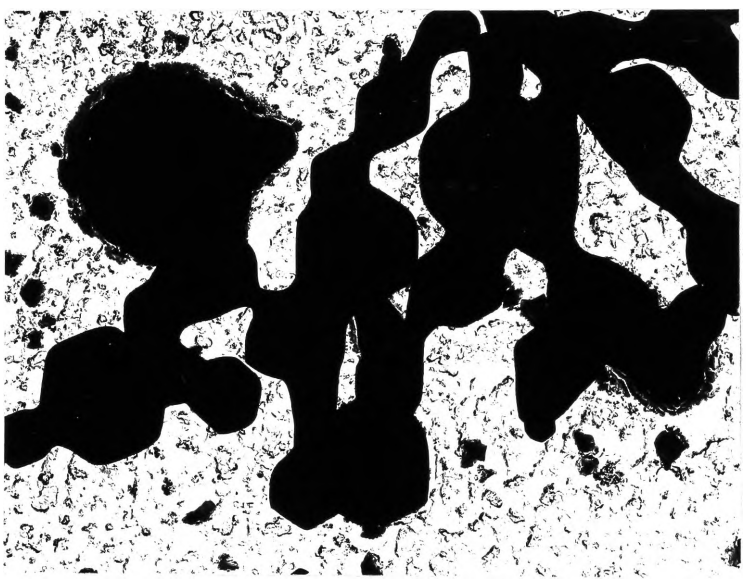

(b)

Fig. A-7 Alumina clusters

(a) 7200X

(b) 8300X

A3-3-2 Iron Ingots. EPMA analysis of inclusions in the iron ingots indicated that many inclusions contained 0.2 to 0.9 wt% Fe_2O_3, however, there were also some large two phase inclusions as shown in Fig. A-2 from ingot 29. Phase A was predominately Fe_2O_3, and phase B was predominately alumina. These observations suggest heterogeneous nucleation of alumina on Fe_2O_3 particles present in the melt.

Figure A-6 gives examples of the dendritic form of alumina observed at the grain boundaries in ingot 29. (This ingot was solidified in the crucible). Adachi et al (236) also reported analogous alumina morphology in melts solidified in their crucibles, whilst Luyckx (24) and von Bogdandy et al (32) described the formation of this inclusion type in regions which were high in aluminium content.

A3-3-3 Alumina Clusters. In both the copper and the iron ingots aggregates of small alumina particles were observed in clusters (Fig. A-7). This result differs from previous reports (48, 16, 32, 78, 233), which claimed that clusters were aggregates of the dendritic alumina. The presence of clusters in the rapidly solidified iron ingots is in agreement with the observations of Hilty (237) and Senda (57). However, in the copper ingots clusters were also

observed when the heats were cast at high as well as low superheats. Thus the quantity of aluminium added (52) rather than the solidification rate appears to be the important factor in cluster formation.

Of the previous hypotheses postulated for cluster formation and reviewed in Section 2-2-2, those requiring air oxidation of the stream or oxidation of aluminium by air seem untenable in the case of the present experimental heats. These heats were melted under a low pressure ($< 10^{-2}$ mm Hg) and cast under 100 mm Hg of dry argon. An alternative explanation comes from considerations of the many observations already discussed which seem to indicate a slow dissolution rate of the deoxidizer in the melt. Thus a more probable explanation of cluster formation in these heats could come from the hypothesis of Chipman (27).

Thus, according to this hypothesis, the clusters would form from numerous nucleations in aluminium rich volume elements and would remain in a cluster because of surface energy considerations (as proposed by Kozakevitch and Lucas (61) . This mechanism would form the "nucleus" of cluster. Further movement of the cluster in the induction currents of the melt would result in further collisions with other alumina particles and hence further growth. The latter cluster growth mechanism is what Torssell and Olette (58)

Fig. A-8 Large $FeO-Al_2O_3$ particle

(660X)

FeO	6-12%
Al_2O_3	88-94%

found in their melts.

One further observation which supports Chipman's hypothesis was the formation of large alumina - hercynite particles (Fig. A-8). Ward (26) has described their formation in oxygen rich - low aluminium content volume elements.

APPENDIX 4

PROGRAM DESCRIPTION AND USAGE

The program consists of a main section, several major subroutines and several minor subroutines. The purpose of the main section is to call the subroutines and set up the control variables for the optimisation routine.

A4-1 MAJOR SUBROUTINES

A4-1-1 Input - reads Data Cards

Card 1 - contains any alphanumeric title for the current data set except when the first four entries are stop.

Card 2 - Contains initial estimates of X_u, X_l, $\bar{y}$ and S_y in format F10.0

Card 3 - Specifies the number of unknowns and which of the parameters X_u, X_l, $\bar{y}$ and S_y are to be used for the optimisation.

Card 4 - contains output control parameters IPRINT and IPLOT in format 2I1, although at this stage IPLOT is not used.

Card 5 - To the end of the data set - contain the experimental data F(I), XXL(I), XXU(I) in format 3F10.0. The last card of the data set should have a negative value for F(I). When the last card is reached the parameters are fitted to the data and a report output, then the next card is read which has the same function as card 1.

A4-1-2 DTACHK - does the checking of the data, e.g.

(a) upper class limit greater than the corresponding lower class limit

(b) class limits must not overlap.

(c) there is not too many very low class frequencies.

For particular sets of data one or more of these checks can be deleted, e.g. check (b) was deleted so that data from counts obtained at two or more magnifications could be used together.

A4-1-3 OUTPUT - the final results of the parameter fit and the first four moments of the distribution are ouput in report form

A4-1-4 FCNZ - calculates the criteria V for a trial set of parameters, V is really - X^2,

where: $X^2 = \sum_{i=1}^{n} \frac{(F_i - FI_i)^2}{FI_i}$

As the fitting critieria operates by maximizing V, thus V equals - X^2

A4-1-5 CLIMBR - is a standard optimizing subroutine based on Rosenbrock's Hillclimbing Method (238) which uses function values only.

The program generates exploratory movements of a vector X the elements of which are selections of the scaled versions Z of the distribution parameters X_u, X_L, $\bar{y}$, Sy, where Z is the unit normal variable.

A4-1-6 MOMENT - is a subroutine to calculate the first four moments of X about zero. The relationship between Y and X defined earlier was:

$$Y = \ln\left(\frac{X - X_L}{X_u - X}\right)$$

where X_u = upper limit of X

X_L = lower limit of X

To calculate the first four moments of X, the transformation used by Johnson (192) was employed, were:

$$Y' = \frac{X - \xi}{\lambda}$$

and $X_L = \xi$

$$X_u = \lambda + \xi$$

The variate X can be transormed to a unit normal variate Z by using the function:

$$Z = \gamma + \delta \ln\left(\frac{X - \xi}{\lambda + \xi - X}\right)$$

or

$$Z = \gamma + \delta \ln\left(\frac{Y'}{1 - Y'}\right)$$

The r^{th} moment of Y' about zero is therefore:

$$E(Y^1)^r = \frac{1}{\sqrt{2\pi}} \int_{-\infty}^{\infty} \exp\left(-\frac{Z^2}{2}\right) \left[1 + \exp\left(\frac{Z-\gamma}{\delta}\right)\right]^{-r} dz$$

The inte gral can be evaluated using a quadrature formula (239) of the form:

$$\int_{-\infty}^{\infty} \exp\,(1-X^2)\, f(X)\, dX$$

$$= \frac{H}{N} \sum_{-\infty}^{\infty} f(NH) \exp\,(-N^2H^2) - E(H)$$

The first four moments of Y^1 can be calculated if γ, δ, N and H are known.

N and H can be chosen arbitrarily, e.g. N = 10 and H = 0.5. While γ and δ can be calculated from $\bar{y}$ and Sy as follows:

$$\bar{y} = -\frac{\gamma}{\delta}$$

and $$Sy = \frac{1}{\delta}$$

The first four moments of X can be determined from those of Y^1 as follows:

$$E(X) = (X_u - X_L)\, E(Y^1) + X_L$$

$$E(X)^2 = (X_u - X_L)^2\, E(Y^1)^2 + 2(X_u - X_L)\, X_L\, E(Y^1) + X_L^2$$

$$E(X)^3 = (X_u - X_L)^3\, E(Y^1)^3 + 3(X_u - X_L)^2\, X_L\, E(Y^1)^2 + 3(X_u - X_L)\, X_L^2\, E(Y^1) + X_L^3$$

$$E(X)^4 = (X_u - X_L)^4\, E(Y^1)^4 + 4(X_u - X_L)^3 X_L\, E(Y^1)^3 + 6(X_u - X_L)^2 X_L^2\, E(Y^1)^2 + 4(X_u - X_L) X_L^3\, E(Y^1) + X_L^4$$

A4-2 Minor Subroutines

A4-2-1 UPROB - obtains the probability density corresponding to a given value by calling function XPROB.

A4-2-2 XPROB - evaluates the probability density for a given value of the random variable, X.

The class interval limits for variate Y are obtained using the following equations:

$$Y_{ui} = \ln\left(\frac{X_u - XX_{ui}}{XX_{ui} - X_L}\right)$$

and

$$Y_{Li} = \ln\left(\frac{X_u - XX_{Li}}{XX_{Li} - X_L}\right)$$

where XX_{ui} = upper boundary of group i

XX_{Li} = lower boundary of group i

The probability for group i is:-

$$P_i = \frac{1}{\sqrt{2\pi}\, S_y} \int_{Y_{Li}}^{Y_{ui}} \exp\left(- \frac{(y-\bar{y})^2}{2\, S_y^2} \right) dy$$

$$= \frac{1}{\sqrt{2\pi}} \int_{\frac{Y_{Li}-\bar{y}}{S_y}}^{\frac{Y_{ui}-\bar{y}}{S_y}} \exp\left(- \frac{t^2}{2} \right) dt$$

The theoretical frequencies for each class interval, FI_i, are calculated as:

$$FI_i = \frac{P_i}{P} \cdot N$$

where $N = \sum_{i=1}^{n} FI_i = \sum_{i=1}^{n} F_i$

and $P = \sum_{i=1}^{n} P_i$

A4-2-3 FCNX - is called by Climbr for evaluation of the function V to be optimised. It assembles the prespecified variables and trial values of X of the unknown variables into a standard order in the vector Z before calling FCNZ to evaluate V.

A4-2-4 NDTR - evaluates by a series approximation the standard integral:-

$$P_T = \frac{1}{\sqrt{2\pi}} \int_{-\infty}^{x} \exp\left(-\frac{t^2}{2}\right) dt$$

The approximation is:-

$$T = 1 \Big/ (1 + 0.2316419 \, |x|)$$

$$D = 0.398942 \exp (- |x|^2 / 2)$$

$$P = 1 - D.T. (((1.330274 \, T - 1.821256) \, T + 1.781478) - 0.3565638) \, T + 10.3193815)$$

$P_T = P$ for $X \geq 0$

$= 1 - P$ for $X < 0$

The complete program is available on request.

A4-3 SPECIFICATION OF CLASS INTERVAL LIMITS

To eliminate the small sampling variations which occur during a sizing assessment and to make the data amenable to computation the length of the class intervals, Δx, were chosen to be either:

1. in a geometric progression with a modulus of $\sqrt{2}$ when the section size was defined as the geometric mean of the major and minor axis, or
2. in an arithmetical progression when the section size was defined as the major or minor axes.

The mid-points of the transformed log-normal distribution can be termed $\ln x_1$, $\ln x_2$, $\ln x_3$, ..., $\ln x_n$. The number of observations, f_j, in the jth class interval is the number of observations satisfying the following inequality:

$$\ln x_j - \frac{\Delta \ln x}{2} \leq f_j \leq \ln x_j + \frac{\Delta \ln x}{2}$$

i.e. where $\Delta \ln x = \ln \sqrt{2}$

$= 0.3464$

and $x = \sqrt{a.b}$

where a = semi major axis of an ellipse

b = semi minor axis of an ellipse

A4-4 TESTING OF THE PROGRAM

The initial trials of the program involved the analysis of published distribution data to which a four parameter distribution had been successfully fitted. The results of these trials, listed in Table A-3, show the computer determined distributions fit the data extremely well. Furthermore, if the parameters and goodness of fit results are examined in this table, it can be readily seen that after 50 iterations the final distributions obtained are comparable to those obtained in the articles by such differing methods as maximum likelihood (240), moments (192) and a combined graphical and analytical procedure (241).

TABLE A-3 COMPUTER ANALYSIS OF PUBLISHED DATA

COMPUTER FIT			PUBLISHED DATA			GOODNESS OF FIT 10% LEVEL		REFERENCE
X_L	X_u	X^2	X_L	X_u	X^2	χ^2	DEGREES OF FREEDOM	
800	12,000	———	700	12,700	---	---	---	240
0.0489	10.072	4.095	0	10.0	5.76	10.6	6	192
0	95.156	4.928	0	95	4.847	13.4	8	241

Confident, therefore, of the ability of the program to obtain an adequate fit to the data when good initial estimates of X_L and X_u were available, it was consequently only necessary to examine the effect on the adequacy of the fit when the initial estimates were poor. The data of Drapal and Horalek (187) were used for this purpose and the results are given in Table A-4.

The first observation which can be made from the results in this table is that a significant fit of a log-normal function to the data wasobtained for all combinations of X_L and X_u. The minimum value of chi-square however, depended on the adequacy of the initial estimates of the size range limits, especially of X_u. The probability of the distribution obtained after 50 iterations having a reliable estimate of X_u seems to depend on the error in the initial estimate of X_u and whether the data has a pronounced tail (i.e. its skewness).

TABLE A-4 ANALYSIS OF DATA FROM PLANE 1, 2 AND 3 (187)

Initial Estimates

X_L	X_u	X_L	X_u	MEAN
Plane 1				
0 (F)	5,000 (F)	0	5,000	9.2791
0	5,000	0.0223	5,051	9.3781
0.00185	496	0.8988	519.6	9.2417
0 (F)	28.25	0	80.05	9.2310
Plane 2				
0 (F)	5,000 (F)	0	5,000	9.4535
0	5,000	1.7088	4,997	9.4919
0.262	497	1.0172	548.6	9.4298
0 (F)	28.25	0	87.94	9.4108
Plane 3				
0 (F)	5,000 (F)	0	5,000	9.2806
0	5,000	0.88×10^{-4}	5,037	9.2711
0 (F)	28.25	0	54.82	9.2250
0.154	53	0.4011	50.06	9.2520

F = FIXED LIMIT

(SIZE IN μm)

MODE	MEDIAN	$\hat{\sigma}^2$	X^2
7.2641	8.5525	15.268	6.484
7.2561	8.6100	16.381	6.762
8.3335	8.4721	15.001	7.313
7.3537	8.5973	14.353	6.429
7.3281	8.6848	16.541	3.883
7.0643	8.5810	17.134	5.117
8.4306	8.6007	16.449	4.228
7.4042	8.7289	15.667	4.609
7.3250	8.5773	14.720	2.368
3.7078	8.5647	14.777	2.374
7.4566	8.6506	13.782	1.845
7.4201	8.6629	13.774	2.009

Thus in the case of the distributions examined, the subsequent estimates of X_u determined for each iteration did not significantly differ from the initial estimate. Hence it must be emphasised that for successful fitting using this program good estimates of X_u are required. One simple way of meeting this requirement is to examine the sample at a low magnification.

APPENDIX 5 - SAMPLE CALCULATIONS

A5-1 DETERMINATION OF DISTRIBUTION OF ECCENTRICITIES

The distribution of eccentricities of the sections assessed on the polished plane were determined using the following equation

$$\epsilon = \sqrt{1 - \frac{b^2}{a^2}} \qquad \text{(A5-1)}$$

where b = minor axes of the elliptical section

and a = major axes of the elliptical section

In order to estimate the distribution of eccentricities of the ellipsoidal particles from the observed distribution of section eccentricities it is necessary to assume either oblate or prolate ellipsoids of revolution so as to simplify the calculations. For example I22 No 5R containing alumina inclusions, the assumed shape of the particles was oblate ellipsoids. This assumption was derived from the dimensions of the largest equiaxed and non-equiaxed sections observed in the assessment.

Thus for oblate ellipsoids of revolution the relationship between the distribution of eccentricities, F(e), of the ellipsoidal particles to that of the elliptical

sections, $f(\epsilon)$, was derived by Wicksell (165):

$$g(\epsilon') = \frac{1}{\delta_0} \cdot \epsilon' \sqrt{1+\epsilon'^2} \cdot \int_{\epsilon'}^{\infty} \frac{F(e')(1+e'^2)^{-\frac{1}{3}}\, de'}{e' \sqrt{e'^2 - \epsilon'^2}} \qquad \text{(A5-2)}$$

where $g(\epsilon') = f(\epsilon)(1+\epsilon'^2)^{-\frac{3}{2}}$

$F(e') = F(e)(1+e'^2)^{-\frac{3}{2}}$

Both distributions $f(\epsilon)$ and $F(e)$ were transformed into distributions $g(\epsilon')$ and $F(e')$ respectively, so that the form of the relationship between $g(\epsilon')$ and $F(e')$ was that of Equ. (6-2-2):

$$\text{i.e.,} \quad m(y) = ky \int_{y}^{x_{max}} \frac{f(x)\, dx}{\sqrt{x^2 - y^2}} \qquad \text{(A5-3)}$$

The integral in Equ. (A5-3) can be solved by any of the three methods mentioned in Section (6-2-1). Equ (A5-2) when rearranged as follows is in the form of Equ. (A5-3):

$$g(\epsilon')' = \frac{g(\epsilon')}{\sqrt{1+\epsilon'^2}} = \frac{1}{\delta_0} \epsilon' \int_{\epsilon'}^{\infty} \frac{\frac{F(e')(1+e'^2)^{-\frac{1}{3}}}{e'}}{\sqrt{e'^2 - \epsilon'^2}}\, de' \qquad \text{(A5-4)}$$

Therefore as (165):

$$f(\epsilon) = g(\epsilon')(1+\epsilon'^2)^{\frac{1}{2}} \qquad \text{(A5-5)}$$

then: $$\frac{g(\epsilon')}{\sqrt{1+\epsilon'^2}} = \frac{f(\epsilon)}{\sqrt{1+\epsilon'^2}\left(1+\epsilon'^2\right)^{\frac{3}{2}}} \qquad (A5\text{-}6)$$

Also as (165):

$$F(e) = F(e')\left(1+e'^2\right)^{\frac{3}{2}} \qquad (A5\text{-}7)$$

$$\frac{F(e')\left(1+e'^2\right)^{-\frac{1}{3}}}{e'} = \frac{F(e)\left(1+e'^2\right)^{\frac{3}{2}}}{e'\left(1+e'^2\right)^{\frac{1}{3}}}$$

or:

$$F(e) = \left[\frac{F(e')\left(1+e'^2\right)^{-\frac{1}{3}}}{e'}\right] e'\left(1+e'^2\right)^{\frac{3}{2}}\left(1+e'^2\right)^{\frac{1}{3}}$$

$$= G(e')\,e'\left(1+e'^2\right)^{\frac{3}{2}}\left(1+e'^2\right)^{\frac{1}{3}} \qquad (A5\text{-}8)$$

The method chosen to solve the integral in Equ. (A5-4) was to group the frequencies $g(\epsilon')'$ into equal size intervals of ϵ' and to use Saltykov's table discussed in Section (6-2). The following table lists the interval limits of ϵ and ϵ' employed:

ϵ			ϵ'		
0.0	-	0.4472	0.0	-	0.5
0.4472	-	0.7071	0.5	-	1.0
0.7071	-	0.8321	1.0	-	1.5
0.8321	-	0.8944	1.5	-	2.0
0.8944	-	0.9285	2.0	-	2.5
0.9285	-	0.9487	2.5	-	3.0
0.9487	-	0.9615	3.0	-	3.5
0.9615	-	1.0	3.5	-	4.0

The first operation is the determination of $g(\epsilon')'$ from $f(\epsilon)$ as in the following table:

$f(\epsilon)$	$(1+\epsilon'^2)^{\frac{1}{2}}$	$(1+\epsilon'^2)^{\frac{3}{2}}$	$g(\epsilon')'$
1	1.0307764	1.0951999	0.88581318
56	1.25	1.953125	22.9376
116	1.600781	4.1020015	17.66567570
114	2.015564	8.1882305	6.90745714
68	2.462214	14.9271751	1.85014382
81	2.926175	25.055373	1.10480047
32	3.400368	39.316751	0.23935717
96	3.881044	58.45822	0.42313318

The values of $g(\epsilon')'$ are then substituted into Equ. (6-2-4) of Section (6-2) as follows:

$$G(e')_8 = \frac{1}{0.5}\ (0.258 \cdot 0.42313318)$$

$$= 0.21833672$$

$$G(e')_7 = \frac{1}{0.5}\ (0.2773 \cdot 0.23935717 - 0.1016 \cdot 0.42313318)$$

$$= 0.04676682$$

$$G(e')_6 = \frac{1}{0.5}\ (0.3015 \cdot 1.10480047 - 0.1081 \cdot 0.23935717$$

$$-0.0346 \cdot 0.42313318)$$

$$= 0.58516484$$

$$G(e')_5 = \frac{1}{0.5}\ (0.3333 \cdot 1.85014382 - 0.1161 \cdot 1.10480047)$$

$$- 0.0366 \cdot 0.23935717 - 0.0095 \cdot 0.42313318)$$

$$= 0.95121074$$

$$G(e')_4 = \frac{1}{0.5}\ (0.3779 \cdot 6.90745714 - 0.1260 \cdot 1.85014382$$

$$- 0.0386 \cdot 1.10480047 - 0.0174 \cdot 0.23935717$$

$$- 0.0095 \cdot 0.42313318)$$

$$= 4.6527601$$

$$G(e')_3 = \frac{1}{0.5}(0.4472 \cdot 17.6656757 - 0.1382 \cdot 6.90745714 - 0.0408 \cdot 1.85014382 - 0.0178 \cdot 1.10480047 - 0.0093 \cdot 0.23935717 - 0.0057 \cdot 0.42313318)$$

$$= 13.69138078$$

$$G(e')_2 = \frac{1}{0.5}(0.5774 \cdot 22.9376 - 0.1529 \cdot 17.6656757 - 0.042 \cdot 6.90745714 - 0.0171 \cdot 1.85014382 - 0.0087 \cdot 1.10480047 - 0.0051 \cdot 0.23935717 - 0.0031 \cdot 0.42313318)$$

$$= 20.41838716$$

$$G(e')_1 = \frac{1}{0.5}(1.0.88581318 - 0.1547 \cdot 22.9376 - 0.036 \cdot 17.6656757 - 0.013 \cdot 6.90745714 - 0.0061 \cdot 1.85014382 - 0.0033 \cdot 1.10480047 - 0.002 \cdot 0.23935717 - 0.0013 \cdot 0.42313318)$$

$$= -6.80871062$$

The frequencies, F(e), in the following table were determined from $G(e')$ with the aid of Equ. (A5-8):

$G(e')$	e'	$(1 + e'^2)^{\frac{1}{3}}$	$(1 + e'^2)^{\frac{3}{2}}$	$F(e)$
-6.80871062	0.25			
20.41838716	0.75	1.1603972	1.953125	19.72320447
13.69138078	1.25	1.3684259	4.1020015	96.06702957
4.6527601	1.75	1.5956261	8.1882305	106.38242855
0.95121074	2.25	1.8234083	14.9271751	58.25333824
0.58516484	2.75	2.0458174	25.055373	82.48569875
0.04676682	3.25	2.2612604	39.316751	13.51292606
0.21833672	3.75	2.4696326	58.45822	118.20503779

The mean eccentricity of the oblate ellipsoids of revolution can now be calculated as follows:

$F(e)$	e	
19.72320447	0.6	
96.06702957	0.7808686	$\bar{e} = \frac{437.09672712}{494.62966343}$
106.38242855	0.868243	
58.25333824	0.9138117	$= 0.884$
82.48569875	0.939793	
13.51292606	0.9557789	
118.20503779	0.966235	

A5-2 Determination of Mean Values of λ_ns

Before the mean values of the shape parameters, λ_n, can be calculated the values of λ_n for each particular value of e, the mid-point of the classes used in grouping e, were determined from interpolations of the values given by Wicksell (165) and from the following equations:

when $e \rightarrow 1$.

$$\lambda_{-1} = (1-e^2)^{-\frac{1}{4}} \cdot \left(1-\tfrac{1}{4}e^2 - \frac{3}{160}e^4 - \frac{5}{896}e^6 - \frac{5}{2048}e^8 \ldots\ldots\right)$$

$$\lambda_0 = (1-e^2)^{-\frac{1}{6}} \cdot \left(1-\frac{1}{6}e^2 - \frac{1}{40}e^4 - \frac{1}{112}e^6 - \frac{5}{1152}e^8 \ldots\ldots\ldots\right)$$

$$\lambda_1 = (1-e^2)^{-\frac{1}{12}} \cdot \left(1-\frac{1}{12}e^2 - \frac{3}{160}e^4 - \frac{1}{128}e^6 - \frac{77}{18432}e^8 \ldots\ldots\right)$$

$$\lambda_2 = 1$$

$$\lambda_3 = (1-e^2)^{\frac{1}{12}} \cdot \left(1+\frac{1}{12}e^2 + \frac{1}{32}e^4 + \frac{15}{896}e^6 + \frac{65}{6144}e^8 \ldots\ldots\right)$$

$$\lambda_4 = (1-e^2)^{\frac{1}{6}} \cdot \left(1+\frac{1}{6}e^2 + \frac{3}{40}e^4 + \frac{5}{112}e^6 + \frac{35}{1152}e^8 \ldots\ldots\right)$$

The above equations are series approximations given by Wicksell (165).

The mean values of λ_n for the distribution of eccentricities, F(e), can be calculated as follows:

F(e)	λ_{-1}	λ_0	λ_1	λ_3	λ_4
19.7230447	1.014	1.009	1.004	0.997	0.996
96.06702957	1.016	1.037	1.0167	0.9881	0.9803
106.38242855	1.131	1.075	1.0338	0.9744	0.9598
58.25333824	1.215	1.127	1.054	0.960	0.9285
82.48569875	1.288	1.172	1.07	0.946	0.906
13.51292606	1.375	1.224	1.1029	0.9152	0.8446
118.20503779	1.435	1.264	1.1236	0.8988	0.8147

$$\overline{\lambda_{-1}} = \frac{603.14568457}{494.62966343} = 1.2194$$

$$\overline{\lambda_0} = \frac{562.15891286}{494.62966343} = 1.1365$$

$$\overline{\lambda_1} = \frac{524.82874324}{494.62966343} = 1.0611$$

$$\overline{\lambda_3} = \frac{470.81113950}{494.62966343} = 0.9518$$

$$\overline{\lambda_4} = \frac{452.45944580}{494.62966343} = 0.9147$$

Similarly the mean of $\lambda(e_2, e_3)$ can be calculated, as for oblate ellipsoids of revolution Equ. (7-5-17) reduces to (165):

$$\lambda_{(e,o)} = (1 - e^2)^{-\frac{1}{3}} \cdot \frac{1}{2}\left(1 + \frac{1-e^2}{2e} \cdot \ln \frac{1+e}{1-e}\right) \quad \text{(A5-9)}$$

and the mean for I18 No 5R is equal to:

$$\lambda = \overline{\lambda_{(e,o)}} = 1.0715$$

A5-3 DETERMINATION OF N_A

The average number of particle sections per unit area was determined for sample I22 No 5R by traversing the sample a number of times and recording the number of particles observed. The following table gives the results:

Traverse (No)	Length of Traverse (LT)	Number of Particles Observed (fi)	fi LT.0.37.0.077243
1	11.27 mm	62	192.4894
2	12.26	49	139.8443
3	12.64	23	63.6678
4	12.66	37	102.2603
5	13.64	32	82.0871
6	12.62	32	88.72168
7	12.56	38	105.8603
8	12.73	27	74.2121
9	9.62	27	98.2037
10	6.69	14	73.2219
11	12.75	19	52.1414

Mean = 97.5191

The mean value determined above represents the number of sections per unit area whose size is greater than that which can be resolved by the optical microscope employed in the assessment. Thus there is a systematic error in this value. To compensate for this error the N_A used in the calculations of S_v and V_v was the value determined by the above method divided by the fraction of the best fit section distribution which includes the range of the assessment data.

That is for sample I22 No 5R

$$N_A = \frac{97.5191}{0.995742}$$

A5-4 DETERMINATION OF MOMENTS AND PARAMETERS OF THE SPATIAL DISTRIBUTION

For oblate ellipsoids of revolution the relationship between the moments of the major axes and that of the geometric mean of the axes is as was given in Section (7-7):

$$E(X^i) = E(S^i)\ E\left[(1-e^2)^{\frac{i}{6}}\right]$$

Using this relationship and assuming that a two parameter log-normal distribution represents both distributions (i.e. variate S and X) then it can be shown that:

$$\frac{E(X^2)}{E(X)} = \frac{E(S^2)}{E(S)} \frac{E\left[(1-e^2)^{\frac{1}{3}}\right]}{E\left[(1-e^2)^{\frac{1}{6}}\right]} \qquad \text{(A5-9)}$$

and

$$\frac{E(X^3)}{E(X)} = \frac{E(S^3)}{E(S)} \frac{E\left[(1-e^2)^{\frac{1}{2}}\right]}{E\left[(1-e^2)^{\frac{1}{6}}\right]} \qquad \text{(A5-10)}$$

Assuming ellipsoids of constant form Equ (A5-9) becomes:

$$\mu e^{\frac{3}{2}\sigma^2} = \bar{x}\, e^{\frac{3}{2}s^2} \cdot (1-e^2)^{\frac{1}{6}} \qquad \text{(A5-11)}$$

and Equ. (A5-10) becomes:

$$\mu^2 e^{4\sigma^2} = \bar{x}^2 e^{4s^2} \cdot (1-e^2)^{\frac{1}{3}} \qquad \text{(A5-12)}$$

where μ = median of L-N distribution of X

σ^2 = variance of L-N distribution of X

$\bar{x}$ = median of L-N distribution of S

s^2 = variance of L-N distribution of S

Solving Equs (A5-11) and (A5-12) simultaneously it can be shown that:

$$\sigma^2 = s^2 \qquad \text{(A5-13)}$$

and $$\ln\mu = \ln\bar{x} + \frac{1}{6}\ln(1-e^2) \qquad \text{(A5-14)}$$

Thus the parameters and the moments of the spatial distribution of the geometric mean diameters of oblate ellipsoids can be readily calculated from the parameters of spatial distribution of major axes.

For sample I22 No 5R the parameters and moments of the distribution of X, assuming oblate ellipsoids of e = 0.85, are as follows:

$$\chi_{median} = \mu = 2.4514$$
$$\sigma^2 = 0.2965$$
$$\chi_{mode} = 1.8222$$

$$E(X) = \chi_{mean} = 2.8432$$

$$E(X^2) = 10.8737$$
$$E(X^3) = 55.947$$
$$E(X^4) = 387.2$$

APPENDIX 6 - EXAMINATION OF Q.T.M. AREA COUNTS USING THE ROSIN-RAMMLER LAW

Samples from aluminium fully killed strip and plate were assessed for inclusion content using the QTM. Initial attempts to count and size the inclusions in these samples resulted in erroneous counts per field because of the elongated form of many of the inclusions. Banks (142) also reported multiple counting of stringer inclusions and concluded that inclusions can only be sized, with reasonable accuracy when they are nearly spherical in form, i.e. before rolling. From his work Banks also concluded that the greater the ratio of the major to minor axis of the inclusions the greater will be the multiple counting or under-estimation of inclusion length.

This observation appears to put a severe limitation on the usefulness of the QTM in assessing inclusionnumber and content in rolled products. It should be noted that the information determined from the QTM for an inclusion assessment is variable, e.g. it can be a size-frequency analysis, or a volume fraction assessment. There are, however, difficulties in applying both of these approaches to the analysis of inclusions in plate and strip samples. Multiple counting of inclusions precludes the use of the size-frequency mehhod; while a volume fraction measurement

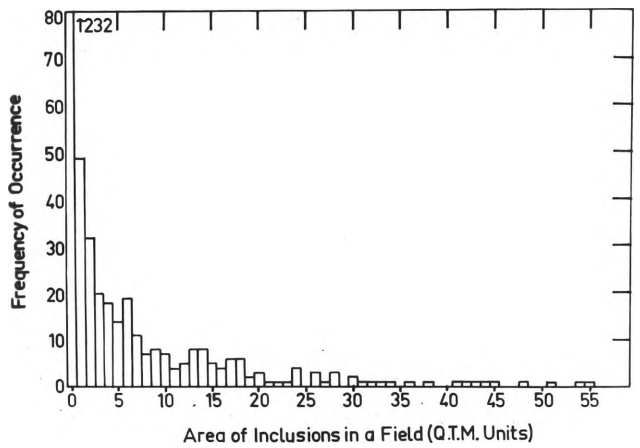

Fig. A-9 The histogram of the frequency of fields containing certain inclusion areas from sample 8c.

does not provide information of the average inclusion size nor the probability of occurrence of the larger size inclusions. In the latter approach it can quite often occur that only a few large inclusions contribute approximately half of the total inclusion area of 500 fields while the other half or so, of the inclusion area consists of numerous small inclusions. Thus, unless this is specificilly noted by the operator such irregularities in inclusion size cannot be inferred from the final total inclusion area.

In order to overcome these difficulties a modified technique was developed which involved the determination of the inclusion areain each of 500 fields. Figure A-9 presents the histogram of an as-rolled stress relieved plate sample, No 8c (chemical composition is given in Table A-5).

It can be seen from this figure that the data shows a large positive skewness. When such data are obtained Herdan (149) advises the use of the Rosin-Rammler law, as it provides a better fit to these distributions which have a greater departure from normality than those obeying the log-normal function. Thus the Rosin-Rammler distribution was tested for adequacy of representation of the data from sample 8C.

However, before the fit is examined it would be useful

TABLE A-5 CHEMICAL COMPOSITION OF PLATE SAMPLE NO 8c

C	Mn	Si	P
0.17-0.20	0.7-0.9	0.10x	0.025x

TABLE A-5 C'tued

S	Al	Ni	Cr	Mo	Cu
0.035x	Nil	0.1	0.1	0.05	0.1

to briefly describe the Rosin-Rammler distribution and to define it for inclusion studies.

As is well known the Rosin-Rammler function was derived empirically by Rosin and Rammler to describe the size distribution of ground materials, powdered coal inparticular (242). Later the function was theoretically derived for the process of fragmentation of coal under impact by Bennett (243). The function has also been applied with success in describing the size distribution of some clastic sediments (244) and of droplets from atomizers (149).

The form of the function is that of a strongly positively skewed distribution. The relative frequency distribution or density function can be expressed as:-

$$f(y) = \frac{d\,G(y)}{dy} = 100nb\, y^{n-1} e^{-by^n} \qquad \text{(A6-1)}$$

where n and b are parameters of the distribution

y is the particle size

G(y) is the cumulative frequency $\leqslant y$ expressed as a percentage of the total frequency

The parameter n is a measure of the total dispersion and is the slope of the straight line obtained when the

data described by the function is plotted in the form of log log $\frac{100}{G(y)}$ versus log y. The larger the value of n the more closely sized is the distribution. For values of $n < 1$ it should be noted that the relative frequency curve does not have a maximum in the region of real values of y(243, 244).

Also there is another theoretical difficulty with the use of this function for representing inclusion area fraction distributions. The function as defined in Equ. (A6-1) has no finite upper limit to the size range.

Important as these considerations are in theoretical statistical studies of this function, they should not, and in fact have not had any inhibiting influence on the practical applications of the function. Indeed it is the extreme skewness of this function which makes it suitable for representing inclusion count data such as is plotted in Fig. A-9

Thus the Rosin-Rammler law for this application is defined as:

$1 - G(y) = R(y) =$ cumulative frequency percent of a field with a given inclusion area $\geq y$

$y =$ total area of inclusions in one field (in QTM units).

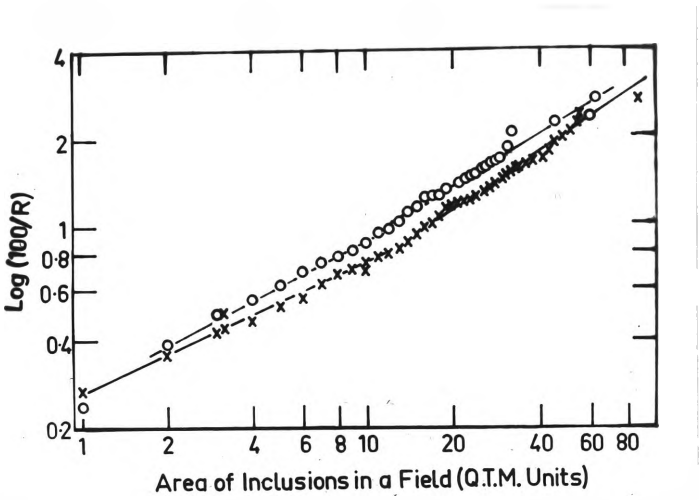

Fig. A-10 Inclusion area per field - frequency data for samples 8c and 7M plotted such that a distribution following the Rosin - Rammler law would be linear.

x — 8c

o — 7M

With these definitions the Rosin-Rammler functions for several samples are then comparable if a standard assessment technique is used. The standard conditions used in this analysis were 500 fields and a field size of 150 x 200 μm^2.

Table A-6 presents the chi-square goodness of fit results for the sample plotted in Fig. A-9. Since the X^2 value in this table considerably exceeds the tabulated value of chi-square at the 1% level (χ^2 = 13.277 for 4 degrees of freedom) it is evident that the fit is inadequate.

The absence of linearity in Fig. A-10 supports the findings in Table A-6. As a log-normal function on Rosin-Rammler coordinates plots as a curve which is concave towards the upper left hand corner of the graph (244), the data was also fitted to a log-normal function using Hald's (212) method for truncated distributions. The result of the chi-square goodness of fit test to the log-normal function was; X^2 = 50.89 for 3 degrees of freedom, which again exceeds the tabulated value of chi-square at the 1% level.

Thus the graph in Fig. A-10 was interpreted as consisting of two linear segments, each of which was fitted to a Rosin-Rammler function. The parameters of these functions are given in Table A-7.

The two linear segments in sample 80 are probably

TABLE A-6 GOODNESS OF FIT CALCULATION FOR SAMPLE NO. 8c TO THE ROSIN-RAMMLER FUNCTION

f_{ex}	f_{ob}	$\frac{(f_{ob} - f_{ex})^2}{f_{ex}}$
62.850	49.0	0.2805
64.800	32.0	16.6025
72.150	39.0	15.2311
69.900	51.0	5.1103
55.115	49.0	0.6785
32.195	34.0	0.1012
12.148	13.0	0.0598
		$X^2 = 38.0639$

TABLE A-7 PARAMETERS OF THE TWO ROSIN-RAMMLER FUNCTIONS REPRESENTING SAMPLE 8c

	DISTRIBUTION 1 0 to 14 (QTM UNITS)	DISTRIBUTION 2 15 to 87 (QTM UNITS)
n	0.448	0.678
b	0.608	0.337
k	3.040	4.811

a consequence of the assessment of both oxides and sulphides from the longitudinal section plane. The distribution with the range of field areas from 15 to 87 QTM area units was, therefore, assumed to represent the distribution of the elongated silicates and sulphides and the distribution with the range 0 to 14 QTM units that of the small oxide particles and probably also any small rounded sulphide particles.

It must berealised that this interpretation is based on the assumption that the fields containing a large total inclusion area contain mainly silicate and sulphide stringers, while the fields of low inclusion area consist of a few small silicate inclusions. Observations made show that for this sample this assumption is valid.

Another sample (7M) of the same grade of steel was also assessed by the QTM and analysed by the present method. The probability plot of the distribution of field areas is also given in Fig. A-10. An attempt to fit the 7M data to a single Rosin-Rammler function resulted in $X^2 = 46.581$, which is greater than the tabulated χ^2 value for the 1% level of 13.277 (4 degrees of freedom). In view of this result the above sample was also examined (Fig. A-10) for the presence of two linear segments. The parameters of the Rosin-Rammler function fitted to each

segment are listed in Table A-8, together with those of the single Rosin-Rammler function which best represents the complete data. Two interpretations are possible for the 7M data, these are:

1. That it is a heterogeneous sample, whose heterogeneity is only slight, or
2. The data is homogeneous and the lack of a significant fit to a single Rosin-Rammler function results from either a bad choice of the empirical function (i.e. one of Pearson's curves may provide a better fit) or the fit may be masked by experimental errors. In order to assess the magnitude of errors in the experimental technique in the absence of heterogeneity a sample containing only one inclusion type was assessed. This was a sample containing FeO particles from ingot No. 28. Table A-9 presents the results of the goodness of fit test of the distribution of field areas to a single Rosin-Rammler function for this sample.

The value of X^2 from Table A-9 is less than the tabulated χ^2 value at the 1% of 6.635 (one degree of freedom). Thus data supplied by this method of analysis will lead to a significant fit to a Rosin-Rammler function

TABLE A-8 PARAMETERS OF THE TWO ROSIN-RAMMLER FUNCTIONS REPRESENTING SAMPLE 7M

	DISTRIBUTION 1 0 to 12 (QTM UNITS)	DISTRIBUTION 2 13 to 62 (QTM UNITS)	COMBINED 1 + 2
n	0.538	0.579	0.569
b	0.594	0.554	0.571
k	2.635	2.776	2.674

TABLE A-9 GOODNESS OF FIT CALCULATION FOR INGOT 28

BOTTOM SAMPLE TO THE ROSIN-RAMMLER FUNCTION

f_{ob}	f_{ex}	$\frac{(f_{ob} - f_{ex})^2}{f_{ex}}$
5	4.7358	2.4860 *
25	17.7822	
68	71.8052	0.2017
178	195.0952	1.4980
155	154.3014	0.0032
		$X^2 = 4.1889$

* frequencies combined so obtain a frequency greater than 5.

when the data is homogeneous.

Consequently, the lack of an adaquate fit of the data of sample 7M to a single Rosin-Rammler function was interpreted as the result of heterogeneity of inclusion type and morphology (similar to that observed in sample 8c). The slight heterogeneity of sample 7M has most probably resulted from its normalising heat treatment. To some extent the heat treatment would re-dissolve the stringers and hence break them up and produce a more globular form (245-247). Inclusion assessment of the heat treated sample would reflect this rearrangement in morphology by a reduction in the slope of the upper range distribution, its slope approximating to that of the lower range distribution. A lower n value for the upper range distribution of 7M compared to that of 8c supports this hypothesis.

To test the reproducibility of this method of inclusion assessment a sample, designated 9A, was taken from aluminium fully killed strip. The same sample area was assessed three times using the QTM. The three sets of data were analysed and the parameters of the respective Rosin-Rammler distributions are given in Table A-10.

The reproducibility of the three sets of data were examined by the chi-square contingency test, and the

TABLE A-10 PARAMETERS OF THE ROSIN-RAMMLER FUNCTIONS REPRESENTING THE THREE ASSESSMENTS OF SAMPLE 9A

	b	k	n
1st count	2.140	0.1185	0.357
2nd count	2.275	0.0709	0.311
3rd count	2.193	0.0953	0.334

TABLE A-11 CHI-SQUARE CONTINGENCY TEST RESULTS FOR SAMPLE 9A

Counts	X^2	χ^2_{10}	χ^2_{05}	Degrees of Freedom
1st - 2nd	0.256	7.779	9.488	4
1st - 3rd	0.333	7.779	9.488	4
2nd - 3rd	0.827	7.779	9.488	4

results of which are listed in Table A-11.

The very low values of X^2 in Table A-11 indicate the very high reproducibility of this assessment method. Thus the parameters in Table A-10 can be considered to give the variability of each parameter which results from statistical or chance errors in the inclusion assessment. Although the results of Tables A-10 and A-11 show excellent reproducibility in assessing a given area of sample, the question of how representative this is of a large area of the rolled product, of course, cannot be deduced from these results. The high number of zero fields in 9A, although reproducible, is a result not only of the cleanness of the sample but also of the high reduction ratio from ingot to strip form. This means that in order to cover an equivalent slab sample area in the plate or strip form, a considerably larger area has to be examined in the latter.

It is therefore suggested that samples for inclusion assessments should whenever possible, be taken from the slab. This should reduce the errors in the assessment resulting from non-representative sampling to the lowest possible level under the practical conditions involved.

If slab samples are assessed by the QTM, the method of

representing the distribution of field inclusion areas by the Rosin-Rammler function has the potential of being a powerful tool in comparing steel "cleanness" as well as investigating inclusion populations and morphologies. The method developed in this section, however, is one of curve fitting and thus, lacks the theoretical basis of the log-normal model previously discussed. It must be recalled, however, that empirical methods have been employed in coal sizing and comparisons for many years with considerable success. Likewise the above method of assessing slab samples by the QTM and representing the resulting data by the Rosin-Rammler law could also be of considerable importance as an analytical measure of relative cleanness.

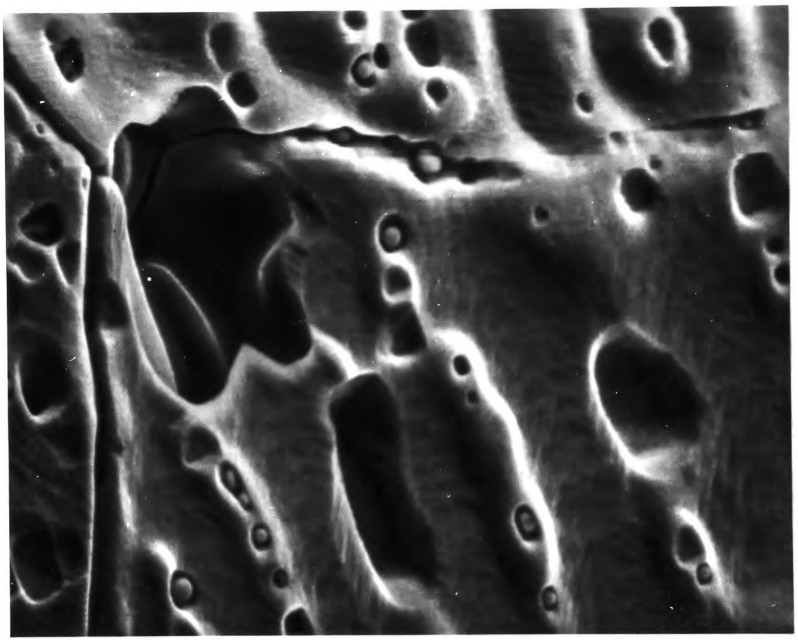

Fig. A-11 Scanning electron micrograph (1500X) of a preliminary antimony deoxidized copper ingot, showing approximately spherical Sb_2O_3 inclusions.

APPENDIX 7

SERIES 3 MELT

The aim of this heat was to examine if there was any similarity between the inclusion size-frequency distributions present in the melt after deoxidation and those which were trapped in the cast ingot.

To simplify the examination of inclusion assessment data, antimony was chosen as the deoxidant, as the shape of the resulting inclusions are approximately spherical (Fig. A-11). The general details of the heat are given in Section 5-4-3; the following are the thermal analysis details and sampling times for the 1300 g melt of copper deoxidized by 23.4 g of antimony.

Sample No.	Time (seconds)	mV	Temperature (°C)
1	-88	13.78	1242
Sb addition	0	13.798	1244
2	11	13.758	1241
3	32	13.646	1233
4	80	13.642	1232
5	200	13.648	1233
6	509	13.820	1245

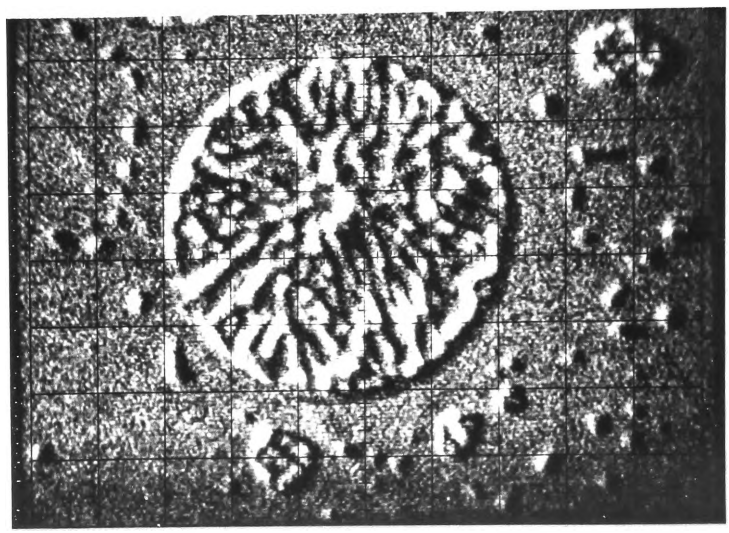

(a)

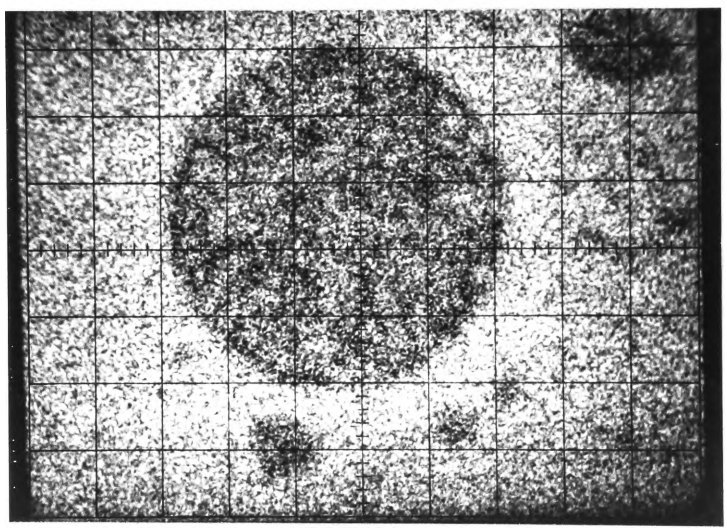

(b)

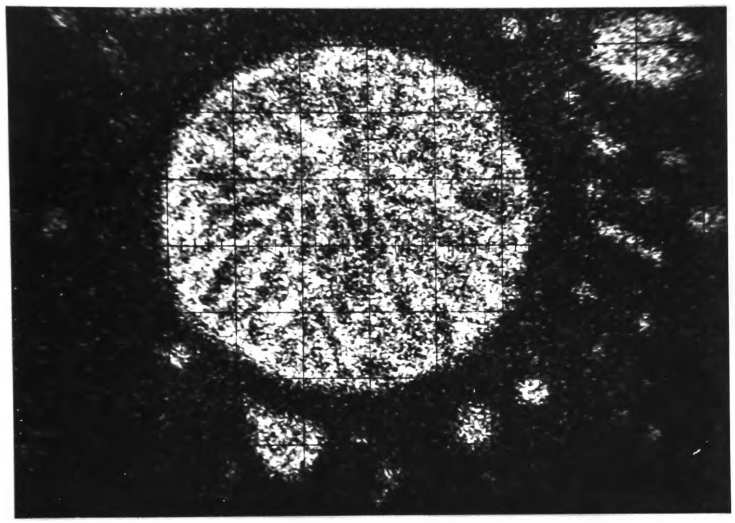

(c)

Fig. A-12 Electron probe microanalysis of a eutectic inclusion (2000X)

(a) back scattered electron image

(b) Cu K radiation

(c) Sb K radiation

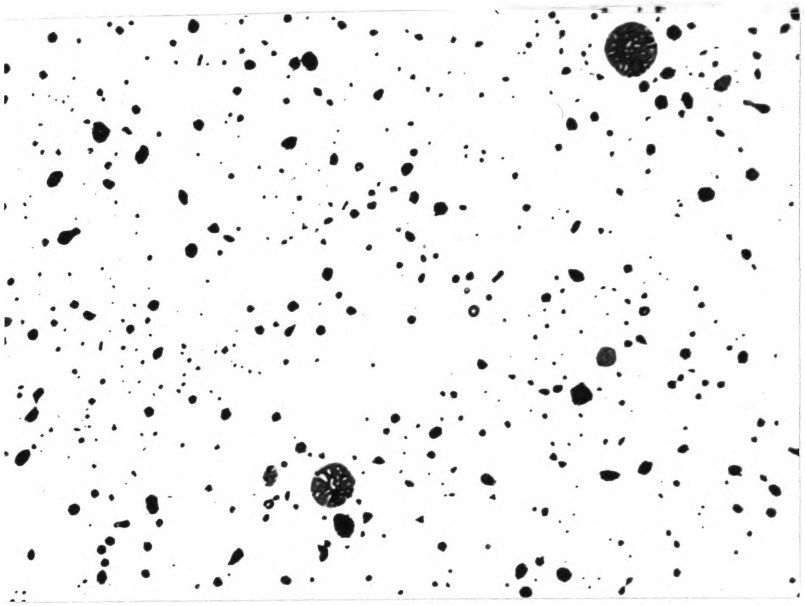

(a) From middle of sample (330X)

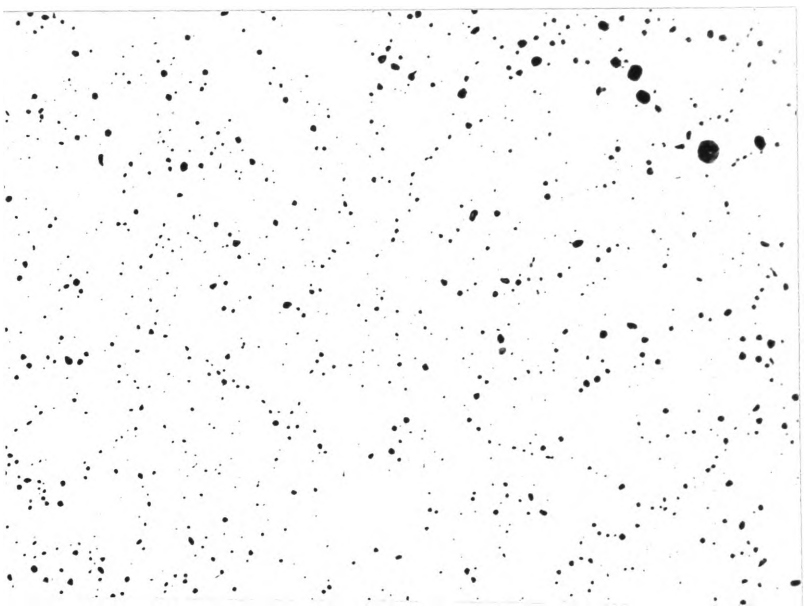

(b) From end of sample (330X)

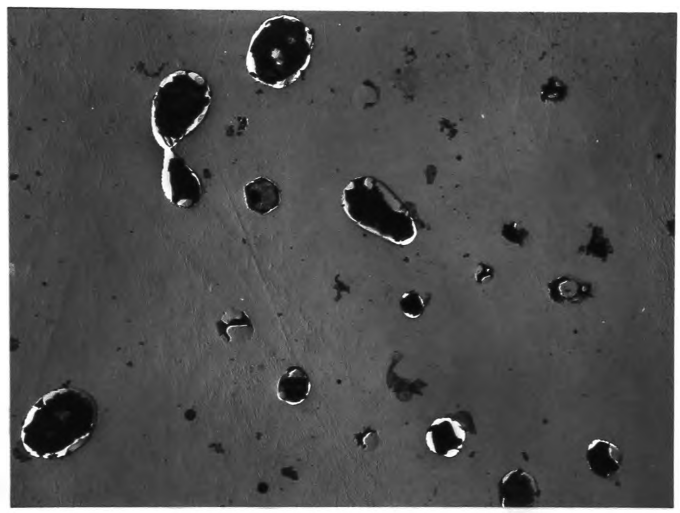

(c) From middle of sample (2600X)

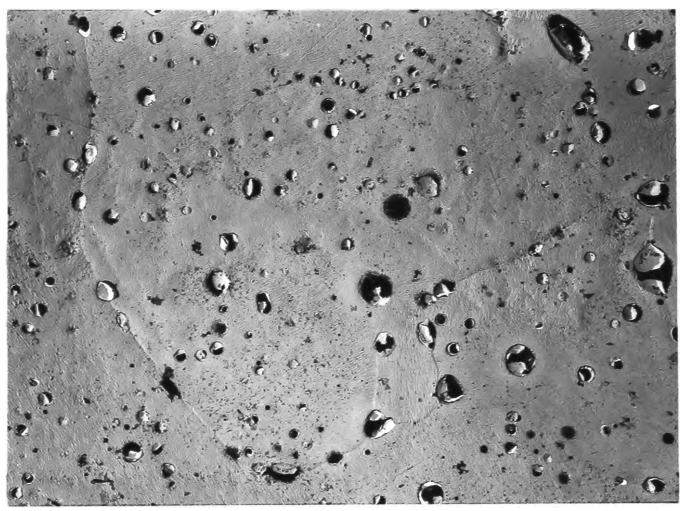

(d) From end of sample (2600X)

FIG. A-13 Inclusion distributions in the same dip tube sample.

7	559	13.846	1247
8	992	13.588	1228
Cast	1774	—	—

Microscopic examination of the dip tube samples revealed that the argon gas shielding had not been successful in preventing oxidation of the melt (probably because the gas flow rate chosen was too low). All samples contained duplex inclusions instead of the expected Sb_2O_3 particles. Electron probe microanalysis of these duplex inclusions identified them as consisting of Cu, Sb and O. The light coloured outer rim (light blue) of the inclusions (see Fig. A-12 and A-13) appears to be Sb_2O_3 and the dark phase in the inclusions CuO.

The lack of thermodynamic data of the Cu-Sb-O system has hindered interpretation of the inclusion assessment data, but as can be observed from Fig. A-13 (b), there is a considerable amount of secondary deoxidation products, as well as the primary deoxidation products.

The size-frequency distributions of inclusions produced by both these deoxidation steps will have different parameters and so the assessment data should be heterogeneous. To test for heterogeneity, firstly the relative frequency curves were examined for the presence of two modes. None

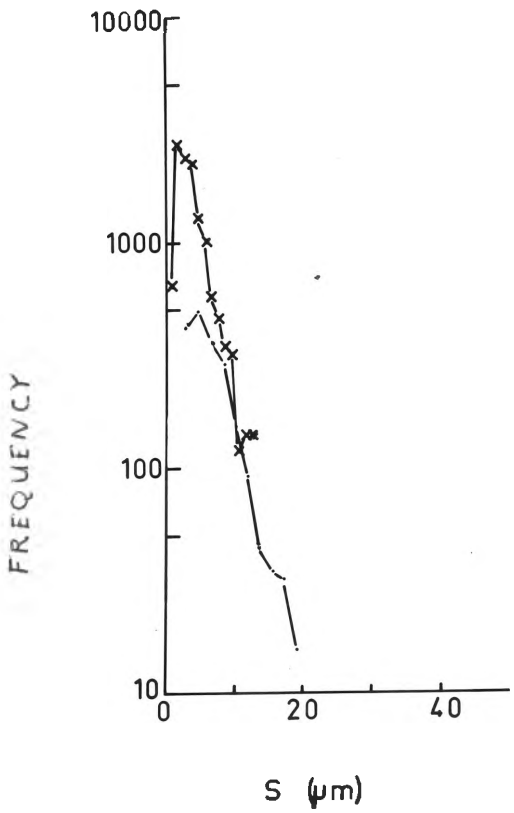

Fig. A-14 Size frequency data from dip tube sample No 5, showing the absence of any bimodal nature.

X-X count at 8300X

.-. count at 1400X

of the samples assessed were bimodal as Fig. A-14 shows for sample No 5.

When heterogeneity is exhibited only as small distortions in the relative frequency curve, the fit of the data to the three parameter log-normal section can be used as a qualitative measure of the degree of heterogeneity. For the samples assessed, a significant fit to the model could not be obtained with either the optical or electron microscope assessment data. (Tables A-12 and A-13). The degree of heterogeneity thus, although not sufficient to allow the separation of the two constituent distributions (as in Section 7-9-2) is sufficient to prevent representation as a single L-N curve. The inclusion distributions thus can only be qualitatively examined and compared.
Firstly the size-frequency distributions of inclusions found in the middle of the dip tube samples were examined. If the proportions of inclusions in each of the size classes are examined, it is noted that for both the optical and electron microscopic assessment data there was a distribution which was common to all dip tube samples and was also present in the ingot sample. (see Table A-14 and A15). If instead of the proportions, the frequencies in each of the size classes for the common distribution are examined, (all data expressed per 0.5 sq mm in Tables

TABLE A-12 CHI-SQUARE GOODNESS OF FIT RESULTS FOR COMBINED OPTICAL AND ELECTRON MICROSCOPE DATA (INCLUSION SIZE = $\sqrt{AB}$)

SAMPLE CODE	X^2	$\chi^2_{0.05}$	DEGREES OF FREEDOM
Dip Tube 2	517.70	18.307	10
Dip Tube 3	221.70	19.675	11
Dip Tube 5	182.41	15.507	8
Dip Tube 8	126.96	11.070	5
Ingot Bottom	130.75	15.507	8

TABLE A-13 CHI-SQUARE GOODNESS OF FIT RESULTS FOR OPTICAL DATA (INCLUSION SIZE = B)

SAMPLE CODE	X^2	$\chi^2_{0.05}$	DEGREES OF FREEDOM
Dip Tube 2	34.392	21.026	12
Dip Tube 3	30.059	23.685	14
Dip Tube 5	101.07	19.675	11
Dip Tube 8	38.030	15.507	8
Ingot Bottom	64.351	18.307	10

TABLE A-14 ASSESSMENT DATA DETERMINED BY THE OPTICAL MICROSCOPE - COMMON DISTRIBUTION

Class Limits (μm)	Proportion by number - sample total frequency equals 100 percent				
	Dip Tube 2	Dip Tube 3	Dip Tube 5	Dip Tube 8	Ingot Bottom
1.1586 - 1.5449	28.6	31.1	31.2	34.5	24.3
1.5449 - 2.3173	36.3	34.3	34.1	31.7	31.2
2.3173 - 3.0897	20.1	20.1	19.0	16.8	19.8
3.0897 - 3.8622	9.4	7.8	8.0	11.4	12.7
3.8622 - 6.6346	2.2	2.3	2.5	2.8	5.6
4.6346 - 5.4070	0.76	1.17	1.55	0.94	2.8
5.4070 - 6.1794	0.29	0.91	1.0	0.41	1.44
6.1794 - 6.9519	0.76	0.56	0.82	0.24	0.99
6.9519 - 7.7243	0.29	0.20	0.18	-	0.19
7.7243 - 8.4967	0.29	0.15	-	0.24	0.27

TABLE A-15 ASSESSMENT DATA DETERMINED BY THE ELECTRON MICROSCOPE - COMMON DISTRIBUTION

Class Limits (μm)	Proportion by number - sample total frequency equals 100 percent				
	Dip Tube 2	Dip Tube 3	Dip Tube 5	Dip Tube 8	Ingot Bottom
0.4116 - 1.2349	8.4	12.3	11.5	11.8	7.3
1.2349 - 2.4699	31.0	21.7	24.7	26.6	27.6
2.4699 - 3.7048	27.9	24.8	22.6	26.0	23.0
3.7048 - 4.9397	18.7	18.5	19.9	15.6	16.5
4.9397 - 6.1747	7.7	11.0	11.8	6.6	8.9
6.1747 - 7.4096	3.0	5.2	7.5	2.3	5.9
7.4096 - 8.6445	0.77	3.0	1.83	1.53	3.4
8.6445 - 9.8795	0.82	1.35	1.06	0.38	2.6
9.8795 -11.1144	0.33	0.75	0.19	0.76	2.3
11.1144 -12.3493	0.27	0.65	0.19	0.31	0.97

A-16, A-17), it can be seen that for all dip tube samples the frequencies in each respective size class are approximately constant in magnitude.

The existence of this common unchanging distribution is partly a consequence of the sampling technique employed which sampled only the deoxidation products which had floated to the top of the melt. Also the distribution does not change with time because once the inclusions have floated to the top of the melt very little further growth occurs, e.g. the distribution 10 seconds after deoxidation is very similar to that in the ingot cast 1774 seconds after deoxidation. The greater variability in the frequencies determined by the electron microscope are probably caused by one or both of the following:

(1) the flatness of the replicated surface

(2) the difficulty in measuring both axes of the inclusions

The inclusion distributions in the dip tube ends, however, show a considerable variation from sample to sample (Table A-18). The only obvious explanation for these differences in distributions is variability in the rate of solidification of the sample ends from sample to sample which will result in differing nucleation and growth conditions for the secondary deoxidation process. It of

TABLE A-16 ASSESSMENT DATA DETERMINED BY THE OPTICAL MICROSCOPE - COMMON DISTRIBUTION

Class Limits (μm)	Frequencies per 0.5 mm^2				
	Dip Tube 2	Dip Tube 3	Dip Tube 5	Dip Tube 8	Ingot Bottom
1.1586 - 1.5449	1138	1078	983	1304	616
1.5449 - 2.3173	1442	1184	1068	1199	790
2.3173 - 3.0897	801	695	596	634	501
3.0897 - 3.8622	372	270	250	429	322
3.8622 - 4.6346	87	79	79	107	141
4.6346 - 5.4070	30	40	48	36	70
5.4070 - 6.1794	11	32	31	16	37
6.1794 - 6.9519	30	19	26	9	25
6.9519 - 7.7243	11	7	6	-	5
7.7243 - 8.4967	11	5	-	9	7

TABLE A-17 ASSESSMENT DATA DETERMINED BY THE ELECTRON MICROSCOPE - COMMON DISTRIBUTION

Class Limits (μm)	Frequencies per 0.5mm^2				
	Dip Tube 2	Dip Tube 3	Dip Tube 5	Dip Tube 8	Ingot Bottom
0.4116 - 1.2349	757	2006	1532	1917	744
1.2349 - 2.4699	2798	3522	3310	4304	2837
2.4699 - 3.7048	2525	4030	3027	4217	2333
3.7048 - 4.9397	1684	3014	2666	2523	1672
4.9397 - 6.1747	693	1796	1584	1064	899
6.1747 - 7.4096	272	849	1005	371	598
7.4096 - 8.6445	69	491	244	247	341
8.6445 - 9.8795	74	219	141	62	268
9.8795 -11.1144	29	123	26	124	228
11.1144 -12.3493	25	105	26	49	98

course follows from this arguement that the solidification rate in the middle of the dip tube sample is similar to that in the base of the ingot, as the inclusion distributions assessed in both cases were similar. Hence in this trial continuity of inclusion distribution from melt to ingot was obtained providing the samples taken from both situations had similar solidification histories, i.e. similar secondary precipitation size-frequency distributions. However, as all samples exhibited heterogeneity of section distributions which could not be graphically separated, the distributions in these samples cannot be represented as log-normal distributions until an efficient method of analysing compounded distributions becomes available. This problem is suggested for future research.